A Thesis Submitted for the Degree of PhD at the University of Warwick

Permanent WRAP URL:

http://wrap.warwick.ac.uk/112171

Copyright and reuse:

For more information, please contact the WRAP Team at: wrap@warwick.ac.uk

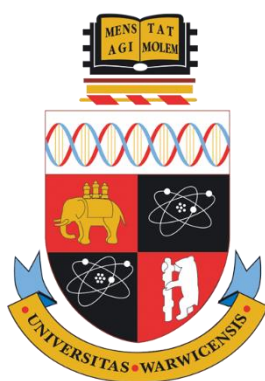**warwick.ac.uk/lib-publications**

Structure-Property Relationships of Conjugated Polymers

Samuel S. Lawton

A thesis submitted for the degree of

Doctor of Philosophy in Chemistry

Department of Chemistry

University of Warwick

July 2018

Easy is a synonym for boring.

Bethan Elaine Morris

Once you eliminate the impossible, whatever remains, no matter how improbable, must be the truth.

Arthur Conan Doyle

Research is what I'm doing when I don't know what I'm doing.

Wernher von Braun

Table of Contents

List of Figures

List of Tables

List of Schemes

List of Abbreviations

***ABA*-PTBnDT(C12)-*b*-PTBT**	*ABA*-(poly-A-4,8-didodecyl-2-(thiophen-2-yl)benzo[1,2-b:4,5-b']dithiophene-block-*b*-poly-5,6-bis(octyloxy)-4-(thiophen-2-yl)benzo[c][1,2,5]thiadiazole)
***AB*-PTBT-*b*-PTBnDT(CO₂C₁₂)**	*AB*-poly-4,8,-didodecyl-2-(thiophen-2-yl)benzo[1,2-b:4,5-b']dithiophene-4,8-dicarboxylate-*block*-*b*-poly-5,6-bis(octyloxy)-4-(thiophen-2-yl)benzo[c][1,2,5]thiadiazole
AFM	Atomic force microscopy
BHJ	Bulk heterojunction
BHT	Butylated hydroxytoluene
BnDT	Benzodithiophene
BnDT(C12)	4,8-didodecylbenzo[1,2-b:4,5-b']dithiophene
BnDT(CO2C12)	Didodecyl benzo[1,2-b:4,5-b']dithiophene-4,8-dicarboxylate
BT	Benzothiadiazol
BTz	Benzotriazol
ClBn	Chlorobenzene
CMD	Concerted metalation-deprotonation
CPDT	Cyclopentadithiophene
CV	Cyclic voltammetry
Đ	Dispersity
D-A	Donor-acceptor
DC	Direct current
DFT	Density functional theory
DHAP	direct hetero(arylation) polymerisation
DP	Degree of polymerisation
DPP	Pyrrole[3,4-c]pyrrole-1,4-dione
DRI	Differential refractive Index
DTBnDT	4,8-didodecyl-2-(thiophen-2-yl)-6-(thiophen-3-yl)benzo[1,2-b:4,5-b']dithiophene
DTBT	Dithiophenyl benzothiadiazol
DTBT	5,6-bis(octyloxy)-4-(thiophen-2-yl)-7-(thiophen-3-yl)benzo[c][1,2,5]thiadiazole
DTBTz	Dithiophenyl benzotriazol

DTTPD	Dithiophenyl thienopyrroledione
Eg	Band gap
EQE	External quantum efficiency
ETL	Electron transport layer
eV	Electron volts
FET	Field effect transistor
FF	Fill factor
GIWAXS	Grazing incidence wide angle X-Ray scattering
GPC	Gel permitation chromotography
GRIM	Gringard methatesis
HOMO	Highest occupied molecular orbital
HTL	Hole transport layer
ICT	Intramolecular charge transfer
IIDDT	Dithenoisoindigo
IPCE	Internal power conversion efficiency
IQE	Internal quantum efficiency
IR	Infrared
ITO	Indium tin oxide
Jsc	Short circuit cureent density
K	Kelvin
LUMO	Lowest unoccupied molecular orbital
MEH-PPV	Poly[2-methoxy-5-(2,ethylhexyloxy)-1,4-phenylenevinylene
MHz	Mega-Hertz
Mn	Number average molecular weight
***multi*-PTBT-*b*-PTBnDT(C$_{12}$)**	*Multi*-poly-a-4,8-didodecyl-2-(thiophen-2-yl)benzo[1,2-b:4,5-b']dithiophene-block-*b*-poly-5,6-bis(octyloxy)-4-(thiophen-2-yl)benzo[c][1,2,5]thiadiazole
***multi*-PTBT-*b*-PTBnDT(CO$_2$C$_{12}$)**	*Multi*-poly-4,8,-didodecyl-2-(thiophen-2-yl)benzo[1,2-b:4,5-b']dithiophene-4,8-dicarboxylate-*block*-*b*-poly-5,6-bis(octyloxy)-4-(thiophen-2-yl)benzo[c][1,2,5]thiadiazole
Mw	Weight average molecular weight
NIR	Near-infrared
NMR	Nuclear magnatic resonance
OLED	Organic light emitting diode

OPV	Organic photovoltaic
P(2,4,6-Me3Ph)3	Tris(2,4,6-trimethylphenyl)phosphine
P(2,4-Me2Ph)3	Tris(2,4-dimethylphenyl)phosphine
P(o-OMePh)3	Tri(o-methoxyphenyl)phosphine
P(o-tolyl)₃	Tri(o-tolyl)phosphine
P3HT	Poly(3-hexylthiophene)
PCBM	phenyl-$C_{61/71}$-butyric acid methyl ester ($PC_{61/71}BM$)
PCE	Power Conversion Efficiency
Pd2(dba)3	Tris(dibenzylideneacetone)dipalladium(0)
POPV	Polymer Organic Photovoltaic
PPH3	Triphenyl Phosphine
PPV	Polyphenylvinylene
PTB7	Poly[[4,8-bis[(2-ethylhexyl)oxy]benzo[1,2-b:4,5-b']dithiophene-2,6-diyl][3-fluoro-2-[(2-ethylhexyl)carbonyl]thieno[3,4-b]thiophenediyl]]
PTB7-Th	Poly[4,8-bis(5-(2-ethylhexyl)thiophen-2-yl)benzo[1,2-b;4,5-b']dithiophene-2,6-diyl-alt-(4-(2-ethylhexyl)-3-fluorothieno[3,4-b]thiophene-)-2-carboxylate-2-6-diyl)]
PTBnDT(C12)	Poly(4,8-didodecyl-2-(thiophen-2-yl)benzo[1,2-b:4,5-b']dithiophene)
PTBnDT(C₁₂)-*stat*-PTBT	4-(5-(4,8-didodecylbenzo[1,2-b:4,5-b']dithiophen-2-yl)thiophen-2-yl)-*stat*-5,6-bis(octyloxy)-7-(thiophen-2-yl)benzo[c][1,2,5]thiadiazole
PTBnDT(CO2C12)	Poly(didodecyl 2-(thiophen-3-yl)benzo[1,2-b:4,5-b']dithiophene-4,8-dicarboxylate)
PTBnDTTBT	4-(5-(4,8-didodecylbenzo[1,2-b:4,5-b']dithiophen-2-yl)thiophen-2-yl)-5,6-bis(octyloxy)-7-(thiophen-2-yl)benzo[c][1,2,5]thiadiazole
PTBT	Poly(5,6-bis(octyloxy)-4-(thiophen-2-yl)benzo[c][1,2,5]thiadiazole)
PTBT-*stat*-PTBnDT(CO₂C₁₂)	Poly(didodecyl 2-(5-(5,6-bis(octyloxy)benzo[c][1,2,5]thiadiazol-4-yl)thiophen-2-yl)-*stat*-6-(thiophen-3-yl)benzo[1,2-b:4,5-b']dithiophene-4,8-dicarboxylate)
Rsh	Shunt resistance
Rsh	Series resistance
SEC	Size exclusion chromotography
STM	Scanning tunneling microscopy
TBAPF₆	Tetrabutylammonium hexafluorophosphate
TBnDT	4,8-didodecyl-2-(thiophen-2-yl)benzo[1,2-b:4,5-b']dithiophene

TBT	5,6-bis(octyloxy)-4-(thiophen-2-yl)benzo[c][1,2,5]thiadiazole
TCB	1,2,4-trichlorobenzene
T$_D$	Decomposition temperature
TGA	Thermogravometric analysis
TPD	Thienopyrroledione
TT	Thieno[3,4-b]thiophene
UV-Vis	Ultraviolet/visible light spectroscopy
Voc	Open Circuit Voltage
VS	Viscometry
XPhos	2-Dicyclohexylphosphino-2',4',6'-triisopropylbiphenyl

Acknowledgments

First and foremost I would like to thank Prof. David Haddleton for accepting my application to undertake this PhD and for his continued supervision and support throughout. I would also like to thank Merck Chemicals Ltd. for the industrial funding and provision of monomers and other supplies. The staff at Merck have been a great help throughout my PhD. From Merck I would like to thank Dr. Agnieszka Pron and Dr. Lana Nanson for their support and supervision throughout my four years at Warwick. On visiting Merck at Chilworth I would like to thank Dr Michal Krompiec and Dr. Ignasi Burgues for their assistance and training in making OPV devices. The post docs that have served in the group alongside my project have been exceptional; thank you to Dr. Kristian Kempe and Dr. Ahmed Elissa. A special shout out to the Wilson group, with which we share a lab, for all the support and inspiration throughout the years, Thanks Dr. Paul Wilson.

There are a number of non-academic staff at Warwick without whom the completion of my PhD would have been impossible, I would like to thank the finance and stores team for all their hard work and for putting up with all my questions and request forms, A special thanks to Suki for helping to sort everything with my trip to the USA. The technical staff have also play a vital role in keeping all the kit up to a high standard for a large number of users. I would especially like to thank Dr. Ivan Prokes for his assistance in the NMR suite as well as Dr. Daniel Lester from the Warwick Polymer Characterisation RTP for his assistance and expertise with SEC.

I would also like to thank my parents for their support both emotionally and financial. My friends away from the university of also played a vital role in helping me maintain my sanity, for this a special thanks goes to "the squad" Ben, Scott, Tev and Vicky.

To anyone reading this in the future I would ask you to hold this in mind; it's not just the science that makes the group, it's the people. I have a lot of people to thank for their support and friendship over the past four years, let's start from the beginning. Three days after starting my PhD I was told to pack my bags and head off to the *Macro Group* Young Researchers' Meeting in Durham, I had no idea what to expect being a wide-eyed fresh faced PhD student, cut to 2 am on the first day (after a heavy "networking session") when Jamie Godfrey, Jennifer Collins and Samuel Lowe stumble out of the establishment behind me claiming "it's too early to close, what is this?" I would like to thank these three

individuals for making me feel immediately welcome and their continued friendship and scientific guidance.

October 2014: Glen, Patrick, Richard and Nikolaos start their PhDs too. Thanks Glen for your musical education in the lab (if sometimes of questionable taste), Pat for constantly answering my questions and being a fellow pun master, Richard, a great house mate (2017/18) with a wicked sense of humour and Nikolaos for teaching me how to drink Sambuca the Greek way.

Christmas 2014: Dr. Daniel Lester has proven himself to be a loyal friend and has taught me everything I know about SEC, we have spent the last six months becoming close friends (the words carnage and rampage were used excessively) and now sit listening to Dave's stories about times past in the group "Davicdotes" as they are now know.

August 2015: I move in with Emma Ravenhill, Connah Burnette and Ross Jaggers who make the next two years of my life great fun and support me through all the shenanigans I get myself into. Special thanks to Ross for dealing with all my drama and being a great friend.

October 2015: Dave only takes on one student, Rachel Hand, who is perhaps the most organised person I know and took on the daunting task of trying to impart some of that on me, thanks!

2016: A combination of energetic summer students, Warwick Polymer Conference 2016 (we had great fun organising the bar crawl and beating Seb's team in the five-a-side), and five new PhD students inject a new lease of life and science into the group.

2017: Another five PhD students enter the group in the final year of my PhD it is safe to say the group will be in good hands! Richard and I move in with Nick Kuht, he turns out to be a hoot.

2018: Writing the thesis and finishing up has been one of the biggest challenges in my PhD I'd like to thank all my proof readers (Dan, Patrick, Ellis, Tammy, Richard, Luke, Lana, Ahmed and Dave) for their input. Tammy and Patrick thanks for the (perhaps an excessive amount of) tea breaks and Luke for all the pints. A special thanks to Chris and Gavin for putting up with all the abuse that accompanied "thesis rage".

It has been a pleasure to work alongside such talented and friendly students across the years, it's been rewarding to see our MChem and MSc students achieve so highly, thank you to everyone who I have worked with. To any future students who have bothered to read this, remember to take some time out and enjoy your life! Balance your research with other activities like teaching and be a well-rounded person... because any old monkey can churn out data, be an individual!

Declaration

Experimental work contained in this thesis is original work carries out by the author, unless otherwise stated, in the *Department of Chemistry* at the *University of Warwick*, between July 2014 and July 2018. No material contained herein has been submitted for any other degree or at any other institution.

Scanning Tunnelling Microscopy (Figure 2.6) was carried out by Daniel Warr under the supervision of Dr. Giovanni Costantini at the *University of Warwick*.

Devices were made and tested by myself at *Merck Chemicals Ltd.* under the supervision of Dr. Michal Krompiec and Dr. Ignasi Burgues (Chapter 4).

Results from other authors are referenced in the usual manner throughout the text.

_____   Date:

_____

Samuel S. Lawton

Abstract

Conjugated polymers for application in optoelectronic devices have been an increasingly popular topic of research over the past two decades, with photovoltaic devices incorporating conjugated polymers now nearing large-scale commercialisation. This work focuses on the structure-property relationships of conjugated polymers.

Firstly, the difference in backbone structure between an alternating copolymer and its statistical counterpart are investigated, the differences in backbone sequence is elucidated by kinetic and microscopic techniques. The resulting polymers are found to be more gradient or block-like and form better BHJ blends with the $PC_{61}BM$ acceptor and have deeper HOMOs resulting in the observed increase in PCE.

Subsequently, alterations to the catalytic system for the synthesis of statistical copolymer by Stille polycondensation are investigated. Variations in the ligands electronic and steric effects are shown to have a profound effect on the relative rates of monomer conversion. Changing the catalyst directly effects the backbone sequence of the polymer. Polymers synthesised using various catalysts are investigated and their optoelectronic and morphological properties are discussed related to the monomer sequence.

Finally, well-defined all-conjugated block copolymers are investigated. Electron deficient PTBT and electron rich PTBnDT blocks are synthesised and characterised. Each of the homoblocks demonstrate distinctly different miscibility and film morphology with the $PC_{61}BM$ electron acceptor. When coupled, the resulting block copolymers show signs of micro-phase separation and the viability of block copolymers as a means of domain size control is investigated.

Chapter 1: An Introduction to Conjugated Polymers in Organic Photovoltaics
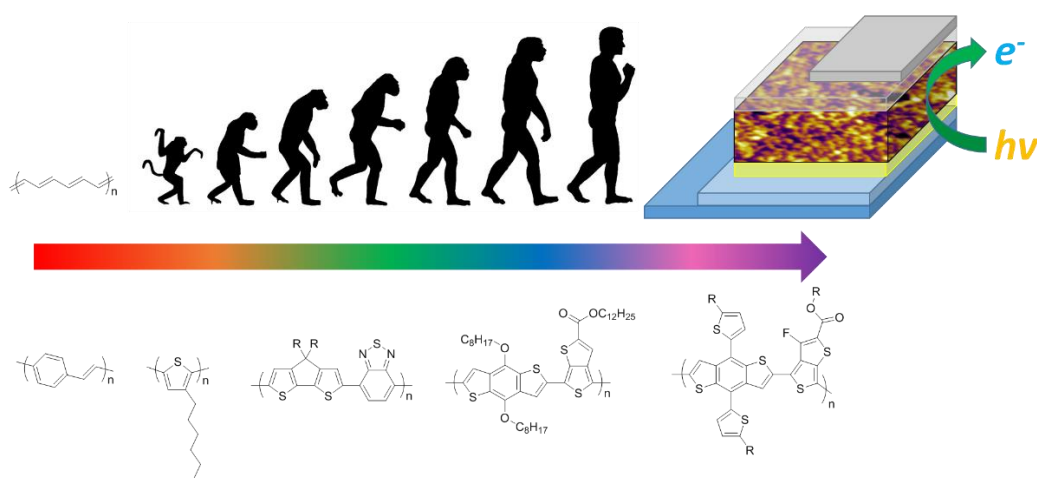
1.0: Introduction

With an ever-growing population in a world that strives to become more technologically advanced, and with many developing countries, the demand for a renewable clean energy supply is quickly becoming both an economic and environmental crisis. With the world's energy demand predicted to increase by 48 % between 2012 and 2020,[1] relying on the limited supply of traditional fuels is no longer a viable option. In addition to their growing scarcity, traditional fuel supplies release large amounts of waste and are a major contributor to annual greenhouse gas emissions. For example, the UK energy supply sector emitted 112 million tonnes of CO_2 alone in 2015.[2] Solar energy is perhaps the most promising candidate to provide a large portion of the world's energy demands, however, the widely used silicon based devices are expensive and require energy intensive processes for their fabrication. As a result, silicon devices are less accessible to developing countries and have a long energy payback time, in the order of years.[3] Despite efficiencies being approximately half that of silicon based devices, organic photovoltaics (OPVs) have greatly reduced the energy payback time from years to days.[4] OPVs offer further benefits such as; their low energy production (on a roll-to-roll basis) and their light weight. The ability of such devices to be flexible and semi-transparent[5,6] furthers the prospects of OPVs, making them particularly appealing for integrated devices in modern architecture. This was recently demonstrated by BELECTRIC and Merck with the solar tree instalment at the Universal Exhibition in Milan.[7]

Perhaps one of the most widely investigated areas of contemporary OPV research has been the polymer donor-fullerene acceptor bulk heterojunction (BHJ) based device. Typically, such BHJs are formed of a physical blend of an electron donating polymer and an electron accepting fullerene. A suitable polymer must principally have a low band gap allowing it to absorb light across the visible and near infrared (NIR) spectrum. As well as a high absorption coefficient, donor polymers must also have sufficient hole transport properties to limit losses due to recombination. Phenyl-C_{61}-butyric acid methyl ester ($PC_{61}BM$) is often used as a cost-effective electron accepting material, although $PC_{71}BM$ may be used instead owing to its improved absorption profile with respect to the solar spectrum.[8] This introduction focuses on polymer OPVs (POPVs) and more specifically the evolution of the design of polymer donor materials over time.

1.1: Operating Principles of OPVs

An OPV device aims to convert photons into electrical energy in the form of direct current (DC). POPVs typically consist of a transparent anode such as indium tin oxide (ITO), a hole transport layer (HTL), the active layer (the BHJ) which directly absorbs photons and generates charge carriers, an electron transport layer (ETL) and finally a reflective cathode (Figure 1.1a). Some devices are made in the inverted stack configuration, where the anode and cathode are switched along with the HTL and the ETL (Figure 1.1b). While interlayers (the HTL and ETL) play an important role in maximising the efficiency and longevity of devices, they are not the main focus of this introduction, for more information the reader should see the referenced literature.[9]
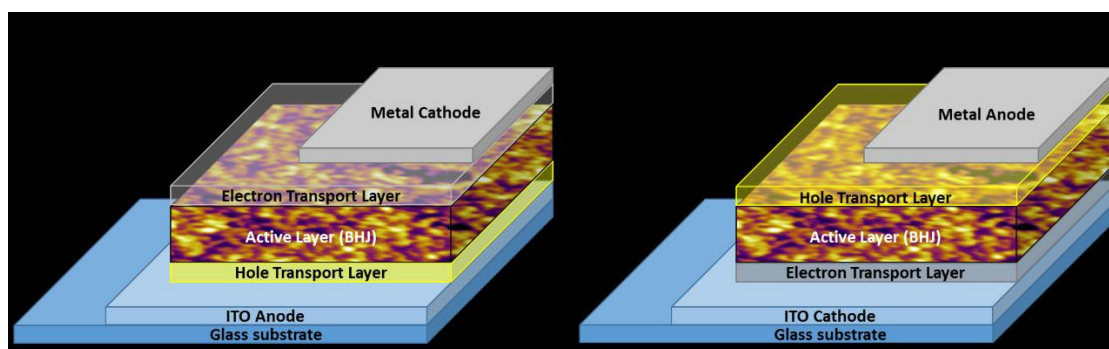
Figure 1.1: Standard structures of BHJ-OPVs, a; normal stack with a transparent anode, b; inverted stack with transparent cathode.

The active layer is the most complex and important layer of the BHJ-OPV, it consists of an electron donating material (*e.g.* a polymer) and an electron accepting material, which is most often phenyl-$C_{61/71}$-butyric acid methyl ester ($PC_{61/71}BM$), although polymer and small molecule acceptors have been increasingly used in non-fullerene OPVs.[10-12] The active layer is responsible for the main photovoltaic process; light absorption/exciton formation, charge separation and charge transport, as detailed in Figure 1.2. Light can be absorbed by the donor or acceptor material; when an incident photon has an energy greater than the highest occupied molecular orbital (HOMO)-lowest occupied molecular orbital (LUMO) band gap of the donor (E_g^{donor}) or acceptor ($E_g^{acceptor}$) an exciton is formed (Figure 1.2a). The exciton has a short lifetime, in the order of picoseconds.[13] In this time it needs to diffuse to the donor-acceptor interface where a sufficient energetic driving force (≥ 0.3 eV)[14] is required for the separation of the coulombically bound charge pair to create a separate hole and electron (Figure 1.2b and 1.2c). The free electron then travels

through the acceptor material and is extracted at the cathode whilst the free hole travels through the donor material and is extracted at the anode (Figure 1.2d).
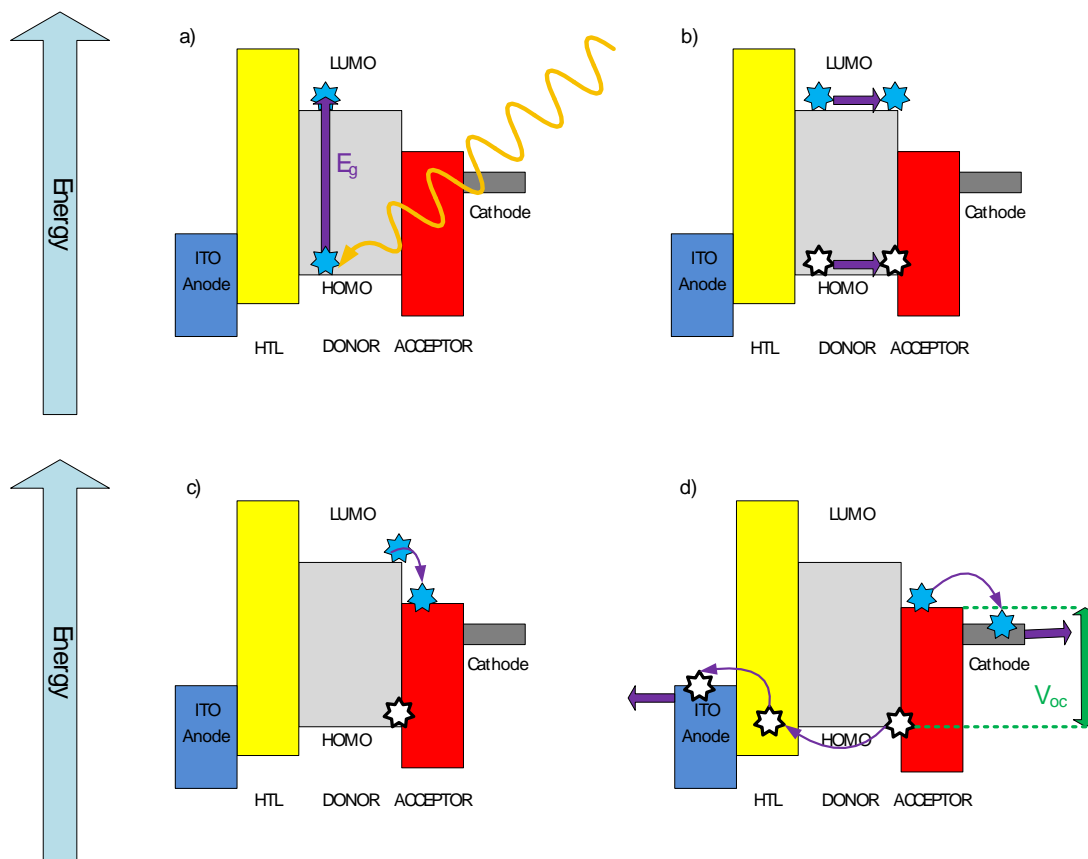
Figure 1.2: Photovoltaic processes in an OPV, a; exciton formation by the absorbance of a photon $hv > E_g$, b; Exciton diffusion to a donor-acceptor interface, c; charge separation d; charge extraction. *n.b.* Excitons may also be formed in the acceptor material which similarly diffuse to the donor acceptor interface and undergo charge separation followed by charge extraction.

In an ideal active layer all incident light should be absorbed, 100 % of the excitons will then be extracted into their separate charges, which must then rapidly travel through the donor and acceptor materials without recombining. In this case, neglecting any other losses, the device would have 100 % external quantum efficiency (EQE) and 100 % internal quantum efficiency (IQE), where EQE is the ratio of charge carriers collected to the number of photons incident to the OPVs exterior, and IQE is the ratio of charge carriers collected to the number of excitons formed.

While a perfect device may never be realised, there are some simple design aspects of the modern OPV that help to maximise both the EQE and the IQE. The movement from a single planar donor-acceptor heterojunction to a BHJ is perhaps the most important engineering advancement in the field of OPVs. The first OPV devices used a single planar junction that leads to very low power conversion efficiencies (PCEs), due to the short lifetime of the exciton. As the exciton is so short lived, its maximum diffusion length is thought to be in the region of 8-10 nm.[15,16] In a single junction device (Figure 1.3a) only light absorbed within 10 nm of the junction can be separated into independent charge carriers. A BHJ uses a physical blend of donor and acceptor materials to create continuous domains with sizes in the order of 20-30 nm (Figure 1.3b), allowing for much thicker active layers, resulting in the absorption of many more photons and subsequent separation of excitons into charge carriers, yielding both a higher EQE and IQE. While a domain size of 10 nm would ensure near quantitative conversion of excitons into charge carriers, a domain size of less than 20 nm can lead to high levels of electron-hole recombination and thus an overall greater loss in charge carriers.[17]
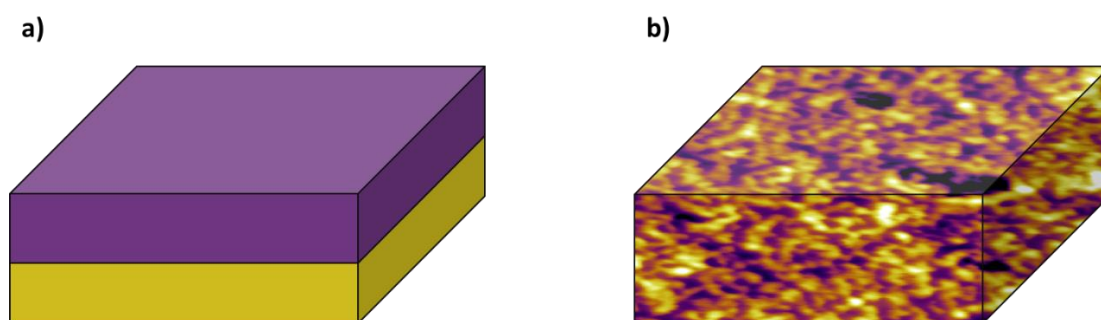
Figure 1.3: heterojunctions: a, single planar heterojunction, a single layer of donor material deposited on a single layer of acceptor material, b; bulk heterojunction, physically blended donor and acceptor materials.

The figure of merit for photovoltaic devices is the PCE which is defined by Equation 1:

$$PCE = \frac{V_{oc} \times J_{sc} \times FF}{P_{in}}$$

Equation 1

Where V_{oc} is the open circuit voltage, J_{sc} is the short circuit current density, FF is the fill factor and P_{in} is the number of photons incident to the device. V_{oc} is the maximum potential available from the device at zero current and is strongly correlated to the energy difference of the HOMO of the donor material and the LUMO of the acceptor material. J_{sc} is the maximum current density the OPV can produce and is dependent on the number of incident photons of $E > E_g$ and the collection probability of free charges. At both the V_{oc} and the J_{sc} the power output of the device is zero. The FF is used to determine the maximum power output of the device, it can be thought of as a measure of "squareness" of the JV curve (Figure 1.4) and is described by Equation 2:

$$FF = \frac{I_{mpp} \times V_{mpp}}{J_{sc} \times V_{oc}}$$
<div align="right">Equation 2</div>

Where I_{mp} and V_{mp} are the current and voltage at the maximum power point, respectively.
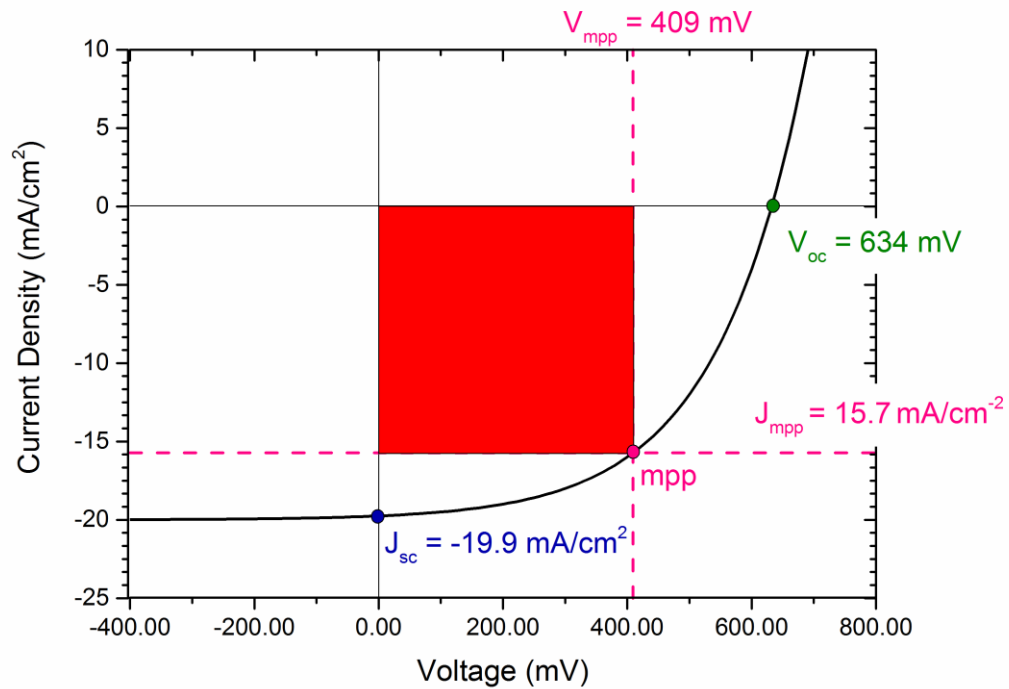
Figure 1.4: Example current-voltage (JV) curve for an OPV device. The J_{sc} is -19.9 mA/cm² indicated by the blue dot at the intersection of the y-axis. The V_{oc} is 634 mV indicated in green at the interaction of the x-axis. The red area represents the largest rectangle that will fit in the curve, this touches the JV curve at the maximum power point (mpp) indicated in pink, J_{mpp} and V_{mpp} are also indicated in pink, and these data can be used to calculate the FF.

Fullerene derivatives such as $PC_{61/71}BM$ are the most commonly used electron acceptor materials in a BHJ. The fullerene derivatives have high electron affinities and electron mobilities in three dimensions as well as a favourable nanoscale morphology.[18] It is also believed that the low lying excited states of the anions contributes to more efficient charge separation.[19] The only disadvantages of fullerene derivatives for OPVs is their low optical absorption and the relatively high cost of the most efficient forms ($PC_{71}BM$). We therefore rely on the donor to generate the majority of the excitons and thus require it to have a high absorption coefficient across the solar spectrum for effective harvesting of light. The remainder of this review focuses on the history and development of donor polymers and the techniques used to optimise their electronic and morphological properties for application in PCBM-based BHJ devices.

1.2: Requirements of Donor Polymers

The donor polymer is an integral part of the modern OPV, as mentioned in Section 1.1, due to the low optical absorption of PCBM acceptors we rely largely on the donor material for the absorption of light and generation of excitons. A strong broad absorption is not enough, however, there are a plethora of other electronic, structural and morphological properties one must consider when designing a donor polymer. To achieve a useful donor polymer which yields an OPV with a high PCE we must consider how the physical and electronic properties of the polymer will affect the J_{sc}, V_{oc}, and the FF of the OPV device, with a view to maximising each.

The first thing one must consider when developing new polymeric materials is the molecular weight. A relatively high molecular weight is what gives polymers their characteristic physical and mechanical properties. Whilst the BHJ must be mechanically flexible and stable, molecular weight plays another role in conjugated polymers. The higher the molecular weight of the polymer, the longer the maximum conjugation length of the material. A long conjugation length leads to a decreased band gap and increased absorption of the solar spectrum.[20] Higher molecular weight polymers can also exhibit more interchain entanglement, thus influencing charge transport and J_{sc}. Due to the rigid aromatic structure of conjugated polymers, at high molecular weights these materials become increasingly insoluble and difficult to process at low temperatures in most

common solvents. It is important to find a balance between the optoelectronic and physical properties when considering the molecular weight of conjugated polymers.

J_{sc} is limited by the number of excitons generated in the BHJ, which is proportional to the number of photons with $hv \geq E_g$ impinging on the exterior of the device. Most solar energy at the Earth's surface lies within the visible wavelength to the NIR region,[21] corresponding to an ideal band gap of 1.4-1.5 eV. This band gap can be lowered, which would allow longer wavelengths of light to generate excitons. The resultant increase in the donor HOMO leads to a decrease V_{oc} and an overall reduction of the PCE. One could achieve a smaller band gap by choosing to lower the LUMO of the donor material and maintain the low lying HOMO thus preserving the high V_{oc}, however, a driving force of approximately 0.3 eV is required for efficient charge separation from the LUMO of the donor to the LUMO of the acceptor.[22] Lowering the LUMO too far may result in more excitons, but the probability of these excitons being split into charge carriers is then greatly reduced resulting in an insufficient J_{sc}.

The open circuit voltage is correlated to the HOMO of the donor and the LUMO of the acceptor.[23] As the acceptor is usually $PC_{61/71}BM$, therefore a minimisation of the donor HOMO is required to give a large V_{oc}. Lowering the HOMO too much will, however, increase the E_g. Only higher energy photons will be able to form excitons, thus underutilising the solar energy that is incident to the earth's surface and resulting in a less than optimal J_{sc}.

FF is a measurement of the rectification of the OPV and is largely dependent on the shunt resistance, R_{sh}, and the series resistance, R_s, which in turn are affected by the morphology of the donor-acceptor blend. Obtaining an optimum morphology with domain sizes in the order of 10-30 nm is required to maximise diffusion of the excitons to the donor-acceptor interface and minimise recombination, further to this sufficient percolation pathways to the electrodes is also vital in achieving a high FF.

For a BHJ OPV device based on a polymer-$PC_{61}BM$ blend, a polymer which has: a LUMO of -3.9 eV (0.3 eV greater than the LUMO of $PC_{61}BM$, -4.2 eV);[22] a band gap that promotes absorption in the NIR region (1.4-1.5 eV) and a corresponding HOMO of -5.4 eV and finally, an extended crystalline morphology to promote charge extraction and forms a stable blend with $PC_{61}BM$ would be required.

1.3: A Brief History of Conjugated Polymers

The 2000 Nobel Prize winners, Professors Heeger, MacDiarmid and Shirakawa, are often accredited with the discovery of conjugated polymers through their work with polyacetylenes.[24-26] In reality, work on conjugated and conducting polymeric materials predates this milestone discovery. Quite possibly the first known organic conducting material is carbon black[27] which was considered to be a three dimensional network of various ill-defined polymers with varying chemical compositions.[28] It was in the 1950s that work began on producing a more defined synthetic polymer alternative to carbon black materials, but it was not until 1963 that Weiss *et al.* would achieve this with the synthesis of polypyrrole from tetraiodopyrrole (Figure 1.5). The crosslinked and unfunctionalised polypyrroles obtained were insoluble black powders which demonstrated conductive properties.[29,30] Later in 1966, Jozefowicz *et al.* developed conducting polyanilines by the oxidative polymerisation of aniline using persulfates (Figure 1.5).[31] In 1967, a student of Shirakawa mistakenly added a 1000 times excess of catalyst while attempting to make polyacetylene resulting in a lustrous and conductive film, the synthetic procedure was later optimised and made more reproducible.[32,33] Finally in 1977 Heeger, MacDiarmid and Shirakawa published their work on iodine doped polyacetylene films[26] for which they later won the 2000 Nobel Prize in Chemistry for "the discovery and development of conductive polymers".

Polypyrrole   Polyaniline   Polyacetylene
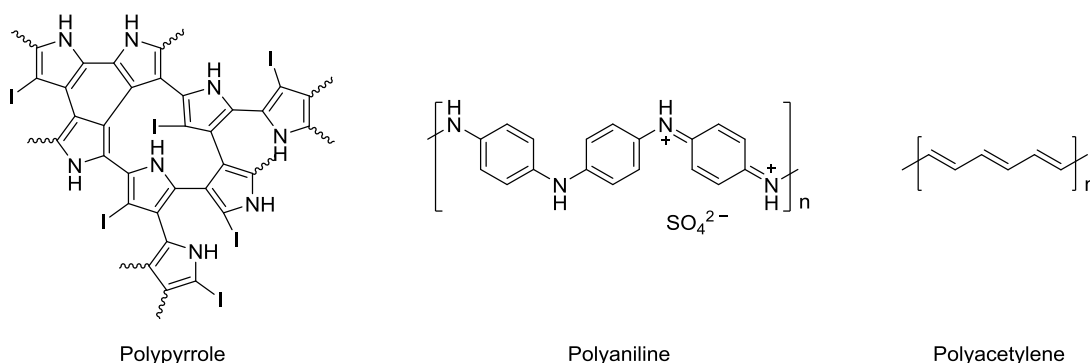
Figure 1.5: Chemical structures of polypyrrole, polyaniline and polyacetylene.

Among the first donor polymers to be used in OPV devices were poly(phenylenevinylene)s (PPVs). The rigid aromatic backbone, however, makes such polymers hard to process in common organic solvents. Poly[2-methoxy-5-(2-ethylhexyloxy)-1,4-phenylenevinylene] (MEH-PPV) and poly[2-methoxy-5-(3,7-dimethyloctyloxy)]-1,4-phenylenevinylene (MDMO-PPV) were among the first solution processable PPVs owing to the introduction of alkyl side chains along the backbone. After

use of various solvents to manipulate the film morphology, MEH-PPV achieved PCEs of up to 3.3 %.[34,35]
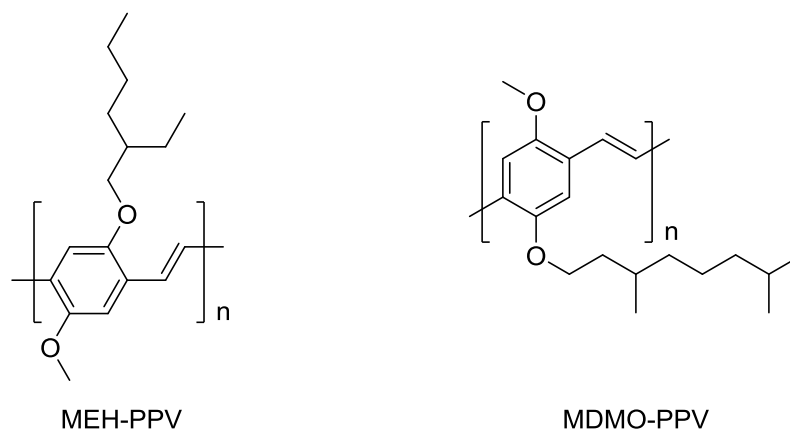
Figure 1.6: Chemical structures of MEH-PPV and MDMO-PPV.

The next major increase in PCE (to above 5 %) was achieved by the use of poly(3-hexylthiophene) (P3HT). P3HT has a much more crystalline structure owing to the greater degree of π-stacking and a regio-regular synthesis yielded P3HT based devices with much higher J_{sc}.[36,37] P3HT is, however, limited due to its relatively high HOMO of 5.1 eV, which restricts the maximum value of V_{oc} as well as its large E_g of 2 eV resulting in limited solar harvesting. Despite its relatively low PCE when compared to more recent advancements, P3HT is still widely used as a standard when varying other aspects of the BHJ OPV as it is very well defined.
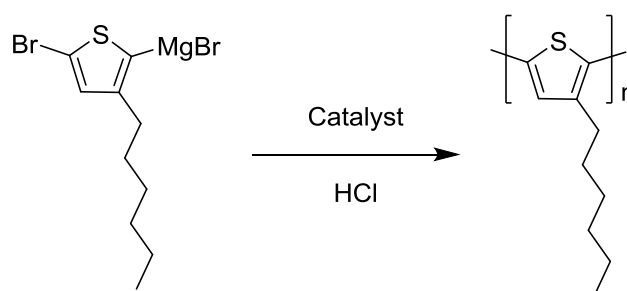
Figure 1.7: Synthesis of regio-regular P3HT by Grignard metathesis.

In attempts to create lower band gap polymers, donor-acceptor (or push-pull) alternating polymers became an area of significant interest.[38,39] In 2010, perhaps one of the most famous donor polymers to be developed to date was reported, poly[[4,8-bis[(2-ethylhexyl)oxy]benzo[1,2-b:4,5-b']dithiophene-2,6-diyl][3-fluoro-2-[(2-ethylhexyl)carbonyl]thieno[3,4-b]thiophenediyl]] (PTB7) (Figure 1.8). PTB7 set the new

record achieving PCEs of 7.4 % in PC$_{71}$BM BHJ devices.[40] The work of Yu *et al.* demonstrated that through careful monomer design, and selection of substituents and side chains that the commercialisation of polymer OPVs could be a not too distant possibility. Since PTB7 was demonstrated many variations of monomer combinations, side chains, substituents and processing conditions have been investigated. To date the most promising OPV donor materials remain low band gap donor-acceptor polymers frequently resulting in single junction devices with PCEs > 10 %.[41-46]
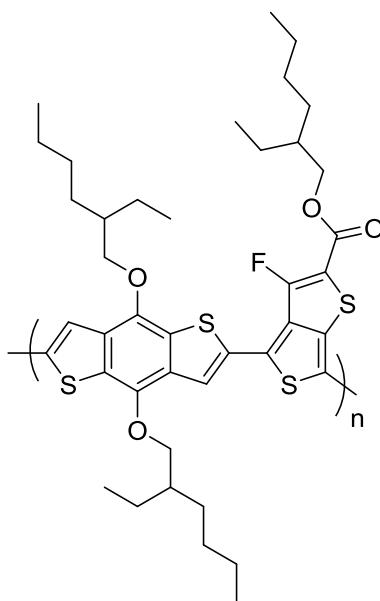
Figure 1.8: Chemical structure of PTB7.[40]

1.4: Synthetic Strategies for Conjugated Polymers

In this section we discuss the various synthetic strategies used in the production of low band gap donor polymers for OPVs. Palladium catalysed coupling techniques such as the Stille cross coupling and Suzuki-Miyaura coupling dominate much of the literature due to their tolerance of functional groups and efficiency at forming sp^2 carbon-carbon bonds. There are, however, emerging new methods of preparing high molecular weight functional conjugated polymers for OPVs. An increasingly popular choice is the much more atom efficient direct hetero(arylation) polymerisation (DHAP), which utilises a palladium catalyst to activate a C-H bond and forgoes the requirement of the toxic stannanes coupling functionalities necessary for Stille coupling. Below is an outline of each of these synthetic strategies and their various advantages and pitfalls.

1.4.1: Stille Polycondensation

The first examples of this type of palladium catalysed cross coupling were reported in 1976 and 1977 by Eaborn[47] and Kosugi,[48,49] it was not until 1978 that Stille published his mechanistic work on the coupling technique[50] which he later reviewed in 1986.[51] The extensive work of Stille revealed the mechanistic intricacies of the coupling system and soon led to the association of his name with the coupling pathway. A simplified version of the Stille cross coupling for an aromatic halide Ar-X and a (trialkylstannyl)aryl Ar-'SnMe$_3$ is shown in Figure 1.9, which is sufficient for the scope of this review. A more comprehensive understanding of some of the finer details of the Stille coupling can be found in the literature.[52]

The Stille coupling consists of four main steps; oxidative addition, transmetalation, a trans/cis isomerisation followed by a reductive elimination, as outlined in Figure 1.9. Often the electron deficient species is functionalised with a halide (either iodine or bromine) as it is expected to undergo oxidative addition more readily than an electron rich species. The oxidative addition of the arylhalide is followed by a rapid cis/trans isomerisation.[53] Transmetalation then occurs between the electron rich arylstannane and the palladium centre. Transmetalation is generally regarded as the rate-determining step and can occur through a number of pathways including open, cyclic or ionic routes.[51,52,54] Transmetalation is followed by a trans/cis isomerisation which then allows for the reductive elimination (the final step) producing the coupled Ar-Ar' and regenerating the Palladium-(0) catalyst.
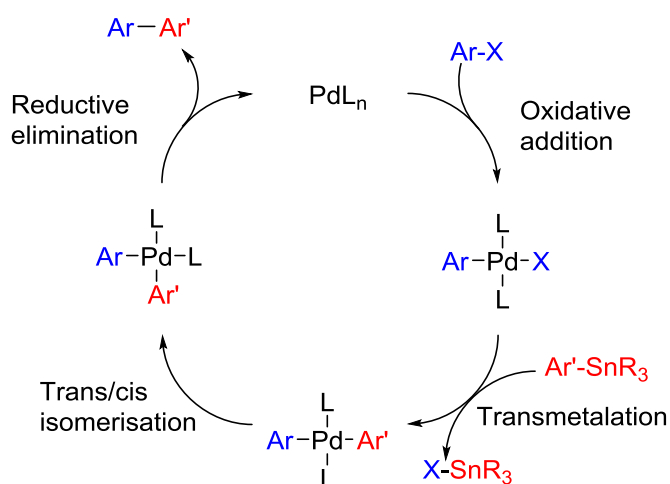
Figure 1.9: Simplified catalytic cycle for the Stille coupling of an aromatic halide Ar-X and a (trialkylstannyl)aryl Ar'-SnMe$_3$.

Choosing the right palladium catalyst is key to obtaining functional materials of a high molecular weight. Choices of monomer, solvent[55,56] and additives[57,58] can all have a significant effect on the catalyst's performance and often each new polymer has its own optimum synthetic conditions. Tetrakis(triphenylphosphine)palladium-(0) [Pd(PPh$_3$)$_4$] has been a popular choice in Stille polycondensations, although excess PPh$_3$ has been shown as an inhibitor of the Stille coupling,[59] further to this [Pd(PPh$_3$)$_4$] is oxidised by even trace amounts of oxygen. To achieve materials of a high molecular weight, high conversion, and thus high catalyst activity, is paramount. Unlike in small molecule reactions where a conversion of < 90 % might be acceptable, polycondensation reactions require a conversion of > 97 % to reach degrees of polymerisation (DPs) of 40. It is therefore important to consider more stable and active catalysts. Tris(dibenzylideneacetonyl)dipalladium [Pd$_2$(dba)$_3$] has been widely used as a more air stable source of palladium-(0) since it was introduced by Ishii *et al.*[60] in conjugation with various ligands such as tri(*ortho*-tolyl)phosphine (P(*o*-tolyl)$_3$) and 2-dicyclohexylphosphino-2',4',6'-triisopropylbiphenyl, more commonly known as XPhos. Recently, You and co-workers demonstrated the profound effect that using two different optimised catalytic systems can have on the resulting polymer.[61] In their work they describe the synthesis of poly[4,8-bis(5-(2-ethylhexyl)thiophen-2-yl)benzo[1,2-b;4,5-b']dithiophene-2,6-diyl-alt-(4-(2-ethylhexyl)-3-fluorothieno[3,4-b]thiophene-)-2-carboxylate-2-6-diyl)] (PTB7-Th) using [Pd(PPh$_3$)$_4$] as a catalyst in one case and Pd$_2$(dba)$_3$: P(*o*-tolyl)$_3$ for the other. They found that the Pd$_2$(dba)$_3$: P(*o*-tolyl)$_3$ system achieved much higher molecular weights (M_n = 22.6 KDa, by GPC) than the [Pd(PPh$_3$)$_4$] system

(M_n = 12.4 kDa, by GPC). The results showed that PTB7-Th synthesised using $Pd_2(dba)_3$: P(o-tolyl)$_3$ gave polymers which performed more than twice as well in devices compared to those synthesised using [Pd(PPh$_3$)$_4$].

Stille polycondensation proceeds under relatively mild conditions and there is no requirement for the addition of base as in Suzuki-Miyaura, as such Stille coupling is tolerant for a much larger range of functional groups than other palladium catalysed cross couplings. Monomer synthesis is often straight forward without the need for protecting groups, moreover generally the monomers are much more stable under ambient conditions. Purification of the bis(trialkylstannyl) monomers can, however, be problematic, their instability on silica means that they often cannot reach the high levels of purity obtained by column chromatography. High monomer purity is vital in maintaining a good stoichiometric balance of reactive functional groups and achieving high molecular weight polymers. A further drawback of the Stille coupling is the production of a stoichiometric amount of trialkyltin halide as a by-product which is very toxic and poses severe environmental issues for industrial scale up. Despite these drawbacks, Stille coupling is still currently the most widely used technique in the synthesis of functional conjugated polymers for OPV devices.

1.4.2: Suzuki Polycondensation

The Suzuki-Miyaura cross coupling, discovered in 1979,[62] is another form of palladium catalysed cross coupling. Suzuki's work on the formation of C-C bonds with palladium catalysed cross coupling reactions earned him the 2010 Nobel Prize with Heck and Negishi. This particular coupling technique uses an arylhalide and an aryl boronic acid (or ester) to form a sp^2 C-C bond between the two aromatic moieties. Similarly, to the Stille coupling the arylhalide (Ar-X) undergoes oxidative addition to a Pd^0 centre which is followed by transmetalation and reductive elimination. Unlike Stille coupling, however, the Suzuki coupling requires the presence of a base to form the [ArPd(OR)] complex as well as the trialkylborate species which takes part in the transmetalation step, finally, the base is believed to accelerate the reductive elimination step.[63]
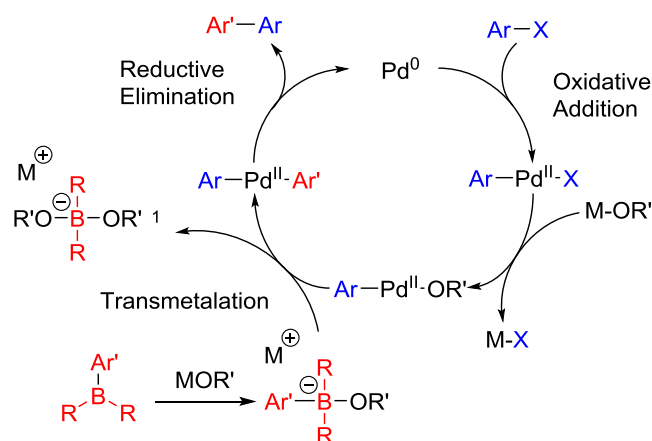
Figure 1.10: Catalytic cycle for the Suzuki coupling of Ar-X with R_2B-Ar', using M-OR' as a base.

Suzuki polycondensation has frequently been used for the synthesis of polyfluorenes[64] over the last two decades for applications in organic electronics such as OPVs, organic light emitting diodes (OLEDs) and field effect transistors (FETs).

Although the Suzuki coupling offers an attractive alternative to Stille coupling, with more benign side products, the requirement of a base makes the Suzuki coupling much less tolerant of a variety of functional groups. While boronic acids might be more reactive, allowing for the use of a gentler base, they become unstable on silica and it becomes challenging to reach the high levels of monomer purity required for step-growth polymerisation.

1.4.4: Direct (Hetero)Arylation Polymerisation.

Efforts to develop a more environmentally friendly and atom efficient synthetic route to conjugated polymers resulted in the first example of direct (hetero)arylation polymerisation (DHAP) in 1999.[65] Using Heck-like conditions, Lemaire and co-workers were able to synthesise poly(3-octylthiophene) with a M_n of 3 kDa and a regioregularity of 90 %.[66] The low molecular weight and lack of selectivity were hurdles, which would need to be overcome if DHAP were to be considered a viable alternative to the more well-established Stille and Suzuki couplings. The progress of DHAP over the last two decades has been the subject of a number of in-depth reviews[67-69] and a greater understanding of the mechanism (Figure 1.11), the role of additives and solvents have led to great improvements in molecular weight and selectivity. As with other palladium coupling reactions the first step is the oxidative addition of the arylhalide to the palladium-(0) centre, after this the most common path way is concerted metalation-deprotonation

(CMD) where a carboxylate deprotonates Ar'-H. The final step is reductive elimination to yield the final product Ar-Ar'.
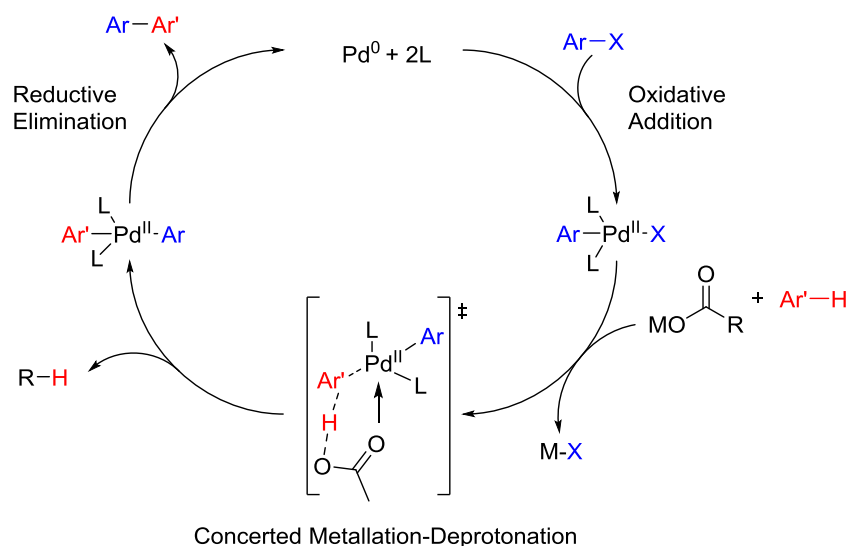
Figure 1.11: Catalytic cycle for DHAP; oxidative addition of arylhalide, followed by concerted metalation-deprotonation utilising a carboxylate, finally reductive elimination to form the final product Ar-Ar' and reform the catalyst.
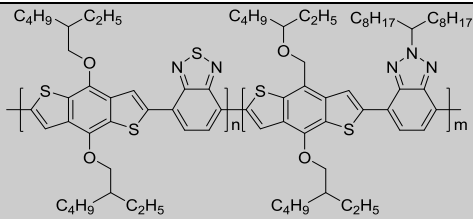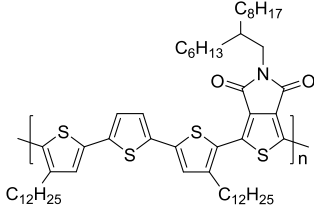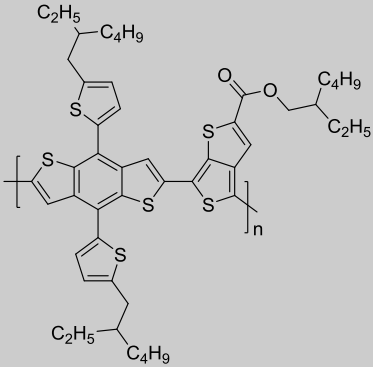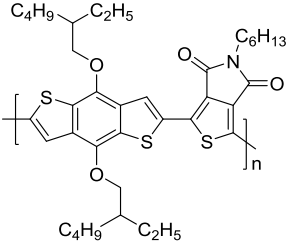
In 2010 Ozawa *et al.* reported P3HT synthesised by DHAP with comparable molecular weights and regioregularities (31 kDa and > 98 %, respectively) to those made by the Grignard metathesis route.[70] Donor-acceptor alternating polymers were later synthesised, the main issues arising from monomers with multiple C-H bonds which can lead to homocoupling, branching and crosslinking.[71] Some efforts have been made to limit the reaction of β-CH groups by adding substituents (so called β-blocking), however, this can lead to excessive torsional strain, a shortened conjugation length and a large band gap.[72]

More recent studies have compared the photovoltaic properties of polymers synthesised by Stille polycondensation with those made by DHAP. Often, due to the higher probability of defects along the backbone, devices that utilise polymers synthesised by DHAP are less efficient than those made by Stille polycondensation (Table 1.1).[73,74] There are, however, some reported cases of polymers made by DHAP out performing those made by Stille polycondensation.[75]

DHAP has progressed significantly in the past decade and is now a useful tool for the synthesis of conjugated polymers which, in some cases, rival those made by the more

traditional Stille polycondensation reaction. Issues with selectivity continue to cause problems and the use of additives may not be compatible with some monomers. Despite this, DHAP is progressing quickly and offers a promising, greener alternative to Stille and Suzuki polycondensations.

Table 1.1: Previous work comparing the PCE of devices created using the same polymer made by Stille polycondensation and DHAP.

Polymer	PCE % Stille	PCE % DAHP	Ref.
	4.88	4.16	72
	7.20	6.86	73
	8.24	8.19	73
	4.65	5.14	74

1.5: Molecular Design of Push-Pull Conjugated Polymers

Whilst it is important to expand the toolbox used for creating semi-conducting polymers, the largest advancements in PCE over the past decade can perhaps be accredited to the meticulous work by many in the field for the design of donor and acceptor monomers and polymers.

When trying to form a material exhibiting a specific band gap, with desirable HOMO and LUMO energy levels and a favourable morphology, there are a number of aspects one has to consider. This is made especially complex by interrelated nature of these properties *i.e.* even slightly altering one may have drastic effects on the next. One can alter the HOMO and LUMO of the polymer by judicious design of core accepting and donating units, which will also influence the band gap. The energy levels may then be adjusted further by the addition of electron donating or withdrawing substituents. The morphology of the polymer backbone, its ability to π-stack and hole transport properties will all be dependent on the factors identified above. Additionally, the polymer must be soluble; alkyl side chains are used to make these materials soluble in common organic solvents and enable to processing at low temperatures. The structure of the side chains will in-turn effect the polymer morphology and can impact the energy levels and band gap of the polymer.

This section of the introduction summarises some of the key moieties used in the area of donor-acceptor polymers for OPVs and highlights recent developments in polymeric semi-conducting materials. The main focuses are on advances made in the development of donor and acceptor core units, the use of substituents to tune energy levels and the implementation of various side chains to achieve good solubility and a favourable morphology.

1.5.1: Electron-Donating Monomers

The role of the donor unit is to influence the HOMO of the polymer as well as influencing the band gap. A deep HOMO (with respect to vacuum level) will lead to a high V_{oc}, however, a HOMO which is too deep will result in a large E_g, leading to a reduction in J_{sc}. Often weak-donors are used, a weak donor encourages intramolecular charge transfer (ICT) with a strong acceptor, allowing for a low E_g whilst maintaining a suitably deep HOMO.

Fused aromatic systems are a popular choice for the donor unit as they not only have favourable electronic properties but are also planar which allows favourable charge transport and an extended conjugation length. Fluorenes (Figure 1.12a) are one species of fused aromatics, which offer a deep lying HOMO owing to the electron deficient benzene rings, making it a very weak donor. Additionally, fluorenes can be functionalised at the 9-position, leading to minimal torsional strain between repeat units, offering an extended conjugation length and increased solubility.
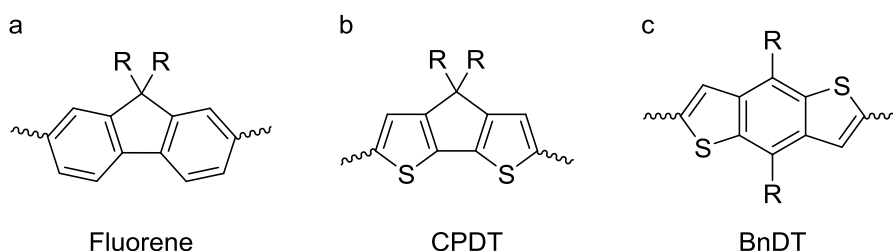
Figure 1.12: Fused aromatic ring donor moieties a; fluorene, b; cyclopentadithiophene (CPDT) and c; benzodithiophene (BnDT).
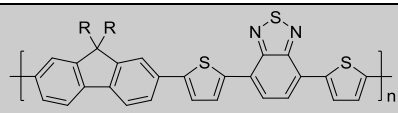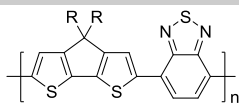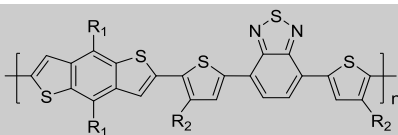
The relative synthetic ease of fluorenes is also attractive in addition to their compatibility with Suzuki coupling, making polymer synthesis more attractive, and avoiding stoichiometric quantities of organostannanes. Deep HOMOs of between -5.5 and -5.7 eV have previously been reported[76-78] giving a V_{oc} of up to 1 V. The concurrent high E_g, however, led to a low J_{sc} and a PCE of < 3 % (Table 1.2). The HOMO of fluorenes can be an issue when considering the materials for use in an OPV device with a PCBM acceptor. The high band gap of fluorene based polymers have, however, recently been utilised for blue organic light emitting diodes (OLEDs).[79]

To overcome the issue of a low J_{sc} resulting from the high E_g a slightly stronger donor is needed with a higher HOMO, this is achieved by making the donating species more electron rich. One such donor is cyclopentadithiophene (CPDT) (Figure 1.12b), the addition of the electron rich flanking thiophenes raises the HOMO of the molecule to -5.3 eV when copolymerised with benzothiadiazol (BT).[80] Brabec *et al.* observed a much higher J_{sc} when using CPDT due to increased solar harvesting, however, a low V_{oc} can limit the PCE.

From these observations a sensible conclusion would suggest that a donor of nature between that of CPDT and fluorene would give a HOMO closer to the optimum value achieving a good balance between V_{oc} and J_{sc}. Replacing the bridging CH_2 of CPDT with

a more electron deficient benzene ring provides one such alternative. Benzodithiophene (BnDT) has been a popular candidate for the electron donating species in donor-acceptor polymers. The fused aromatic system is weakly donating, has a rigid planer structure resulting in higher crystallinity as well as extended conjugation length. Finally, the ability to functionalise the BnDT unit at the 4- and 8-position allows for the addition of solubilising side chains while minimising steric clashing results in reduced torsional strain along the backbone.
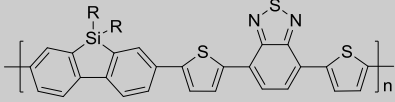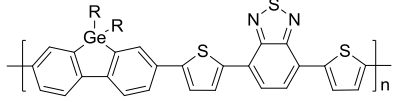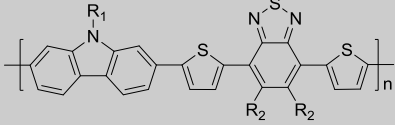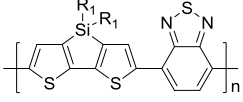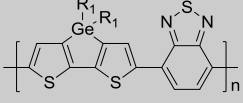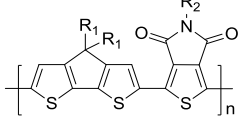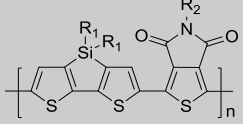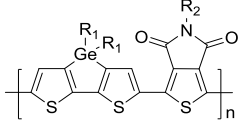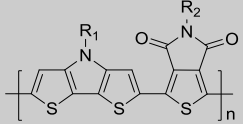
Table 1.2: Copolymers incorporating fluorene, CPDT and BnDT and their photovoltaic properties.

Polymer	HOMO (eV)	E_g (eV)	V_{oc} (V)	J_{sc} (mA/cm²)	PCE (%)	Ref
	-5.7	1.9	1.04	4.66	2.2	76
	-5.3	1.4	0.62	16.2	5.5	80
	-5.4	1.7	0.87	10.03	5.0	81

The copolymer of BnDT and dithienobenzodithiophene (DTBT) does indeed give a moderate HOMO of -5.4 eV and an E_g of 1.7 eV between that of fluorene and CPDT based D-A polymers.[81] While, in this case, the PCE is slightly lower than that of CPDT based copolymers, later modifications of the side chains and additional substituents make BnDT one of the most effective donor choices.

Another well-explored avenue for altering the properties of the donor units is the introduction of additional heteroatoms, such as nitrogen, silicon and germanium, into the fused cycles, which are summarised in Table 1.3.

Table 1.3: Photovoltaic properties of donor polymers containining various heteroatoms.

Polymer	HOMO (eV)	E_g (eV)	V_{oc} (V)	J_{sc} (mA/cm²)	PCE (%)	Ref
	-5.4	1.8	0.90	9.5	5.4	83
	5.6	1.8	0.79	6.9	2.8	84
	-5.5	1.9	0.88	10.6	6.1	86
	-5.3	1.4	0.57	17.3	5.9	88
	-	-	0.56	18.64	4.56	89
	-5.4	1.7	0.80	10.0	3.74	90
	-5.7	1.7	0.89	11.5	6.6	91
	-5.6	1.7	0.85	12.6	7.30	91
	-5.1	1.6	0.66	4.98	1.65	92

A popular route of investigation is to replace the sp³ bridging carbon in fluorenes and CPDTs with other group four elements (Table 1.3). The HOMOs of the resulting fluorene based polymers are slightly higher, perhaps owing to the slightly more diffuse nature of the frontier orbitals of Si and Ge.[82-84] The main contributor to the increased efficiency of the Si and Ge based polymers is the enhanced J_{sc}, which is a result of

improved morphology of the blends. Longer Si-C and Ge-C bonds reduce steric clashing and torsional strain along the back bone resulting in solution phase aggregation, better solid state stacking and more efficient charge extraction.[85] Heeger *et al.* also replaced the carbon bridge in fluorene with the more electron donating nitrogen to make a carbazole derivative with the aim of increasing the donor ability. They found that the resulting polymer had a higher HOMO of -5.5 eV and a similar band gap of 1.9 eV to the fluorene conjugate.[86] The carbazole polymer demonstrated much higher J_{sc}, a result of its excellent charge transport properties as demonstrated previously.[87]

In contrast to fluorine, varying the bridging atom in CPDT from carbon to Si or Ge has little effect on the HOMO and V_{oc} due to the presence of the electron donating thiophene units. In Si/Ge-PCPDTBT copolymers a large increase in the J_{sc} results in an increase in PCE. The enhancement in J_{sc} is expected to be a result of better charge transport enhanced by more favourable interchain interactions of the Si and Ge equivalents.[88,89] Copolymers of CPDT derivatives with thienopyrroledione (TPD) have also been widely investigated, showing a similar trend to the PCPDTBT polymers discussed previously, and increasing PCE from 3.74 % to 5.30 % to 7.30 % as the bridging atom is changed from carbon to silicon to germanium, respectively.[90,91] Replacing the bridging atom with an electron donating nitrogen atom in CPDT results in a significantly higher HOMO (-5.1 eV) resulting in a device with a low V_{oc} and low PCE of 1.65%.[92]

An ideal donor will have a sufficiently low lying HOMO (around -5.4 eV) to promote a high V_{oc}, whilst remaining high enough to minimise the band gap and optimise J_{sc}. Fused cycles demonstrate strong aggregation and favourable morphologies promoting good charge transport and higher J_{sc}.

1.5.2: Electron Accepting Monomers
The role of the electron accepting unit is primarily to maximise ICT by having a high electron affinity as well as offering some control over the LUMO position of the donor polymer. As BnDT has shown great potential and is a very popular choice for the electron donating species in donor-acceptor polymers, all the electron accepting moieties reviewed in this section will be used in conjunction with alkyl or alkoxy substituted BnDT when comparing devices, the effects of varying side chains will be discussed in Section 1.5.3.

Thieno[3,4-*b*]thiophene (TT) has been a popular choice for an acceptor unit since it was first reported in 1997[93] due to its stable quinodal form. Many polymers which utilise TT as an electron accepting species exhibit low band gaps resulting from their high HOMO when copolymerised with BnDT (Table 1.1).[94] The addition of further substituents and side chain modification (Sections 1.5.3 and 1.5.4) yielded the well documented high performance polymers PTB7[40] and PTB7-Th.[95]

Benzo[1,2,3]triazol BTz (Figure 1.13) is a prevalent choice for solution processable materials, the ability to functionalise with an alkyl chain at the 2-position on the nitrogen allows for increased solubility, and further substituents can be added to the 5 and 6-positions on the benzene ring to increase solubility or modify the electronic properties of the polymer (Section 1.5.4). The ability of the nitrogen to donate its lone pair into the aromatic system, however, makes BTz a weaker acceptor than others reviewed in this section, its resulting copolymers (PBnDTBTz)[96] shown in Table 1.4 have high band gaps and lower J_{sc} and PCEs.[97,98]

TT   BTz   BT   TPD
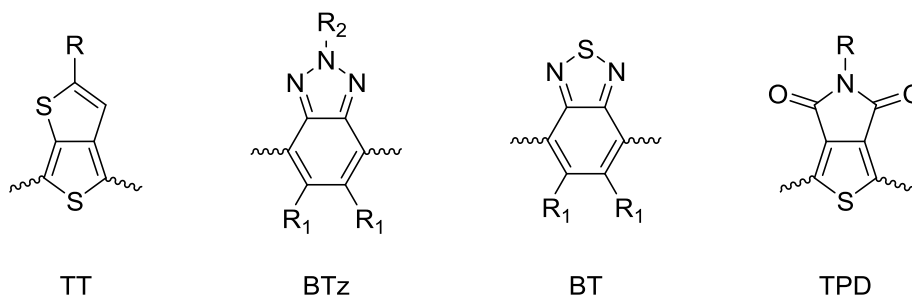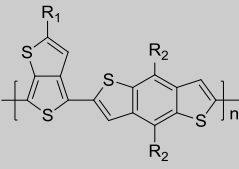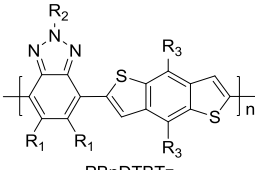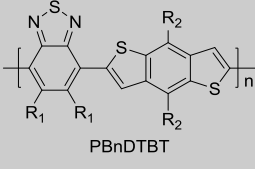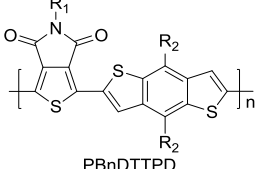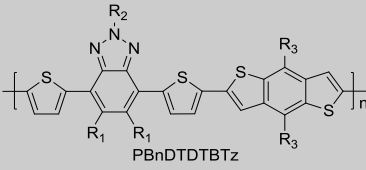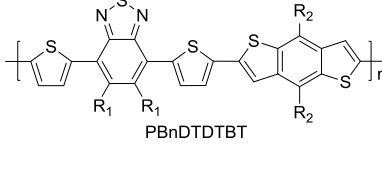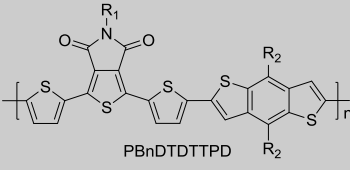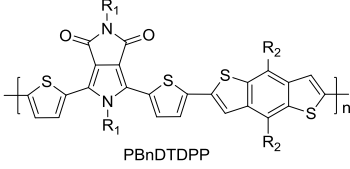
Figure 1.13: Chemical structures of commonly used acceptor units.

A structurally similar acceptor to BTz is 2,1,3-benzothiadiazole (BT), the sulphur lone pair is less basic than that of nitrogen and therefore this electron density is donated into the aromatic system to a lesser extent, making BT a stronger acceptor. Although it has one less position for alkyl functionalisation BT has been shown to give planer backbones and more crystalline films in the copolymer PBnDTBT (Table 1.4).[99] Thieno[3,4-*c*]pyrrole-4,6-dione (TPD) incorporates electron withdrawing amide groups, which makes it a strong planer acceptor unit with a deep HOMO. When copolymerised with BnDT (PBnDTTPD) it gave a high V_{oc} of 1.0 V but demonstrated low PCEs due to a large band gap of 1.9 eV and concurrent low J_{sc}.[100]

Table 1.4: Photovoltaic properties of BnDT copolymerised with various electron accepting units.

Polymer	HOMO (eV)	E_g (eV)	V_{oc} (V)	J_{sc} (mA/cm^2)	PCE (%)	Ref
PBnDTTT	-5.0	1.6	072	13.9	5.85	94
PBnDTBTz	-5.0	2.0	0.61	4.8	1.4	96
PBnDTBT	-4.9	1.7	0.73	8.93	2.99	99
PBnDTTPD	-5.7	1.9	1.0	2.0	0.8	100
PBnDTDTBTz	-5.1	2.0	0.61	4.5	1.7	103
PBnDTDTBT	-5.4	1.7	0.87	10.03	5.0	104
PBnDTDTTPD	-5.6	1.9	0.89	7.6	3.9	23
PBnDTDPP	-5.2	1.5	0.71	9.4	4.1	23

It has become increasingly popular to synthesise alternating copolymers with thiophene flanked acceptor units (Figure 1.14). The thiophene spacer reduces steric clashing between the donor and acceptor units and their solubilising side chains,[101] resulting in a more planer backbone, extended conjugation length and a reduced band gap. The thiophene units are also thought to help aid hole transport and improve the J_{sc} of devices.[102]

The polymers of DTBTz, DTBT and DTTPD (PBnDTDTBTz,[103] PBnDTDTBT[81] and PBnDTDTTPD[104] respectively) shown in Table 1.4 all exhibit lower lying HOMOs than their non thiophene flanked relatives (PBnDTBTz, PBnDTBT and PBnDTTPD respectively). In particular, the HOMO of PBnDTDTBT is close to the "ideal HOMO level"[105] and the polymer exhibits a good V_{oc} of 0.87 V with moderated J_{sc} of 10.03 mA/cm^2, this is indeed a promising candidate for photovoltaic devices.

A final acceptor worth noting is pyrrole[3,4-c]pyrrole-1,4-dione (DPP, Figure 1.14), which has demonstrated high carrier mobilities in field effect transistors (FETs)[106] and its polymers result in a low band gap and wider absorption profile. The high lying HOMO of the DPP based polymers (possibly a result of the flanking thiophenes) limits the V_{oc} to some extent, nonetheless PBnDTDPP achieved respectable PCEs of 4.1%.[30]
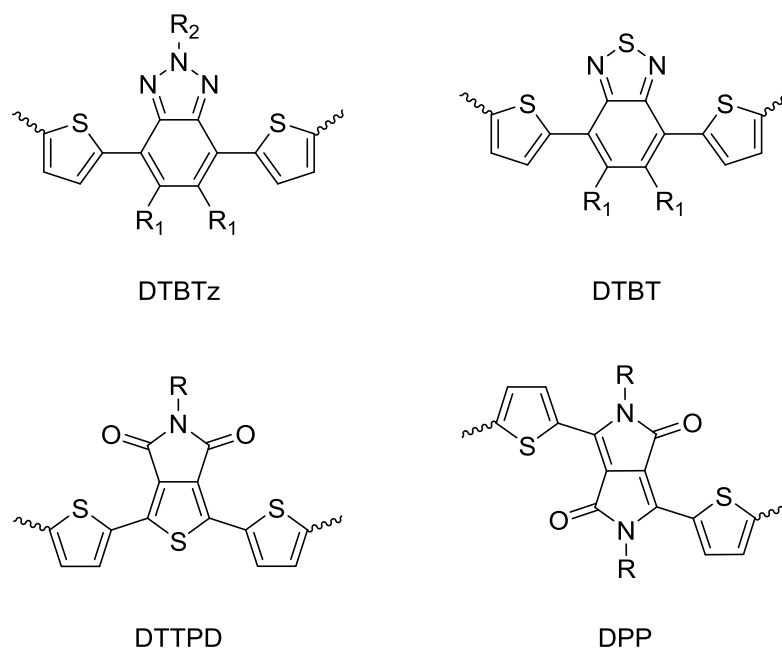
Figure 1.14: Chemical structures of thiophene flanked acceptor units.

In summary, ideal acceptor units should be strongly electron accepting (to promote a lower E_g), additional room for solubilising side chains and substituents for the modification of energy levels is also desirable. The acceptor units should maintain the low HOMO of the polymer and allow for a high V_{oc}. Flanking thiophene units can be used to decrease steric clashing and increase polymer conjugation length to result in a reduced E_g.

1.5.3: Side Chain Engineering

The primary function of the side chains in conjugated polymers is to increase the solubility of the rigid π-backbone polymers. Without these solubilising side chains interchain interactions would be so great that the polymers would be insoluble and unprocessable in common solvents. In addition to solubility, side chains can be used to finely tune the electronic properties of the polymer by the addition of electron withdrawing/donating side chains or by extending conjugation. Side chains have been shown to not only influence the solubility and electronic properties of the polymers, but they can also play a significant role in directing the film morphology, effecting charge transport and device efficiency. In this section of the introduction, we discuss each of the aspects of conjugated polymer side chains outlined above.

Throughout this introduction, we have discussed the need to minimise torsional strain along the polymer backbone and increase the conjugation length to help maintain a low E_g. With this in mind, one must judiciously consider where the solubilising side chains are placed along the polymer backbone. Li *et al.* showed that the hole mobility of polymer films could be significantly influenced by the positioning of side chains in PDTTPD-TT polymers (Figure 1.15). Adding the side chains in the 3- and 4-position of the thienopyrroledione flanking thiophenes leads to large amounts of steric clashing with the TPD unit and its bulky branched alkyl side chain. As a result, there is increased torsional strain along the backbone and greater π-stacking distances are observed hindering both intra- and inter-chain hole mobilities. Placing the alkyl chains on the TT unit, far away from the TPD, however, yields much higher hole mobilities resulting from the greater inter-chain pi-stacking and reduced torsional disorder.[107]
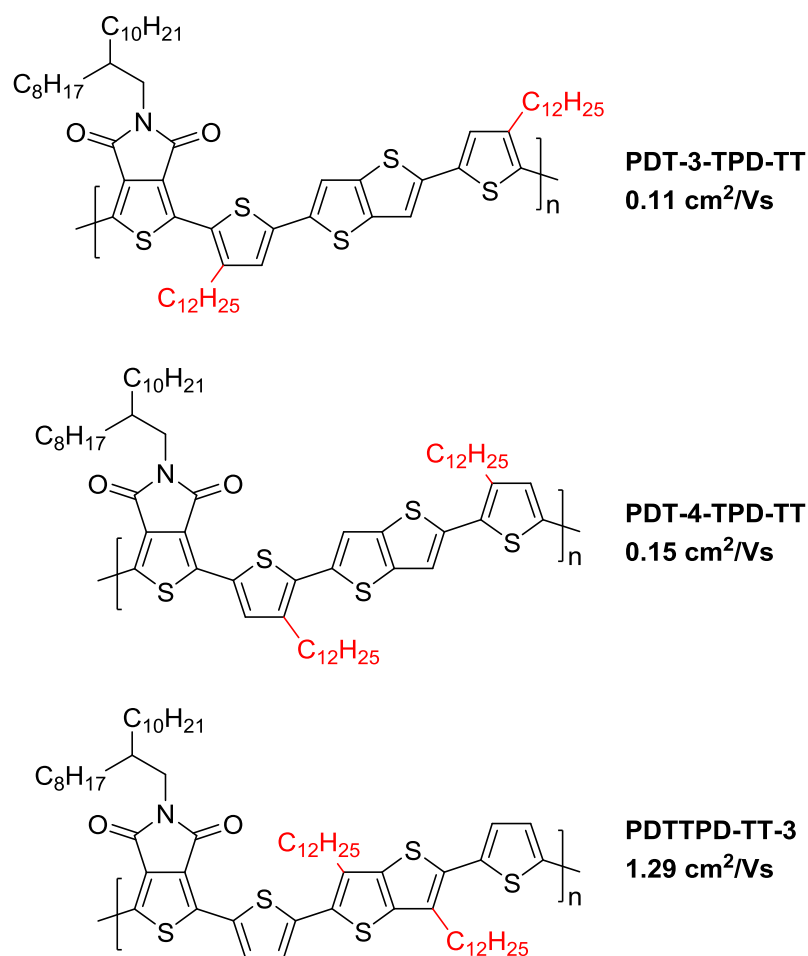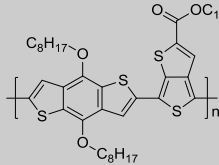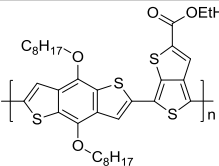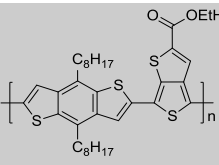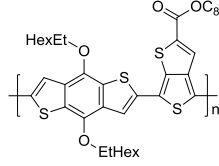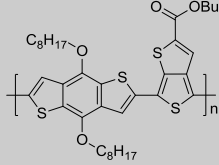
Figure 1.15: PDTTPD-TT polymers alkylated in various positions, hole mobilities are indicated under the polymers abbreviation. [107]

While increased steric clashing can reduce inter-chain interactions by unfavourable amounts, reducing charge transport properties, the introduction of branched alkyl side chains can introduce enough inter-chain separation to offer good solubility whilst maintaining adequate hole transport for FET devices.[108-110]

The series of PTB polymers summarised in Table 1.5 are a good example of how branched alkyl side chains can effect hole mobility and PCE.[111] PTB1 with linear alky chains on both the BnDT and TT unit has a moderate hole mobility of 4.7×10^{-4} cm^2/Vs resulting in a respectable PCE of 4.76 %. Replacing the long dodecyl chain on the TT unit with the branched 2-ethylhexyl yields PTB2 with similar hole mobilities (4.0×10^{-4} cm^2/Vs) and a slightly enhanced PCE of 5.10 %. PTB3 has the highest hole mobility (7.1×10^{-4} cm^2/Vs) of the five polymers, replacing the octyoxy side chains of the BnDT unit with *n*-octyl, which also result in a lower HOMO of -5.0 eV, giving the highest PCE of

5.53 %. Addition of two 2-ethylhexyl groups to the BnDT unit (PTB5) gives similar hole mobilities to PTB2 of 4 x 10^{-4} cm^2/Vs, however, a reduced J_{sc} of 10.3 mA/cm^2 and PCE of 3.02 % is observed, which is assigned to a less than optimal BHJ morphology. PTB6 is comprised of octyoxy bearing BnDT units and a 2-butyloctyl bearing TT unit, the addition of this large bulky chain interrupts π-stacking, resulting in the lowest observed hole mobility of 2.6 x 10^{-4} cm^2/Vs and a low PCE of only 2.26 %.

Table 1.5: Polymer structures and photovoltaic properties of PTB1, PTB2, PTB5 and PTB6, where EtHex is 2-ethyheyl and BuOct is 2-butyloctyl.

Polymer	HOMO (eV)	E_g (eV)	V_{oc} (V)	J_{sc} (mA/cm²)	PCE (%)	Ref
PTB1	-4.9	1.6	0.58	12.5	4.76	111
PTB2	-4.9	1.6	0.60	12.8	5.10	111
PTB3	-5.0	1.6	0.74	13.1	5.53	111
PTB5	-5.0	1.6	0.68	10.3	3.02	111
PTB6	-5.0	1.6	0.62	7.74	2.26	111

When utilising the solubilising nature of branched side chains one must consider not only the length but also the branching point. For example Pei *et al.*[112] demonstrated that moving the branching point further away from the conjugated back bone of a dithenoisoindigo polymer (PIIDDT, Figure 1.16) lead to better π-stacking and increased

hole mobilities in PIIDDT-C3 and PIIDDT-C4 (Table 1.6). Similarly Bronstein *et al.* reported improved crystallinity and charge transport of indolonaphthyridine polymers when sidechains branched at C3 rather than C1.[113]
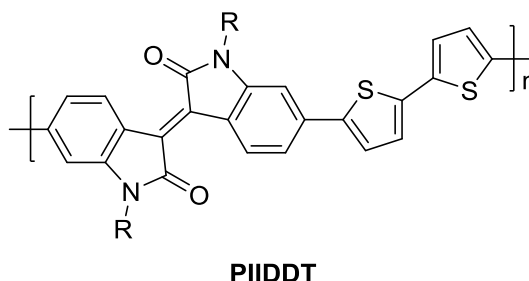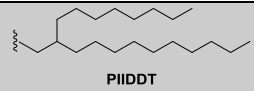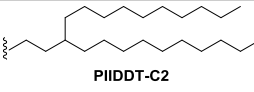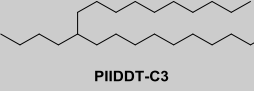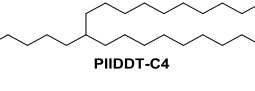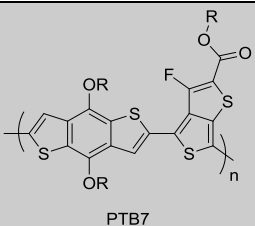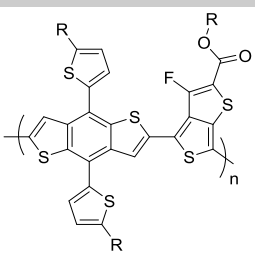
Figure 1.16: Chemical structure of polydithienoisoindigo.

Table 1.6: Effect of branching point of side chains in PIIDDT on π-π stacking distances and hole mobility.

Side Chain (R)	π-π Stacking distance (Å)	HOMO (eV)	E_g (eV)	Hole Mobility μ (cm²/Vs)	Ref
PIIDDT	3.8	-5.7	2/00	1.06	112
PIIDDT-C2	3.6	-5.6	1.90	0.40	112
PIIDDT-C3	3.6	-5.5	1.78	3.62	112
PIIDDT-C4	3.6	-5.5	1.76	1.76	112

One last aspect of conjugated polymer side chains that must be discussed is the introduction of conjugated side chains, such as alkyl substituted thiophenes, this modification produces what are commonly known as two dimensional conjugated polymers. Extending conjugation to the side chains can influence the band gap as well as leading to stronger intermolecular π-stacking resulting in improved hole mobilities, J_{sc} and PCEs as demonstrated by BTB7[40] and PTB7-Th[114] in Table 1.7.
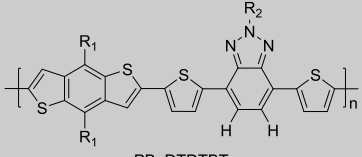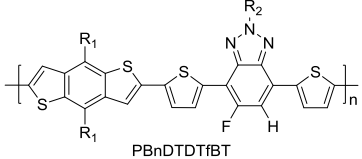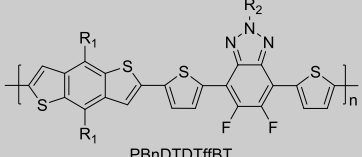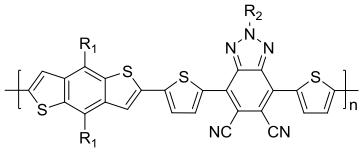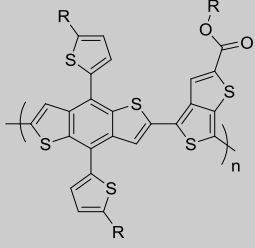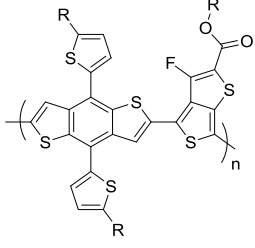
Table 1.7: Structure and photovoltaic properties of PTB7 and PTB7-Th.

Polymer	HOMO (eV)	E_g (eV)	V_{oc} (V)	J_{sc} (mA/cm²)	PCE (%)	Ref
PTB7	-5.2	1.6	0.74	14.5	7.4	40
PTB7-Th	-5.2	1.6	0.78	16.86	9.00	114

1.5.4: Substituents

One method of maximising the V_{oc}, with the aim of achieving high PCEs is to lower the HOMO level of a conjugated polymer by introducing electron-withdrawing substituents into the backbone, usually on an electron accepting unit such thienothiophene or benzotriazole. Another advantage arises from adding electron withdrawing substituents to the already electron deficient accepting unit, the increased electron deficiency favours a strong inter-molecular π-stacking interaction with electron donating units.[115] This leads to a more crystalline morphology and often higher J_{sc}. Perhaps two of the most seminal demonstrations of the power of electron withdrawing groups are; the work of You and co-workers on fluorine and cyano substituted benzotriazoles[116,117] and the work of Hou *et al.* in the development of the famous high performance PTB7-Th polymer summarised in Table 1.8.[114,118]

Table 1.8: Photovoltaic properties of polymers containing F and CN substituents in the backbone.

Polymer	HOMO (eV)	E_g (eV)	V_{oc} (V)	J_{sc} (mA/cm²)	PCE (%)	Ref
PBnDTDTBT	-5.4	1.7	0.81	10.1	3.14	116
PBnDTDTfBT	-5.5	1.7	0.85	11.4	4.91	116
PBnDTDTffBT	-5.5	1.7	0.91	12.7	6.51	116
PBnDTDT(CN)BT	-5.7	1.8	0.96	14.07	8.37	117
PDTTT-E-T	-5.1	1.6	0.68	14.59	6.21	114
PTB7-Th	-5.2	1.6	0.78	16.86	9.00	118

In the work of You the sequential addition of fluorine to the benzotriazol units leads to a lower HOMO and greater V_{oc} and PCE in the order of PBnDTDTBT < PBnDTDTfBT < PBnDTDTffBT. There is also an increasing trend in the J_{sc} for these polymers which is assigned to the more morphological changes in the BHJ affected by increasing fluorination. Addition of the more electron withdrawing CN groups to DTBT gives an exceptionally low HOMO of -5.73 V and, while the band gap increases slightly, it still allows for good solar harvesting, this combined with the improved morphology induced by the electron withdrawing CN groups yields devices with notable PCEs of over 8 %. Similar observations were made by Hou and co-workers, the fluorination of the TT unit in PBDTTT-E-T to yield PTB7-Th led to a lower HOMO, higher V_{oc} and improved J_{sc} culminating in impressive PCEs of over 9 %.[118]

This section of the review has provided a brief summary of many of the factors one has to consider when designing conjugated donor-acceptor polymers for photovoltaic applications. Great care must be taken to achieve a suitably low lying HOMO, which can be tuned by both careful donor and acceptor coupling and the introduction of side chains and electron withdrawing substituents. Perhaps one of the best case studies is that of the PTB family, which has evolved from a simple copolymer of BnDT and TT to incorporate branched and conjugated side chains as well as introducing electron withdrawing substituents, culminating in one of the highest performing and most famous polymers of its field.[118]

1.6: Varying Architecture of Conjugated Polymers

The previous section of this introduction focused on the development of various donor and acceptor units and their resulting polymers over the last decade. As the development of new donor and acceptor units slows and PCEs begin to reach a plateau, an emerging point of enquiry is the sequence of donor and acceptor units along the polymer backbone. Whilst synthetically simple, alternating donor-acceptor polymers may not be the most effective way to combine monomers and develop materials for use in OPVs. This section of the introduction focuses on the limited number of investigations into the effect of backbone composition and sequence on the optoelectronic and physical properties of this class of material.

One of the first comprehensive studies into varying the backbone composition (donor to acceptor ratio) was by Brabec *et al.*[119] Brabec found that an imbalance in the D:A ratio

could lead to broader spectral absorbance and devices with competitive efficiencies. In 2010, Wei and co-workers investigated how the introduction of randomness along the backbone affected BnDT donor and CPDT acceptor based copolymers and found that their semi-random polymers outperformed their alternating counterparts.[120] Chen showed that varying D:A from the traditional 1:1 could lead to more efficient devices in 2013, however, their best device efficiencies were low still when compared with the contemporaries.[121]

Later in 2013 Kim *et al.* demonstrated one of the first donor-acceptor polymers to utilise multiple species of donor distributed in a semi-random fashion along the polymer backbone. They used an AA, BB and B'B' type system (Figure 1.17) to achieve a series of semi-random terpolymers with varying HOMOs and E_g (Table 1.9).[122]

P1 : PBnDTT-DPP100
P2 : PBnDTT-DPP90-TPD10
P3 : PBnDTT-DPP75-TPD25
P4 : PBnDTT-DPP50-TPD50
P5 : PBnDTT-DPP25-TPD75
P6 : PBnDTT-DPP10-TPD90
P7 : PBnDTT-TPD100
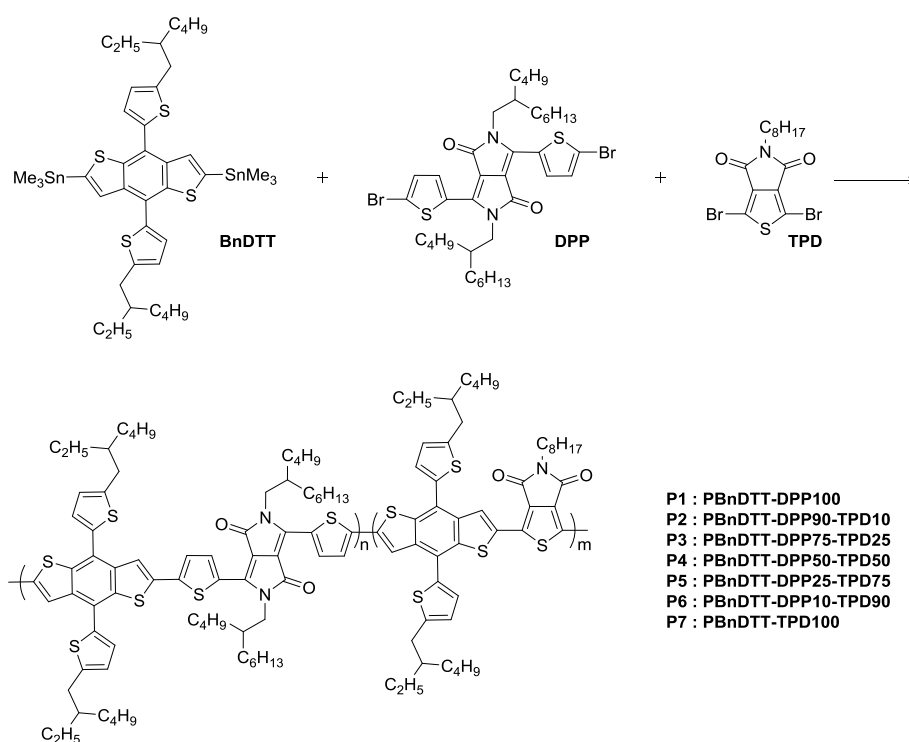
Figure 1.17: Reaction scheme for the synthesis of; alternating poly[thienyl-substituted benzo[1,2-b:4,5-b']dithiophene-pyrrolo[3,4-c]pyrrole (P1), semi-random poly[thienyl-substituted benzo[1,2-b:4,5-b']dithiophene-pyrrolo[3,4-c]pyrrole-1,4- dione-thieno[3,4-c]pyrrole-4,6-dione]copolymers (P2-P6) and poly[thienyl-substituted benzo[1,2-b:4,5-b']dithiophene-1,4-dione-thieno[3,4-c]pyrrole-4,6-dione] (P7).[122]

As the more electron deficient DPP was replaced with the weaker acceptor TPD, the HOMO of the polymer dropped and the E_g increased resulting in an expected increase in V_{oc}. The PCE of the devices, however, did not form a linear correlation with polymer composition. Kim found that P3 performed best, closely followed by P4 due to their

broad spectral absorption and subsequent high J_{sc}. P7 interestingly showed a relatively high J_{sc} of 9.25 mA/cm^2 despite its large E_g of 0.97 V and an agreeable PCE of 5.10 %. It was hypothesised, after computational experiments, that P5 and P6 exhibit poor ICT as the DPP rich regions act as trap sites, and combination with more favourable blend morphology of P7 (with PCBM) accounted for the higher J_{sc} and PCE observed in the non-DPP baring P7 chain.

Table 1.9: Photovoltaic properties of polymers P1-P7.[122]

Polymer	n:m	HOMO (eV)	E_g (eV)	V_{oc} (V)	J_{sc} (mA/cm^2)	PCE (%)
P1	100:0	-5.3	1.4	0.73	12.20	5.03
P2	90:10	-5.3	1.4	0.74	10.95	4.91
P3	75:25	-5.4	1.4	0.74	13.99	5.61
P4	50:50	-5.4	1.4	0.76	12.95	5.26
P5	25:75	-5.5	1.5	0.79	7.61	3.02
P6	10:90	-5.5	1.6	0.82	6.09	2.09
P7	0:100	-5.5	1.9	0.97	9.25	5.10

Similarly to the system above, isoindigo and DPP were used as the two accepting units when copolymerised with thiophene in an AA, BB, B'B' type polymerisation, to yield a variety of copolymers P8-P12 (Figure 1.18). Polymers with increasing DPP content were reported to have lower E_g (as previously) owing to DPP's strong electron withdrawing nature, however, perhaps the most interesting parallel to Kim's work is the non-linear relationship between polymer composition and, J_{sc} and PCE (Table 1.10). Whilst the homopolymers P8 and P9 exhibited mediocre PCEs of 3.43 % and 4.56 % respectively, P11 (a statistical distribution of isoindigo and DPP along the backbone) showed a high PCE of 6.04 % and had a greater J_{sc} than P9 despite its greater E_g. The hole mobility of each of the polymers was calculated using the space charge limit current (SCLC) model, the random polymers P10, P11 and P12 had mobilities of 0.046, 0.102 and 0.023 cm^2/Vs which were all higher than the homopolymers P8 and P9 (0.023 and 0.009 respectively). Grazing incidence wide angle X-Ray scattering (GIWAXS) of P11 (which exhibited the highest mobilities) showed the polymers preference for a face-on orientation with respect to the electrode. The face-on orientation is thought to enhance charge transport in the

vertical direction, helping to limit charge recombination and maximise J_{sc}, perhaps explaining why P11 has a greater J_{sc} than P9 despite is larger E_g.
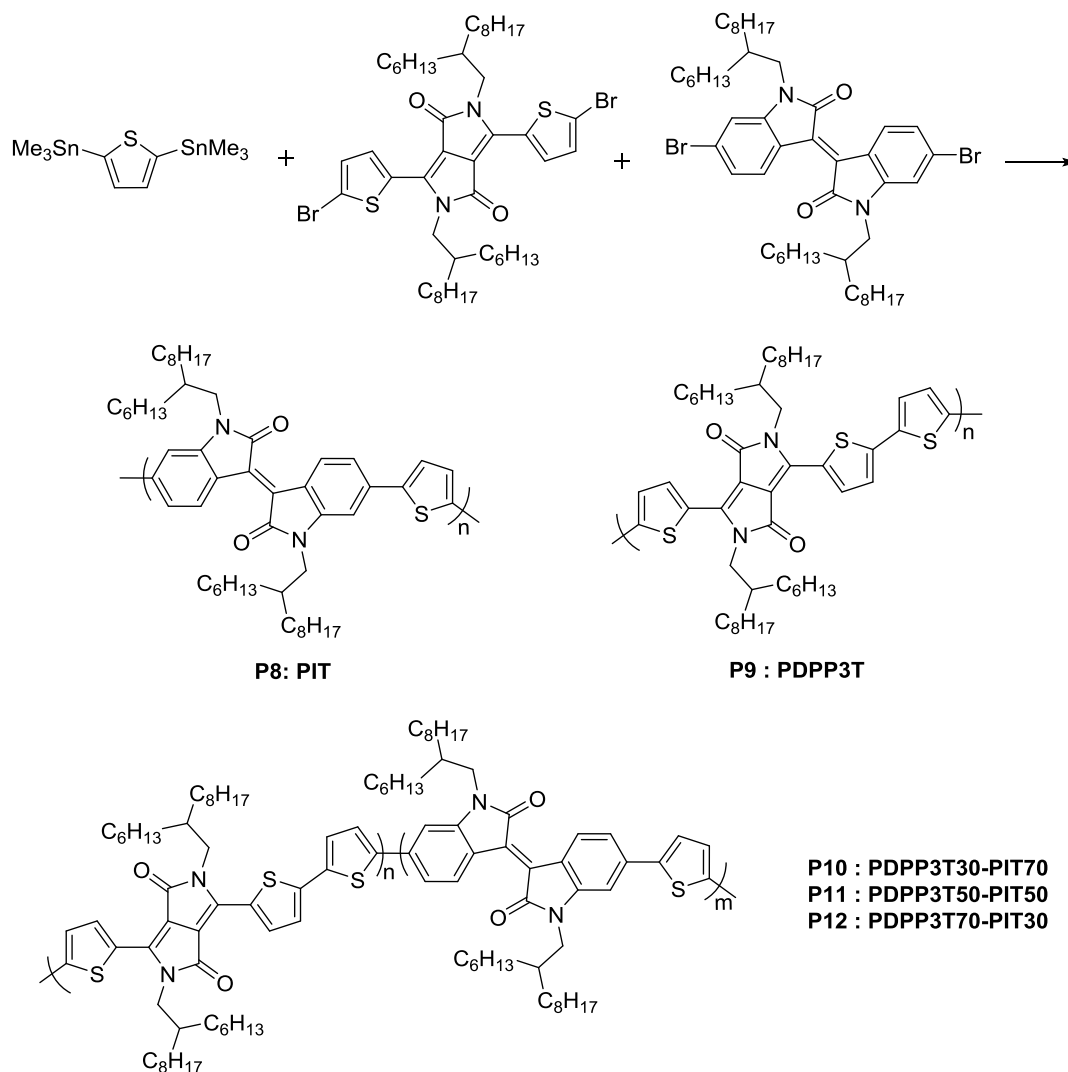
Figure 1.18: Chemical structure of; P8 polyisoindigo-alt-thiophene, P9 PDPP3T, and P10-12 PIT-*stat*-DPP3T.

Table 1.10: Photovoltaic properties of polymers P8-P12.[123]

Polymer	n:m	HOMO (eV)	E_g (eV)	V_{oc} (V)	J_{sc} (mA/cm^2)	PCE (%)
P8	100:0	-5.7	1.6	0.81	7.06	3.43
P10	30:70	-5.5	1.5	0.78	7.84	3.49
P11	50:50	-5.6	1.4	0.77	13.52	6.04
P12	70:30	-5.6	1.4	0.69	12.35	4.86
P9	0:100	-5.4	1.4	0.63	11.67	4.56

Another method of constructing a random conjugated polymer is to use both a di-bromine and di-stannyl functionalised (diborinic ester in the case of Suzuki coupling) donor or acceptor, as demonstrated by Kim and co-workers (Figure 1.19).[124] In this way, one can investigate the sequence of two monomers without having to introduce a second donor, acceptor or bridging unit. Kim also demonstrated that a donor to acceptor ratio of 1:1 was not ideal. Density functional theory (DFT) calculations indicated that DPP-DPP couplings could lead to trap sites and decrease J_{sc}. This is reflected in the experimental results of more DPP rich polymers P15-P17 (Table 1.11). Whilst DPP-DPP coupling was absent in the alternating polymer P18 it suffered from a lower spectral absorbance compared to some of its random counterparts and as such the J_{sc} was not as high as the statistical polymers P13 and P14.

Table 1.11: Photovoltaic properties of random polymers P13-P17 and alternating polymer P18 reported by Kim et al..[124]

Polymer	BnDT:DPP	HOMO (eV)	E_g (eV)	V_{oc} (eV)	J_{sc} (mA/cm^2)	PCE (%)
P13	4:1	-5.4	1.5	0.75	15.06	5.04
P14	2:1	-5.4	1.6	0.74	14.84	5.63
P15	1:1	-5.3	1.3	0.71	6.41	2.42
P16	1:2	-5.3	1.3	0.70	5.10	1.64
P17	1:4	-5.3	1.2	0.68	2.98	0.79
P18	1:1 (alt)	-5.3	1.4	0.73	12.20	5.03

Despite these observations not all random copolymers outperform alternating copolymers. Ong and co-workers demonstrated that alternating PDTBTff-TT had vastly superior J_{sc} and PCE when compared to its random counterpart (Table 1.12).[125] Random copolymers were achieved by using a distannylated thiophene bridge (Figure 1.20) and demonstrated inferior hole mobilities (0.030 cm^2/Vs) compared to the alternating copolymer (0.061 cm^2/Vs). Optical absorption studies in solution and of films showed the alternating polymer to have a higher vibronic character, which is indicative of a greater degree of π-stacking and suggest a more defined film morphology or higher crystallinity. The two polymers P19 and P20 perform very similarly except for their J_{sc}, a result of the

morphology mentioned above, but also possibly due to trap sites of acceptor rich regions of the polymer backbone as previously mentioned by Kim *et al.*[122,124]
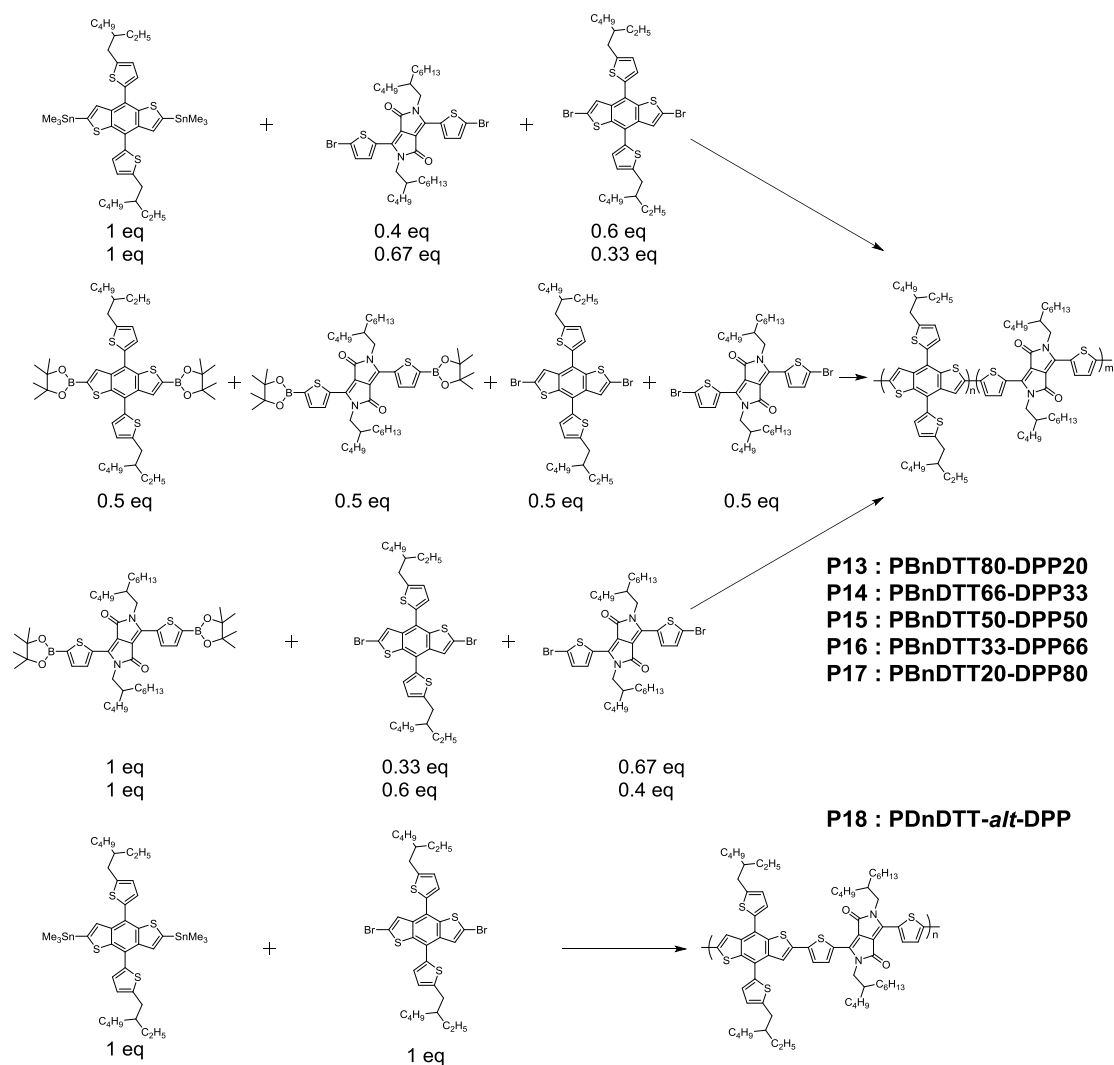
Figure 1.19: Use of both di-brominated and di-stannylated/di-boronic ester donor and acceptor monomers to introduce disorder along the backbone by Kim *et al.*[124]
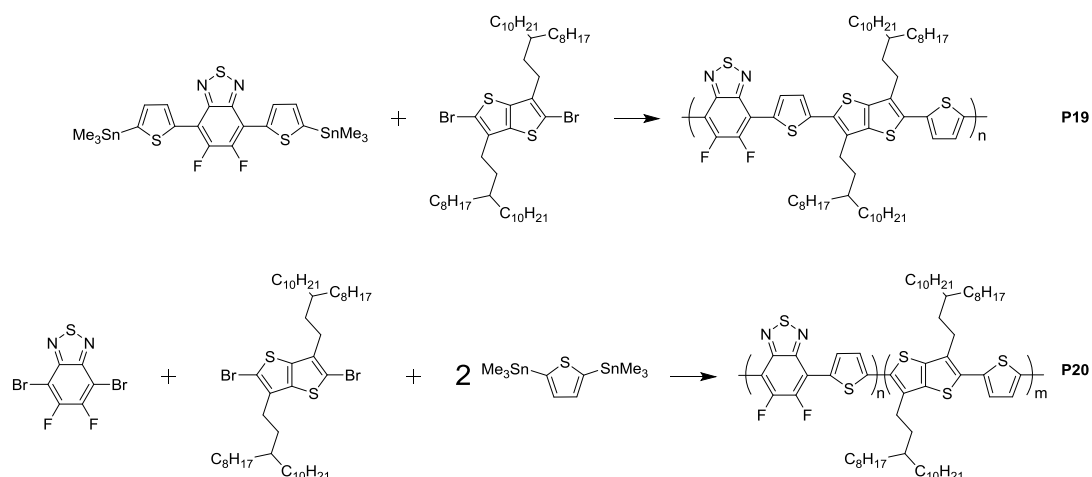
Figure 1.20: Monomers used for the synthesis of polymer P19 and P20.[126]

Table 1.12: Photovoltaic properties of P19 and P20.[125]

Polymer	M_n	HOMO	E_g	V_{oc}	J_{sc}	PCE
	(KDa)	(eV)	(eV)	(eV)	(mA/cm²)	(%)
P19	16.5	-5.4	1.7	0.79	9.68	4.96
P20	14.6	-5.4	1.7	0.78	14.56	7.57

As previously mentioned at the end of Section 1.5, PTB7 and related polymers have been subject to in-depth investigation since their development, the order of the backbone and degree of randomness is no exception. In 2016 Huang and co-workers introduced an electron rich bithiophene unit (TT) into the PTB7 to produce the random copolymer PTB7-Thh-TT (P22).[126] After device optimisation and introduction of an amino-substituted perylene diimide hole blocking interlayer they found that the random copolymer P22 outperformed the regioregular PTB7 (P21). Despite having a marginally lower J_{sc} and V_{oc} than P21, P22 has a greater PCE owing to its increased fill factor (FF P21 = 62.71, FF P22 = 67.38) and its superior hole mobility (P21 = 1.67 x 10^{-4} cm²/Vs, P22 = 2.49 x 10^{-4} cm²/V).
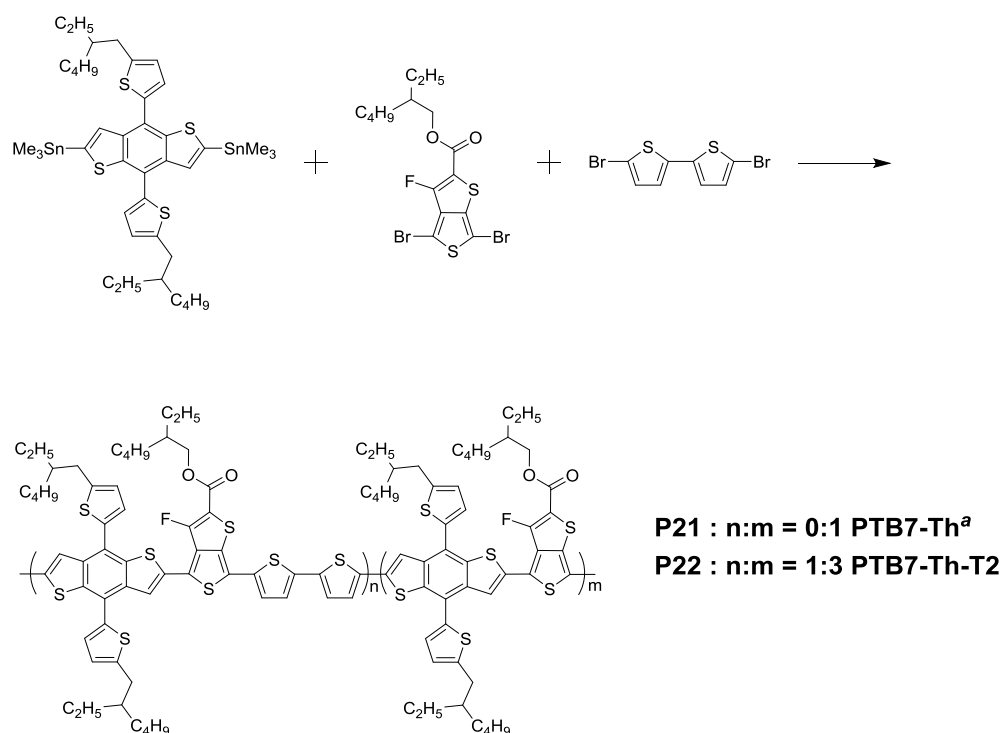
Figure 1.21: Synthesis and structure of polymers P21 and P22.[126]

While this study showed that PTB7 based random polymers could perform well, it is hard to draw a direct comparison between the two polymers as they differ not just in their sequence, but also in their constituents.

Table 1.13: Photovoltaic properties of P21 and P22.[126]

Polymer	M_n (KDa)	HOMO (eV)	E_g (eV)	V_{oc} (eV)	J_{sc} (mA/cm^2)	PCE (%)
P21	59	-5.3	1.6	0.80	15.70	7.89
P22	45	-5.3	1.6	0.79	15.40	8.19

A later study by Kim and co-workers investigated varying the composition of PTB7-Th altering the donor acceptor ratio from 3:1 to 5:1 and finally 7:1 for polymers P24, P25 and P26 respectively (Figure 1.22). The lower lying HOMO of the electron rich polymers lead to an enhanced V_{oc} but the resulting increase in E_g lead to a reduction in J_{sc} and ultimately PCE for PCBM based devices (Table 1.14).[127]
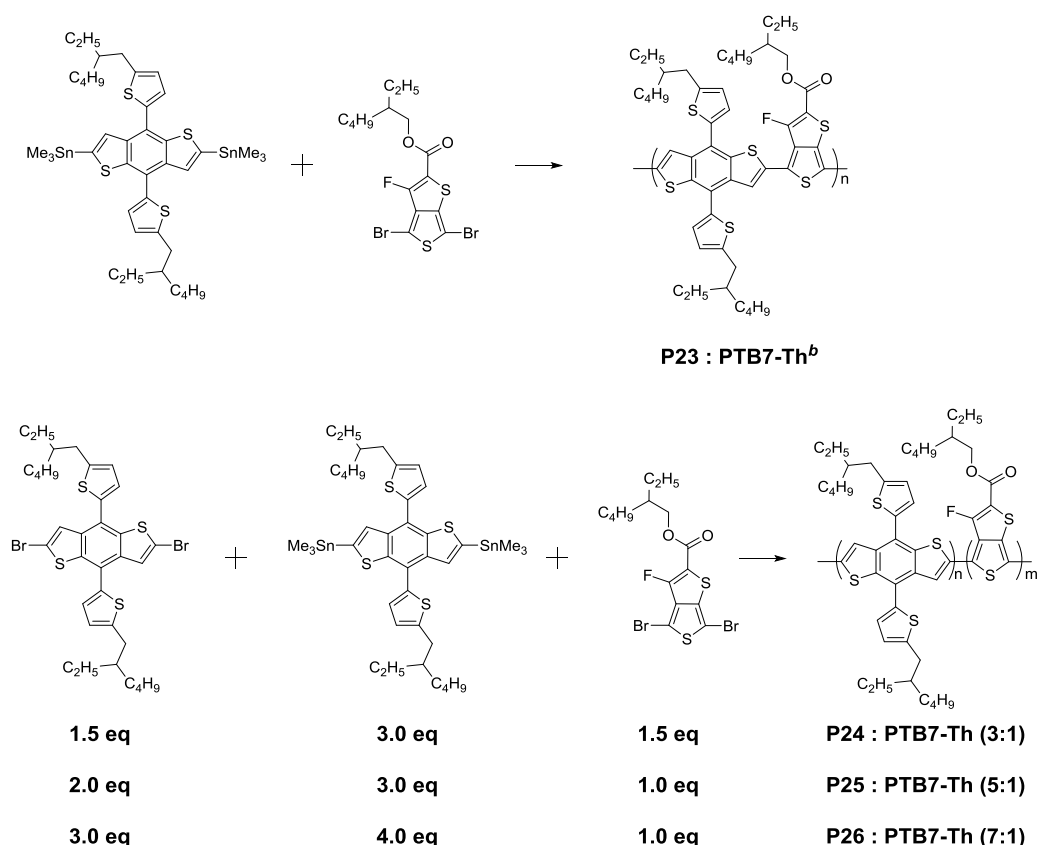
Figure 1.22: Chemical structures of P23-26 and the monomers used for their formation.[127]

The ability to tune the band gap was an attractive feature of polymers P24-26 especially when used with strongly absorbing non-fullerene acceptors such as naphthalenedi-imide based polymers in all polymer BHJs owing to the complementary absorption of the two components of the active layer.[127]

Table 1.14: Photovoltaic properties of polymers P23-P26.[127]

Polymer	n:m	HOMO (eV)	E_g (eV)	V_{oc} (eV)	J_{sc} (mA/cm^2)	PCE (%)
P23	1:1 (alt)	-5.2	1.6	0.81	13.76	6.47
P24	3:1	-5.3	1.7	0.88	11.43	5.63
P25	5:1	-5.4	1.8	0.88	11.13	5.58
P26	7:1	-5.4	1.8	0.89	10.06	4.66

While regular or alternating donor polymers have a better defined monomer sequence, random or statistical copolymers will have a distribution of monomers throughout the backbone. This distribution of different sequences in random and semi-random

copolymers, coupled with variations in conjugation length along the back bone, can give rise to a plethora of effective chromophores. This leads to the broadening of the absorption into the NIR region and more complete harvesting of the solar spectrum, ultimately resulting in a higher short circuit current density (J_{sc}).[124] While a broad absorption and low E_g may lead to an increase in J_{sc}, the more unpredictable and less crystalline structure of "random" and "semi-random" copolymers compared to the extended crystalline structure of their alternating counterparts can be undesirable. The nanocrystaline morphologies often found in random copolymers have been shown to hinder charge extraction and work to lower J_{sc}[128] and, as such, this could potentially impact their large scale use in OPVs in the near future.[129] The tendency of random copolymers to aggregate less than their alternating counterparts can be advantageous, leading to materials which are more readily soluble and easier to process in non-chlorinated solvents.[130] The same randomness can also lead to large batch-to-batch variations which could make them a less appealing option for product design.[129] There is a great deal of trial and error to establish whether a "random" or "semi-random" copolymer will outperform its alternating counterpart where performance is dependent on a careful balance of V_{oc}, E_g and morphology. While, in separate cases, both random and alternating copolymers have outperformed their counterparts and there is currently no accurate way to predict which the more desirable choice is.[130-132]

In this thesis, the main focus is on disentanglement of the differences in properties that arise from monomer composition and monomer sequence. One monomer system in particular is scrutinised very closely as we try to discern which structural differences give rise to more favourable photovoltaic properties and aim to enhance them from the knowledge we gain.

1.7: References

(1)   Government, U. S. *International Energy Outlook 2016*, 2016.

(2)   Government, U. K. *2016 UK Greenhouse Gas Emissions, Provisional Figures*, 2016.

(3)   Knapp, K.; Jester, T. *Sol. Energy* **2001**, *71*, 165.

(4)   Espinosa, N.; Hosel, M.; Angmo, D.; Krebs, F. C. *Eng. & Env. Sci.* **2012**, *5*, 5117.

(5)   Brabec, C. J. *Sol. Energ. Mat. Sol. C.* **2004**, *83*, 273.

(6)   Sirringhaus, H. *Adv. Mater.* **2014**, *26*, 1319.

(7)   Berny, S.; Blouin, N.; Distler, A.; Egelhaaf, H. J.; Krompiec, M.; Lohr, A.; Lozman, O. R.; Morse, G. E.; Nanson, L.; Pron, A.; Sauermann, T.; Seidler, N.; Tierney, S.; Tiwana, P.; Wagner, M.; Wilson, H. *Adv. Sci.* **2016**, *3*.

(8)   M., W. M.; M., K. J.; H., V. W. J.; Joop, K.; C., H. J.; A., v. H. P.; J., J. R. A. *Angew. Chem. Int. Edit.* **2003**, *42*, 3371.

(9)   Yin, Z.; Wei, J.; Zheng, Q. *Adv. Sci.* **2016**, *3*.

(10)   Chen, W.; Zhang, Q. *J. Mater. Chem. C* **2017**, *5*, 1275.

(11)   Hou, J.; Inganas, O.; Friend, R. H.; Gao, F. *Nat. Mater.* **2018**, *17*, 119.

(12)   Yan, C.; Barlow, S.; Wang, Z.; Yan, H.; Jen, A. K. Y.; Marder, S. R.; Zhan, X. *Nat. Rev. Mater.* **2018**, *3*.

(13)   Tamai, Y.; Ohkita, H.; Benten, H.; Ito, S. *J. Phys. Chem. Lett* **2015**, *6*, 3417.

(14)   Shoaee, S.; Clarke, T. M.; Huang, C.; Barlow, S.; Marder, S. R.; Heeney, M.; McCulloch, I.; Durrant, J. R. *J. Am. Chem. Soc.* **2010**, *132*, 12919.

(15)   Huijser, A.; Savenije, T. J.; Shalav, A.; Siebbeles, L. D. A. *J. Appl. Phys.* **2008**, *104*, 10.

(16)   Shaw, P. E.; Ruseckas, A.; Samuel, I. D. W. *Adv. Mater.* **2008**, *20*, 3516.

(17)   Groves, C.; Marsh, R. A.; Greenham, N. C. *J. Chem. Phys.* **2008**, *129*.

(18)   Yu, G.; Gao, J.; Hummelen, J. C.; Wudl, F.; Heeger, A. J. *Science* **1995**, *270*, 1789.

(19)   Liu, T.; Troisi, A. *Adv. Mater.* **2013**, *25*, 1038.

(20)   Meier, H.; Stalmach, U.; Kolshorn, H. *Acta Polymerica* **1997**, *48*, 379.

(21)   Moliton, A.; Nunzi, J. M. *Polym. Int.* **2006**, *55*, 583.

(22)   Thompson, B. C.; Frechet, J. M. J. *Angew. Chem. Int. Edit.* **2008**, *47*, 58.

(23)   Scharber, M. C.; Wuhlbacher, D.; Koppe, M.; Denk, P.; Waldauf, C.; Heeger, A. J.; Brabec, C. L. *Adv. Mater.* **2006**, *18*, 789.

(24)   Shirakawa, H. *Angew. Chem.Int. Edit.* **2001**, *40*, 2575.

(25)   Chiang, C. K.; Fincher, C. R.; Park, Y. W.; Heeger, A. J.; Shirakawa, H.; Louis, E. J.; Gau, S. C.; Macdiarmid, A. G. *Phys. Rev. Lett.* **1977**, *39*, 1098.

(26)   Shirakawa, H.; Louis, E. J.; Macdiarmid, A. G.; Chiang, C. K.; Heeger, A. J. *J. Chem. Soc. Chem. Comm.* **1977**, 578.

(27)   Reife, A. In *Abstr. Pap. Am. Chem. S.*; 4 ed.; Wiley & Sons: New York, **1992**; *204*,1037.

(28)   Weiss D. E., *Phys. Chem. Org. Solid State*; Intersci. Pub.: New York, **1965**; *2*.

(29)   McNeill, R.; Siudak, R.; Wardlaw, J.; Weiss, D. *Austr. J. Chem* **1963**, *16*, 1056.

(30)   Bolto, B.; McNeill, R.; Weiss, D. *Austr. J. Chem.* **1963**, *16*, 1090.

(31)   Jozefowicz, M.; Yu, L. T.; Perichon, J.; Buvet, R. *J. Polym. Sci. C: Polymer Symposia* **1969**, *22*, 1187.

(32)   Shirakawa, H.; Ikeda, S. *Polym. J.* **1971**, *2*, 231.

(33)   Ito, T.; Shirakawa, H.; Ikeda, S. *J. Polym. Sci. a Polym. Chem.* **1974**, *12*, 11.

(34)   Shaheen, S. E.; Brabec, C. J.; Sariciftci, N. S.; Padinger, F.; Fromherz, T.; Hummelen, J. C. *Appl. Phys. Lett.* **2001**, *78*, 841.

(35)   Brabec, C. J.; Shaheen, S. E.; Winder, C.; Sariciftci, N. S.; Denk, P. *Appl. Phys. Lett.* **2002**, *80*, 1288.

(36)   McCullough, R. D.; Lowe, R. D. *Abstr. Pap. Am. Chem. Soc.* **1992**, *203*, 240.

(37)   McCullough, R. D.; Lowe, R. D. *J. Chem. Soc. Chem. Comm.* **1992**, *70*.

(38)   Bundgaard, E.; Krebs, F. C. *Sol. Eng. Mater. Sol. C.* **2007**, *91*, 954.

(39)   Qian, G.; Wang, Z. Y. *Can. J. Chem.* **2010**, *88*, 192.

(40)   Liang, Y. Y.; Xu, Z.; Xia, J. B.; Tsai, S. T.; Wu, Y.; Li, G.; Ray, C.; Yu, L. P. *Adv. Mater.* **2010**, *22*,135.

(41)   He, Z.; Xiao, B.; Liu, F.; Wu, H.; Yang, Y.; Xiao, S.; Wang, C.; Russell, T. P.; Cao, Y. *Nat. Photonics* **2015**, *9*, 174.

(42)   Liu, J.; Li, X.; Zhang, S.; Ren, X.; Cheng, J.; Zhu, L.; Zhang, D.; Huo, L.; Hou, J.; Choy, W. C. H. *Adv. Mater. Int.* **2015**, *2*.

(43)   Huang, J.; Li, C.-Z.; Chueh, C.-C.; Liu, S.-Q.; Yu, J.-S.; Jen, A. K. Y. *Adv. Eng. Mater.* **2015**, *5*.

(44)   Liu, Y.; Zhao, J.; Li, Z.; Mu, C.; Ma, W.; Hu, H.; Jiang, K.; Lin, H.; Ade, H.; Yan, H. *Nat. Comm.* **2014**, *5*.

(45)   Huang, J.; Carpenter, J. H.; Li, C.-Z.; Yu, J.-S.; Ade, H.; Jen, A. K. Y. *Adv. Mater.* **2016**, *28*, 967.

(46)   Zhao, J.; Li, Y.; Yang, G.; Jiang, K.; Lin, H.; Ade, H.; Ma, W.; Yan, H. *Nat. Eng.* **2016**, *1*.

(47)   Azarian, D.; Dua, S. S.; Eaborn, C.; Walton, D. R. M. *J. Organomet. chem.,* **1976**, *117*, 55.

(48)   Kosugi, M.; Shimizu, Y.; Migita, T. *Chem. Lett.* **1977**, 1423.

(49)   Kosugi, M.; Sasazawa, K.; Shimizu, Y.; Migita, T. *Chem. Lett.* **1977**, 301.

(50)   Milstein, D.; Stille, J. K. *J. Am. Chem. Soc.* **1978**, *100*, 3636.

(51)   Stille, J. K. *Angew. Chem. Int. Edit.* **1986**, *25*, 508.

(52)   Cordovilla, C.; Bartolome, C.; Martinez-Ilarduya, J. M.; Espinet, P. *Acs Cat.* **2015**, *5*, 3040.

(53)   Casado, A. L.; Espinet, P. *Organomet.* **1998**, *17*, 954.

(54)   Espinet, P.; Echavarren, A. M. *Angew. Chem. Int. Edit.* **2004**, *43*, 4704.

(55)   Bao, Z. N.; Chan, W. K.; Yu, L. P. *J. Am. Chem. Soc.* **1995**, *117*, 12426.

(56)   Beletskaya, I. P. *j. Organomet. Chem.* **1983**, *250*, 551.

(57)   Farina, V.; Krishnan, B.; Marshall, D. R.; Roth, G. P. *J. Org. Chem.* **1993**, *58*, 5434.

(58)   Farina, V.; Kapadia, S.; Krishnan, B.; Wang, C. J.; Liebeskind, L. S. *J. Org. Chem.* **1994**, *59*, 5905.

(59)   Farina, V.; Krishnan, B. *J. Am. Chem. Soc.* **1991**, *113*, 9585.

(60)   Ishii, Y. *Ann. NY. Acad. Sci.* **1974**, *239*, 114.

(61)   Gao, J. H.; Wang, W.; Zhang, S. J.; Xiao, S. Q.; Zhan, C.; Yang, M. Y.; Lu, X. H.; You, W. *J. Mater. Chem. A* **2018**, *6*, 179.

(62)   Miyaura, N.; Yamada, K.; Suzuki, A. *Tet. Lett.* **1979**, *20*, 3437.

(63)   Amatore, C.; Jutand, A.; Le Duc, G. *Chme. Eur. J.* **2011**, *17*, 2492.

(64)   Rusu, R. D.; Schluter, A. D. *RSC Adv.* **2014**, *4*, 57026.

(65)   Sevignon, M.; Papillon, J.; Schulz, E.; Lemaire, M. *Tet. Lett.* **1999**, *40*, 5873.

(66)   Hassan, J.; Schulz, E.; Gozzi, C.; Lemaire, M. *J. Mol. Cat. a-Chem.* **2003**, *195*, 125.

(67)   Morin, P. O.; Bura, T.; Leclerc, M. *Mater. Horiz.* **2016**, *3*, 11.

(68)   Yu, S. M.; Liu, F. C.; Yu, J. W.; Zhang, S. M.; Cabanetos, C.; Gao, Y. Q.; Huang, W. *J. Mater. Chem. C* **2017**, *5*, 29.

(69)   Bohra, H.; Wang, M. F. *J. Mater. Chem. A* **2017**, *5*, 11550.

(70)   Wang, Q. F.; Takita, R.; Kikuzaki, Y.; Ozawa, F. *J. Am. Chem. Soc.* **2010**, *132*, 11420.

(71)   Lu, W.; Kuwabara, J.; Kanbara, T. *Macromolecules* **2011**, *44*, 1252.

(72)   Chu, T.-Y.; Lu, J.; Beaupre, S.; Zhang, Y.; Pouliot, J.-R.; Wakim, S.; Zhou, J.; Leclerc, M.; Li, Z.; Ding, J.; Tao, Y. *J. Am. Chem. Soc.* **2011**, *133*, 4250.

(73)   Marzano, G.; Kotowski, D.; Babudri, F.; Musio, R.; Pellegrino, A.; Luzzati, S.; Po, R.; Farinola, G. M. *Macromolecules* **2015**, *48*, 7039.

(74)   Dudnik, A. S.; Aldrich, T. J.; EasthamP, N. D.; Chang, R. P. H.; Facchetti, A.; Marks, T. J. *J. Am. Chem. Soc.* **2016**, *138*, 15699.

(75)   Marzano, G.; Carulli, F.; Babudri, F.; Pellegrino, A.; Po, R.; Luzzati, S.; Farinola, G. M. *J. Mater. Chem. A* **2016**, *4*, 17163.

(76)   Li, W. W.; Qin, R. P.; Zhou, Y.; Andersson, M.; Li, F. H.; Zhang, C.; Li, B. S.; Liu, Z. P.; Bo, Z. S.; Zhang, F. L. *Polymer* **2010**, *51*, 3031.

(77)   Janietz, S.; Krueger, H.; Schleiermacher, H. F.; Wurfel, U.; Niggemann, M. *Macromol. Chem. Phys.* **2009**, *210*, 1493.

(78)   Svensson, M.; Zhang, F. L.; Veenstra, S. C.; Verhees, W. J. H.; Hummelen, J. C.; Kroon, J. M.; Inganas, O.; Andersson, M. R. *Adv. Mater.* **2003**, *15*, 988.

(79)   Sun, W.; Zhou, N. L.; Xiao, Y.; Wang, S. R.; Li, X. G. *Chem. Asian J.* **2017**, *12*, 3069.

(80)   Muhlbacher, D.; Scharber, M.; Morana, M.; Zhu, Z.; Waller, D.; Gaudiana, R.; Brabec, C. *Adv. Mater.* **2006**, *18*, 2931.

(81)   Zhou, H.; Yang, L.; Stuart, A. C.; Price, S. C.; Liu, S.; You, W. *Angew. Chem. Inter. Edit.* **2011**, *50*, 2995.

(82)   Wang, E.; Wang, L.; Lan, L.; Luo, C.; Zhuang, W.; Peng, J.; Cao, Y. *Appl. Phys. Lett.* **2008**, *92*.

(83)   Allard, N.; Aich, R. B.; Gendron, D.; Boudreault, P. L. T.; Tessier, C.; Alem, S.; Tse, S. C.; Tao, Y.; Leclerc, M. *Macromolecules* **2010**, *43*, 2328.

(84)   McCulloch, I.; Ashraf, R. S.; Biniek, L.; Bronstein, H.; Combe, C.; Donaghey, J. E.; James, D. I.; Nielsen, C. B.; Schroeder, B. C.; Zhang, W. *Accounts Chem. Res.* **2012**, *45*, 714.

(85)   Chen, H. Y.; Hou, J. H.; Hayden, A. E.; Yang, H.; Houk, K. N.; Yang, Y. *Adv. Mater.* **2010**, *22*, 371.

(86)   Park, S. H.; Roy, A.; Beaupre, S.; Cho, S.; Coates, N.; Moon, J. S.; Moses, D.; Leclerc, M.; Lee, K.; Heeger, A. J. *Nat. Photonics* **2009**, *3*, 297.

(87)   Drolet, N.; Morin, J. F.; Leclerc, N.; Wakim, S.; Tao, Y.; Leclerc, M. *Adv. Funct. Mater.* **2005**, *15*, 1671.

(88)   Coffin, R. C.; Peet, J.; Rogers, J.; Bazan, G. C. *Nat. Chem.* **2009**, *1*, 657.

(89)   Kim, J. S.; Fei, Z. P.; Wood, S.; James, D. T.; Sim, M.; Cho, K.; Heeney, M. J.; Kim, J. S. *Adv. Eneg. Mater.* **2014**, *4*.

(90)   Zhang, Y.; Zou, J. Y.; Yip, H. L.; Sun, Y.; Davies, J. A.; Chen, K. S.; Acton, O.; Jen, A. K. Y. *J. Mate Chem* **2011**, *21*, 3895.

(91)   Amb, C. M.; Chen, S.; Graham, K. R.; Subbiah, J.; Small, C. E.; So, F.; Reynolds, J. R. *J. Am. Chem. Soc.* **2011**, *133*, 10062.

(92)   Guo, X. G.; Xin, H.; Kim, F. S.; Liyanage, A. D. T.; Jenekhe, S. A.; Watson, M. D. *Macromolecules* **2011**, *44*, 269.

(93)   Pomerantz, M.; Gu, X. M. *Synthetic Met.* **1997**, *84*, 243.

(94)   Liang, Y. Y.; Feng, D. Q.; Wu, Y.; Tsai, S. T.; Li, G.; Ray, C.; Yu, L. P. *J. Am. Chem. Soc.* **2009**, *131*, 7792.

(95)   Liao, S. H.; Jhuo, H. J.; Cheng, Y. S.; Chen, S. A. *Adv. Mater.* **2013**, *25*, 4766.

(96)   Yao, H. F.; Zhang, H.; Ye, L.; Zhao, W. C.; Zhang, S. Q.; Hou, J. H. *ACS Appl. Mater. Inter.* **2016**, *8*, 3575.

(97)   Kim, J. H.; Song, C. E.; Kang, I. N.; Shin, W. S.; Zhang, Z. G.; Li, Y. F.; Hwang, D. H. *B. Kor. Chem. Soc.* **2014**, *35*, 1356.

(98)   Kim, J. H.; Song, C. E.; Shin, N.; Kang, H.; Wood, S.; Kang, I. N.; Kim, B. J.; Kim, B.; Kim, J. S.; Shin, W. S.; Hwang, D. H. *Acs Appl. Mater. Inter.* **2013**, *5*, 12820.

(99)   Coffin, R. C.; MacNeill, C. M.; Peterson, E. D.; Ward, J. W.; Owen, J. W.; McLellan, C. A.; Smith, G. M.; Noftle, R. E.; Jurchescu, O. D.; Carroll, D. L. *J. Nanotech.* **2011**, *2011*, 10.

(100)   Braunecker, W. A.; Owczarczyk, Z. R.; Garcia, A.; Kopidakis, N.; Larsen, R. E.; Hammond, S. R.; Ginley, D. S.; Olson, D. C. *Chem Mater.* **2012**, *24*, 1346.

(101)   Song, S.; Jin, Y.; Kim, S. H.; Moon, J.; Kim, K.; Kim, J. Y.; Park, S. H.; Lee, K.; Suh, H. *Macromolecules* **2008**, *41*, 7296.

(102)   Kline, R. J.; McGehee, M. D.; Kadnikova, E. N.; Liu, J. S.; Frechet, J. M. J.; Toney, M. F. *Macromolecules* **2005**, *38*, 3312.

(103)   Zhang, Z. H.; Peng, B.; Liu, B.; Pan, C. Y.; Li, Y. F.; He, Y. H.; Zhou, K. C.; Zou, Y. P. *Polym. Chem.* **2010**, *1*, 1441.

(104)   Najari, A.; Beaupre, S.; Berrouard, P.; Zou, Y. P.; Pouliot, J. R.; Lepage-Perusse, C.; Leclerc, M. *Adv. Funct. Mater.* **2011**, *21*, 718.

(105)   Zhou, H. X.; Yang, L. Q.; Stoneking, S.; You, W. *Acs Appl. Mater. Inter.* **2010**, *2*, 1377.

(106)   Li, Y. N.; Sonar, P.; Murphy, L.; Hong, W. *Eneg. Env. Sci.* **2013**, *6*, 1684.

(107)   Wu, Q.; Wang, M.; Qiao, X.; Xiong, Y.; Huang, Y.; Gao, X.; Li, H. *Macromolecules* **2013**, *46*, 3887.

(108)   Osaka, I.; Zhang, R.; Sauve, G.; Smilgies, D.-M.; Kowalewski, T.; McCullough, R. D. *J. Am. Chem. Soc.* **2009**, *131*, 2521.

(109)   Howard, J. B.; Thompson, B. C. *Macromol. Chem. Phys* **2017**, *218*.

(110)   Olivier, Y.; Niedzialek, D.; Lemaur, V.; Pisula, W.; Muellen, K.; Koldemir, U.; Reynolds, J. R.; Lazzaroni, R.; Cornil, J.; Beljonne, D. *Adv. Mater.* **2014**, *26*, 2119.

(111)   Liang, Y.; Feng, D.; Wu, Y.; Tsai, S.-T.; Li, G.; Ray, C.; Yu, L. *J. Am. Chem. Soc.* **2009**, *131*, 7792.

(112)   Lei, T.; Dou, J. H.; Pei, J. *Adv. Mater.* **2012**, *24*, 6457.

(113)   Fallon, K. J.; Santala, A.; Wijeyasinghe, N.; Manley, E. F.; Goodeal, N.; Leventis, A.; Freeman, D. M. E.; Al-Hashimi, M.; Chen, L. X.; Marks, T. J.; Anthopoulos, T. D.; Bronstein, H. *Adv. Funct. Mater.* **2017**, *27*.

(114)   Zhang, S. Q.; Ye, L.; Zhao, W. C.; Liu, D. L.; Yao, H. F.; Hou, J. H. *Macromolecules* **2014**, *47*, 4653.

(115)   Bronstein, H.; Frost, J. M.; Hadipour, A.; Kim, Y.; Nielsen, C. B.; Ashraf, R. S.; Rand, B. P.; Watkins, S.; McCulloch, I. *Chem. Mater.* **2013**, *25*, 277.

(116)   Stuart, A. C.; Tumbleston, J. R.; Zhou, H.; Li, W.; Liu, S.; Ade, H.; You, W. *J. Am. Chem. Soc.* **2013**, *135*, 1806.

(117)   Li, W.; Yan, L.; Zhou, H.; You, W. *Chem. Mater.* **2015**, *27*, 6470.

(118)   Huo, L. J.; Zhang, S. Q.; Guo, X.; Xu, F.; Li, Y. F.; Hou, J. H. *Angew. Chem. Int. Edit.* **2011**, *50*, 9697.

(119)   Zhu, Z.; Waller, D.; Gaudiana, R.; Morana, M.; Muhlbacher, D.; Scharber, M.; Brabec, C. *Macromolecules* **2007**, *40*, 1981.

(120)   Yuan, M. C.; Chiu, M. Y.; Chiang, C. M.; Wei, K. H. *Macromolecules* **2010**, *43*, 6270.

(121)   Li, J.; Ong, K. H.; Sonar, P.; Lim, S. L.; Ng, G. M.; Wong, H. K.; Tan, H. S.; Chen, Z. K. *Polym. Chem.* **2013**, *4*, 804.

(122)   Kang, T. E.; Cho, H. H.; Kim, H. J.; Lee, W.; Kang, H.; Kim, B. J. *Macromolecules* **2013**, *46*, 6806.

(123)   Jung, J. W.; Liu, F.; Russell, T. P.; Jo, W. H. *Eneg. Env. Sci.* **2013**, *6*, 3301.

(124)   Kang, T. E.; Choi, J.; Cho, H. H.; Yoon, S. C.; Kim, B. J. *Macromolecules* **2016**, *49*, 2096.

(125)   Deng, P.; Wu, B.; Lei, Y.; Cao, H.; Ong, B. S. *Macromolecules* **2016**, *49*, 2541.

(126)   Jiang, T.; Yang, J.; Tao, Y.; Fan, C.; Xue, L.; Zhang, Z.; Li, H.; Li, Y.; Huang, W. *Polym. Chem.* **2016**, *7*, 926.

(127)   Kim, S. W.; Choi, J.; Bui, T. T. T.; Lee, C.; Cho, C.; Na, K.; Jung, J.; Song, C. E.; Ma, B.; Lee, W. S.; Kim, B. J. *Adv. Funct. Mater.* **2017**, *27*.

(128)   Menelaou, C.; Tierney, S.; Blouin, N.; Mitchell, W.; Tiwana, P.; McKerracher, I.; Jagadish, C.; Carrasco, M.; Herz, L. M. *J.Phys. Chem. C* **2014**, *118*, 17351.

(129)   Fang, L.; Zhou, Y.; Yao, Y. X.; Diao, Y.; Lee, W. Y.; Appleton, A. L.; Allen, R.; Reinspach, J.; Mannsfeld, S. C. B.; Bao, Z. A. *Chem. Mater.* **2013**, *25*, 4874.

(130)   Duan, C. H.; Gao, K.; van Franeker, J. J.; Liu, F.; Wienk, M. M.; Janssen, R. A. J. *J. Am. Chem. Soc.* **2016**, *138*, 10782.

(131)   Braunecker, W. A.; Oosterhout, S. D.; Owczarczyk, Z. R.; Kopidakis, N.; Ratcliff, E. L.; Ginley, D. S.; Olson, D. C. *ACS Macro Letters* **2014**, *3*, 622.

(132)   Hendriks, K. H.; Heintges, G. H. L.; Wienk, M. M.; Janssen, R. A. J. *J. Mater. Chem. A* **2014**, *2*, 17899.

Chapter 2: Elucidation of the Backbone Structure of Statistical Conjugated Polymers
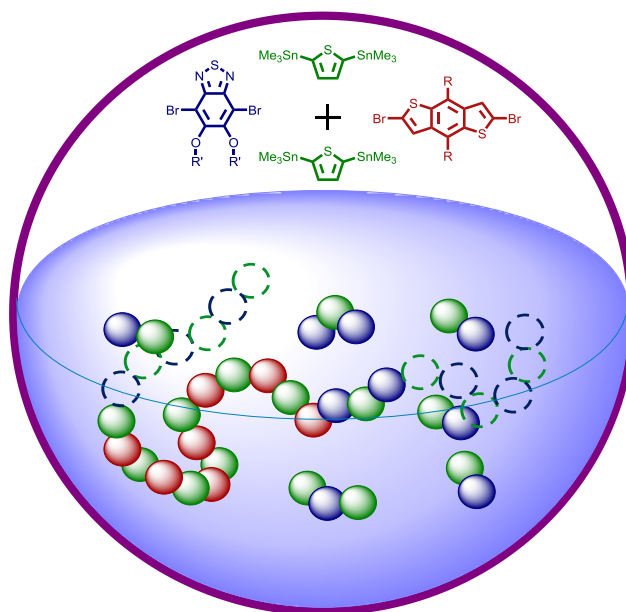
Abstract: Random, statistical and alternating copolymers have different properties. Statistical copolymers have become a more popular choice in the field of photovoltaics, owing to their increased solubility and high performance in some cases, the investigation herein asks why. An investigation into the backbone sequence of one statistical conjugated polymer is carried out, the optoelectronic and morphological properties are compared to its alternating counterpart and the factors underlying their improved performance are revealed.

2.1: Introduction

While alternating donor-acceptor polymers have well defined monomer sequence, "random" or statistical copolymers have a less well defined distribution of monomers throughout the backbone. This distribution of different sequences in random and semi-random copolymers, coupled with variations in conjugation length along the backbone, can give rise to a plethora of chromophores. This often leads to changes in the spectral absorption and adjustments in the HOMO, which in-turn influence the J_{sc} and V_{oc} respectively.[1-4] Electronic effects are not the only cause for a discrepancy in photovoltaic performance between alternating and statistical polymers; changes in π-stacking, aggregation and crystallinity can also affect the interactions with the fullerene acceptor, the charge transport and ultimately deceive performance. The nanocrystalline morphologies sometimes found in random copolymers have been shown to hinder charge extraction and decrease J_{sc}.[5,3,6] The tendency of random copolymers to aggregate less than their alternating counterparts can, however, be advantageous, leading to materials which are more readily soluble and easier to process in non-chlorinated solvents.[7] Conversely, the random nature of such polymers can lead to batch-to-batch variation of the polymer, which could potentially deter the large scale use of such materials in OPVs in the near future.[6] There is a great deal of trial and error as to whether a "random" or "semi-random" copolymer will outperform its alternating counterpart, where performance is dependent on a delicate balance of V_{oc}, J_{sc}, E_g and morphology (see Section 1.6). Explicitly, in separate cases, both random and alternating copolymers have outperformed their counterparts and there is currently no way of predicting which will win out.[4,7,8]

In the macromolecular world, sequence is often the key to achieving desirable and specialist properties from something as specific as an enzyme, to the self-assembly of bespoke block copolymers into a desired micro-structure. Sequence, therefore, could have a vital role to play for conjugated polymers, giving rise to the differences in performance between some random and alternating counterparts. Despite this assertion the effect of backbone sequence is seldom investigated. One study by Meyer *et al.* investigated a range of benzothiadiazol-phenylvinylene oligomers and concluded that sequence had a profound effect on both optoelectronic properties and solid state packing, although their investigations did not extend beyond tetramers which are more accurately

described as small molecules.[9] A second study investigated how the properties of PTB7-Th vary when synthesised using different catalysts [Pd(PPh₃)₄] *vs.* Pd₂(dba)₃ : P(*o*-tol)₃. A profound difference in monomer ratios within the polymer backbone was observed, which could lead to enhanced pre-aggregation in solution and photovoltaic properties.[10] The molecular weight of the polymers synthesised by the two systems was, however, vastly different. Molecular weight and dispersity have been shown to have significant effects on the morphology and electronic properties of conjugated polymers films,[11-14] as such the direct comparison of the properties of these two polymers is problematic.

In the present work we investigate the relative rates of reactivity of monomers in a "semi-random" copolymer (from here on referred to, as a statistical copolymer) of one such system, with the aim of gaining more insight into the sequence and structure of the backbone. Herein, the Merck PTBnDT(C₁₂)-*stat*-PTBT formulation (Scheme 2.1) which has been shown to outperform its alternating counterpart (Figure 2.1 and Table 2.1) is investigated. The aim is to understand the structural differences between the alternating and statistical copolymers and how these could lead to enhanced performance.
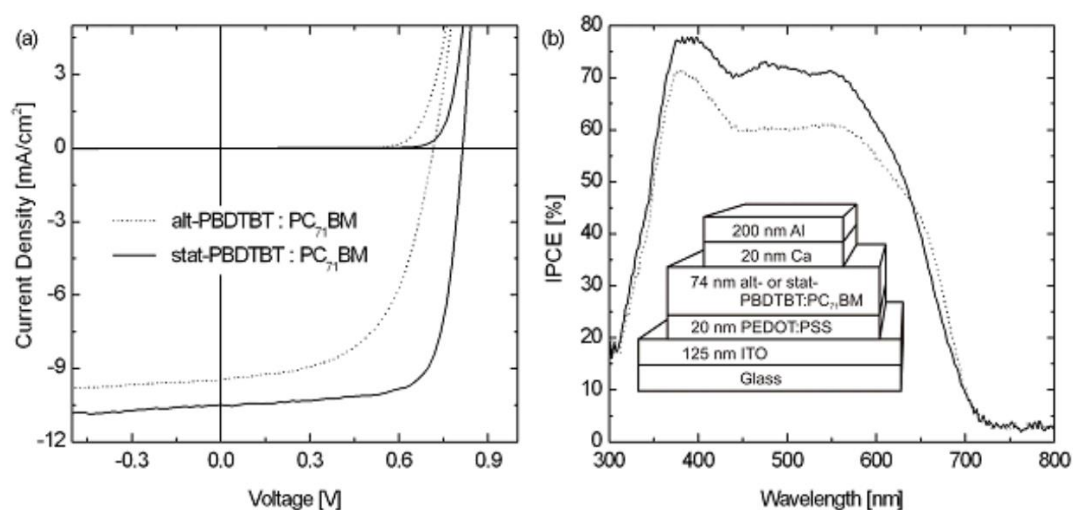
Figure 2.0.1: a; Current, voltage curves of PTBnD-*stat*-PTBT and *alt*-PBnDTDTBT b; ICPE.

a) Alternating copolymer
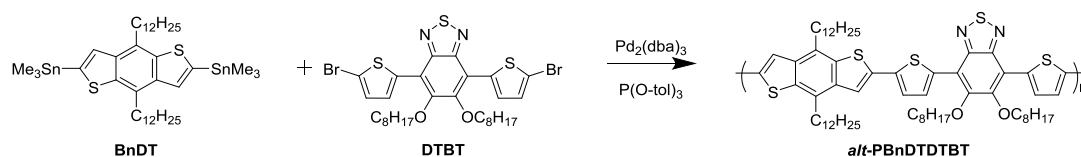
b) Statistical Copolymer
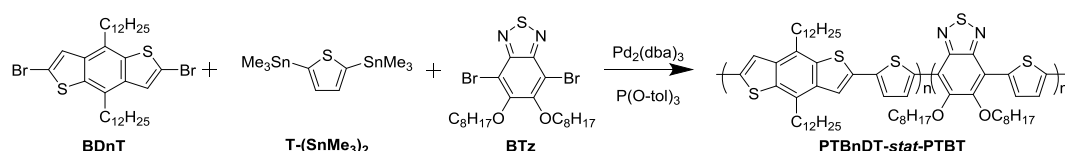
Scheme 2.1: Reaction scheme for the formation of a; *alt*-PBnDTDTBT and b; PTBnDT-*stat*-PTBT.

Table 2.1: Photovoltaic properties of *alt*-PBnDTDTBT and PTBnDT-*stat*-PTBT.

Polymer	J_{sc} (mA/cm²)	V_{oc} (V)	FF (%)	PCE (%)
Alternating	9.8	0.7	63.8	4.50
Statistical	11.7	0.8	71.3	6.51

Inspection of the photovoltaic properties of the two polymers (alternating PTBnDTTBT and the statistical PTBnDT-*stat*-PTBT) displayed in Figure 2.1a indicates that the higher performance of the statistical copolymer can be assigned to an increase in both J_{sc} and V_{oc}. Figure 2.1b displays the internal power conversion efficiency (IPCE) of the devices across the solar spectrum, the statistical copolymer follows the same trend as the alternating polymer but with a higher IPCE. The similar shape of the IPCE plots and the higher J_{sc} of the statistical copolymer suggest these devices have better charge separation and transport properties than the alternating polymer, indicative of a more favourable device morphology. The increased V_{oc} also indicates that the polymers energetics differ favouring the statistical polymer, most likely the result of a deeper HOMO.

In this Chapter the backbone structure of the statistical copolymer is elucidated through both kinetic and microscopic studies. The influence of changes in monomer order on the electronic, optical and morphological properties of the polymer are also investigated. The overall aim is to assign desirable properties to differences in structure.

The PTBnDT(C_{12})-*stat*-PTBT polymer backbone is comprised of a statistical distribution of benzothiadiazole (BT) accepting units and benzodithiophene (BnDT) donating units, each separated by a thiophene bridge (Scheme 2.1). When in the excited state the BT is in the stable quinodal form which helps to maintain a suitable LUMO for an appropriate E_g and charge separation. Compared to the benzotriazole (BTz) analogue BT has been shown to produce materials with much lower LUMOs than BTz (when copolymerised with BnDT) leading to a lower E_g and improved J_{sc}.[15,16] BnDT has been a popular choice as an electron donating (push) species since it was introduced in 2008 by Hou *et al.*,[17] its fused aromatic structure favours a greater degree of π-stacking leading to more crystalline films and enhancing hole mobilities.[18,19] The thiophene bridge acts as a spacer between two adjacent units lowering the torsional strain caused by the solubilising side chains and acts as a secondary acceptor to BT.[20]

2.2: Results and Discussion

2.2.1: Elucidation of Statistical Polymer Backbone Structure

We hypothesised that the two di-brominated monomers (di-bromo BnDT and di-bromo BT), selected for their distinctly different electronic properties, proceed through the Stille catalytic cycle at differing rates. This gives rise to a statistical rather than random arrangement of the donor and acceptor units along the polymer backbone.

Whilst ^{1}H and ^{13}C NMR analysis of the final product can be a powerful tool for characterisation, it becomes increasingly complex as regularity decreases in polymeric chains. The large variety of monomer combinations and associated perturbations in shielding, caused by a complex chain environment, lead to broad and complex NMR spectra. As such, analysing the NMR spectra for both the alternating and the statistical copolymer does not provide significant structural information. In this instance monomer conversion can be followed by ^{1}H NMR with relative ease. When BnDT and BT are converted a shift in the signal at 3.15 and 4.35 ppm (respectively) can be observed. These signals correspond to the α-CH$_2$ groups of the side chains on each monomer. Covalent coupling to the thiophene and an increase in conjugation in the system leads to a significant change in the local electron density of the α-CH$_2$ resulting in the observed shift (Figure 2.2).
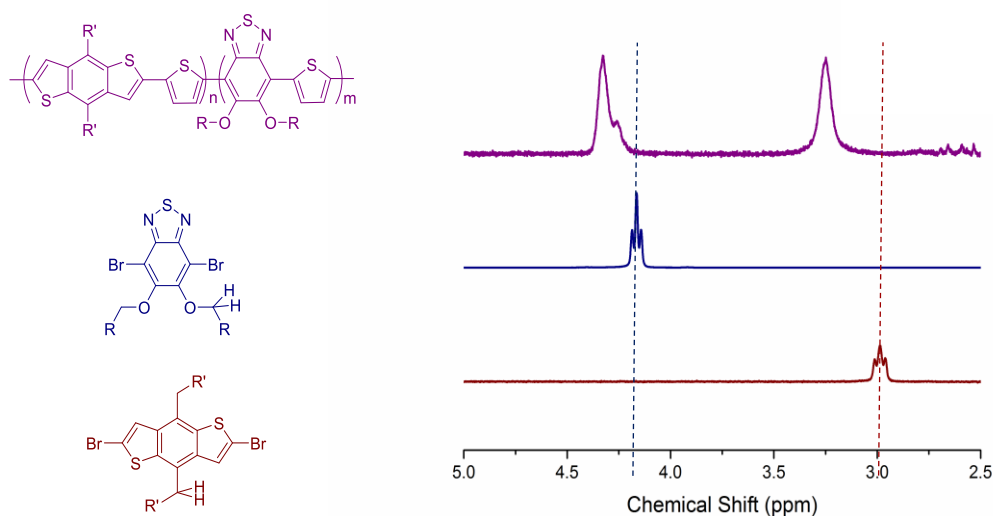
Figure 2.2: Shift of the α-CH$_2$ protons after the monomers BnDT (red) and BT (Blue) are incorporated into a polymer backbone (purple).

For the initial investigation of the conversion of BnDT and BT in this Stille polycondensation we replaced the di-functional bis-2,5-(trimethylstannyl) thiophene with the mono-functional 2-tri-butystannyl thiophene (Scheme 2.2). The mono-functional thiophene limits the number of possible products from an almost infinite number to just 4, thus making ^{1}H NMR interpretation simple and negating the need of a high field instrument to achieve good peak-to-peak resolution. The use of the bulkier *n*-butyl chains in the stannane moiety slows the rate of the transmetallation step and allows for better temporal resolution of the reaction (Figure 2.3). The reaction was carried out on a small scale in an NMR tube fitted with a Young's tap, under a blanket of argon with which *in-situ* ^{1}H NMR spectra could be recorded up to every two minutes.
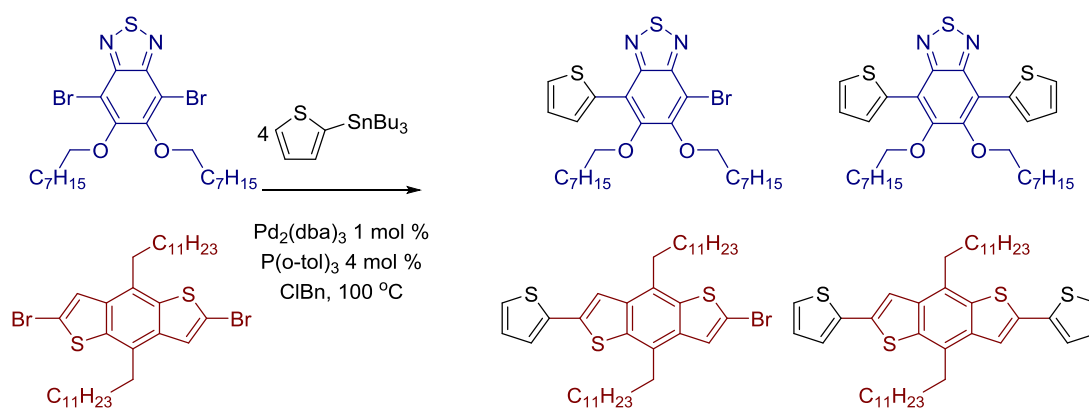
Scheme: 2.2: Competitive reactions between BnDT and BT with a mono-stannylated thiophene.

The triplet from the BnDT monomer was observed at δ = 3.15 ppm, as the reaction progresses the intensity of this peak diminishes and the emergence of two new triplets are observed. One triplet is centred at δ = 3.30 ppm and the second at δ = 3.45 ppm, which are assigned to the mono (TBnDT) and di-substituted (DTBnDT) BnDT monomer unit respectively (Figure 2.3). The BT monomer behaves in a similar manner shifting from δ = 4.35 to δ = 4.45 ppm, albeit to a much lesser extent. At t = 120 min a low intensity peak at δ = 4.45 ppm can be observed which is assigned to the mono-substituted BT unit (TBT), while there is no visible peak for the di-substituted species (DTBT) observed within this reaction time frame. The consumption of BT and BnDT is plotted against time in Figure 2.4 and shows initial (t = 0 to t = 10 min) rapid conversion of BnDT followed by a steady rate of consumption. BT shows no conversion (within the noise limit/error of NMR (5 %)) unitl much later at t = 70.
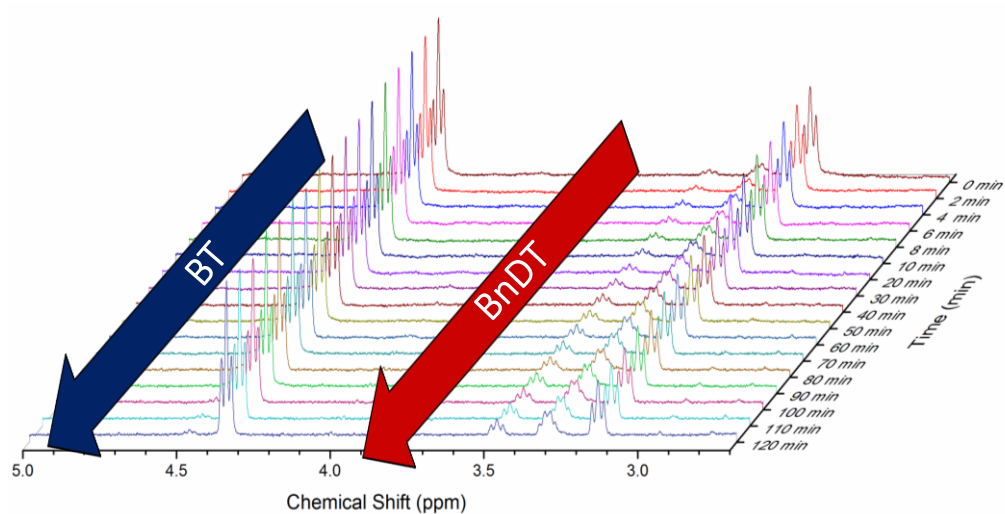
Figure 2.3: ^{1}H spectra taken *in-situ* of a competitive Stille coupling between BT and BnDT to a monostannylated thiophene at 100 ° C over 120 minutes.
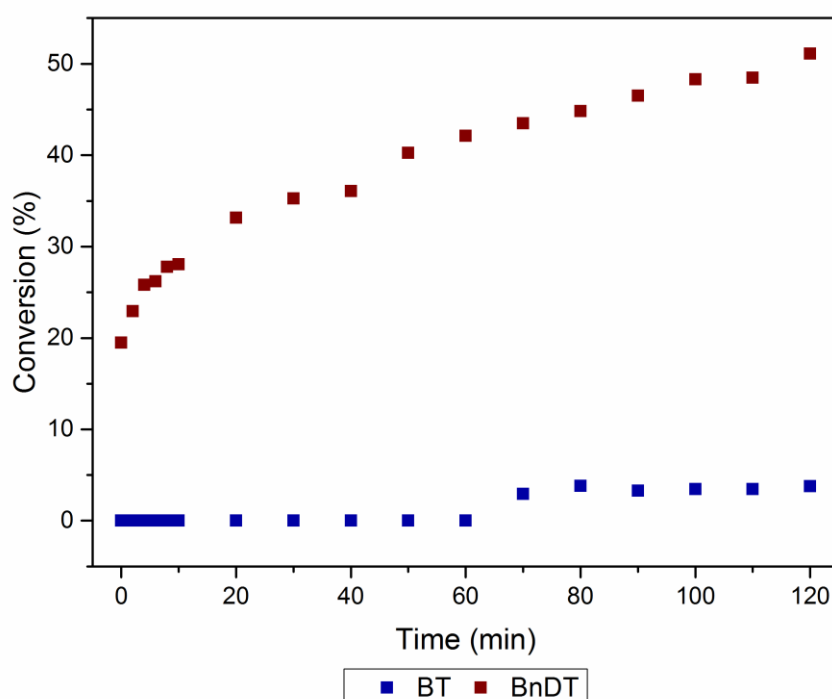
Figure 2.4: Plot of BnDT and BT conversion during in-situ ^{1}H NMR competitive reaction.

In-situ ^{1}H NMR studies offer a good insight into how each monomer proceeds through the Stille catalytic cycle, however, there are various limitations to the procedure. These include: the small scale of the reaction, temperature limitations on the NMR equipment and the inability to mechanically stir the system. It is necessary to monitor the progression of the Stille polycondensation in a system which is more comparable to that of an

industrial synthetic procedure. While microwave synthesis is largely reported in the literature as the standard synthetic procedure,[21,22] we elected to use a conventional heating method. Although conventional heating is slower than microwave synthesis, it has greater industrial appeal due to its scalability and compatibility with well-established industrial reactor design, as well as allowing for ease of sampling throughout the reaction unlike microwave synthesis.

To investigate the effect of different monomer activities in a Stille polycondensation by conventional heating, a reaction mixture containing 1.0 mmol of 2,5-bis(trimethylstannyl) thiophene, 0.5 mmol of BnDT and 0.5 mmol of BT in 48 ml of chlorobenzene was heated to 133 °C. 2.0 ml of catalyst solution containing 0.020 mmol $Pd_2(dba)_3$ and 0.120 mmol P(o-tolyl)$_3$ was added and the reaction was sampled over time. Whilst resolution of individual products is more difficult in the case of polymerisation, owing to the plethora of molecular species formed, it is possible to observe the consumption of monomer with ^{1}H NMR by measuring the depletion of the monomer peak against all other species α-CH$_2$ signals. In agreement with the *in-situ* studies the BnDT monomer is depleted more rapidly than the BT monomer. More rapid conversion of both the BnDT and BT monomer is also observed, resulting from the more mobile and faster reacting 2,5-bis(trimethylstannyl) thiophene. Figure 2.5 demonstrates that the BnDT monomer is converted from its pure unsubstituted form rapidly within the first 10 minutes of reaction. Interestingly, unlike the in-situ reaction discussed above, the BT monomer shows initial rapid conversion, before slowing at approximately 30 minutes, when the 2,5-bis(trimethylstannyl) thiophene monomeric species becomes more scarce.

Functional molecular weights (M_n > 15 kDa by GPC) are reached at lower conversions than expected for a traditional polycondensation reaction. The polymers formed in the first 200 minutes of the reaction are enriched in the BnDT monomer and as time progresses more BT is incorporated into the polymer backbone. Interestingly the number average molecular weight profile of the polymerisation (Figure 2.5) is what one would expect from a chain growth mechanism such as those seen by GRIM. It is possible the catalyst migrates along the BnDT unit and rarely fully dissociates from it. In this instance the Stille polycondensation behaves more like a chain growth polymerisation than a step growth process. From the evidence presented we determined that the materials being produced in this particular Stille polycondensation are gradient or block-like copolymers.
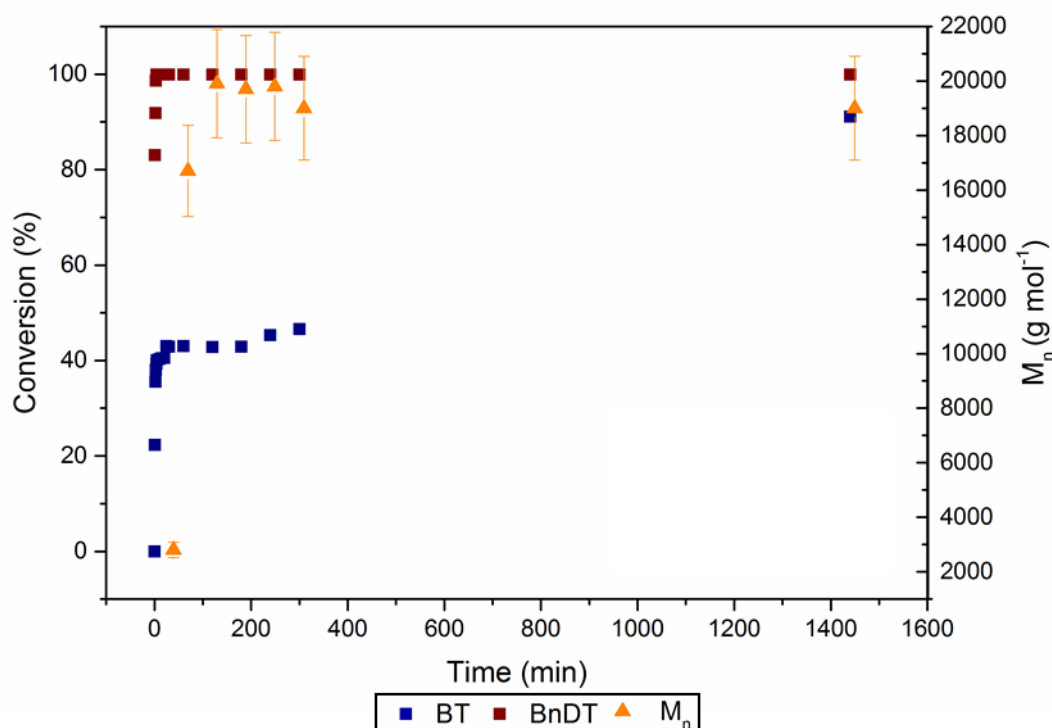
Figure 2.5: Conversion of BnDT and BT during polycondensation reaction, overlaid is M_n of the polymer at t_x.

Further evidence of the block-like structure resulting from the statistical copolymerisation is provided by scanning tunnelling microscopy (STM). Figure 2.6a shows STM images revealing contrast of two parallel bright lines, which are assigned to the conjugated backbone. Their semiconducting nature provides density of states near to the fermi level and exhibits 'bright' contrast in the constant current mode used here. Features can also be seen perpendicular to the backbones which are assigned as alkyl chains protruding in one direction, as such this section of the polymer is assigned to the PTBT block, an overlay of the chemical structure is shown in Figure 2.6c for clarity. Similarly in Figure 2.6b, two parallel bright regions are depicted with alkyl chains protruding from each side and are assigned to the PTBnDT rich blocks, the chemical structure overlay is depicted in Figure 2.6d.
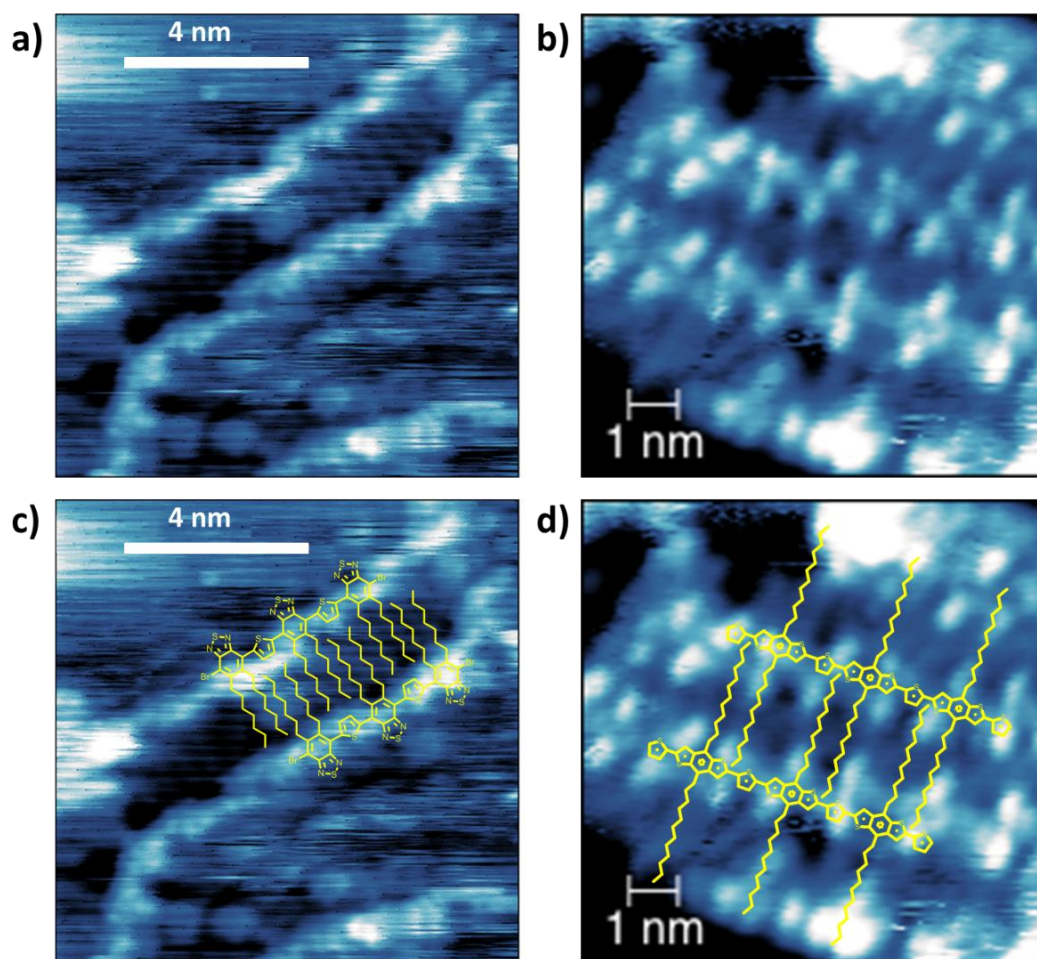
Figure 2.6: STM images of PTBnDT-stat-PTBT electro-sprayed in vacuum onto an atomically flat Au(111)/Mica surface. a; shows, a BT rich region, b; shows a BnDT rich region, c and d; show an overlay of the chemical structure on images a and b respectively (STM provided by Daniel Warr and Dr. Giovanni Costantini).

In order to investigate how the extent of the block-like structure of the statistical polymer PTBnDT-*stat*-PTBT gives rise to higher PCE we synthesised both the alternating and statistical copolymers, without perturbing the system through kinetic sampling (Scheme 2.1). The resultant polymers were characterised the by GPC, ^{1}H NMR, ^{13}C NMR and TGA, further to this we investigated the optoelectronic and morphological properties of the polymers were measured by UV/Vis spectroscopy, cyclic voltammetry (CV) and atomic force microscopy (AFM).

The two polymers were synthesised as shown in Scheme 2.1 (and described in Section 2.4 of this thesis) and their physical properties are summarised in Table 2.1. Both polymers show a similar ratio of BT : BnDT in the backbone by ^{1}H NMR. The ^{1}H NMR of the statistical copolymer shown in black in Figure 3.7, exhibits some differences when

compared to that of the alternating (shown in red). Firstly, in the region of $\delta = 7\text{-}9$ ppm there are some clear variances in the aromatic protons located on the flanking thiophenes of the BnDT and the thiophene bridging unit of the two polymers. The alternating copolymer exhibits one doublet at 7.55 ppm which is assigned to the two protons on the bridging thiophene units adjacent to the BT unit, the second doublet at 7.72 ppm is assigned to two protons, one on each thiophene unit adjacent to the BnDT species and the third centred at 8.54 ppm is assigned to two protons in the BnDT aromatic system. In the same region ($\delta = 7\text{-}9$ ppm) for the statistical copolymer a number of peaks can be identified owing to the variety of proton environments occurring from the varying sequence of BT and BnDT units.

The second region of interest is $\delta = 3\text{-}5$ ppm which contains peaks relate to the $\alpha\text{-}CH_2$ groups of the BT and BnDT units. The peak centred at $\delta = 3.26$ ppm is assigned to $\alpha\text{-}CH_2$ groups of the BnDT units and there is no noticeable difference between those in the statistical polymer and those in the alternating polymer. The difference worth noting in this region concerns the peak centred at $\delta = 4.35$ ppm ($\alpha\text{-}CH_2$ of the BT unit). A shoulder is observed in both the alternating and statistical copolymers (although it is much less pronounced for alternating copolymer) this shoulder is assigned to BT units close to the chain end. The proportion of BT units near the chain end in the statistical copolymer is markedly higher as the BT unit reacts more slowly and is therefore more likely to be positioned near to a chain end than in the alternating counterpart which has a defined sequence.
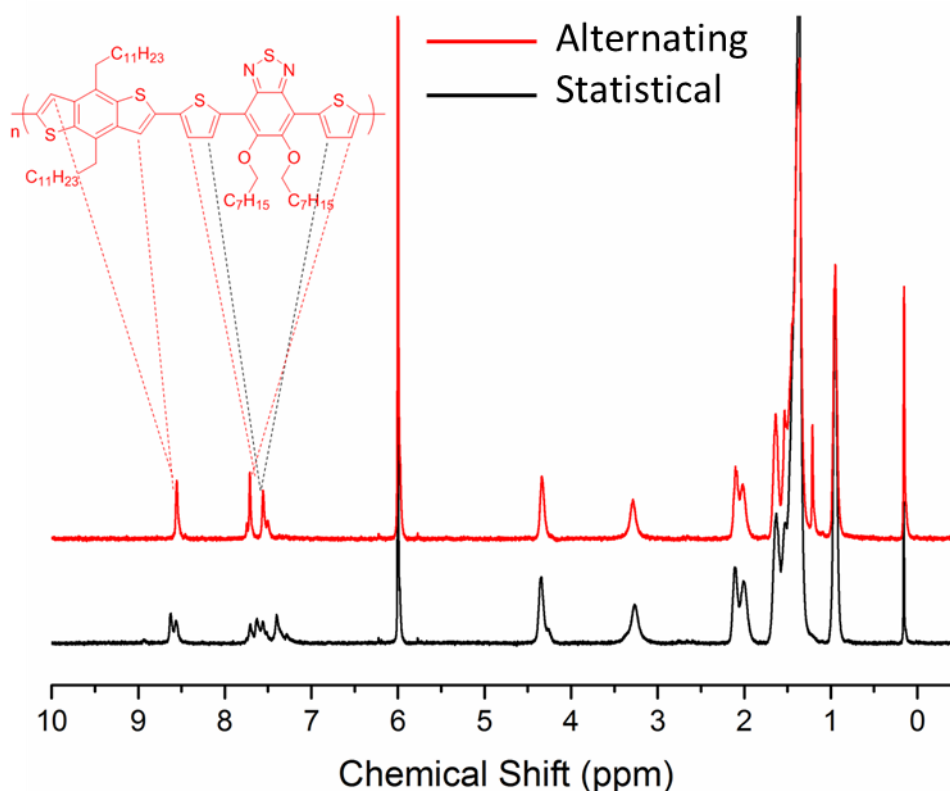
Figure 2.7: ^{1}H NMR of PTBnDT-stat-PTBT (black trace) and alternating PTBnDTTBT (red trace) in 1,1,2,2-teterachloroethane at 100 °C.

The molecular weight distributions for the two polymers (Figure 2.8 and Table 2.2) have a similar shape, the statistical copolymer does show some low molecular weight tailing which could possibly be attributed to PTBT homo-polymer formed in the later stages of the reaction and thus accounting for the higher observed dispersity. Both polymers display good thermal stability with 5 % mass loss (T_D) at T > 325 °C. The first initial mass loss at 325 °C (Figure 2.9) is attributed to the loss of OC_8H_{17} side chains. The second mass loss is assigned to the breakdown of the C-C bond and loss of the $C_{12}H_{25}$ side chains of the BnDT unit.

Table 2.2: Characterisation of PTBnDT-stat-PTBT and *alt*-PBnDTDTBT, molecular weights by GPC.

Polymer	M_n (g/mol)	M_w (g/mol)	Đ	T_D (° C)	% BT (^{1}H NMR)	% BnDT (^{1}H NMR)
Statistical	17600	44800	2.55	329	50	50
Alternating	27500	52800	1.92	326	50	50
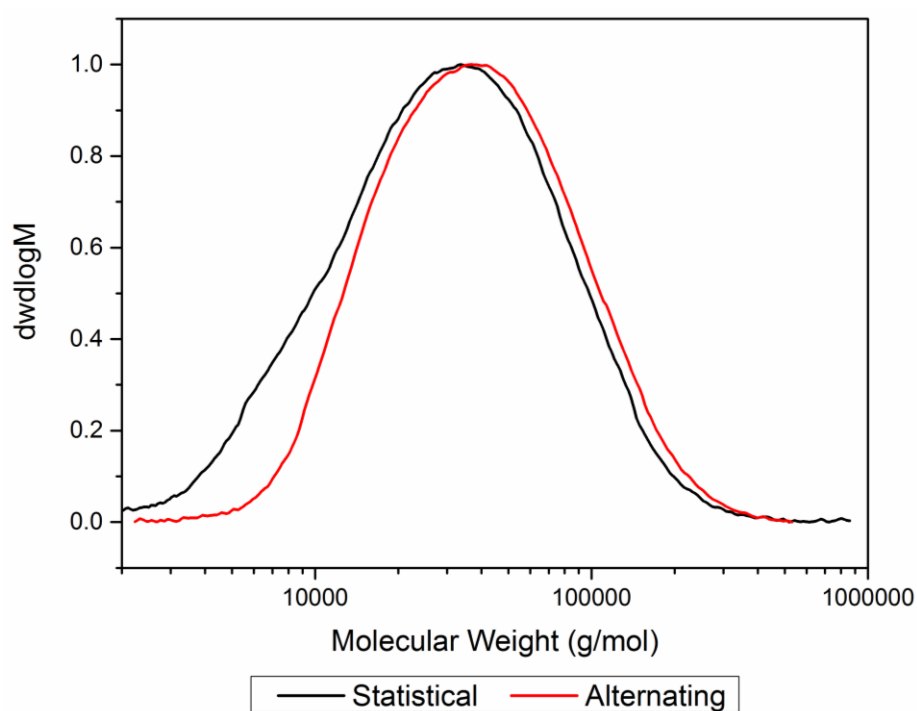
Figure 2.8 : Molecular weight distributions of PTBnDT-*stat*-PTBT *alt*-PBnDTDTBT.
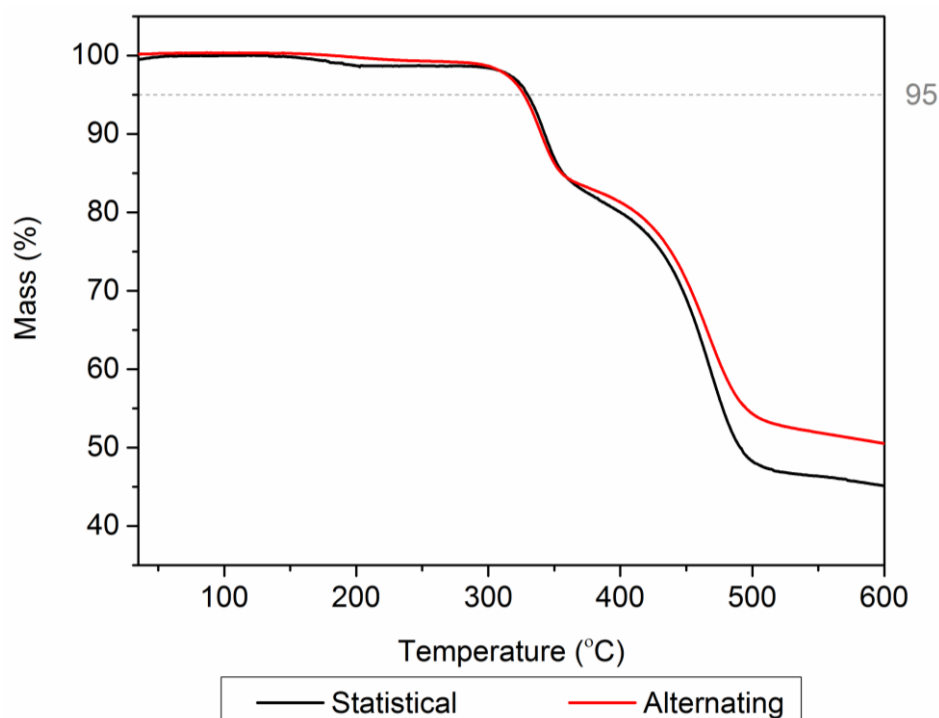
Figure 2.9: Thermogravometric analysis (TGA) of PTBnDT-s*tat*-PTBT *alt*-PBnDTDTBT, 5 % mass loss is indicated by intersection with the dashed grey line.

2.2.2: Optoelectronic Properties of Alternating and Statistical Polymers

To understand how the structural differences between PTBnDT-*stat*-PTBT and alternating PTBnDTTBT effect the polymers performance in BHJ-OPVs, we first examined their optoelectronic properties, summarised in Table 2.3.

Table 2.3: Summary of optoelectronic properties of PTBnDT-*stat*-PTBT and *alt*-PTBnDTTBT.

Ligand	$\lambda_{max}^{soln(25)}$ (nm)	$\lambda_{max}^{soln(90)}$ (nm)	λ_{max}^{film} (nm)	λ_{onset}^{film} (nm)	E_g (eV)	E_{HOMO} (eV)	E_{LUMO} (eV)
Statistical	545	511	554	697	1.78	-5.5	-3.7
Alternating	590	545	590	695	1.78	-5.3	-3.5

Both the alternating and statistical copolymer have a similar onset to absorption (λ_{onset}^{film}) and E_g therefore increased J_{sc} cannot be assigned to a more complete harvesting of the solar spectrum (*i.e.* generation of a greater number of excitons). The alternating copolymer exhibits a strong absorption with λ_{max}^{film} of 590 nm which can be assigned to intramolecular charge transfer (ICT) between the donor and accepting species (Figure 2.6). A pronounced shoulder at $\lambda = 650$ nm is also visible indicating a significant degree of intermolecular interaction through π-stacking. This shoulder is less pronounced in solution at 25 °C and has no contribution at 90 °C as the weak intermolecular π-interactions breakdown.

The main ICT peak of the statistical copolymer film (Figure 2.10) is blue shifted compared to that of the alternating polymer and occurs at $\lambda = 554$ nm, most noticeably two more peaks are visible in the ICT region for the statistical copolymer, the first centred at $\lambda = 510$ nm and the second at $\lambda = 480$ nm. This evidence suggests the presence of more than one ICT couple, which may be expected due to the varying distribution of BT and BnDT throughout the backbone resulting in a number of distinct covalently bound chromophores. Similarly to the alternating polymer a shoulder centred at $\lambda = 650$ nm is attributed to intermolecular π-stacking which breaks down as the solution is heated. The contribution of π-stacking is noticeably weaker in the statistical copolymer, the regular structure of the alternating copolymer leads to better packing and formation of large aggregates which is indicative of a more crystalline polymer in the solid state. While crystalline polymers have been shown to have good hole transport properties, more

ordered polymers have been reported to be less miscible with $PC_{61}BM$, leading to undesirable BHJ morphology ultimately resulting in a drop in J_{sc}.[23,24]
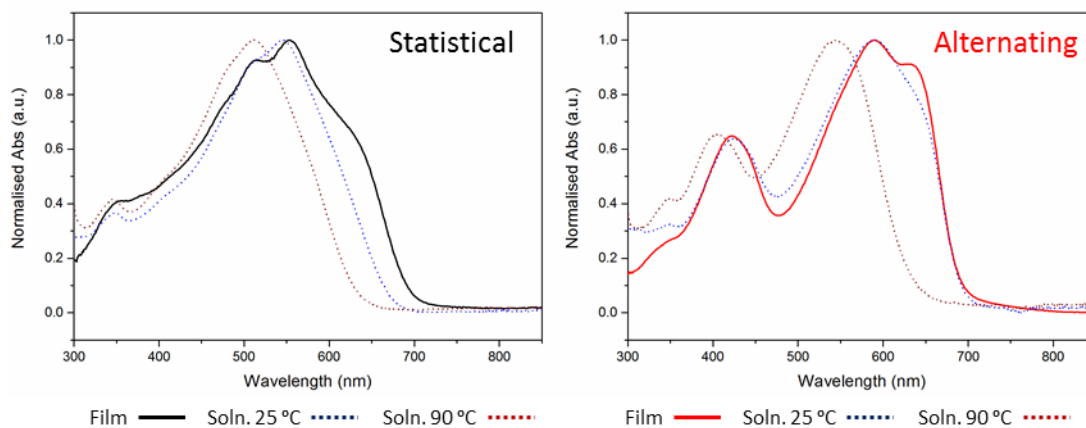
Figure 2.10: Left; normalised UV-Vis absorption of PTBnDT-*stat*-PTBT in a film and, hot and cols solution of chlorobenzene. Right; normalised UV-Vis absorption of alternating PTBnDTTBT in a film and hot and cold solution of chlorobenzene.

The energy with respect to vacuum of the HOMO level of each polymer was estimated from the onset to the oxidation (V_{onset}) potential as measured by CV *vs.* a ferrocene standard; the LUMO was then calculated by considering the optical band gap ($E_{HOMO)}$ + E_g^{opt}).[25,26] The oxidative cyclic voltammograms are shown in Figure 2.11, where the statistical copolymer exhibits a lower onset to oxidation at 1.22 V corresponding to HOMO of -5.46 eV which is lower than that of the alternating polymer (V_{onset} = -1.07 V, HOMO = -5.31 V). The deeper lying HOMO of the statistical polymer is, in part, responsible for the higher V_{oc} exhibited by the polymer (Figure 2.1 and Table 2.1).[27] The shape of the CVs differ greatly, with the large, sharp peak at approximately 1.2 V in the alternating polymer film indicative of more crystalline domains with a lower oxidation energy. The broad multi-modal peak observed for the statistical copolymer suggests there may be some degree of crystallinity combined with amorphous regions, which require slightly more energy to remove an electron.[23]
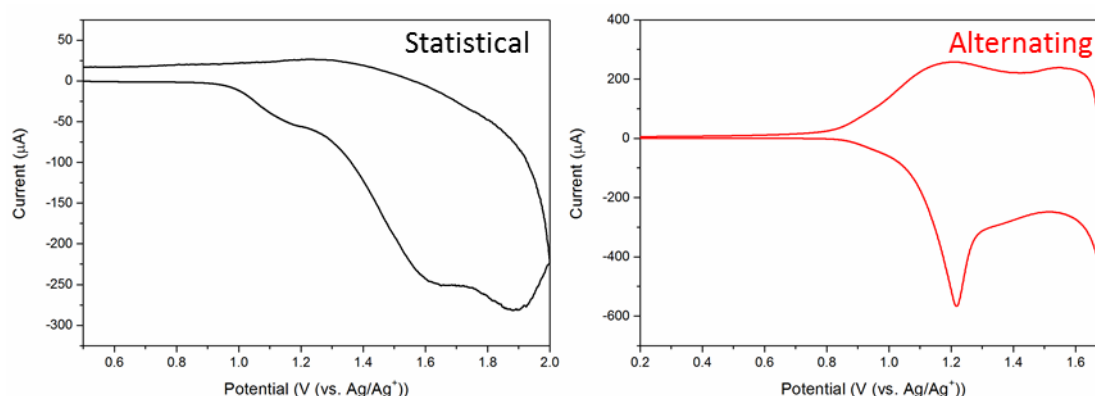
Figure 2.11 : Cyclic voltammograms showing the oxidative process of PTBnDT-stat-PTBT (left, black) and *alt*-PBnDTDTBT (right, red).

2.2.3: Morphological Properties of Alternating and Statistical Polymers

The morphology of the polymers and their $PC_{61}BM$ blends on a clean ITO surface were investigated by AFM. Polymer films were spin cast from 10 mg/ml solution on to ITO and annealed for 5 minutes at 180 °C, polymer : $PC_{61}BM$ (1 : 1.5) blends were spin cast from a 25 mg/ml solution and annealed. The 5 μm^2 (Figure 2.12a and Figure 2.12c) image of the *alt*-PBnDTDTBT polymer shows few features of intrigue although small aggregates of 200-500 nm can be identified. Closer inspection of the film with a 1 μm^2 scan (Figure 2.12b and Figure 2.12d) reveals that the film is homogenous (aside from the aggregates) and there is unlikely to be microphase separation of the polymer chains as expected.

In the *alt*-PBnDTDTBT polymer : $PC_{61}BM$ blend film large crystallite structures are observed which are likely to be $PC_{61}BM$ crystals (Figure 2.13), some of which are greater than 3 μm in length. Inspection of the surrounding film (figure 2.13b) shows regions of surface rougher than that of the pure polymer film (route mean square 1.554 nm of *vs.* 0.744 nm), this is indicative of local incorporation of $PC_{61}BM$. The large pure domains of $PC_{61}BM$ are undesirable, while they will have good charge transport properties[28] they reduce the volume of $PC_{61}BM$-polymer interface and limit charge separation, which may be responsible for the lower observed J_{sc} in devices fabricated using the alternating polymer.[29,30]
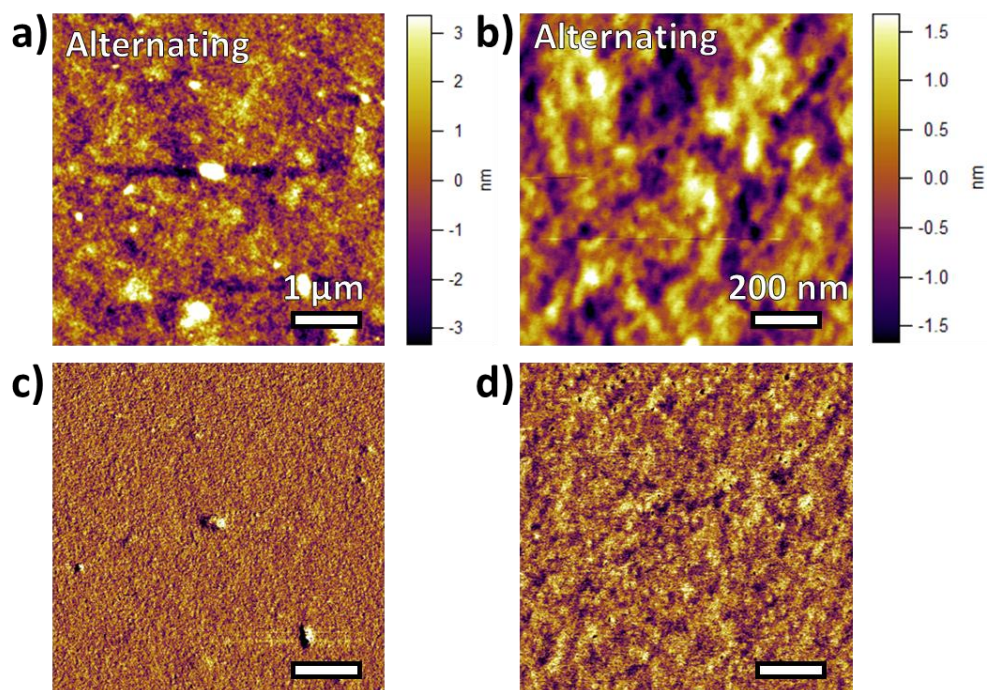
Figure 2.12: a; 5 μm² AFM height image of the *alt*-PBnDTDTBT polymer on ITO (scale bar 1 μm), b; 1 μm² AFM height image of the *alt*-PBnDTDTBT polymer on ITO (scale bar 200 nm), c; phase image of 2.12a, d; phase image of 2.12b.
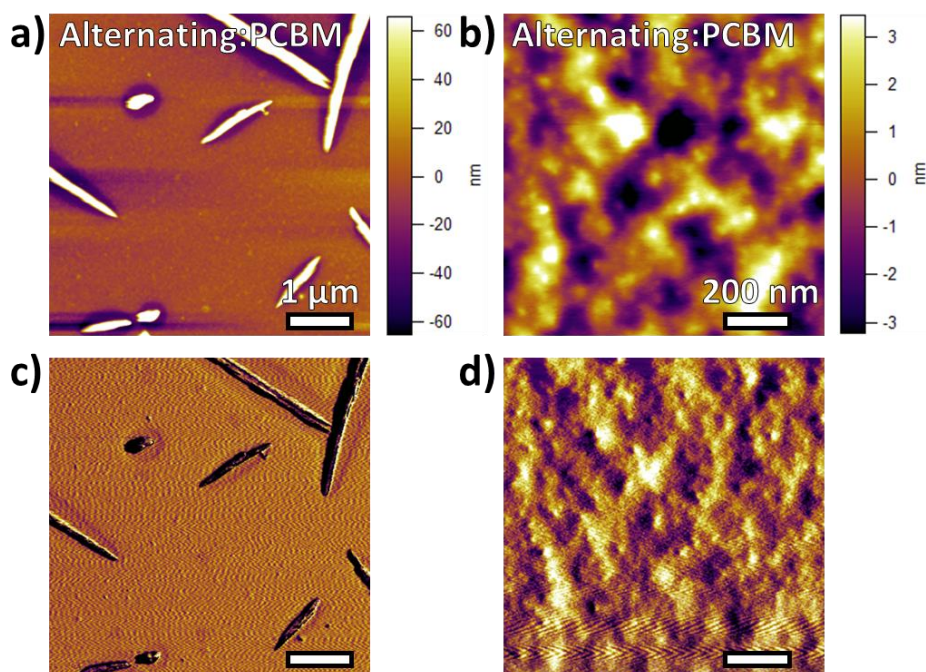
Figure 2.13: a; 5 μm² AFM height image of the *alt*-PBnDTDTBT polymer : PC$_{61}$BM blend on ITO (scale bar 1 μm), b; 1 μm² AFM height image of the *alt*-PBnDTDTBT polymer : PC$_{61}$BM blend on ITO (scale bar 200 nm), c; phase image of 2.13a, d; phase image of 2.13b.

The height and phase images of the PTBnDT(C$_{12}$)-*stat*-PTBT polymer film are presented in Figure 2.10. The statistical copolymer exhibits a similar roughness of 1.187 nm to its alternating counterpart (Figure 2.12) but is devoid of any aggregates. The homogeneity of the statistical film is reflected in the smooth featureless phase images (Figure 2.14c and 2.14d). Analysis of the PTBnDT(C$_{12}$)-*stat*-PTBT : PC$_{61}$BM blend reveals no large aggregates or phase separation of PC$_{61}$BM into crystal-like structures in contrast to the alternating polymer (Figure 2.13). The smooth film demonstrates that the statistical copolymer has superior miscibility with the PC$_{61}$BM, and in the phase image (Figure 2.15) there is also indication of sub 100 nm domain sizes with the possibility of some mixed domains which have been observed in successful devices.
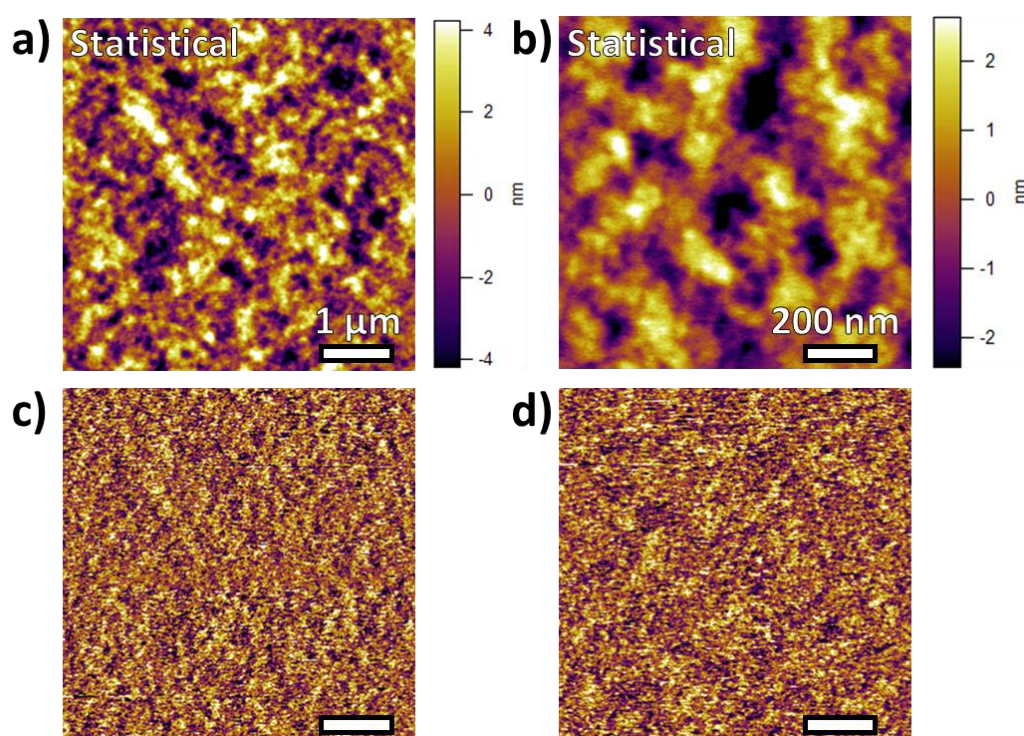
Figure 2.14: a; 5 μm² AFM height image of the PTBnDT-*stat*-PTBT polymer on ITO (scale bar 1 μm), b; 1 μm² AFM height image of the PTBnDT-*stat*-PTBT polymer on ITO (scale bar 200 nm), c; phase image of 2.14a, d; phase image of 2.14b.
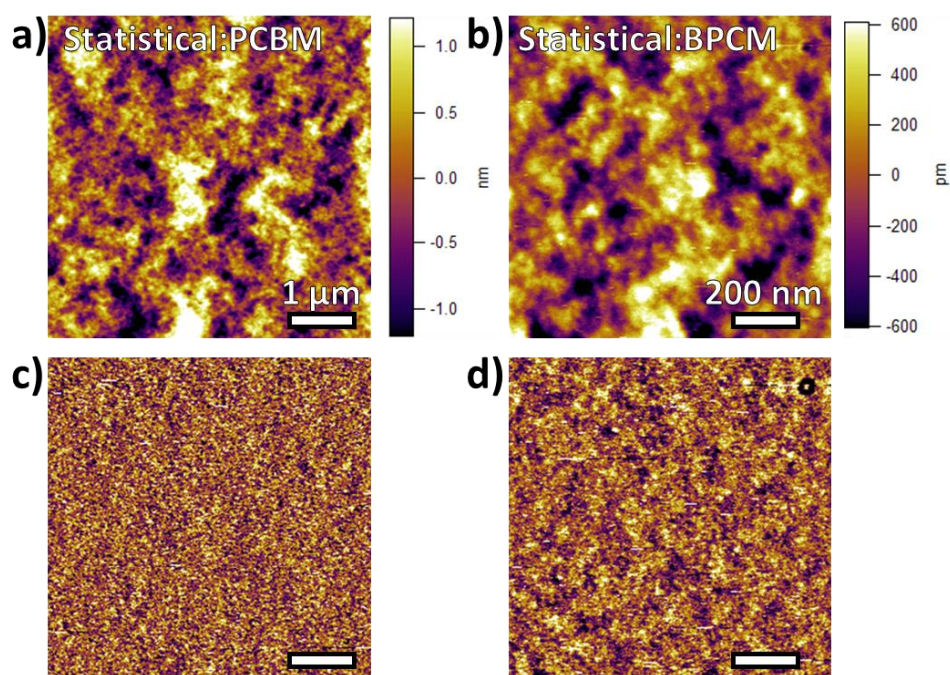
Figure 2.15: a; 5 μm² AFM height image of the PTBnDT-*stat*-PTBT polymer : PC₆₁BM blend on ITO (scale bar 1 μm), b; 1 μm² AFM height image of the PTBnDT-*stat*-PTBT polymer : PC₆₁BM blend on ITO (scale bar 200 nm), c; phase image of 2.15a, d; phase image of 2.15b.

2.3: Conclusions

The structural differences between the alternating polymer *alt*-PBnDTDTBT and its statistical counterpart PTBnDT-*stat*-PTBT where elucidated through kinetic studies and STM. This work has demonstrated that the monomers used in this particular system proceed through the Stille coupling reaction at different rates and result in gradient or block-like polymer structures. We assign the differing rates to the distinctly different electronic properties of the monomeric species. The resulting statistical polymer shows similar optical properties to the alternating counterpart, although some additional ICT states are inferred. Largely the superior performance of the statistical copolymer can be assigned to morphological differences in the BHJ of the OPVs. The diminished miscibility of the alternating copolymer with $PC_{61}BM$, a result of its lower solubility arising from its more regular structure and ability to form large aggregates, causes some phase separation in the in the BHJ. While the large $PC_{61}BM$ crystallites will have good electron transport properties, the reduction in the polymer-$PC_{61}BM$ interfacial area results in decreased charge separation and reduction in the J_{sc} of the devices. The greater efficiency of the statistical copolymer may also be ascribed to the deeper HOMO of the polymer, the increased polymer-HOMO fullerene-LUMO gap results in a greater V_{oc}.

2.4: Experimental

2.4.1: Materials

2,6-Dibromo-4,8-didodecylbenzo[1,2-b:4,5-b']dithiophene, 4,7-dibromo-5,6-bis(octyloxy)benzo[c][1,2,5]thiadiazol, 2,5-bis(trimethylstannyl)thiophene and phenyl-C_{61}-butyric acid methyl ester ($PC_{61}BM$) were provided by Merck ltd. Anhydrous chlorobenzene (99.9 %) was purchased from ACROS Organics and used without further purification. Tris(dibenzylideneacetone)dipalladium(0) ($Pd_2(dba)_3$) was purchased from sigma Aldrich and recrystallised from chloroform to obtain $Pd_2(dba)_3.CHCl_3$. Tri(*o*-tolyl)phosphine was purchased from Sigma Aldrich and recrystallised from hexane. Tetreabutylammonium hexafluorophosphate (99.9 %), silver nitrate, ferrocene (99.9 %), butylated hydroxytoluene and 2-tributylstannyl thiophene were purchased from Sigma-Aldrich and used without further purification.

2.4.2: Methods

NMR. ^{1}H NMR was run on a Bruker Avance 300 MHz spectrometer in deuterated chloroform at 25 °C. High temperature and *in-situ* kinetic data was obtained using Bruker Avance III 400 MHz spectrometer at 100 °C.

Optoelectronic properties. UV-Vis spectra where obtained using an Agilent Technologies Cary 60 UV-Vis spectrometer. Samples were made up to a concentration of 0.01 mg/ml by serial dilution in chlorobenzene. Cyclic voltammetry was conducted on a CH-Instruments 600 E potentiostat using a 3 mm glassy carbon disc electrode which was polished with 0.05 μm alumina powder, rinsed sequentially with acetone, IPA and MilliQ water prior to each use. The counter electrode was a platinum wire coil which was annealed in a blue flame prior to use. The reference electrode was Ag/Ag^+, the silver wire was polished and rinsed sequentially with acetone, IPA and MilliQ water the wire was then placed into a glass capillary tube fitted with a vycor frit and filled with 0.01 mM $AgNO_3$ solution. The system was calibrated using the ferrocene(Fc)/ferrocenium(Fc^+) redox couple. 0.100 M tetrabutylammonium hexafluorophosphate ($TBAPF_6$) was used as the supporting electrolyte. Analytes were dissolved at a concentration of 2 mg/ml in a solution of 2 mg/ml of $TBAPF_6$ in chlorobenzene, drop cast onto the clean glassy carbon disk electrode and allowed to dry under ambient conditions.

Gel permeation chromatography. GPC was run on an Agilent PL220 instrument equipped with differential refractive index (DRI) and viscometry (VS) detectors. The system was equipped with 2 x PLgel Olexis columns (300 x 7.5 mm) and a PLgel Olexis 10 μm guard column. The mobile phase was 1,2,4-trichlorobenzene (TCB) with 250 ppm BHT (butylated hydroxytoluene) as the stabilising additive. Samples were run at 1 ml/min at 160 °C. The system was calibrated between M_p = 164 and 6,035,000 g/mol using 12 polystyrene narrow standards (Agilent EasyVials) to create a third order calibration. Analyte samples were filtered through a stainless steel frit with 10 μm pore size at 140 °C prior to injection. Experimental molar mass (M_n, GPC) and dispersity ($Đ$) values of synthesised polymers were determined by conventional calibration using Agilent GPC/SEC software.**TGA Measurements.** TGA spectra were recorded on a Mettler Toledo TGA/DSC1. Samples were analysed from 25 to 600 °C at a 10 °C min^{-1} heating rate under a nitrogen atmosphere.**AFM measurements.** Polymer and Polymer : PC$_{61}$BM films were spin cast at 2000 RPM for 60 seconds from a 10 mg/ml solution of polymer and 25 mg/ml 1 : 2 polymer:PC$_{61}$BM in chlorobenzene. Films were cast onto ITO coated glass and annealed at 180 ° C for 5 minutes. Atomic Force Microscopy images were obtained using an Asylum Research MFP-3D AFM, using AC 240-TS probes with a spring constant of 0.67 - 3.51 N/m purchased from oxford instruments in intermittent contact (tapping) mode. Images were analysed and processed using the Igor software package.

2.4.3: Experimental Procedures

***In-situ* kinetics.** All solids were dried overnight under vacuum at < 1 mbar at 25 ° C, 99.9 % anhydrous chlorobenzene was purged with nitrogen prior to use. 1 ml, 0.100 M stock solutions of 2,6-dibromo-4,8-didodecylbenzo[1,2-b:4,5-b']dithiophene (BnDT) 68.5 mg (0.100 mmol), 4,7-dibromo-5,6-bis(octyloxy)benzo[c][1,2,5]thiadiazol (BT) 55.0 mg (0.100 mmol) and 2-(tributylstannyl)thiophene 37.3 mg (32 μL, 0.100 mmol) were made up and stored under an atmosphere of nitrogen. 1 ml of catalyst solution was made up from of Pd$_2$(dba)$_3$.CHCl$_3$ 2.0 mg (2 μmol) and of P(o-tolyl)$_3$ 3.6 mg 6 μmol. To a dry NMR tube fitted with a Young's tap, under a blanket of Argon 50 μL BnDT, 50 μL BT, 100 μL 2-(tributylstannyl)thiophene and 100 μL catalysts solutions were added with an additional 100 μL of dry chlorobenzene. A capillary tube filled with degassed 1,1,2,2-tetrachloroehtane-D$_2$ was added as a locking agent. The NMR tube was placed in liquid

nitrogen to effectively halt any reaction prior to loading. An NMR was taken at 25 °C before the probe cavity was heated to 100 °C and a second spectrum (T 373 K, t = 0) was taken, after which the ^{1}H NMR spectrum was recorded every 120 seconds for two hours.

Polycondensation kinetics. To a dry 100 ml, 3-neck-round bottom flask 275.3 mg (0.500 mmol) 4,7-Dibromo-5,6-bis(octyoxy)-benzo-2,1,3-thiadiazole, 342.3 mg (0.500 mmol) 2,6-dibromo-4,8-di(dodecyl)benzo-[1,2-b:4,5-b']dithiophene and 409.8 mg (1.000 mmol) of 2,5-bis(trimethylstannyl)thiophene were added. The central neck was fitted with a condenser, the top of which was sealed with a rubber septum and the remaining two necks were fitted with rubber septa. The system was evacuated and refilled with nitrogen gas for three cycles. 48.0 mL of dry, degassed chlorobenzene was cannulated into the flask which thereafter was kept under a positive nitrogen pressure.

To a separate glass sinter vial 31.1 mg (0.030 mmol) of tris(dibenzylideneacetone)dipalladium(0)-chloroform adduct and 54.8 mg of P(*o*-tolyl)$_3$ (0.18 mmol) were added. The glass sinter vial was sealed with a rubber septum, evacuated and back filled with nitrogen for three cycles. 3 ml of dry chlorobenzene was added via a degassed syringe.

The main reaction vessel was refluxed to 133 °C. A t = 0 sample (100 μL) was taken before 2 ml of the fully solvated catalyst solution was added via a degassed syringe. Further 100 μL samples were taken at t = 1, 2, 3, 4, 5, 10, 15, 20, 25, 30, 60, 120, 180, 240, 300 and 1440 min, and quenched by bubbling with air. Monomer conversion was followed by ^{1}H NMR in Chloroform-D at 25 °C.

Statistical Polymer Synthesis. To a dry 100 ml, 2-neck 100 ml round bottom flask 55.1 mg (0.100 mmol) 4,7-Dibromo-5,6-bis(octyoxy)-benzo-2,1,3-thiadiazole, 68.5 mg (0.100 mmol) 2,6-dibromo-4,8-di(dodecyl)benzo-[1,2-b:4,5-b']dithiophene and 77.8 mg (0.190 mmol) of 2,5-bis(trimethylstannyl)thiophene were added. The central neck was fitted with a condenser, the top of which was sealed with a rubber septum, and the remaining neck was fitted with rubber septum. The system was evacuated and refilled with nitrogen gas for three cycles. 8.0 mL of dry, degassed chlorobenzene was cannulated into the flask which thereafter was kept under a positive nitrogen pressure.

To a separate glass sinter vial 4.1 mg (0.004 mmol) of tris(dibenzylideneacetone)dipalladium(0)-chloroform adduct and 7.3 mg (0.024 mmol) of

P(*o*-tolyl)₃ were added. The glass sinter vial was sealed with a rubber septum, evacuated and back filled with nitrogen for three cycles. 3 ml of dry chlorobezene was added *via* a degassed syringe. 2.0 ml of the premixed catalyst solution was then added to the reaction mixture.

The reaction mixture was refluxed at 133 °C for 24 hours, the resulting polymeric solution was then reduced under vacuum to approximately 2 ml. The polymer was precipitated into 150 ml of methanol and filtered through a cellulose thimble. The polymer was then purified by Soxhlet extraction with acetone, hexanes and chloroform. The chloroform fraction was precipitated into 150 ml of methanol and collected by vacuum filtration. The polymer was dried under vacuum at 40 °C for 24 hours.

The resulting polymer was characterised by ^{1}H NMR (Figure 2.16) δ(ppm) =: 8.70-8.43 (2H, d) corresponding to the two hydrogens an the benzodithiphene unit, 7.74-7.16 (4H, m) result from the four protons of the bridging thiophene, 4.34 (4H, s) is assigned the α-CH₂ protons of the alkoxy side chains on the BT unit, 3.29 (4H, s) are assigned to the α-CH₂ of the alkyl side chains of the BnDT unit, 2.50-0.68 area is assigned to the remaining protons of the alkylside chains on both the BT and BnDT unit. Characterisation by TGA (Figure 2.17) show the T_D = 329 °C. Molecular weight averages as determined by GPC (Figure 2.18) are M_n = 17,600 g/mol, M_w = 44,800 g/mol and the dispesity is 2.55. The optical properties were characterised by UV/Vis and CV (Figure 2.19 and Figure 2.20, respectively) and are summarised in Table 2.3 (Section 2.2.2.).
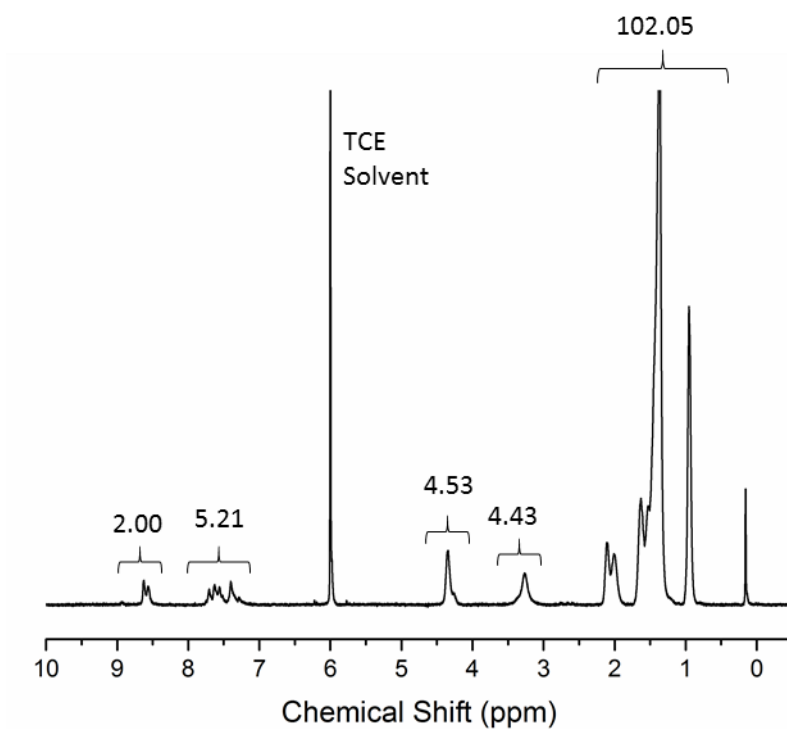
Figure 2.16: ¹H NMR of statistical PTBnDT-*stat*-PTBT in 1,1,2,2-rtetrachloroethane-D₂.
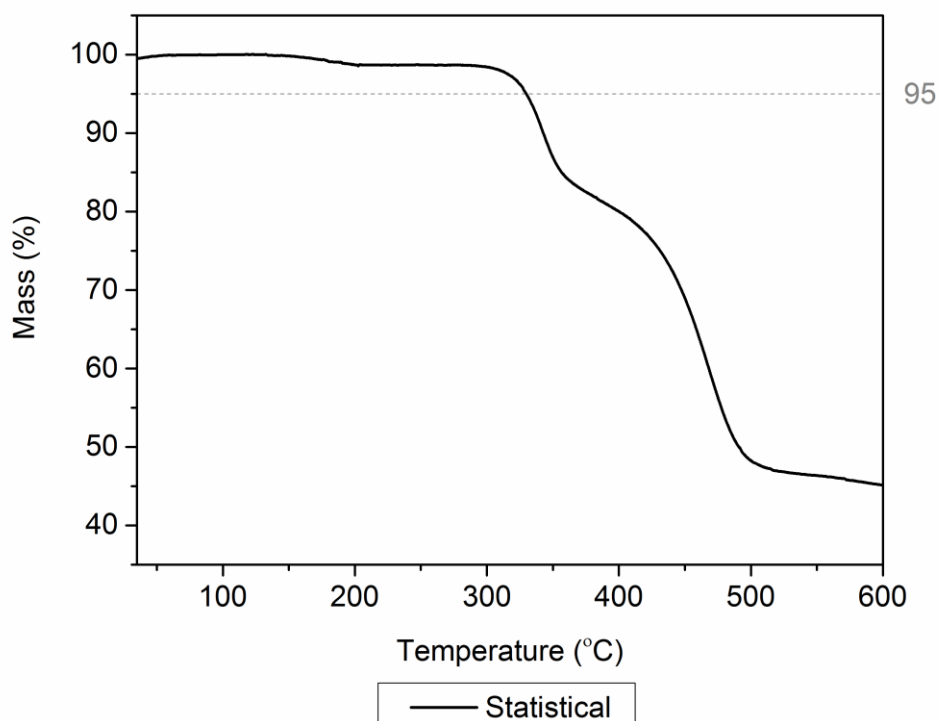
Figure 2.17: TGA of statistical PTBnDT-*stat*-BTBT.
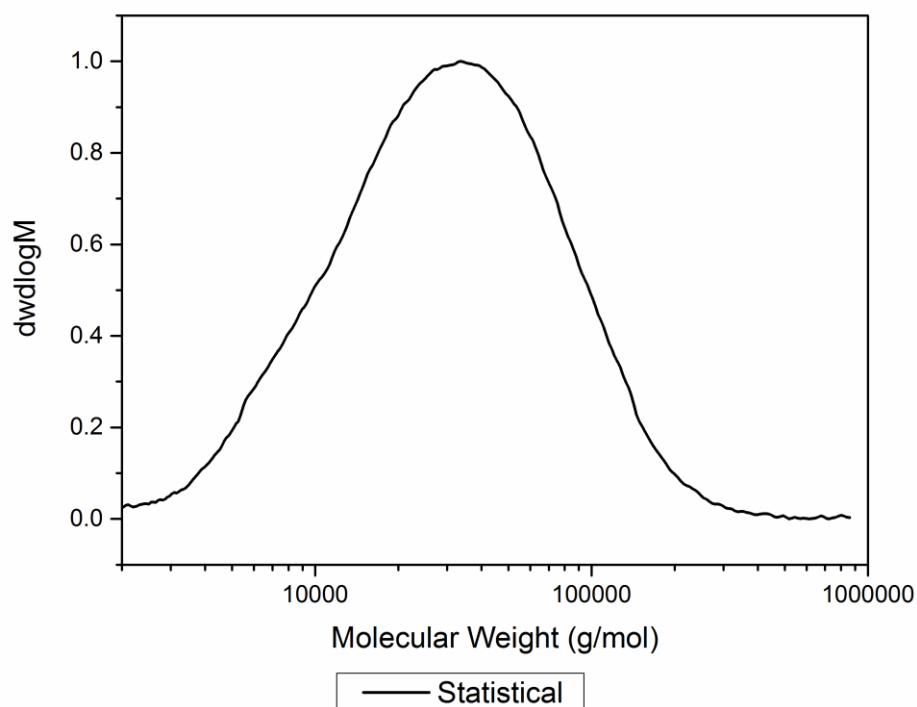
Figure 2.18: Molecular weight distribution of PTBnDT-*stat*-PTBT.
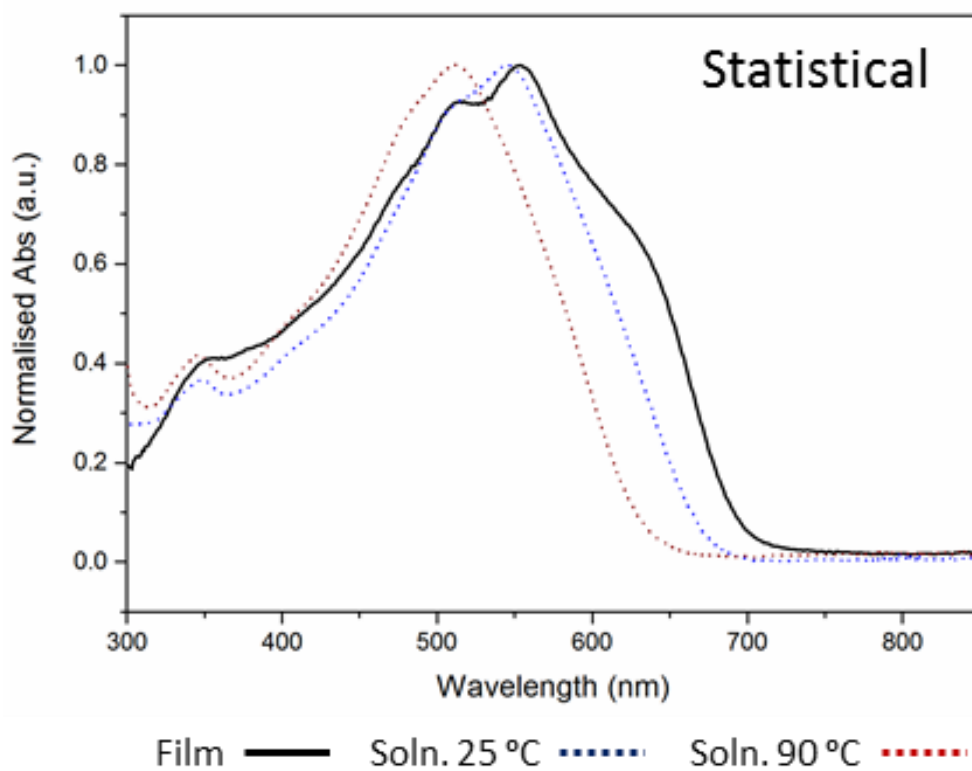
Figure 2.19: UV/Vis trace of PTBnDT-*start*-PTBT, thin film on ITO and, hot and cold solution of chlorobenzene.
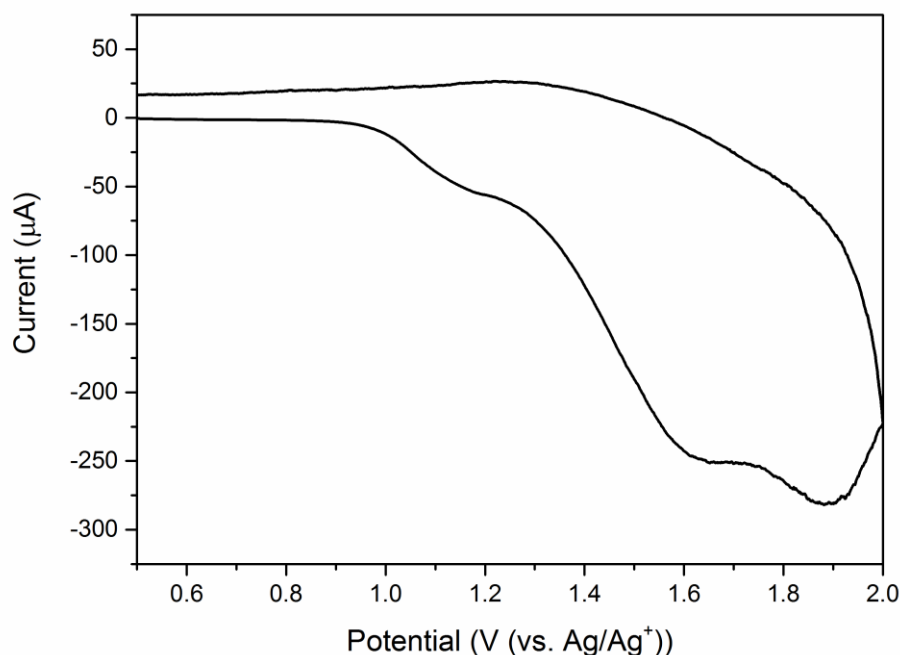
Figure 2.20: Cyclic voltamogramme of PTBnDT-*stat*-PTBT showing the oxidation peak.

Alternating Polymer Synthesis. To a dry 100 ml, 2-neck 100 ml round bottom flask 142.9 mg (0.200 mmol) of 4,7-bis(5-bromothiophen-2-yl)-5,6-bis(octyloxy)benzo[c][1,2,5]thiadiazole and 162.0 mg (0.190 mmol) of (4,8-didodecylbenzo[1,2-b:4,5-b']dithiophene-2,6-diyl)bis(trimethylstannane) were added. The central neck was fitted with a condenser, the top of which was sealed with a rubber septum, and the remaining neck was fitted with rubber septum. The system was evacuated and refilled with nitrogen gas for three cycles. 8.0 mL of dry, degassed chlorobenzene was cannulated into the flask which thereafter was kept under a positive nitrogen pressure.

To a separate glass sinter vial 4.1 mg (0.004 mmol) of tris(dibenzylideneacetone)dipalladium(0)-chloroform adduct and 7.3 mg (0.024 mmol) of P(*o*-tolyl)₃ were added. The glass sinter vial was sealed with a rubber septum, evacuated and back filled with nitrogen for three cycles. 3 ml of dry chlorobezene was added *via* a degassed syringe. 2.0 ml of the premixed catalyst solution was then added to the reaction mixture.

The reaction mixture was refluxed at 133 °C for 24 hours, the resulting polymeric solution was then reduced under vacuum to approximately 2 ml. The polymer was precipitated

into 150 ml of methanol and filtered through a cellulose thimble. The polymer was then purified by Soxhlet extraction with acetone, hexanes, chloroform and chlorobenzene (owing to the limited solubility of the alternating polymer). The chlorobenzene fraction was precipitated into 150 ml of methanol and collected by vacuum filtration. The polymer was dried under vacuum at 40 °C for 24 hours.

The resulting polymer was characterised by ^{1}H NMR (Figure 2.121) δ(ppm) =: 8.57 (2H, s) corresponding to the two hydrogens an the benzodithiophene unit, 7.83-7.62 (2H d) result from the protons of the bridging thiophene unit which are spatially close to the BnDT unit, 7.62-7.43 (2H, d) arise from the remaining two protons on thiophene bridging unit which are spatially close to the BT unit, 4.34 (4H, s) is assigned the α-CH$_2$ protons of the alkoxy side chains on the BT unit, 3.29 (4H, s) are assigned to the α-CH$_2$ of the alkyl side chains of the BnDT unit, 2.50-0.68 area is assigned to the remaining protons of the alkylside chains on both the BT and BnDT unit. Characterisation by TGA (Figure 2.22) show the T_D = 326 °C. Molecular weight averages as determined by GPC (Figure 2.23) are M_n = 27,500 g/mol, M_w = 52,800 g/mol and the dispesity is 1.92. The optical properties were characterised by UV/Vis and CV (Figure 2.24 and Figure 2.25, respectively) and are summarised in Table 2.3 (Section 2.2.2.).
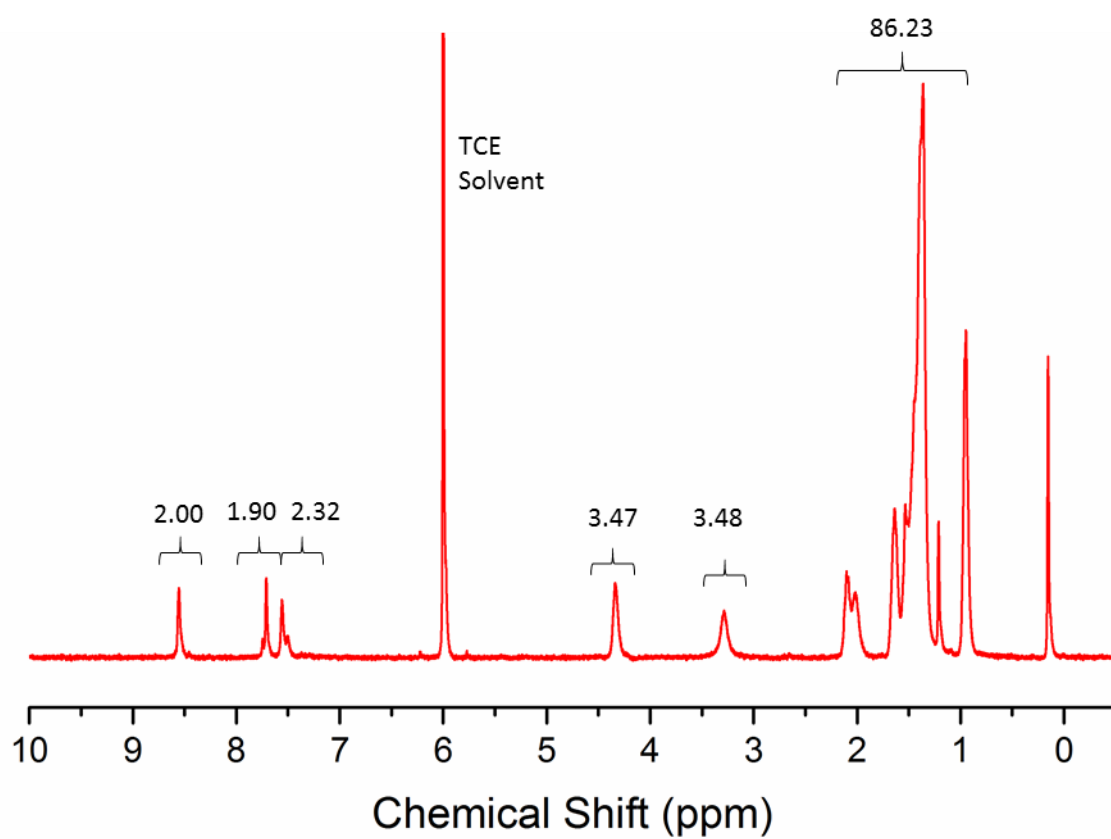
Figure 2.21: ^{1}H NMR of alternating PBnDTDTBT in 1,1,2,2-tetrachloroethane-D$_2$.
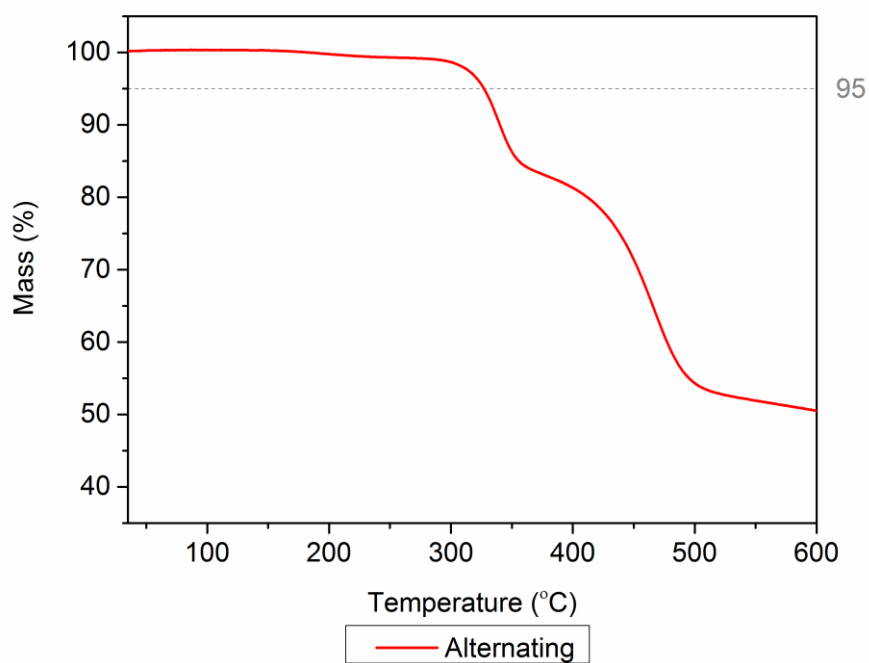
Figure 2.22: TGA of alternating PBnDTDTBT.
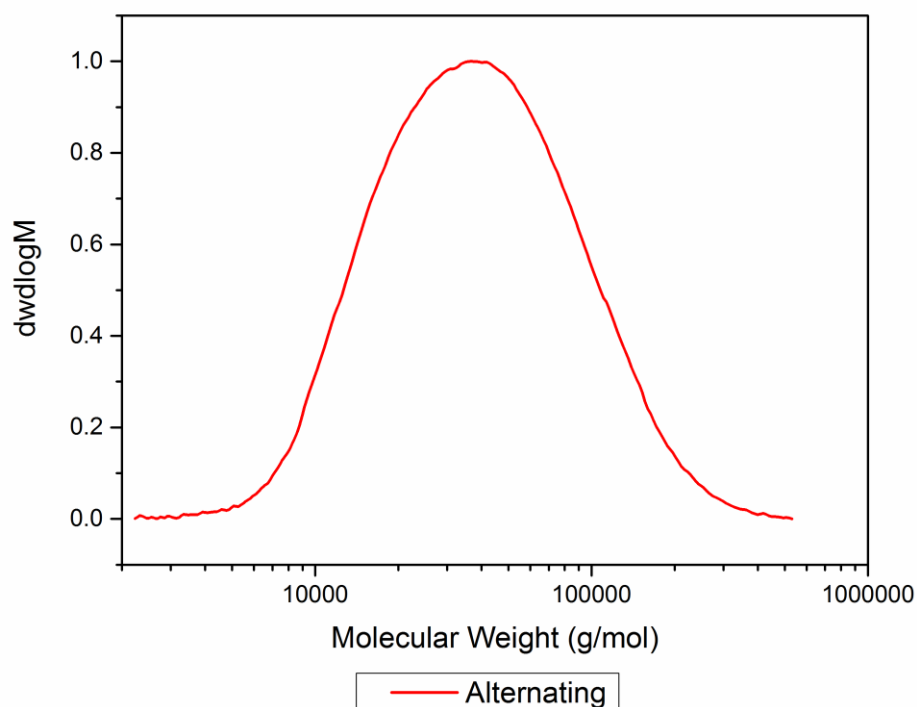
Figure 2.23: Molecular weight distribution of alternating PBnDTDTBT.
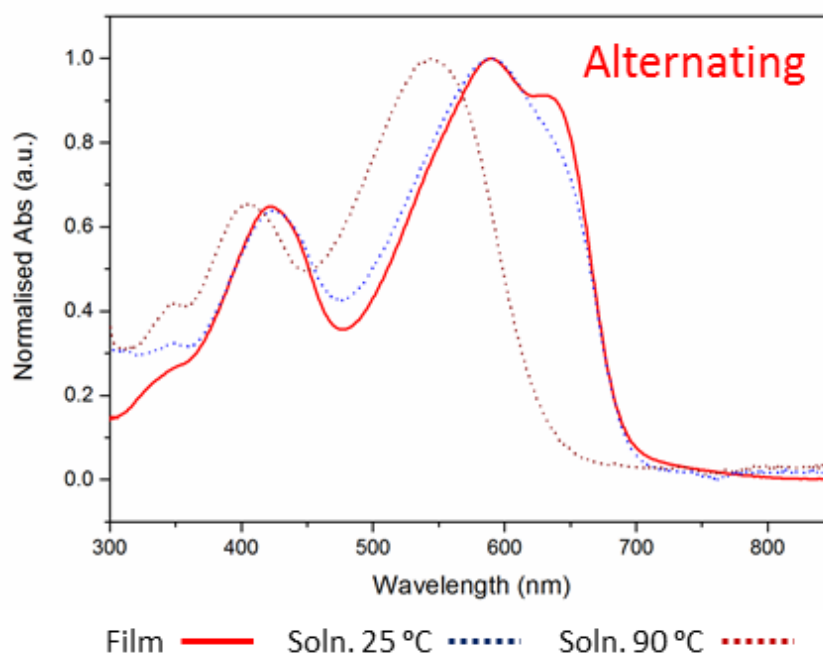
Figure 2.24: UV/Vis trace of alternating PTBnDTDTBT, thin film on ITO and, hot and cold solution of chlorobenzene.
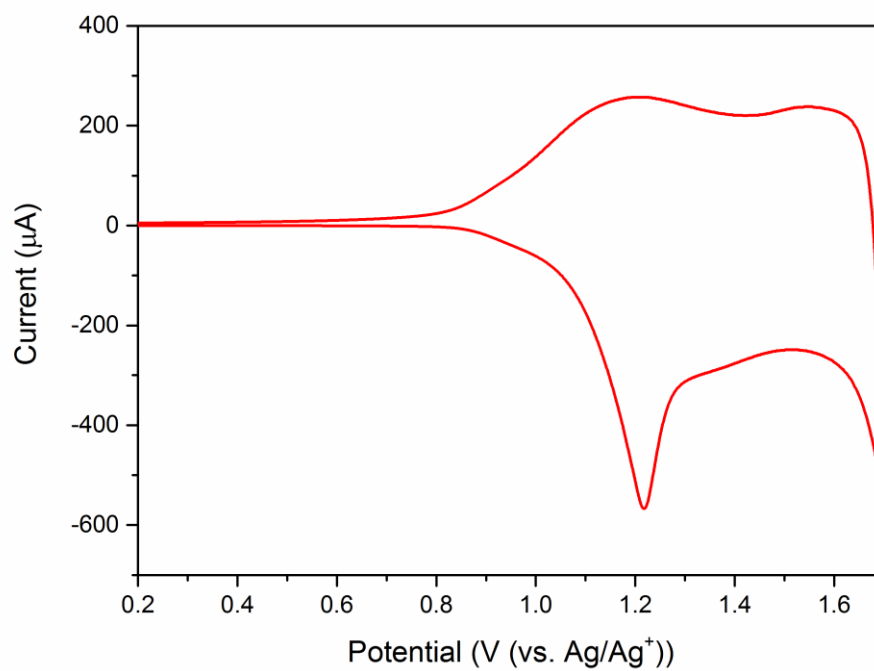
Figure 2.25: Cyclic voltamogramme of alternating PBnDTDTBT showing the oxidation peak.

2.5: References

(1)   Kang, T. E.; Choi, J.; Yoon, S. C.; Kim, B. J. *Macromolecules* **2016**, *49*, 2096.

(2)   Su, Q.; Tong, J.; Li, J.; Zhang, P.; Yang, C.; Zhang, C.; Wang, F.; Chen, D.; Xia, Y. *Polym. J.* **2015**, *47*, 803.

(3)   Wang, X. C.; Wang, K.; Wang, M. F. *Polym. Chem.* **2015**, *6*, 1846.

(4)   Hendriks, K. H.; Heintges, G. H. L.; Wienk, M. M.; Janssen, R. A. J. *J. Mater. Chem. A* **2014**, *2*, 17899.

(5)   Menelaou, C.; Tierney, S.; Blouin, N.; Mitchell, W.; Tiwana, P.; McKerracher, I.; Jagadish, C.; Carrasco, M.; Herz, L. M. *J. Phys. Chem. C* **2014**, *118*, 17351.

(6)   Fang, L.; Zhou, Y.; Yao, Y. X.; Diao, Y.; Lee, W. Y.; Appleton, A. L.; Allen, R.; Reinspach, J.; Mannsfeld, S. C. B.; Bao, Z. A. *Chem. Mater.* **2013**, *25*, 4874.

(7)   Duan, C. H.; Gao, K.; van Franeker, J. J.; Liu, F.; Wienk, M. M.; Janssen, R. A. J. *J. Am. Chem. Soc.* **2016**, *138*, 10782.

(8)   Braunecker, W. A.; Oosterhout, S. D.; Owczarczyk, Z. R.; Kopidakis, N.; Ratcliff, E. L.; Ginley, D. S.; Olson, D. C. *Acs Macro Letters* **2014**, *3*, 622.

(9)   Zhang, S.; Bauer, N. E.; Kanal, I. Y.; You, W.; Hutchison, G. R.; Meyer, T. Y. *Macromolecules* **2017**, *50*, 151.

(10)   Gao, J.; Wang, W.; Zhang, S.; Xiao, S.; Zhan, C.; Yang, M.; Lu, X.; You, W. *J. Mater. Chem. A* **2018**, *6*, 179.

(11)   Zhang, Q. Q.; Kelly, M. A.; Bauer, N.; You, W. *Accounts Chem. Res.* **2017**, *50*, 2401.

(12)   Li, W. T.; Yang, L. Q.; Tumbleston, J. R.; Ade, H.; You, W. *Abstr. Pap. Am. Chem. S.* **2014**, *247*.

(13)   Ding, Z.; Kettle, J.; Horie, M.; Chang, S. W.; Smith, G. C.; Shames, A. I.; Katz, E. A. *J. Mater. Chem. A* **2016**, *4*, 7274.

(14)   Kim, J.-H.; Gadisa, A.; Schaefer, C.; Yao, H.; Gautam, B. R.; Balar, N.; Ghasemi, M.; Constantinou, I.; So, F.; O'Connor, B. T.; Gundogdu, K.; Hou, J.; Ade, H. *J. Mater. Chem. A* **2017**, *5*, 13176.

(15)   Zhou, H.; Yang, L.; Stuart, A. C.; Price, S. C.; Liu, S.; You, W. *Angew. Chem. Int. Edit.* **2011**, *50*, 2995.

(16)   Price, S. C.; Stuart, A. C.; Yang, L.; Zhou, H.; You, W. *J. Am. Chem. Soc.* **2011**, *133*, 4625.

(17)   Hou, J. H.; Park, M. H.; Zhang, S. Q.; Yao, Y.; Chen, L. M.; Li, J. H.; Yang, Y. *Macromolecules* **2008**, *41*, 6012.

(18)   Yao, H. F.; Ye, L.; Zhang, H.; Li, S. S.; Hou, J. H. *Chem. Revs.* **2016**, *116*, 7397.

(19)   Huo, L.; Hou, J. *Polym. Chem.* **2011**, *2*, 2453.

(20)   Zuo, G.; Li, Z.; Zhang, M.; Guo, X.; Wu, Y.; Zhang, S.; Peng, B.; Wei, W.; Hou, J. *Polym. Chem.* **2014**, *5*, 1976.

(21)   Tierney, S.; Heeney, M.; McCulloch, I. *Synthetic Metals* **2005**, *148*, 195.

(22)   Bronstein, H.; Chen, Z. Y.; Ashraf, R. S.; Zhang, W. M.; Du, J. P.; Durrant, J. R.; Tuladhar, P. S.; Song, K.; Watkins, S. E.; Geerts, Y.; Wienk, M. M.; Janssen, R. A. J.; Anthopoulos, T.; Sirringhaus, H.; Heeney, M.; McCulloch, I. *J. Am. Chem. Soc.* **2011**, *133*, 3272.

(23)   Sweetnam, S.; Graham, K. R.; Ngongang Ndjawa, G. O.; Heumüller, T.; Bartelt, J. A.; Burke, T. M.; Li, W.; You, W.; Amassian, A.; McGehee, M. D. *J. Am. Chem. Soc.* **2014**, *136*, 14078.

(24)   Treat, N. D.; Brady, M. A.; Smith, G.; Toney, M. F.; Kramer, E. J.; Hawker, C. J.; Chabinyc, M. L. *Adv. Eng. Mater.* **2011**, *1*, 82.

(25)   Leonat, L.; Beatrice Gabriela, S.; Branzoi, I. V. *Cyclic voltammetry for energy levels estimation of organic materials*, 2013; Vol. 75.

(26)   Bredas, J. L.; Beljonne, D.; Coropceanu, V.; Cornil, J. *Chem. Revs.* **2004**, *104*, 4971.

(27)   Brabec, C. J.; Cravino, A.; Meissner, D.; Sariciftci, N. S.; Fromherz, T.; Rispens, M. T.; Sanchez, L.; Hummelen, J. C. *Adv. Funct. Mater.* **2001**, *11*, 374.

(28)   Mayer, A. C.; Toney, M. F.; Scully, S. R.; Rivnay, J.; Brabec, C. J.; Scharber, M.; Koppe, M.; Heeney, M.; McCulloch, I.; McGehee, M. D. *Adv. Funct. Mater.* **2009**, *19*, 1173.

(29)   He, Y.; Li, Y. *Phys. Chem. Chem. Phys.* **2011**, *13*, 1970.

(30)   Hedley, G. J.; Ward, A. J.; Alekseev, A.; Howells, C. T.; Martins, E. R.; Serrano, L. A.; Cooke, G.; Ruseckas, A.; Samuel, I. D. W. *Nat. Comm.* **2013**, *4*, 2867.

Chapter 3: Varying Backbone Sequence through Modification of the Catalyst

Abstract: In Chapter One the different rates of monomer conversion in a statistical Stille polycondensation were discussed. Herein, the catalytic system is investigated with the aim of modifying the relative rate of conversion of the electron rich and electron deficient monomers. Use of different ligands on the palladium centre results in differing relative rates of monomer conversion and alters backbone sequence. The optoelectronic and morphological properties of the resulting polymers are found to vary with the degree of "randomness".

3.1: Introduction

In Chapter Two the backbone sequence of the Merck PTBnDT(C$_{12}$)-*stat*-PTBT formulation resulting from the catalyst (Pd$_2$(dba)$_3$:P(*o*-tolyl)$_3$) was investigated. It was hypothesised that, after oxidative addition with the active palladium catalyst, BnDT forms a more stable complex than BT, as a result of their distinctly different electronic properties (Section 2.2.1). The result of this is a blocky/gradient copolymer as BnDT was consumed up to 20 times faster than BT. The resulting polymer exhibited a lower lying HOMO and more favourable morphological properties for BHJ-OPVs accounting for the increased V$_{oc}$, J$_{sc}$ and FF observed in device tests.

The catalyst for a Stille polycondensation has been widely investigated,[1-7] however, most studies have focused on achieving a high catalytic stability and turnover, yielding high molecular weight materials.[8] While one recent study examined the effect of different catalysts on homo-coupling defects in the alternating copolymer PTB7-Th,[9] to our knowledge there has been no previous investigation into how altering the catalytic system effects the backbone sequence of a statistical terpolymerisation involving two competing brominated monomers.

In this study a range of ligands, with varying electron donation abilities, for Stille polycondensation are screened. The effect of each ligand (of differing donor abilities and steric bulk) on the rate of consumption of BnDT and BT is observed in a series of kinetic studies and the resulting polymeric materials have varying backbone structures (degrees of "randomness"). We then investigate how the "degree of randomness" effects the polymers morphological and optoelectronic properties and discuss which show more potential for use in polymer-fullerene BHJ-OPV devices.

3.2: Results and Discussion

3.2.1: Electronic and Steric Properties of Ligands

A Stille polycondensation commences with the oxidative addition of an alkynyl or aryl halide, in this instance 4,7-dibromo-5,6-bis(octyloxy)benzo[*c*][*1,2,5*]thiadiazole (BT) or 2,6-dibromo-4,8-didodecylbenzo[*1,2-b:4,5-b'*]dithiophene (BnDT) to a palladium centre. Building on Chapter Two, where it was demonstrated that the differing rates of conversion of BT and BnDT could lead to more block-like structure, Chapter Three explores alterations to the catalyst with the aim of achieving varying degrees of "randomness". We have hypothesised that the reduced rate of conversion of BT (relative to BnDT) is a consequence of its electron withdrawing nature creating an unstable palladium centre following oxidative addition. In an attempt to stabilise the palladium centre after oxidative addition we investigate the effect of modification of the ligands electron donation ability and additionally hope to influence the backbone sequence.

Ligands with additional electron donating groups on the phenyl rings such as methyl or methoxy substituent were selected, their donor ability was screened qualitatively by cyclic voltammetry and their results presented in Figure 3.1. In addition to the more electron rich triphenyl phosphine derivatives we also examine the use of the popular Buchwald ligand XPhos which is frequently used in the palladium catalysed cross-coupling reactions.[1,10] In addition, we also employ a more electron withdrawing ligand, triphenyl phosphite. Whilst electron donor ability is the focus of this study one must also consider the steric impact of each of these ligands, as such the electronic and steric properties (cone angle) are summarised in Table 3.1.

The values for the onset for oxidation of the ligands follow an expected trend, the most difficult to oxidise is the triphenyl phosphite, the electron withdrawing oxygens adjacent to the phosphine result in a more tightly bound lone pair and thus a greater potential is required to remove an electron. Tris(*o*-tolyl)phosphine (P(*o*-tolyl)$_3$) oxidises with relative ease compared to the triphyl phosphite species owing to the reduced electron withdrawing ability of the phenyl rings, although, the phosphorous lone pair is involved in conjugation with aromatic rings. The *ortho*-methoxy group in tris(2-methoxyphenyl)phosphine (P(*o*-OMePh)$_3$) pushes more electron density into the aromatic system, resultantly the lone pair of the phosphine is involved in conjugation with the phenyl rings to a lesser extent (than P(*o*-tolyl)$_3$). For tris-(2,4-dimethylphenyl) phosphine (P(2,4-Me$_2$Ph)$_3$) the two methyl groups increase the electron density of the

ring and therefore ease of oxidation from the phosphorus via lone pair, there is no literature value for the cone angle of this rarely used ligand. Unfortunately it is expected to be between that of P(o-tolyl)₃ and tris(2,4,6-trimethylphenyl)phosphine (P(2,4,6-Me₃Ph)₃). XPhos has two electron donating cyclohexyl groups and the sterically encumbering bisphenyl group and consequently is easily oxidised and has a large cone angle of 210°. The most readily oxidised ligand P(2,4,6-Me₃Ph)₃ also has the largest cone angle of 212°. The methyl groups which are in close proximity result in rotation of the aromatic systems to minimise steric clashing thus accounting for the high cone angle. Not only do the methyl groups result in a large steric effect but their electron donation into the phenyl rings results in a greatly reduced participation of the phosphorous lone pair in conjugation with the aromatic system resulting in the lowest oxidation potential observed of 0.92 V.
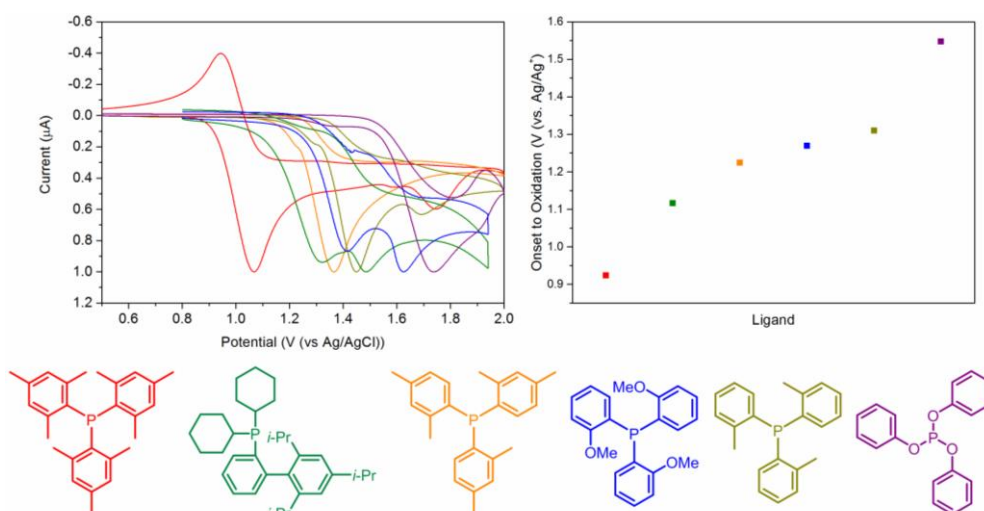
Figure 3.1: Summary of electronic properties of ligands; left CV of 10 μM solutions of ligand, right, onset of oxidation of ligand solution.

Table 3.1: Summary of donor ability and steric effects (cone angle) of ligands in this study.

Ligand	Onset to Oxidation (V (vs. Ag/AgCl)	Cone angle (°)
Tris-(2,4,6-trimethylphenyl)phosphine	0.92	212[11]
XPhos	1.12	210[11]
Tris(2,4-dimethylphenyl)phosphine	1.22	150-210
Tris(2-methoxyphenyl)phosphine	1.27	137[11]
Tris(o-tolyl)phosphine	1.31	147[11]
Triphenyl phosphite	1.55	140-160[12]

3.2.2: Kinetic Studies of Different Catalysts

The effect of each ligand on the relative rate of BT and BnDT conversion during polycondensation was determined by monitoring the consumption of each monomer during a polycondensation (Scheme 3.1 and Figures 3.2-3.7) reaction which was discussed for the ligand P(o-tolyl)$_3$ in Chapter Two.
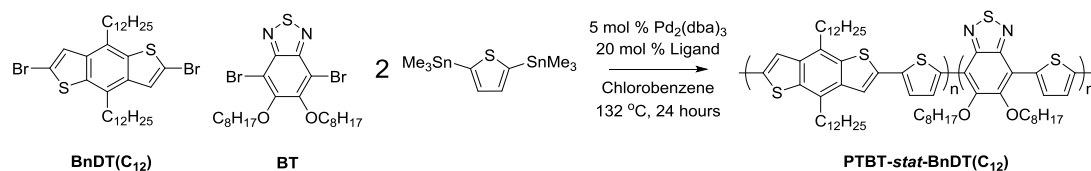
Scheme 3.1: Polycondensation reaction scheme for kinetic studies.
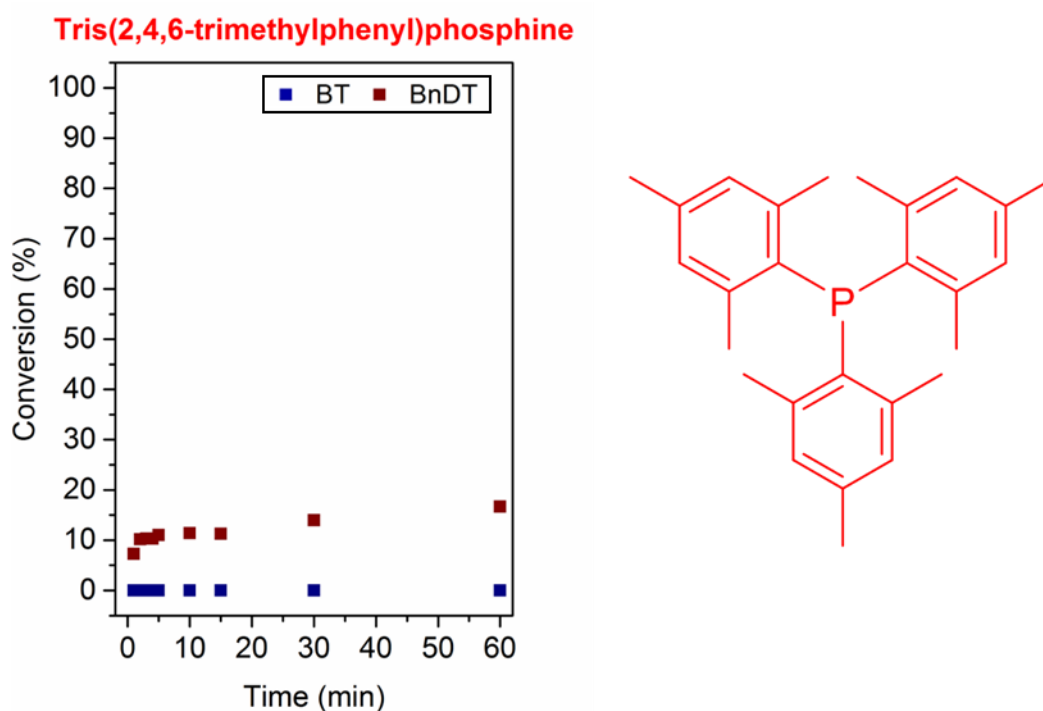
Figure 3.2: The conversion of BT (blue) and BnDT (red) during Stille polycondensation using P(2,4,6-Me$_3$Ph)$_3$ as a ligand.

The most electron donating ligand P(2,4,6-Me$_3$Ph)$_3$ results in poor conversion of both monomers, failing to yield any polymeric material. The strong electron donating ability of the ligand results in decomposition of the palladium catalyst into the insoluble and inactive palladium black.[2] Before all the catalyst is deactivated, however, a small amount of BnDT is converted while no observable amount of BT is converted. The strongly electron donating ligand not only fails to produce polymer but has also shown little to no

effect on the bias of the stile coupling towards the BnDT monomer and was therefore discounted from further studies.
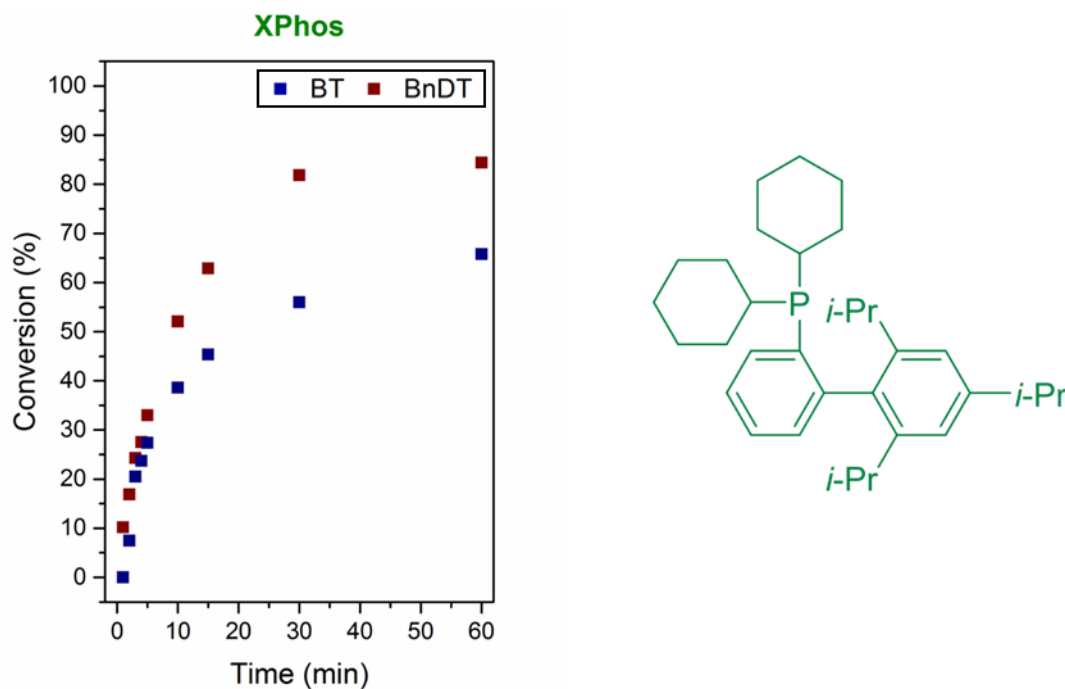
Figure 3.3: The conversion of BT (blue) and BnDT (red) during Stille polycondensation using the Buchwald ligand XPhos.

The Buchwald ligand 2-dicyclohexylphosphino-2',4',6'-triisopropylbiphenyl or XPhos is a popular ligand for Buchwald-Hartwig amination reactions[13] but has also shown high activity in other carbon-carbon bond cross coupling reactions, such as the Suzuki coupling for example.[14,15] Using XPhos as a ligand results in good conversion of both BT and BnDT yielding a polymer with M_n = 20,700 g/mol by GPC The resulting polymer is assigned the name **P3.1-XPhos**. Figure 3.3 also demonstrates that XPhos can be used to largely correct the bias of the Stille coupling for the more electron rich species. It is likely that the superior electron donating ability of XPhos (compared to P(*o*-tolyl)$_3$) makes the L$_2$Pd^{II}BrBT intermediate more thermodynamically stable, accounting for the increased rate of conversion of BT. This is accompanied by a reduction in the rate of conversion of the electron rich BnDT monomer, it is possible that the sterically bulky ligand inhibits the more bulky BnDT monomer (with its long dodecyl side chains). Both of these effects result in BT and BnDT having similar rates of conversion and achieve the closest example

of a random copolymer discussed in this thesis.
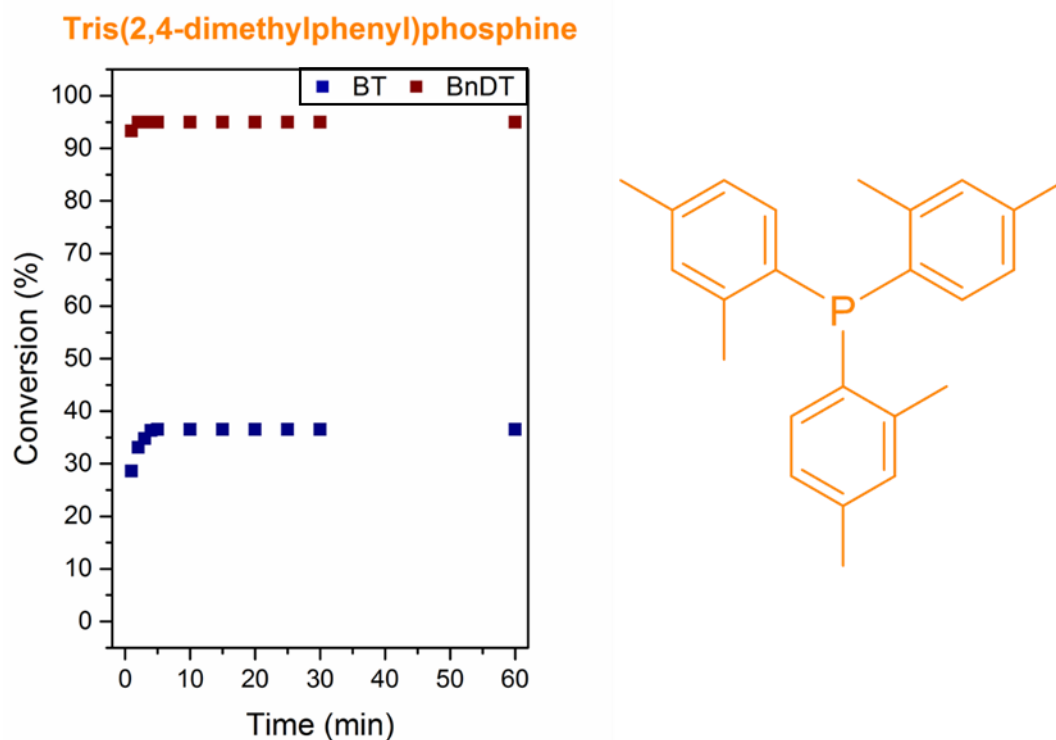
Figure 3.4: The conversion of BT (blue) and BnDT (red) during Stille polycondensation using P(2,4,-Me₂Ph)₃ as a ligand.

P(2,4-Me₂Ph)₃ is perhaps the most anomalous result in terms of the rate of conversion of monomers with respect to the electron donating ability of the ligand. Despite its superior electron donating ability V_{ox}^{onset} = 1.22 V (P(*o*-tolyl) V_{ox}^{onset} = 1.31 V) P(2,4-Me₂Ph)₃ exhibits similar rates of conversion to P(*o*-tolyl)₃ (Figures 3.4 and 3.6 respectively). One possible rationalisation for this is that the planar phenyl rings such as those in P(2,4-Me₂Ph)₃ and P(*o*-tolyl)₃ stabilise the L₂Pd^{II}BrBnDT intermediate through π-stacking interactions. When the π-stacking is inhibited by longer more flexible groups such as methoxy groups in P(*o*-OMePh)₃ or XPhos a decreased rate of BnDT conversion is observed. While BnDT conversion is still rapid, BT conversion reaches a plateau (although at lower conversion) more quickly than the reference system (P(*o*-tolyl₃) (5 min vs. 30 min) possibly due to the increased donor ability of the ligand. This catalyst yielded a polymer with a suitable M_n of 18,100 g/mol. The resulting polymer is assigned the name **P3.2-DMPP**.
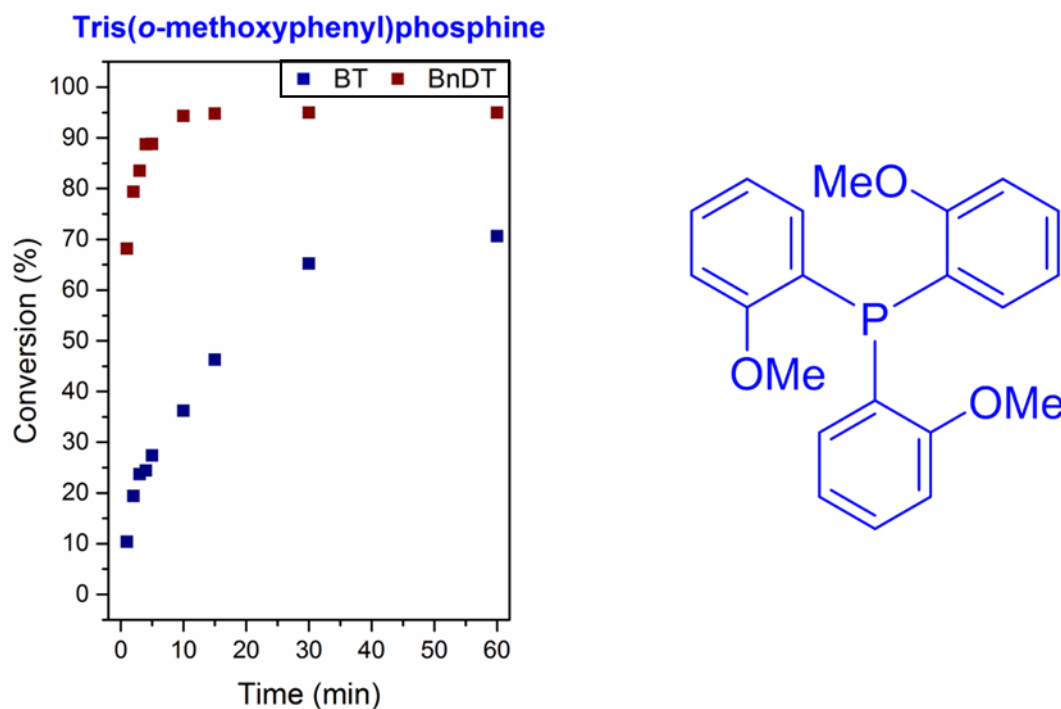
Figure 3. 5: The conversion of BT (blue) and BnDT (red) during Stille polycondensation using P(*o*-OMePh)₃ as a ligand.

The P(*o*-OMePh)₃ system (Figure 3.5), like the XPhos system, experiences a reduction in bias towards the conversion of BnDT. As discussed above, the longer more flexible methoxy groups help to inhibit π-stacking retarding the oxidative addition product of BnDT to the palladium centre relative to the Pd:P(*o*-tolyl)₃ system. The extra stability provided by the greater electron donating ability of the ligand produces an increase in the conversion of the BT unit resulting in a polymer between that of a gradient and random copolymer with a respectable M_n of 18,200 g/mol by GPC The resulting polymer is assigned the name **P3.3-oOMeP**. The catalyst containing the P(*o*-tolyl)₃ ligand (Figure 3.6) has largely been discussed in Chapter Two and is used here as a reference system. P(*o*-tolyl)₃ results in rapid conversion of the BnDT monomer, the BT monomer, however, is converted to a lesser extent resulting in a gradient or block like copolymer. This polymer is assigned the name **P3.4-PoTol**.
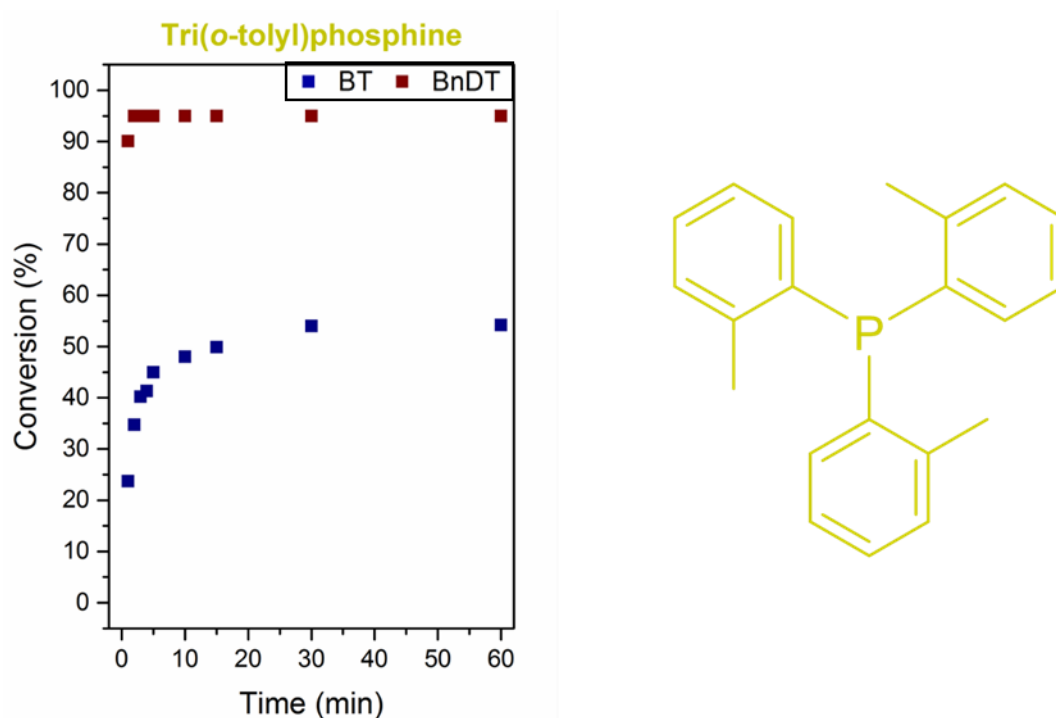
Figure 3.6: The conversion of BT (blue) and BnDT (red) during Stille polycondensation using P(*o*-tolyl)₃ as a ligand.
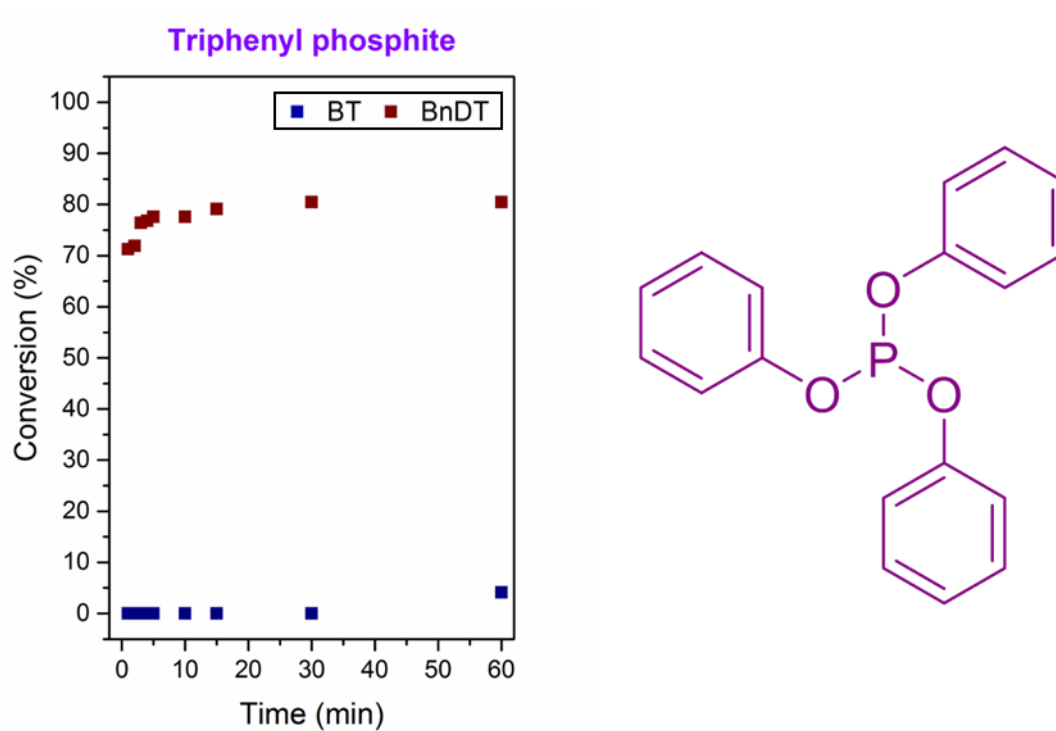
Figure 3.7: The conversion of BT (blue) and BnDT (red) during Stille polycondensation using triphenyl phosphite as a ligand.

The most electron withdrawing ligand triphenyl phosphite (Figure 3.7) results in rapid but not complete conversion of BnDT (plateau at 80 %) and < 5 % conversion of BT

resulting in a predominantly BnDT containing oligomer (M_n = 2,300 g/mol tri-tetramer). The flexible arms of the ligand possibly allow for effective π-stacking forming a stable $L_2Pd^{II}BnDTBr$ intermediate. Due to the low molecular weight of the materials obtained from this triphenyl phosphite systems its investigation was pursued no further.

While much of the discussion into how these ligands effect the relative rates of conversion of the BT and BnDT has been speculative, through these kinetic studies we have demonstrated that while ligands are often screened for their ability to yield polymers of a high molecular weight, it is also essential to consider (when using statistical systems) how the ligand choice effects the backbone sequence in the polymeric material obtained. In the rest of this chapter the variation of morphological and optoelectronic properties of polymers synthesised using different ligands are investigated.

3.2.3: Characterisation of PTBnDT(C₁₂)-*stat*-PTBT Polymers

Table 3.2: Summary of physical properties of PTBnDT(C₁₂)-*stat*-PTBT synthesised using different catalysts.

Polymer	Yield (%)	M_n (g/mol)	M_w (g/mol)	$Đ$	% BnDT (NMR)	% BT (NMR)	T_D (°C)
P3.1-XPhos	90.8	20700	53900	2.42	47	53	330
P3.2-DMPP	76.9	18100	33400	1.85	57	43	329
P3.3-oOMeP	84.2	18200	35800	1.97	52	48	333
P3.4-PoTol	81.6	17600	44800	2.55	50	50	329

Each catalyst produced polymers of a molecular weight between 17,000 g/mol and 21,000 g/mol corresponding to an average maximum conjugation length of 20 repeat units. This allows for the maximum persistence length to be achieved,[16-18] resulting in a lower E_g whilst maintaining good solubility in common organic solvents such as chloroform and toluene. The similar number average molecular weights and dispersities (Figure 3.8) of the polymers also validates the comparison of the optoelectronic properties and morphology with respect to sequence and backbone composition alone. Each polymer also exhibits good thermal stability with a decomposition temperature (T_D, 5 % weight loss) of > 325 °C (Figure 3.9) which is sufficient for their application in POPVs. The first mass loss of 15-20 % at 330 °C is assigned to the loss of the octyoxy side chains while the second mass loss at 350 °C is assigned to the loss of the dodecyl side chains.
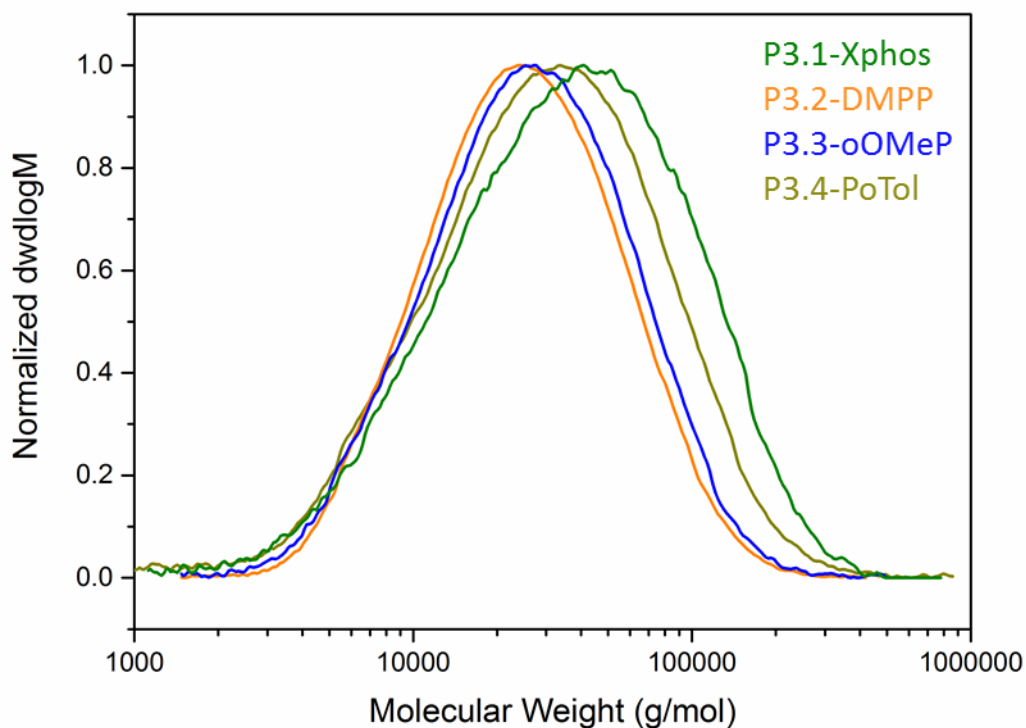
Figure 3.8: Molecular weight distributions (by GPC) of PTBnDT(C$_{12}$)-*stat*-PTBT polymers; P3.1-XPhos, P3.2-DMPP, P3.3-oOMeP and P3.4-PoTol.
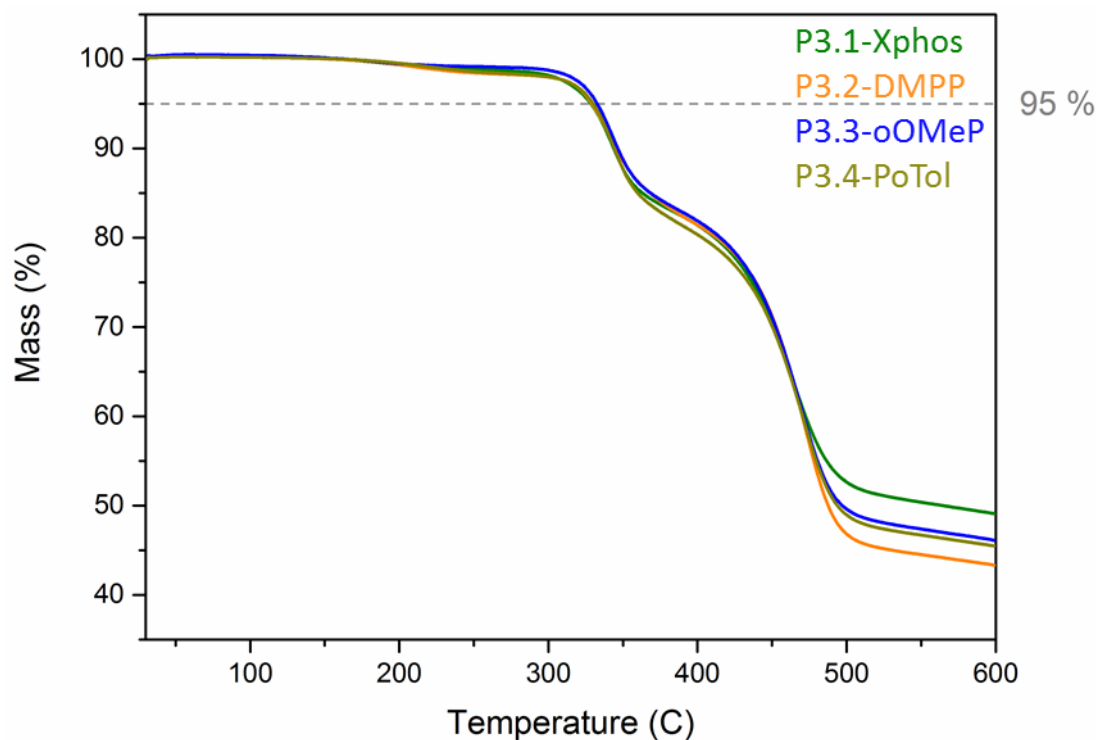
Figure 3.9: TGA traces of PTBnDT(C$_{12}$)-*stat*-PTBT polymers; P3.1-XPhos, P3.2-DMPP, P3.3-oOMeP and P3.4-PoTol..

The ^{1}H NMR spectra (Figure 3.10) at first glance, are similar with δ: = 8.4-8.6 ppm being assigned to the two protons on then BnDT(C$_{12}$) unit , δ: = 7.0-7.7 is assigned to the two

protons on each thiophene bridging unit, δ: = 4.2 is assigned to the α-CH$_2$ of the octyoxy side chains of the BT repeat units, δ: = 3.1 is the α-CH$_2$ of the dodecyl side chains of the BnDT repeat unit and finally δ: = 0.0-2.25 ppm region is assigned to the remaining alkyl protons on both the BT and BnDT(C$_{12}$) units.
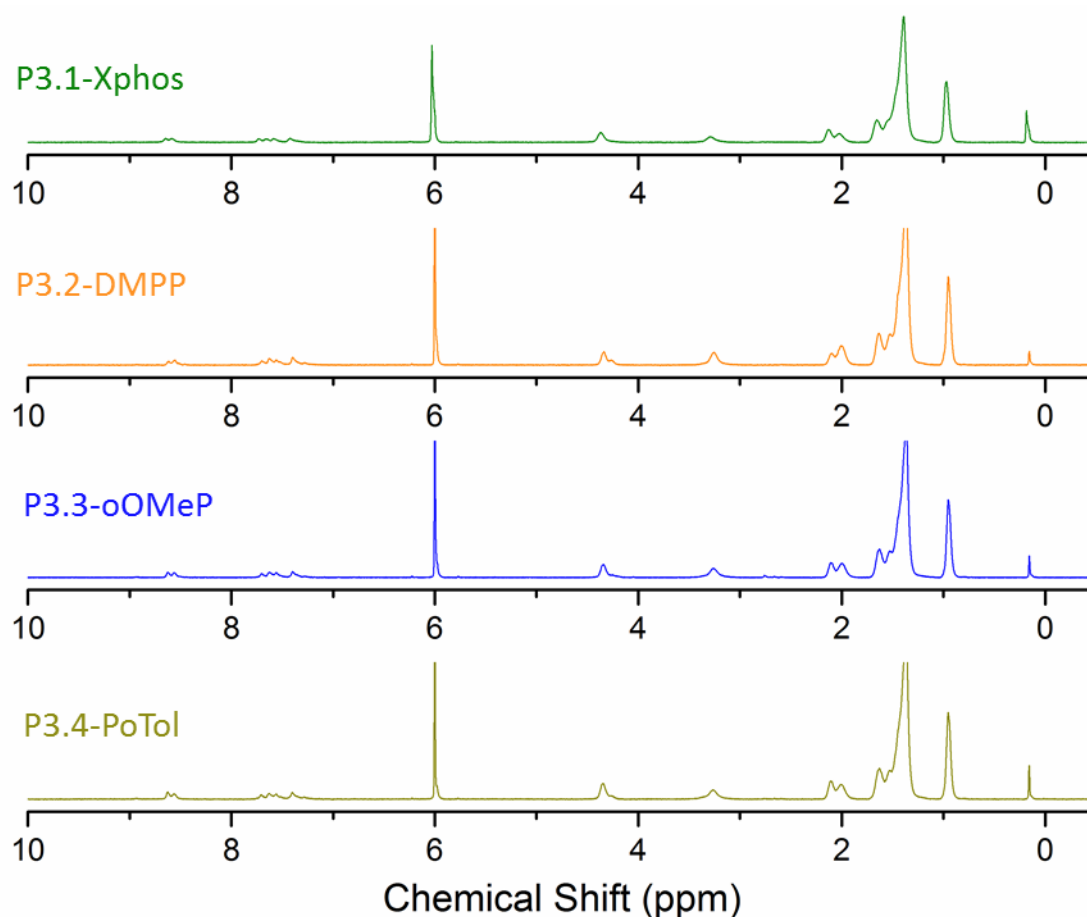
Figure 3.10: ^{1}H NMR spectra of PTBnDT(C$_{12}$)-*stat*-PTBT polymers synthesised using different catalytic systems. Green; P3.1-XPhos, orange; P3.2-DMPP, blue, P3.3-oOMeP and dark yellow; P3.4-PoTol.

On closer inspection of the region δ = 2.5-5.0 ppm which contains the α-CH$_2$ protons for each monomer unit (Figure 3.11) indicate some changes in structure and composition with the catalytic system. These differences can be rationalised using the kinetic studies discussed above. The green trace in Figure 3.11 corresponds to the Pd:XPhos catalyst which exhibited a more even consumption of BT and BnDT monomers throughout the polymerisation (Figure 3.3). Each of the α-CH$_2$ present a monomodal peak indicative of an even distribution of each monomer throughout the backbone, as expected from examination of the kinetic studies.
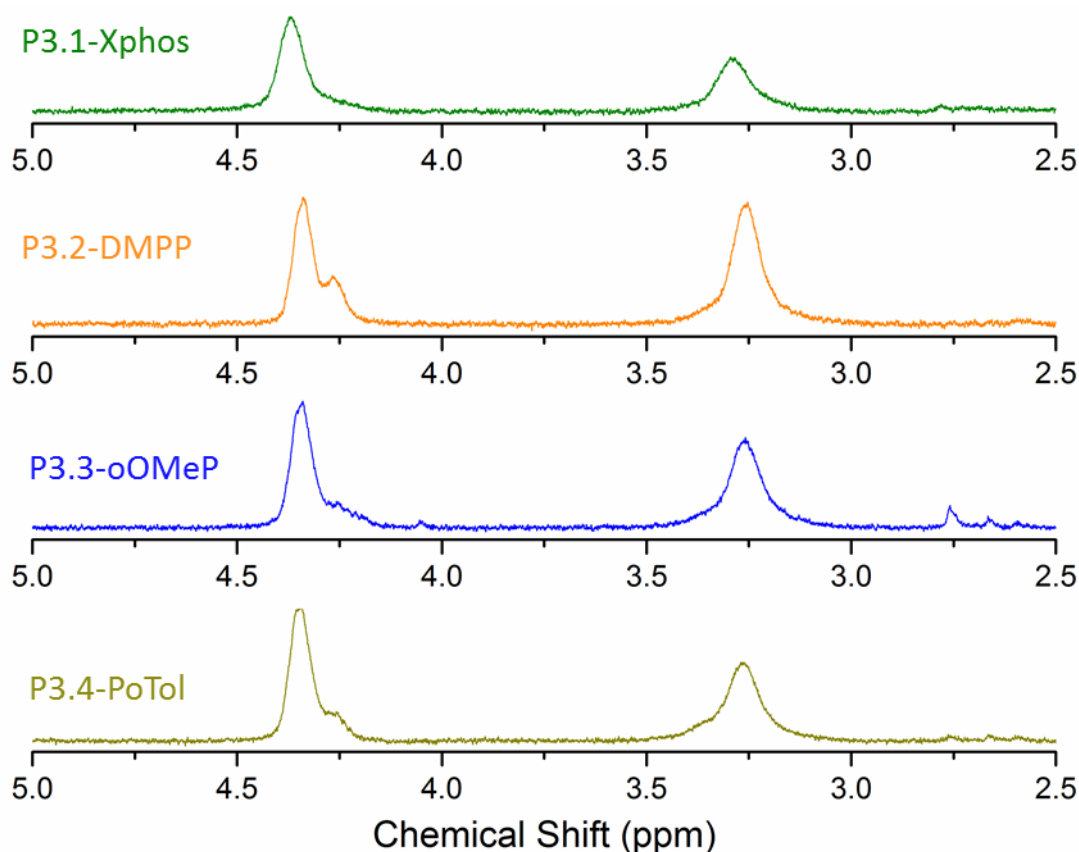
Figure 3.11: ^{1}H NMR spectra (between 2.5-5.0 ppm) of PTBnDT(C$_{12}$)-*stat*-PTBT polymers synthesised using different catalytic systems P3.1-XPhos, P3.2-DMPP, P3.3-oOMeP and P3.4-PoTol.

The orange trace of the Pd:P(2,4-Me$_2$Ph)$_3$ catalyst (Figure 3.11) exhibits a monomodal peak for the BnDT α-CH$_2$ protons and a bimodal distribution for the BT α-CH$_2$ protons. Of the three systems that feature this bimodal behaviour Pd:P(2,4-Me$_2$Ph)$_3$ is the most pronounced. The smaller of the two peaks originates from BT units located at the chain end as discussed in Chapter 2. The Pd:P(2,4-Me$_2$Ph)$_3$ catalyst exhibits the greater discrepancy in rate of consumption between BnDT and BT monomer units, resulting in a greater number of BT end groups and thus the most pronounced shoulder of the four products. The dark yellow trace showing the purified PTBnDT-*stat*-PTBT polymer synthesised using a Pd:P(*o*-tolyl)$_3$ catalyst displays a marginally smaller shoulder than that of the Pd:P(2,4-Me$_2$Ph)$_3$ polymer. The BT in the Pd:P(*o*-tolyl)$_3$ system reaches a conversion of 50 % in the first 60 minutes versus 40 % in the Pd:P(2,4-Me$_2$Ph)$_3$ system, resultantly more of the BT unit is incorporated into the backbone and a samller signal is observed for their presence as near the chain ends groups. A similar effect is observed for the Pd:(*o*-OMePh)$_3$ catalyst, at t = 60 minutes BT conversion is at 70 versus 95 % of BnDT(C$_{12}$) (Δϱ = 25 %) and a concurrent drop in the end group density of the BT unit is observed. Finally the Pd:XPhos catalyst demonstrates the most similar rates of

conversion for BT and BnDT(C$_{12}$) with a $\Delta\varrho$ at t = 60 of only 20 %. Further to this, the BnDT(C$_{12}$) has not rapidly reached full conversion. The resulting polymer has the lowest counts of BT at its chain ends of the four systems examined, as such the end-group peak is much less visible and is lost in the higher field tailing of the peak centred at δ = 4.35 ppm.

3.2.4: Optoelectronic Properties of PTBnDT(C$_{12}$)-*stat*-PTBT Polymers

The optoelectronic properties of the polymers resulting from the use of the four different catalysts where examined by UV-Vis spectroscopy and CV (Figures 3.12 and 3.13, respectively) and are summarised in Table 3.3. The tendency of each polymer to aggregate was also investigated by comparing the UV-Vis spectra of the polymer films with the solution phase UV-Vis spectra at 25 °C and 90 °C in dilute chlorobenzene solutions.
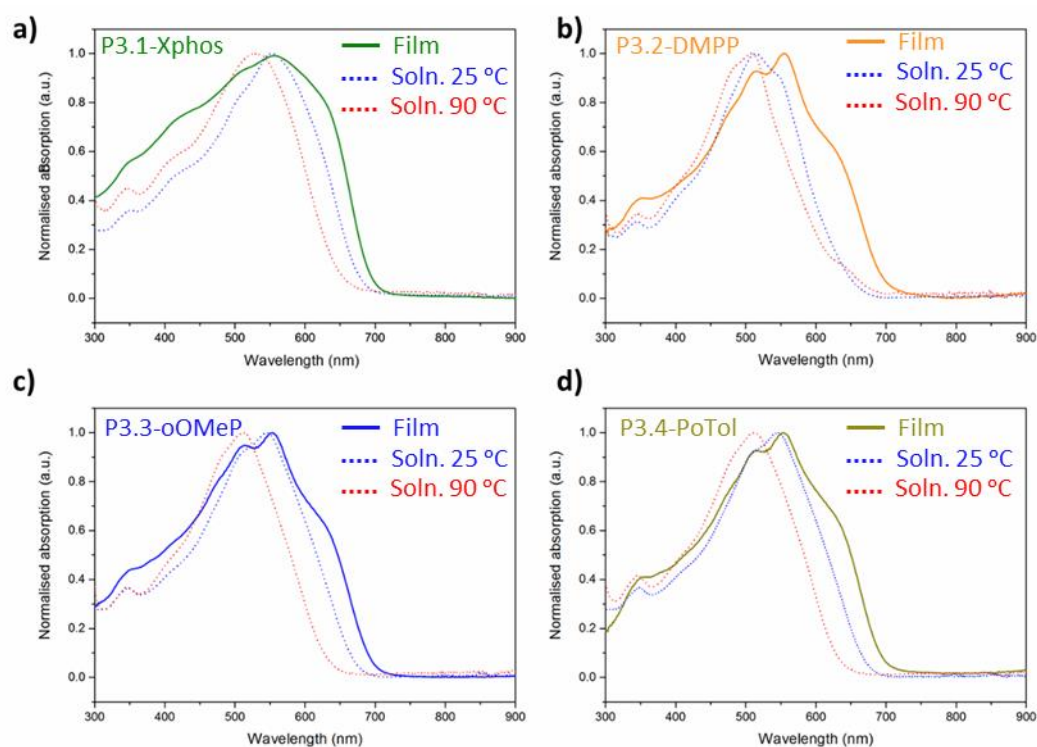
Figure 3.12: UV-Vis traces of PTBnDT(C$_{12}$)-*stat*-PTBT polymers synthesised using different catalytic systems. In each graph the blue and red dashed traces correspond to the UV-Vis spectra in chlorobenzene at 25 °C and 90 °C respectively, the solid trace is the spin cast film on ITO substrate. a; P3.1-XPhos, b;P3.2-DMPP, c; P3.3-oOMeP and d; P3.4-PoTol.

Each polymer film exhibits a vibronic shoulder in the region of 650-700 nm indicating a large degree of aggregation and π-stacking. The vibronic shoulder is most pronounced in the XPhos system (Figure 3.12a) which is the "most random" of the four polymers. In addition this system exhibits a broader absorption profile extending into the shorter wavelengths which may be the result of the increased number of effective chromophores

introduced by the more random distribution of donor $BnDT(C_{12})$ and acceptor BT units along the back bone. Inter molecular charge transfer (ITC) peaks are seen in all four polymers in the region of 500-650 nm, ICT states are more defined in polymers with a less random nature such as those synthesised using the $Pd:P(2,4-Me_2Ph)_3$ and $Pd:(P(o-tolyl)_3$ systems (Figure 3.12b and Figure 3.12d respectively).

Even in dilute solutions of chlorobenzene each polymer still displays a shoulder characteristic of aggregation, this is most noticeable with the $Pd:P(2,4-Me_2Ph)_3$ system. Its tendency to form the "blockiest" polymers, resulting in $BnDT(C_{12})$ rich regions along the backbone which lead to efficient π-stacking and aggregation, which could be beneficial for morphology and structure in thin films. As each solution is heated from 25 °C to 90 °C each polymer exhibits a blue due to the removal of aggregates.
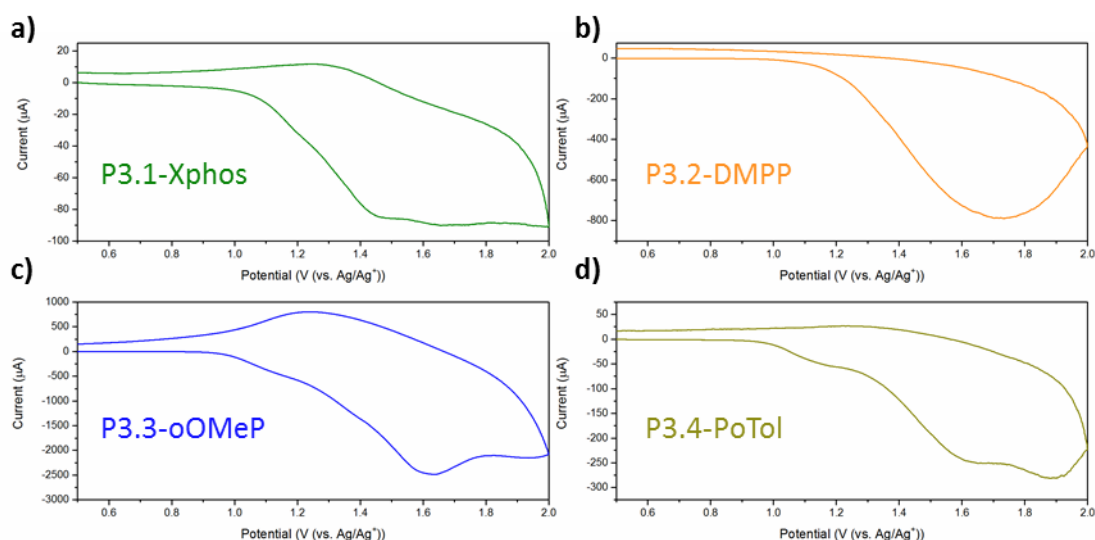
Figure 3.13: Cyclic voltammograms of polymers a; PTBnDT(C_{12})-*stat*-PTBT polymers . a; P3.1-XPhos, b;P3.2-DMPP, c; P3.3-oOMeP and d; P3.4-PoTol.

The HOMO level of each polymer was estimated from the onset to oxidation potential as measured by CV vs. a ferrocene standard, the LUMO was then calculated ($E_{HOMO)}$ + E_g^{opt}).[19,20] The four polymers exhibit similar E_g of 1.77-1.78 eV (Table 3.3) the HOMOs of the more block-like copolymers, however, are lower lying by approximately 0.1 eV, which is favourable for a greater V_{oc}.[21] Shoulders at lower potentials observed in the CV of PTBnDT-*stat*-PTBT synthesised with Xphos, P(*o*-OMePh)$_3$ and P(*o*-tolyl)$_3$ (green, blue and dark yellow traces in Figure 3.13) can often be indicative of more crystalline domains which are more easily oxidised.[22]

Table 3.3: Summary of optical and electronic properties of PTBnDT(C$_{12}$)-*stat*-PTBT polymers; P3.1-XPhos, P3.2-DMPP, P3.3-oOMeP and P3.4-PoTol.

Ligand	$\lambda_{max}^{soln(25)}$ (nm)	$\lambda_{max}^{soln(90)}$ (nm)	λ_{max}^{film} (nm)	λ_{onset}^{film} (nm)	E$_g$ (eV)	E$_{HOMO}$ (eV)	E$_{LUMO}$ (eV)
P3.1-XPhos	553	529	569	695	1.8	-5.3	-3.6
P3.2-DMPP	515	509	555	699	1.8	-5.4	-3.7
P3.3-oOMeP	547	512	554	700	1.8	-5.3	-3.6
P3.4-PoTol	545	511	554	697	1.8	-5.45	-3.7

3.2.5: Morphological Studies PTBnDT(C$_{12}$)-*stat*-PTBT Polymers

The morphology of the polymers synthesised using each of the four catalysts was investigated by AFM. Figure 3.14 and Figure 3.15 show the height and phase images of the polymer film and polymer : PC$_{61}$BM blend respectively for the Pd : XPhos catalyst. Figure 3.14a is a 5x5 μm scan of the polymer film. Polymer aggregates/particles in the order of 200-300 nm can be seen which results from preaggregation in solution demonstrated by the large shoulder at 650 nm in the UV-Vis spectrum (Figure 3.12). The smaller 1x1 μm scan (Figure 3.14b) shows no major features or indication of polymer self-assembly. Both of the phase images (Figure 3.14c and Figure 3.14d) show a continuous phase response with no variation which is expected of an amorphous polymer film.

The AFM height images of the polymer : PC$_{61}$BM film in Figure 3.15 demonstrate a good mixing of polymer and fullerene with no aggregates present which is favourable for devices.[23,24] In Figure 3.15c and Figure 3.15d a mixture of phases can clearly been seen, this interpenetrating network of polymer and PC$_{61}$BM has domains in the region of 50-100 nm which is towards the upper limit of the ideal domain size (30-50 nm being optimum) to maximise charge separation whilst limiting recombination and a lowering of the J$_{sc}$.[25]
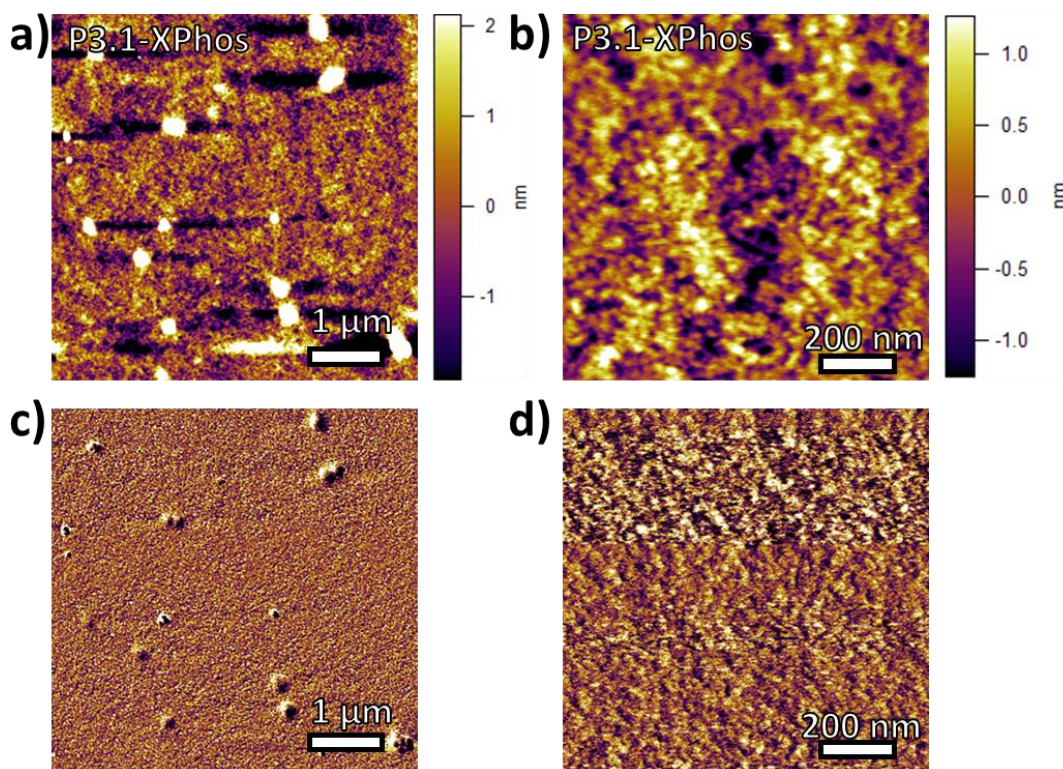
Figure 3.14: AFM height (a and b) and phase (c and d) images of PTBnDT(C$_{12}$)-*stat*-BTBT polymer P3.1-XPhos spin cast on to ITO and annealed at 180 °C for 5 minutes: a and c; 5x5 μm² (scale bar 1 μm), b and d; 1x1 μm² (scale bar 200 nm).
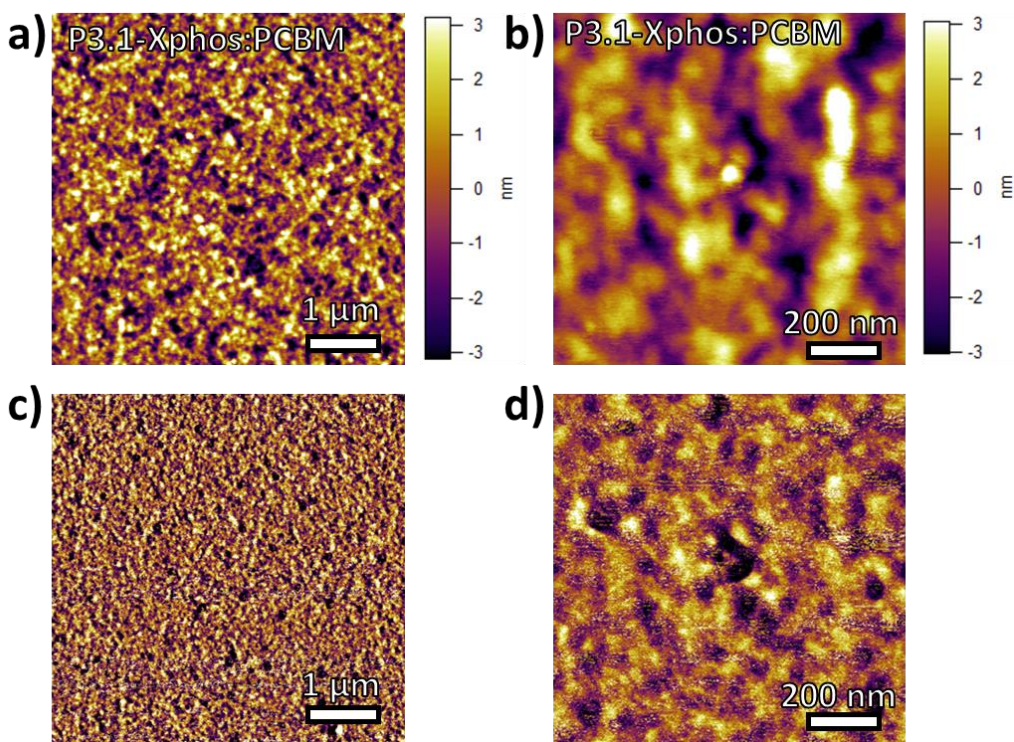
Figure 3.15: AFM height (a and b) and phase (c and d) images of PC$_{61}$BM : PTBnDT(C$_{12}$)-*stat*-BTBT polymer P3.1-XPhos catalyst spin cast on to ITO and annealed at 180 °C for 5 minutes: a and c; 5x5 μm² (scale bar 1 μm), b and d; 1x1 μm² (scale bar 200 nm).

The polymer film of PTBnDT(C$_{12}$)-*stat*-PTBT synthesised with Pd : P(2,4-Me$_2$Ph)$_3$ results in a smooth homogeneous film (Figure 3.16) which resembles a similar morphology to that of the polymer synthesised using Pd:P(*o*-tolyl)$_3$ owing to their similarities in their kinetic plots. Surprisingly these more block-like copolymers show little evidence of micro-phase separation or ordering within the resolution limits of the AFM, examination of the phase images (Figure 3.13c and Figure 3.16d) shows a continuous contrast.

Mixing of the polymer synthesised with Pd:P(2,4-Me$_2$Ph)$_3$ with PC$_{61}$BM results in a very smooth film indicating a suitable miscibility for achieving good BHJ-OPV devices (Figure 3.17b). Examination of the corresponding phase image (Figure 3.17d) is indicative of a mixture of phases with domains in the order of 50-100 nm which is suitable for charge extraction, while slightly smaller domains may be more desirable to maximise polymer : PC$_{61}$BM interface and increase charge separation.
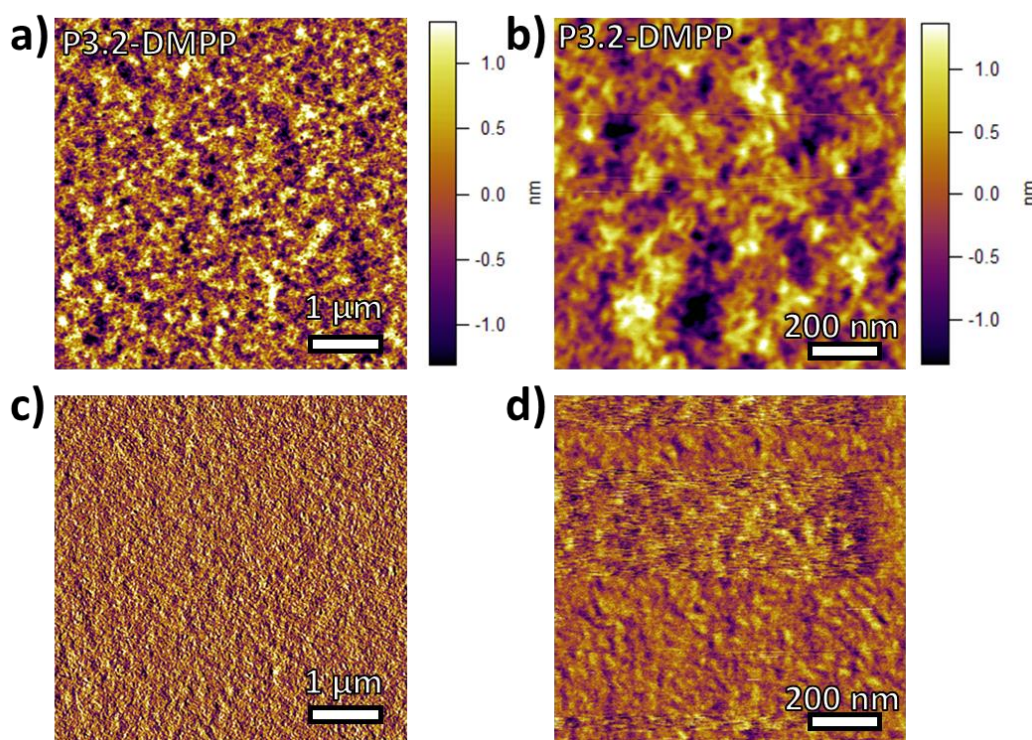
Figure 3.16: AFM height (a and b) and phase (c and d) images of PTBnDT(C$_{12}$)-*stat*-BTBT polymer P3.2-DMPP catalyst spin cast on to ITO and annealed at 180 °C for 5 minutes: a and c; 5x5 μm² (scale bar 1 μm), b and d; 1x1 μm² (scale bar 200 nm).
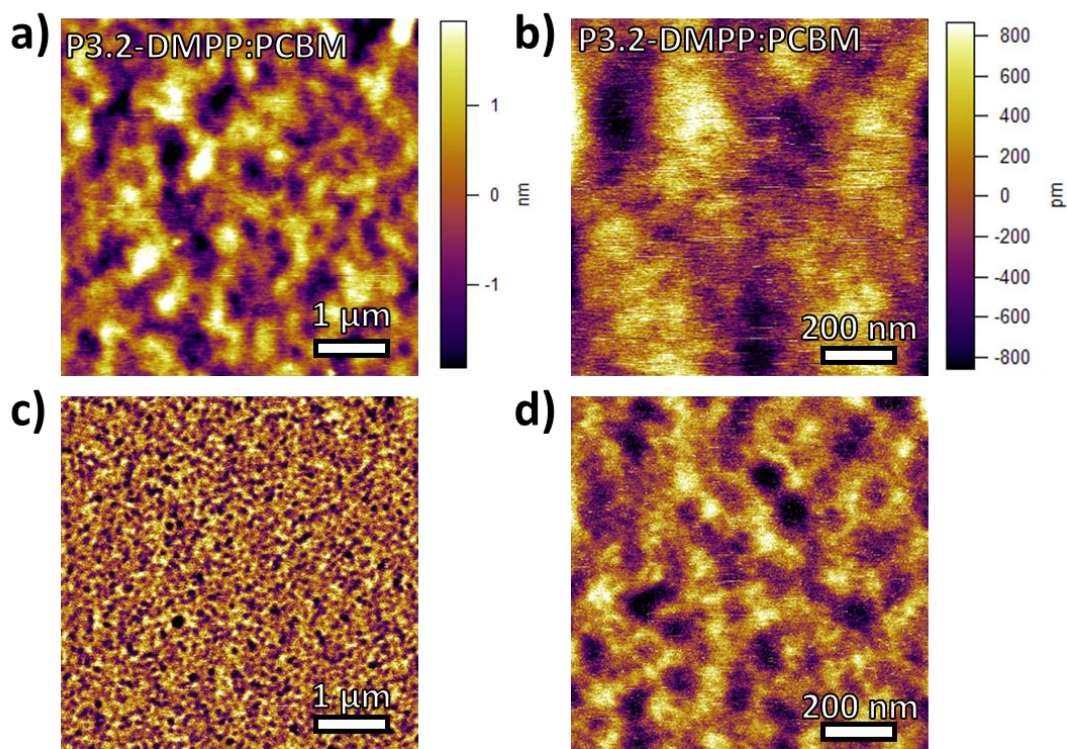
Figure 3.17: AFM height (a and b) and phase (c and d) images of $PC_{61}BM$: PTBnDT(C_{12})-*stat*-BTBT polymer P3.2-DMPP spin cast on to ITO and annealed at 180 °C for 5 minutes: a and c; 5x5 µm² (scale bar 1 µm), b and d; 1x1 µm² (scale bar 200 nm).
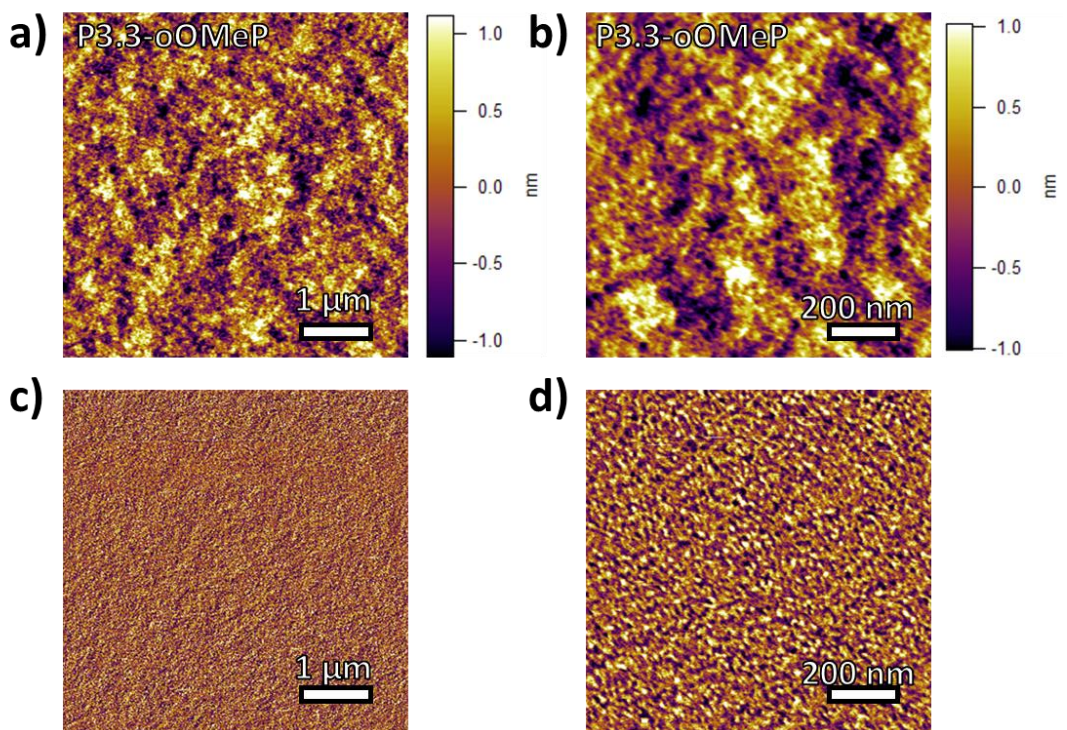
Figure 3.18:AFM height (a and b) and phase (c and d) images of PTBnDT(C_{12})-*stat*-BTBT polymer P3.3-oOMeP spin cast on to ITO and annealed at 180 °C for 5 minutes: a and c; 5x5 µm² (scale bar 1 µm), b and d; 1x1 µm² (scale bar 200 nm).
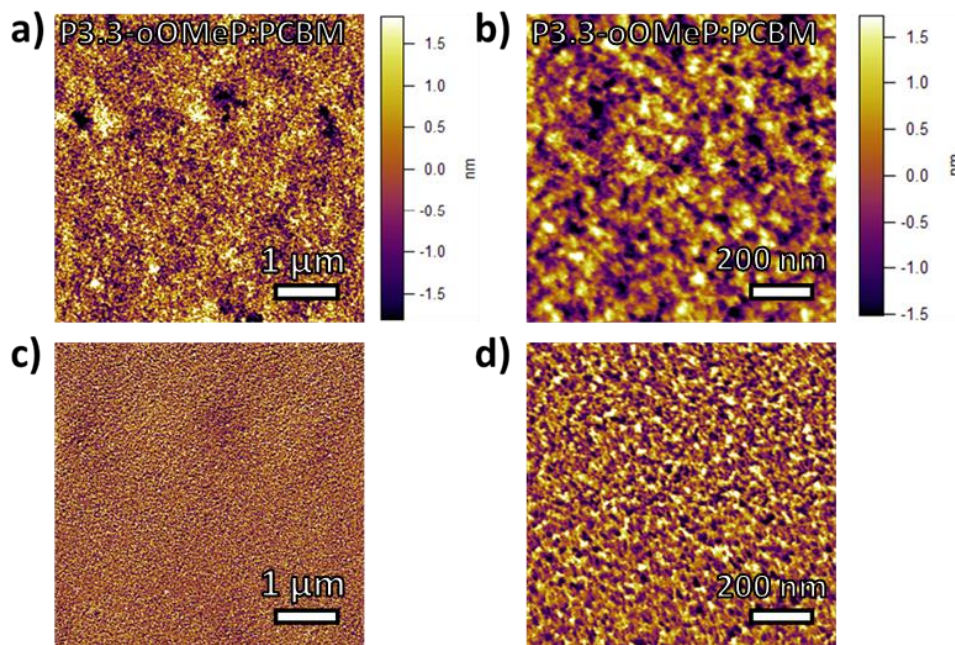
Figure 3.19: AFM height (a and b) and phase (c and d) images of $PC_{61}BM$: $PTBnDT(C_{12})$-*stat*-BTBT polymer P3.3-oOMeP spin cast on to ITO and annealed at 180 °C for 5 minutes: a and c; 5x5 μm² (scale bar 1 μm), b and d; 1x1 μm² (scale bar 200 nm).

Unlike the polymer synthesised using Pd:Xphos, the slightly less random polymer resulting from the Pd:P(*o*-OMePh)$_3$ catalyst shows no aggregates and a relatively smooth film (Figure 3.18). Examination of Figure 2.18d, the 1x1 μm phase image, shows some indication of phase separation in the polymer with small domain sizes < 50 nm which suggests a gradient structure intermediate between block and random polymers may be more favourable for achieving desired domain sizes.

The addition of $PC_{61}BM$ results in a slightly rougher film (RMS = 0.790 nm *vs.* 0.495 nm for the polymer film), the height images Figure 3.19a (5x5 μm) and Figure 3.19b (1x1 μm) show the large scale and continuous mixing of the blend, while phase features are too small to see in the 5x5 μm phase image (Figure 3.19c) small variations in phase can be observed in the 1x1 μm phase image (Figure 3.19d) on the scale of <50 nm which is towards the desired domain size for BHJ-OPV devices.

The polymer synthesised using the Pd:P(*o*-tolyl)$_3$ catalyst results in a film that shows some features in the height images (Figure 3.20a and Figure 3.20b), it is however difficult to confirm this with the phase images as the instruments noise limit was reached. The $PC_{61}BM$ blends of the polymer (Figure 3.21) show a similarly smooth topography indicating good mixing of the polymer and $PC_{61}BM$, it is possible to identify variations of

phase in Figure 3.19d although once again the instruments is approaching its noise limit and the features become hard to distinguish.
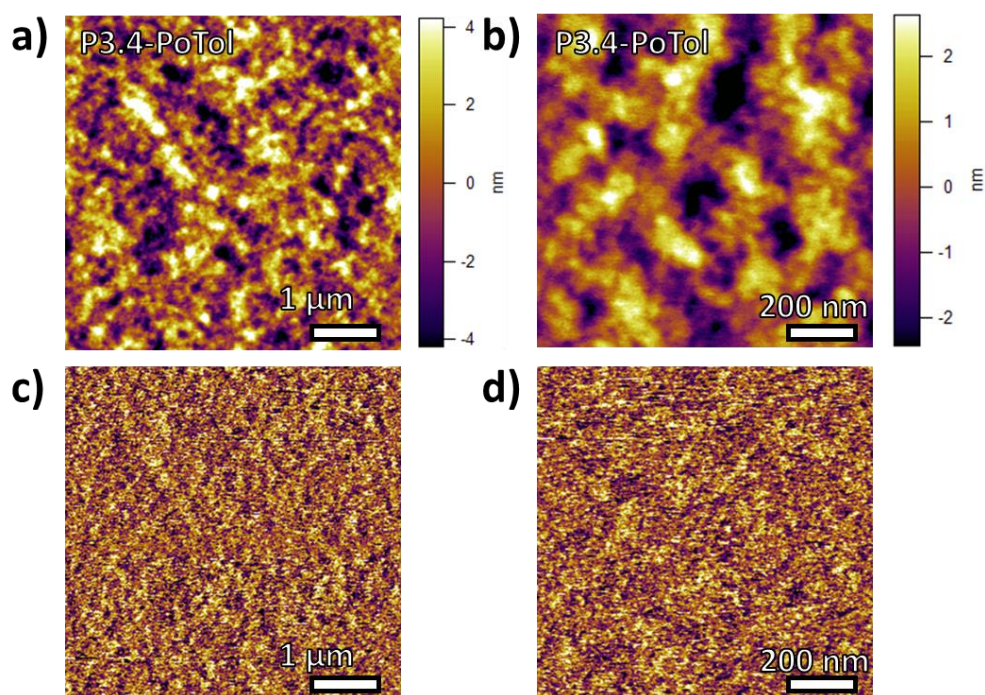
Figure 3.20: AFM height (a and b) and phase (c and d) images of PTBnDT(C$_{12}$)-*stat*-BTBT polymer P3.4-PoTol spin cast on to ITO and annealed at 180 °C for 5 minutes: a and c; 5x5 μm² (scale bar 1 μm), b and d; 1x1 μm² (scale bar 200 nm).

Figure 3..21: AFM height (a and b) and phase (c and d) images of $PC_{61}BM$: $PTBnDT(C_{12})$-*stat*-BTBT polymer P3.4-PoTol spin cast on to ITO and annealed at 180 °C for 5 minutes: a and c; 5x5 µm² (scale bar 1 µm), b and d; 1x1 µm² (scale bar 200 nm).

3.2.6: Characterisation of $PTBnDT(CO_2C_{12})$-*stat*-PTBT Polymers

Similarly to the polymers synthesised above polymers in which the $BnDT(C_{12})$ donor unit bares dodecyl side chains, dodecylcarboxylate side chains in the 4- and 8-position were also synthesised (Scheme 3.2). The addition of the ester groups has been shown to break up intermolecular π-stacking and result in greater solubility.[26] In addition the electron withdrawing CO_2 moiety makes the BnDT a ~~stronger~~ weaker and also results in a lower HOMO and potentially higher V_{oc}. Kinetic studies of this system were more challenging due to the protons now being at the γ-position, as such the changes in backbone structure cause little variation in the protons' electronic environment and concurrently their chemical shift. The polymers were synthesised in the same way as the PTBT-*stat*-$PTBnDT(C_{12})$ conjugate (scheme 3.2), however the kinetics were not followed. The physical properties of the resulting polymers are summarised in Table 3.4. $PTBnDT(CO_2C_{12})$-*stat*-PTBT polymers are assigned the following names P3.5-XPhos (synthesised using Pd : XPhos), P3.6-DMPP (synthesised usoing Pd : tris(2,4-dimethylphenyl)phosphine), P3.7-oOMeP (synthesised using Pd : tris(2-methoxyphenyl)phosphine) and P3.8-PoTol (synthesised using Pd : tris(*o*-tolyl)phosphine).
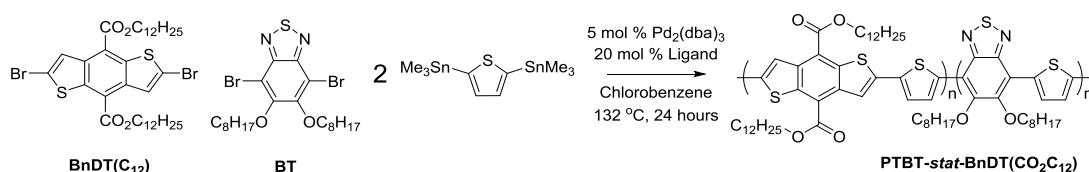
Scheme 3.2 Polycondensation synthesis of PTBT-*stat*-PTBnDT(CO$_2$C$_{12}$) with different catalysts.

Table 3.4: Physical properties of PTBT-*stat*-PTBnDT(CO$_2$C$_{12}$) synthesised different catalysts.

Ligand	Yield (%)	M_n (g/mol)	M_w (g/mol)	Đ	% BnDT (NMR)	% BT (NMR)	T_D (°C)
P3.5-XPhos	85.4	17900	52200	2.92	52	48	323
P3.6-DMPP	86.3	21800	77400	3.55	54	46	328
P3.7-oOMeP	88.0	18300	54900	3.01	54	46	325
P3.8 PoTol	85.0	20900	62800	3.00	53	47	326

Each catalyst produced polymers with a good M_n (17,000 – 22,000 g/mol by GPC) as previously. Each polymer has an acceptable conjugation length whilst maintaining their solubility in chloroform. The dispersities of the diester system are noticeably higher than the didodecyl equivalents; the higher solubility instilled by the ester groups allows for higher molecular weight species to disolve in chloroform resulting in the increased M_w and concurrent dispersity. Each of the molecular weight distributions displayed in Figure 3.22 show a monomodal peak with little evidence of low molecular weight tailing. This is potentially disadvantageous as it has previously been shown that the presence of low molecular weight species can give rise to morphological disorder, negatively effecting the transport properties of the polymer.[17,27,28]

The thermal stability of each polymer was examined by TGA, all polymers show good thermal stability showing T_D > 320 °C (5 % weight loss). At 600 °C each polymer has exhibited approximately 55 % weight loss which is attributed to the decomposition of the side chains, unlike the PTBnDT(C$_{12}$)-*stat*-PTBT system both the CO$_2$C$_{12}$H$_{25}$ and OC$_8$H$_{17}$ side chains displayed a similar lability.
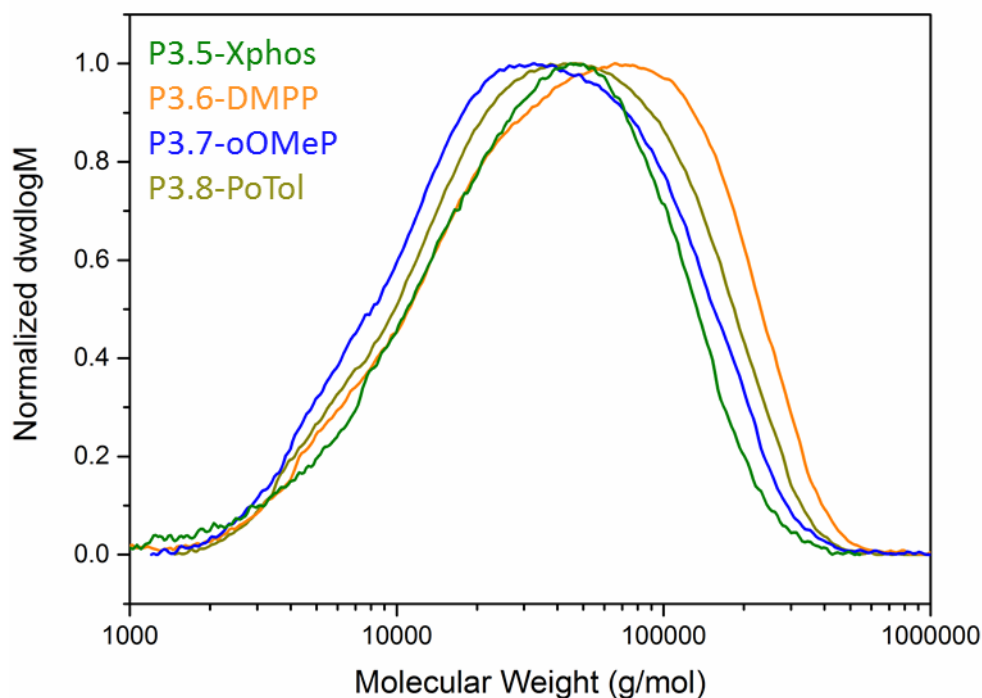
Figure 3.22: Molecular weight distributions (by GPC) of PTBnDT(CO_2C_{12})-*stat*-PTBT polymers; P3.5-XPhos, P3.6-DMPP, P3.7-oOMeP and P3.8-PoTol.
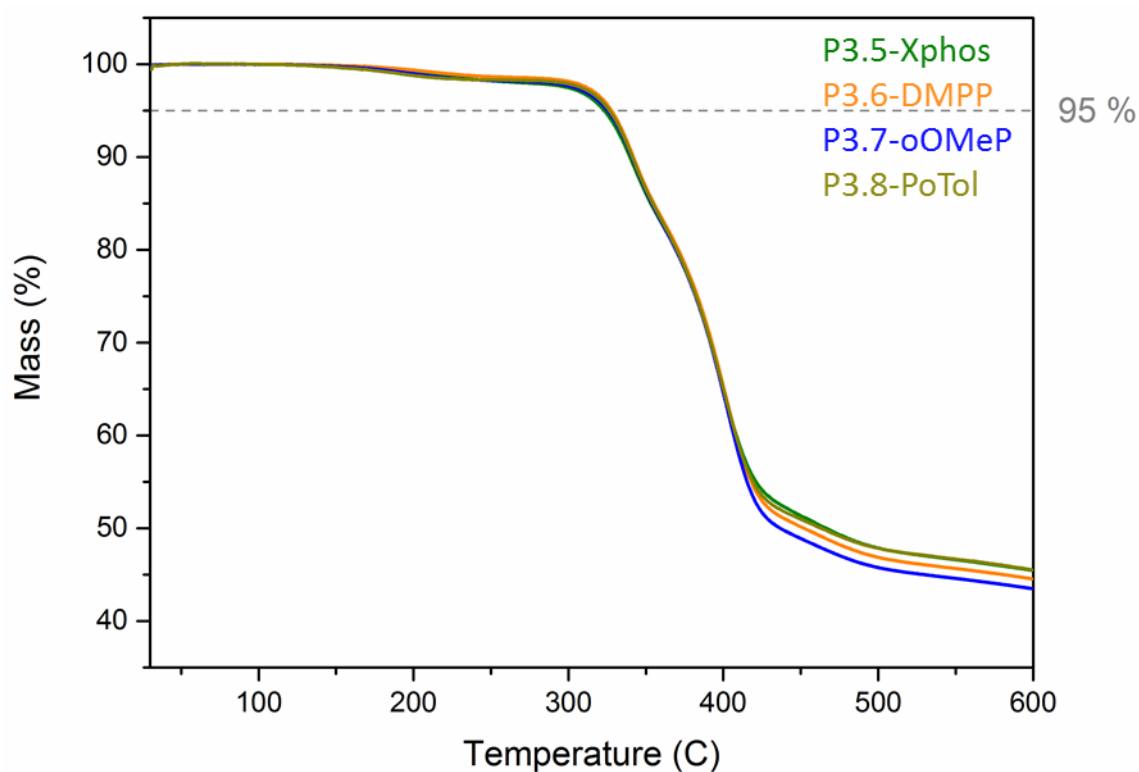
Figure 3.23: TGA plots of PTBnDT(CO_2C_{12})-*stat*-PTBT polymers; P3.5-XPhos, P3.6-DMPP, P3.7-oOMeP and P3.8-PoTol.).

Each of the purified polymers was characterised by ^{1}H NMR in 1,1,2,2-tetrachloroethane at 100 °C. The full spectra are displayed in Figure 4.24 whereas Figure 4.25 shows an

enlargement of the spectra in the region of 5.5 -3.5 ppm. The peaks centred at 4.75 ppm and 4.35 ppm indicate the presence of both the $CO_2C_{12}H_{25}$ α-CH$_2$ (BnDT) and CO_8H_{17} α-CH$_2$ respectively. The integration of these peaks is used to determine the ratio of BnDT(CO_2C_{12}) : BT in the polymer backbone (Table 3.4). Examination of the BT(OC_8H_{17}) α-CH$_2$ peaks reveals similar trends to the PTBnDT(C_{12})-*stat*-PTBT counterparts. Polymers synthesised with catalysts that favour the conversion of BnDT result in a shoulder at 4.25 ppm which is assigned to BT α-CH$_2$ protons at the chain end. The catalysts which favour more balanced monomer conversion (Pd : P(*o*-OMePh)$_3$ and Pd:XPhos) result in a smaller shoulder, which is only visible as tailing in the Pd : XPhos system.
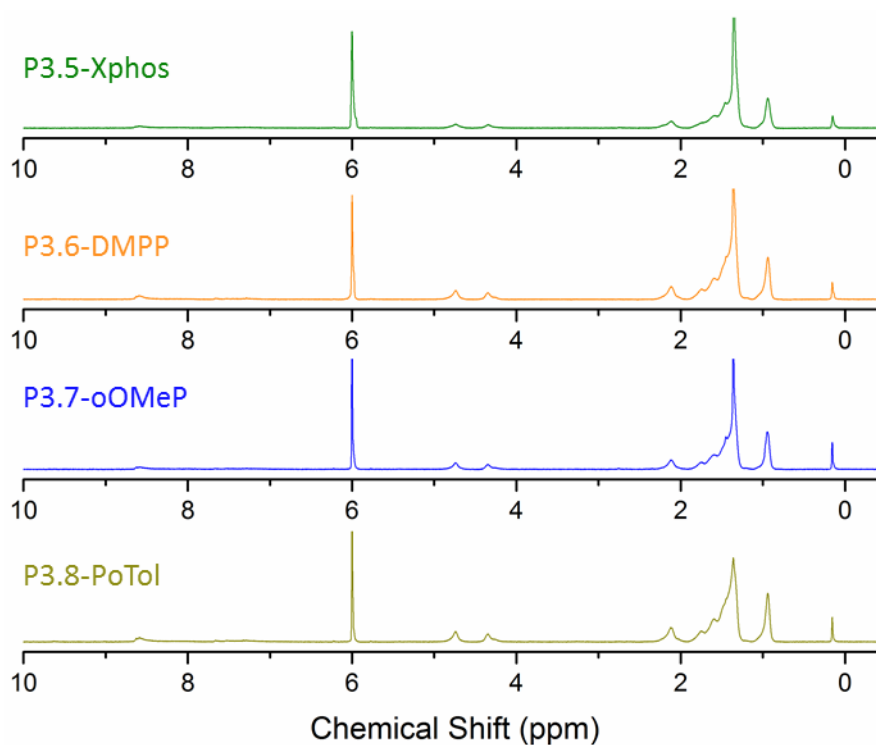
Figure 3.24: ^{1}H NMR spectra of PTBnDT(CO_2C_{12})-*stat*-PTBT polymers; P3.5-XPhos, P3.6-DMPP, P3.7-oOMeP and P3.8-PoTol.).
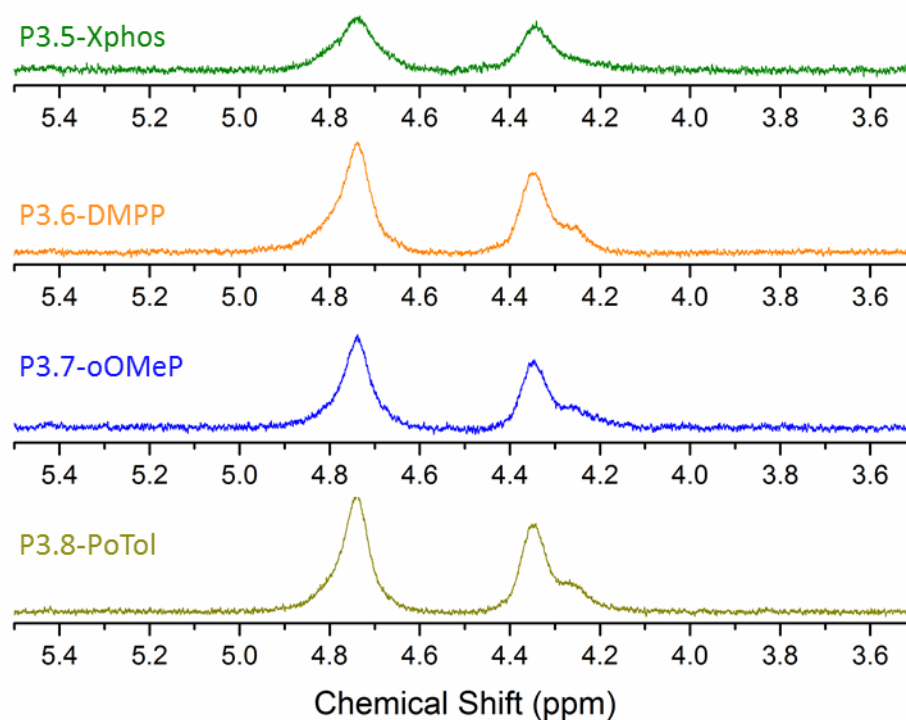
Figure 3.25: ¹H NMR spectra (between 3.5-5.5 ppm) of PTBnDT(CO$_2$C$_{12}$)-*stat*-PTBT polymers; P3.5-XPhos, P3.6-DMPP, P3.7-oOMeP and P3.8-PoTol.).

3.2.7: Optoelectronic Properties PTBnDT(CO$_2$C$_{12}$)-*stat*-PTBT

The optoelectronic properties of the various PTBnDT(CO$_2$C$_{12}$)-*stat*-PTBT polymers were analysed by UV-Vis spectroscopy (Figure 3.26) and CV (Figure 3.27) and are summarised in Table 3.5. Each of the PTBnDT(CO$_2$C$_{12}$)-*stat*-PTBT exhibits an onset to absorption at a longer wavelength than its PTBnDT(C$_{12}$)-*stat*-PTBT counterpart, the ester functionalities along the backbone work to lower the E$_g$ giving these polymers a strong blue appearance when compared to the purple PTBnDT(C$_{12}$)-*stat*-PTBT polymers. The onset to oxidation potential is also slightly larger indicating a deeper HOMO which is a promising feature for achieving high V$_{oc}$. For PTBnDT(CO$_2$C$_{12}$)-*stat*-PTBT UV-Vis spectra of each of the films exhibits a similar shape, with a peak in the region of 530 nm which is assigned to ICT, unlike their C$_{12}$ counterparts only one peak is distinguishable in the ICT region. Each of the four polymers shows strong aggregation characteristics in both the film and solution, indicated by the large shoulder/peak in the region of 670 nm. This shoulder becomes much less pronounced on heating as intermolecular stacking is disrupted for each polymer except for PTBnDT(CO$_2$C$_{12}$)-*stat*-PTBT synthesised with Pd:P(2,4-Me$_2$Ph)$_3$ (Figure 3.26) which still displays a large contribution due to

intermolecular stacking even at 90 °C (as did the C_{12} conjugate) which could possibly be assigned to its more block like nature.

Table 3.5: Summary of optoelectronic properties of For PTBnDT(CO₂C₁₂)-*stat*-PTBT synthesised using different catalyst.

Ligand	$\lambda_{max}^{soln(25)}$ (nm)	$\lambda_{max}^{soln(90)}$ (nm)	λ_{max}^{film} (nm)	λ_{onset}^{film} (nm)	E_g (eV)	E_{HOMO} (eV)	E_{LUMO} (eV)
P3.5-XPhos	635	588	600	735	1.7	-5.5	-3.8
P3.6-DMPP	638	595	595	709	1.7	-5.5	-3.7
P3.7-oOMeP	633	579	596	709	1.7	-5.4	-3.7
P3.8-PoTol	633	578	598	718	1.7	-5.5	-3.8

The variation in optoelectronic properties for the PTBnDT(CO₂C₁₂)-*stat*-PTBT is small although the Pd:Xphos system yields the polymer with the deepest HOMO and lowest E_g, perhaps owing to the more even distribution of donor-BnDT(CO₂C₁₂) and acceptor-BT units along the backbone. Each of the CVs for PTBnDT(CO₂C₁₂)-*stat*-PTBT (Figure 3.27) exhibits a similar shape in contrast to those of PTBnDT(C₁₂)-*stat*-PTBT (Figure 3.13). The lack of secondary peaks is indicative of a more consistent and amorphous film for each of the PTBnDT(CO₂C₁₂)-*stat*-PTBT polymers.
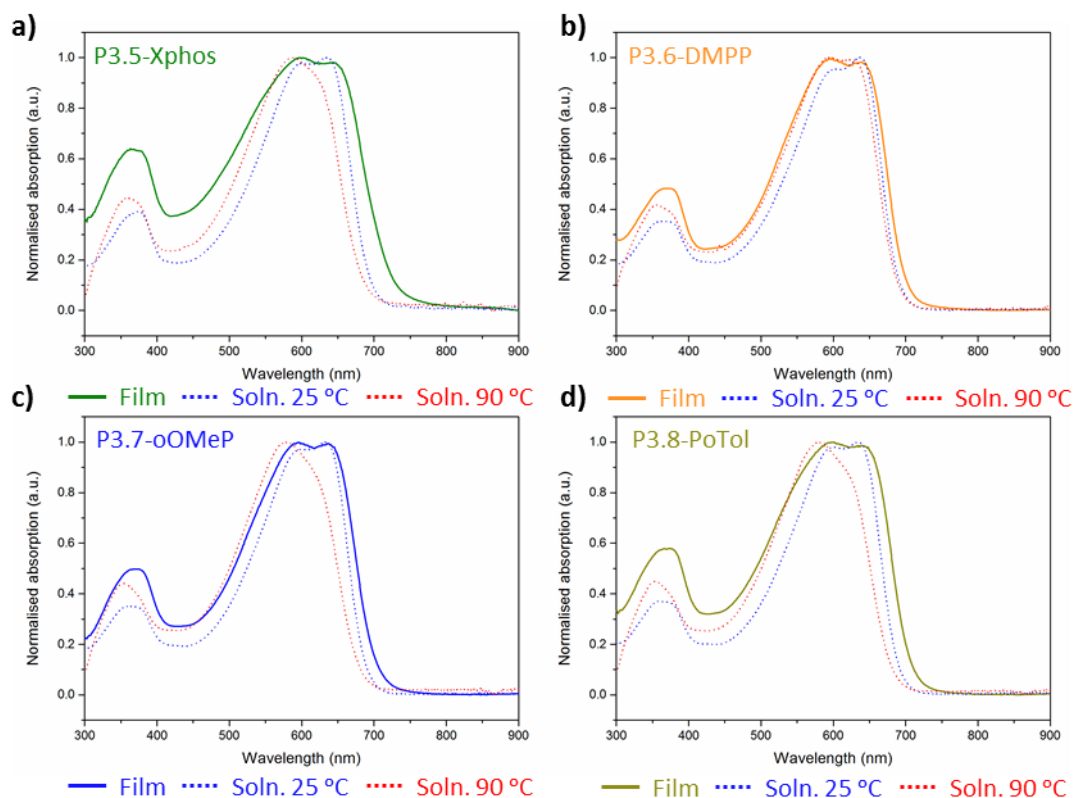
Figure 3.26: UV-Vis traces of PTBnDT(CO$_2$C$_{12}$)-*stat*-PTBT polymers synthesised using different catalytic systems. In each graph the blue and red dashed traces correspond to the UV-Vis spectra in chlorobenzene at 25 °C and 90 °C respectively, the solid trace is the spin cast film on ITO substrate. a; P3.5-XPhos, b; P3.6-DMPP, c; P3.7-oOMeP and d P8.4PoTol.
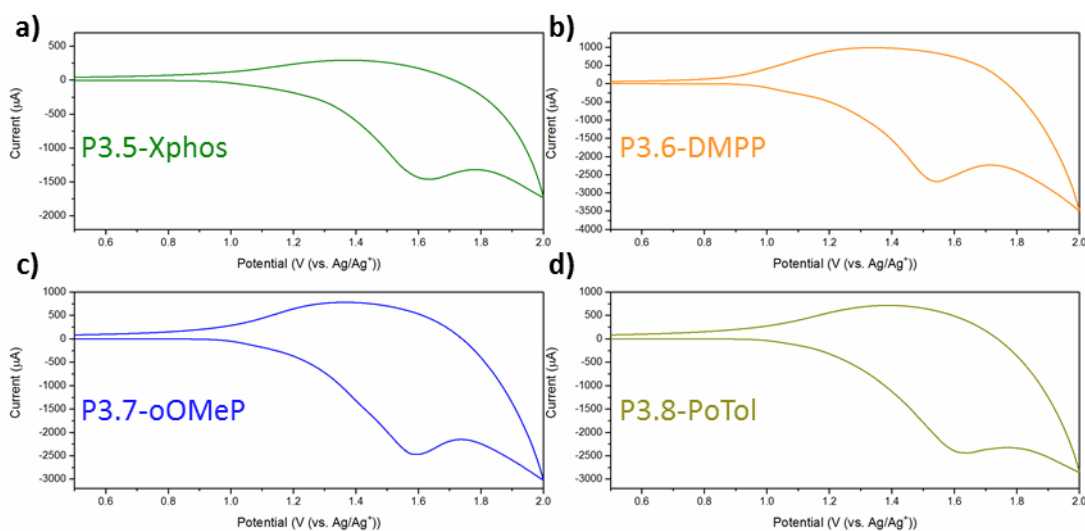
Figure 3.27: Cyclic voltammograms of PTBnDT(CO$_2$C$_{12}$)-*stat*-PTBT polymers: a; P3.5-XPhos, b; P3.6-DMPP, c; P3.7-oOMeP and d P8.4PoTol.

3.2.8: Morphological Studies PTBnDT(CO$_2$C$_{12}$)-*stat*-PTBT Polymers

The morphology of the PTBnDT(CO$_2$C$_{12}$)-*stat*-PTBT polymers synthesised using each of the four catalysts were studied using intermittent contact mode AFM, along with the polymer PC$_{61}$BM blends. The PTBnDT(CO$_2$C$_{12}$)-*stat*-PTBT polymer synthesised using the Pd : XPhos system shows a smooth homogenous film with no variations in phase or indication of self-assembly (Figure 3.28), which is what one would expect for a more even distribution of the BnDT(CO$_2$C$_{12}$) and BT units along the polymer backbone. Unlike its C$_{12}$ counterpart the polymers shows no sign of forming large aggregates or particles which can be assigned to the superior solubility of PTBnDT(CO$_2$C$_{12}$)-*stat*-PTBT when compared to PTBnDT(C$_{12}$)-*stat*-PTBT.

When blended with PC$_{61}$BM an interpenetrating network can be seen in the height images (Figure 3.29a and Figure 3.29b) with a corresponding variation in the phase images (Figure 3.29c and Figure 3.29d). On examination of Figure 3.29d it is possible to assign these variations in phase to small (100 nm) crystallites. Whilst extended crystal structures are thought to be favourable for charge transport and obtaining higher J$_{sc}$,[29,30] small crystal structures can create trap sites at grain boundaries, result in in higher levels of recombination and limit the interfacial area between the PC$_{61}$BM and the polymer-donor.[31]
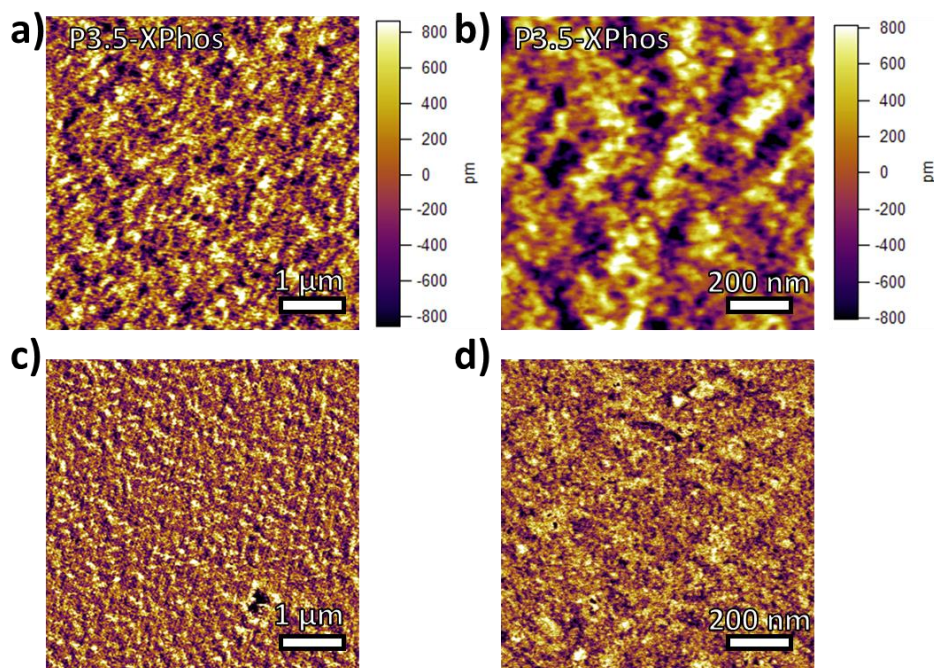
Figure 3.28: AFM height (a and b) and phase (c and d) images of PTBnDT(CO$_2$C$_{12}$)-*stat*-BTBT polymer P3.5-XPhos spin cast on to ITO and annealed at 180 °C for 5 minutes: a and c; 5x5 μm² (scale bar 1 μm), b and d; 1x1 μm² (scale bar 200 nm).
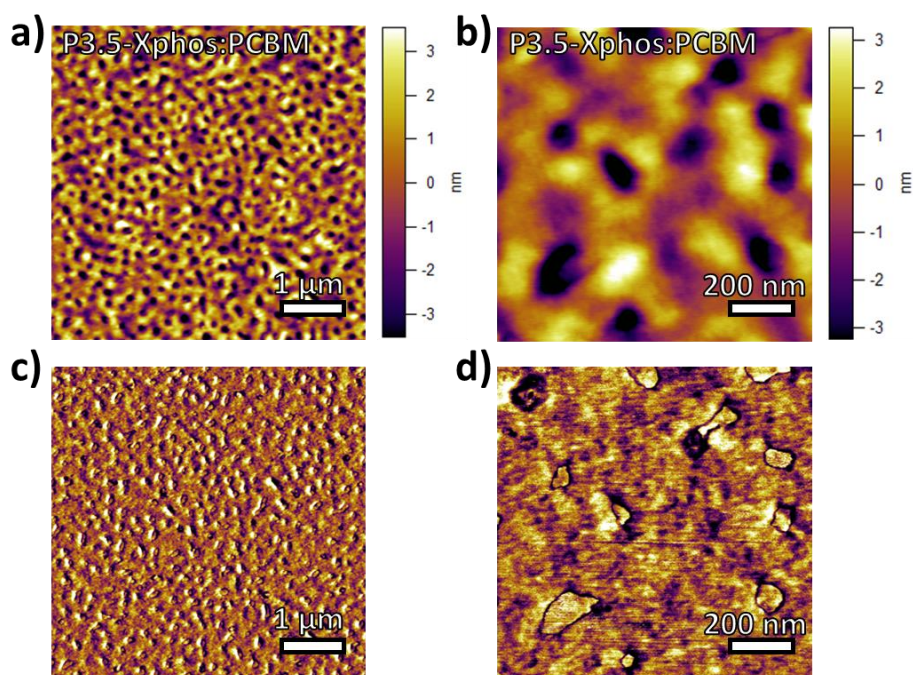
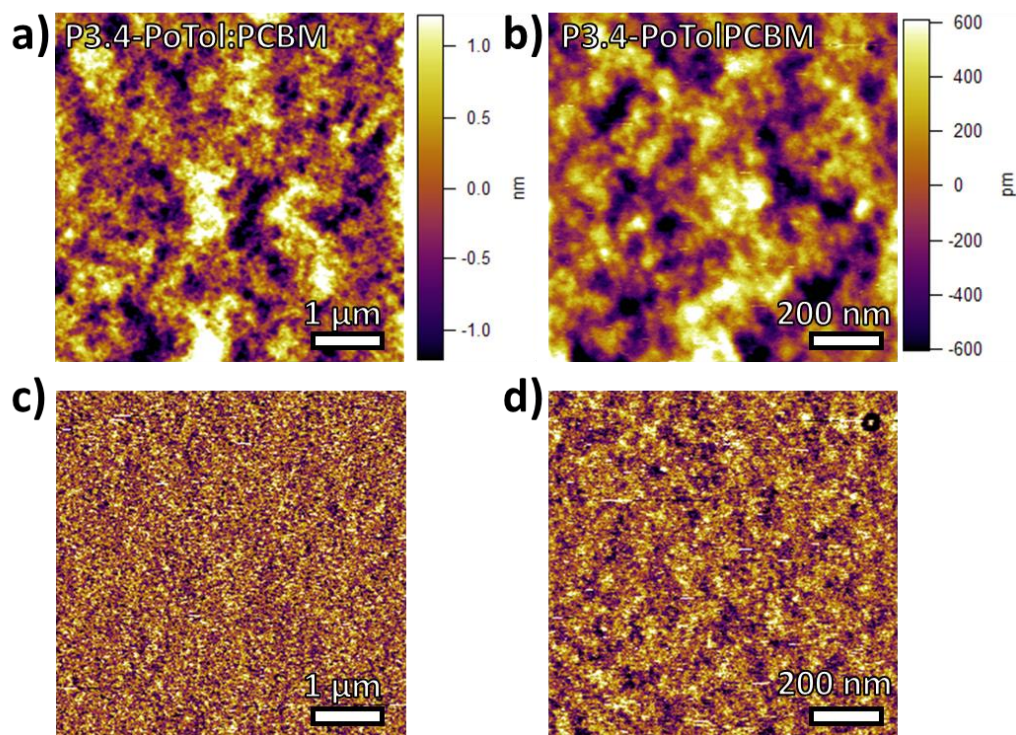Figure 3.29: AFM height (a and b) and phase (c and d) images of $PC_{61}BM$: $PTBnDT(CO_2C_{12})$-*stat*-BTBT polymer **P3.5-XPhos** spin cast on to ITO and annealed at 180 °C for 5 minutes: a and c; 5x5 μm² (scale bar 1 μm), b and d; 1x1 μm² (scale bar 200 nm).

The polymer $PTBnDT(CO_2C_{12})$-*stat*-PTBT resulting from the $Pd:(P(2,4-Me_2Ph)_3$ catalyst presents a smooth film with no phase contrast (Figure 3.30) and shows no signs of self-assembly or aggregation. The polymer : fullerene blend topography in Figure 3.31a and Figure 3.31b is indicative of an interpenetrating bulk heterojunction. Closer examination of the film (1x1 μm scan Figure 3.30b and Figure 3.30d) shows domains in the range of 50-70 nm which is promising for efficient charge separation and subsequent charge extraction.
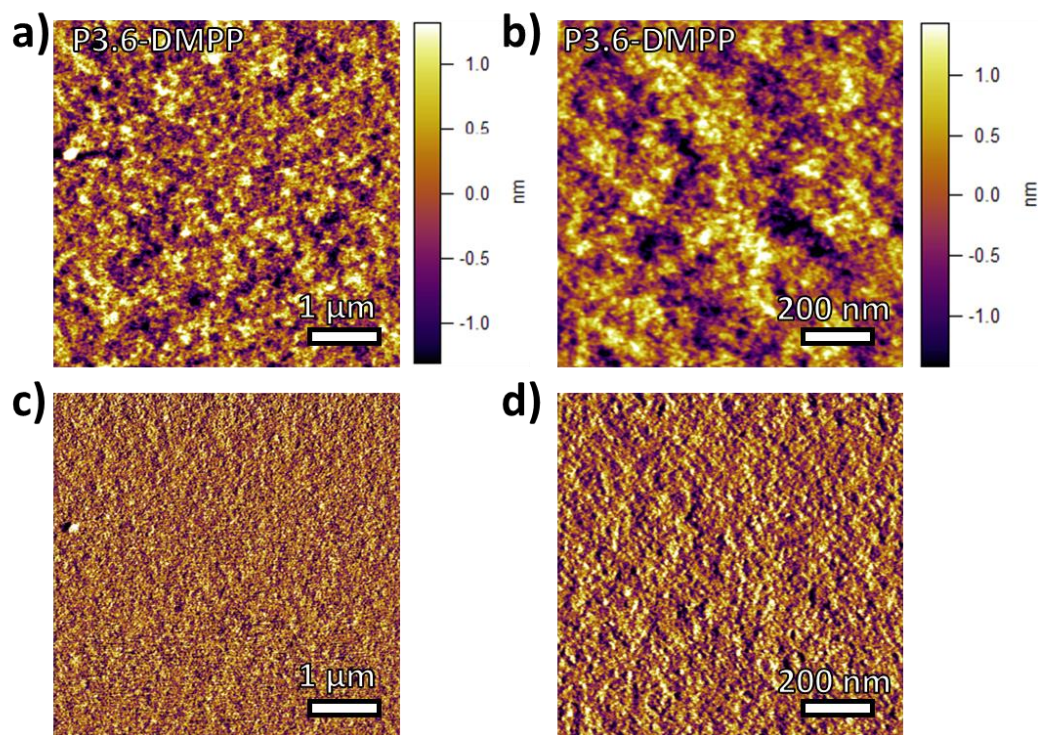
Figure 3.30: AFM height (a and b) and phase (c and d) images of PTBnDT(CO₂C₁₂)-*stat*-BTBT polymer P3.6-DMPP spin cast on to ITO and annealed at 180 °C for 5 minutes: a and c; 5x5 μm² (scale bar 1 μm), b and d; 1x1 μm² (scale bar 200 nm).
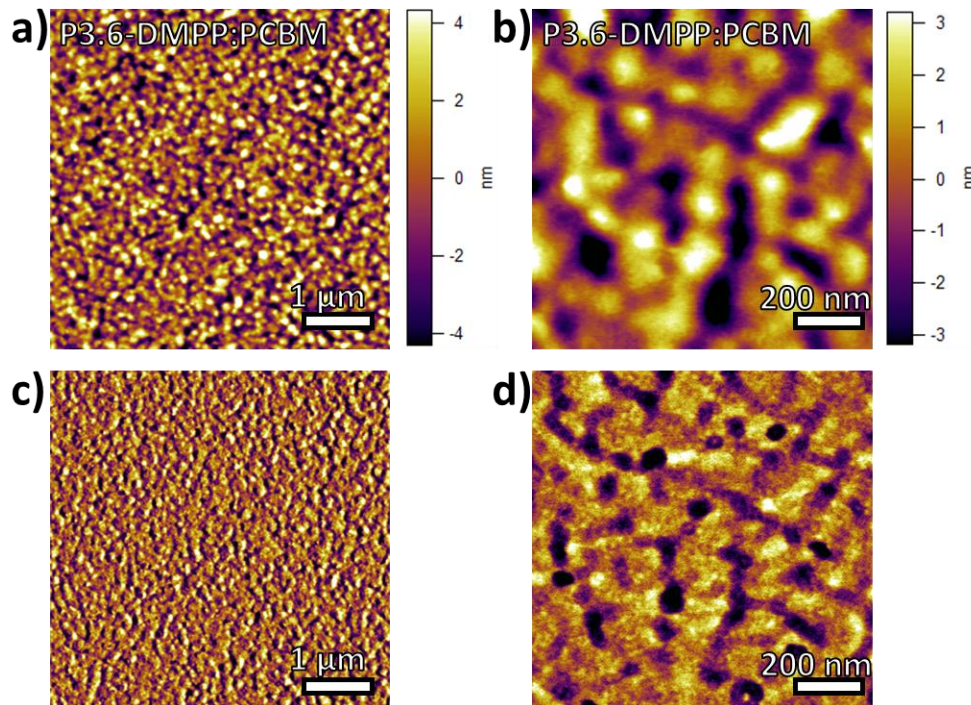
Figure 3.31: AFM height (a and b) and phase (c and d) images of PC₆₁BM : PTBnDT(CO₂C₁₂)-*stat*-BTBT polymer P3.6-DMPP spin cast on to ITO and annealed at 180 °C for 5 minutes: a and c; 5x5 μm² (scale bar 1 μm), b and d; 1x1 μm² (scale bar 200 nm).

The polymer PTBnDT(CO_2C_{12})-*stat*-PTBT synthesised using Pd:P(*o*-OMePh)$_3$ demonstrates unusual morphology with small particles observed which are 100-200 nm in size (Figure 3.32a and Figure 3.32c). A smaller 1x1 μm scan reveals that these small particles could have a crystal-like nature and grain boundaries can be seen in the phase image (Figure 3.32d). The polymer:PC$_{61}$BM blend 5x5 μm scan (Figure 3.33a) shows similar features to the polymer film, when the blend is examined more closely (Figure 3.33b and Figure 3.33d) it is difficult to distinguish any boundaries indicating thorough mixing of the polymer and fullerene may be present. The resulting film lacks distinct domains of polymer and fullerene which will result in poor charge generation and poor charge extraction. This is in contrast to the PTBnDT(C_{12})-*stat*-PTBT equivalent which shows demonstrates a promising morphology with domains < 50 nm (Figure 3.19).
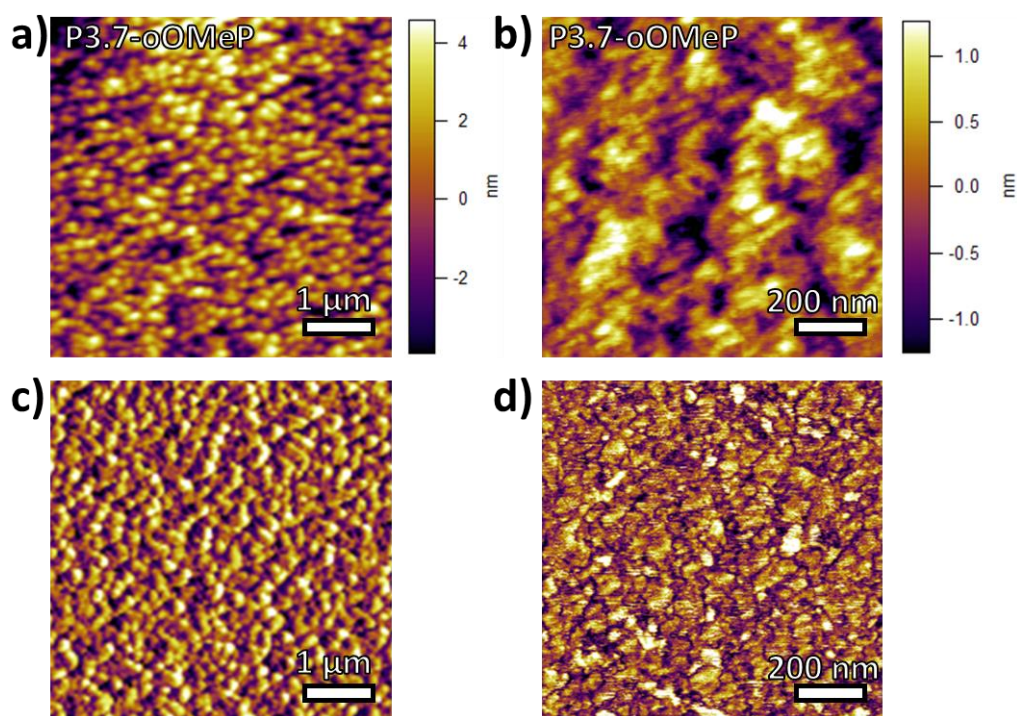
Figure 3.32: AFM height (a and b) and phase (c and d) images of PTBnDT(CO_2C_{12})-*stat*-BTBT polymer 3.7-oOMeP spin cast on to ITO and annealed at 180 °C for 5 minutes: a and c; 5x5 μm^2 (scale bar 1 μm), b and d; 1x1 μm^2 (scale bar 200 nm).
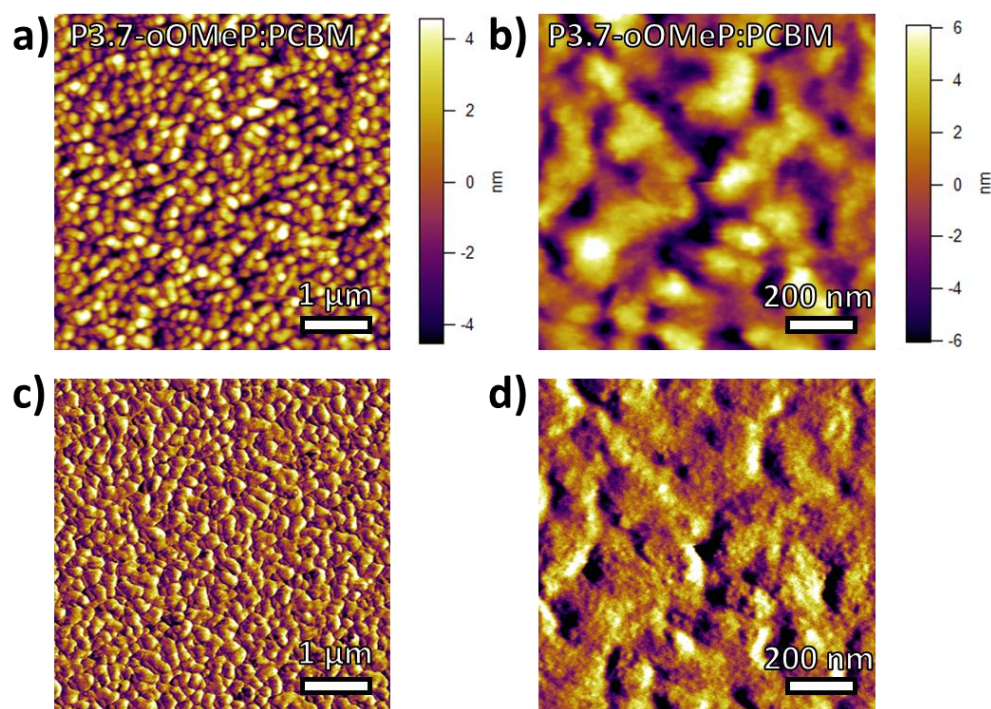
Figure 3.33: AFM height (a and b) and phase (c and d) images of $PC_{61}BM$: $PTBnDT(CO_2C_{12})$-*stat*-BTBT polymer 3.7-oOMeP spin cast on to ITO and annealed at 180 °C for 5 minutes: a and c; 5x5 µm² (scale bar 1 µm), b and d; 1x1 µm² (scale bar 200 nm).

The polymer film for $PTBnDT(CO_2C_{12})$-*stat*-PTBT synthesised by Pd:P(*o*-tolyl)$_3$ catalyst (Figure 3.34) is a smooth film, examination of the phase image Figure 3.34d could suggest some micro-phase separation owing to the block-like structure of the polymer, however, these domains are on the edge of the instrument's resolution (10-15 nm). Each of the $PTBnDT(CO_2C_{12})$-*stat*-PTBT has demonstrated a largely amorphous film devoid of any large aggregates as suggested by evaluation of the CV data (Figure 3.27). Blending with $PC_{61}BM$ (Figure 3.35) exhibits a film similar to that of $PTBnDT(CO_2C_{12})$-*stat*-PTBT synthesised by Pd:P(2,4-Me$_2$Ph)$_3$ which is suspected to have a similar block-like structure. The smaller scan size (1x1 µm), Figure 3.35b, shows a smooth film demonstrating the miscibility of the electron donating polymer and the electron accepting fullerene. The phase image (Figure 3.35d) shows evidence of phase separation and domain sizes in the order of 100 nm, similar to other block-like polymers discussed in this Chapter (Figure 3.17 and Figure 3.31).
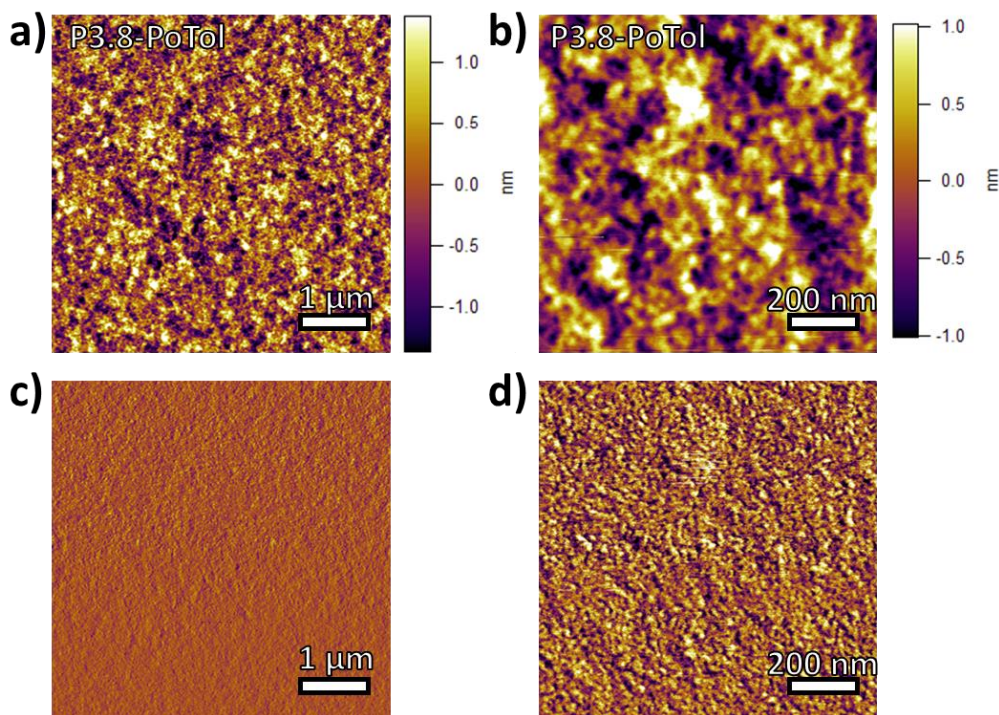
Figure 3.34: AFM height (a and b) and phase (c and d) images of PTBnDT(CO$_2$C$_{12}$)-*stat*-BTBT polymer P3.8-PoTol spin cast on to ITO and annealed at 180 °C for 5 minutes: a and c; 5x5 μm² (scale bar 1 μm), b and d; 1x1 μm² (scale bar 200 nm).
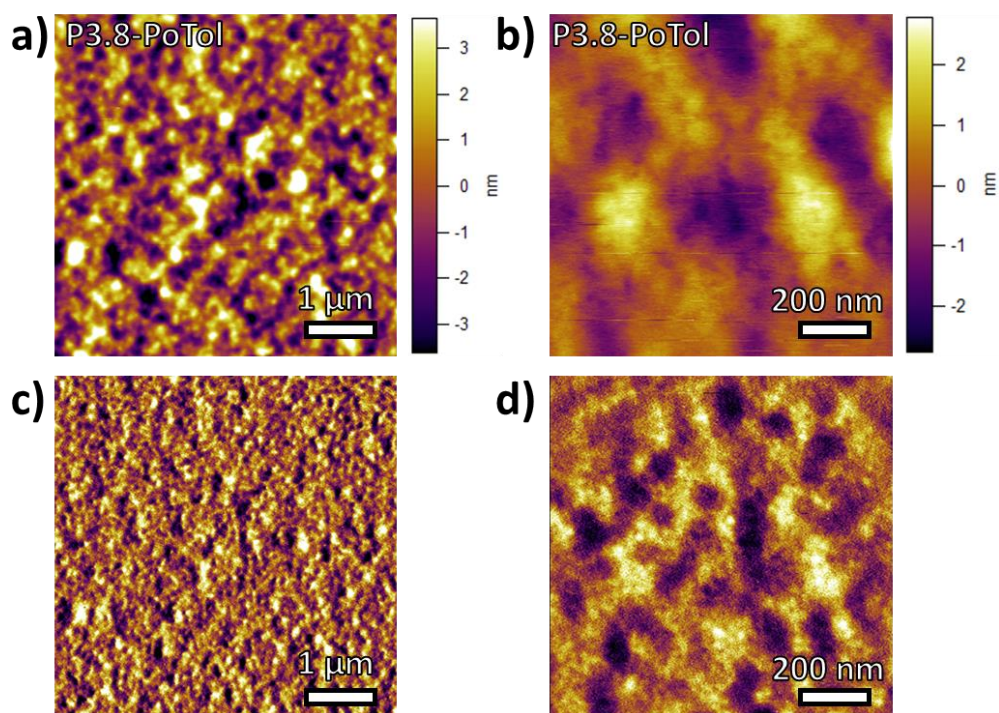
Figure 3.35: AFM height (a and b) and phase (c and d) images of PC$_{61}$BM : PTBnDT(CO$_2$C$_{12}$)-*stat*-BTBT polymer P3.8-PoTol spin cast on to ITO and annealed at 180 °C for 5 minutes: a and c; 5x5 μm² (scale bar 1 μm), b and d; 1x1 μm² (scale bar 200 nm).

3.3: Conclusions

In this Chapter the significance of the choice of catalyst on polymer backbone sequence and resulting physical and optoelectronic properties has been demonstrated. Whilst most catalytic systems are optimised to achieve functional molecular weights and high yields this work has demonstrated that the effect of catalyst on monomer sequence in ternary Stille polycondensation reactions is something that must be considered carefully when designing functional materials for BHJ-OPV devices. Both the electronic and steric properties of the ligand can have profound effects on monomer sequence and one must also consider the electronic and steric properties of the monomers. While the kinetic data presented here may not be transferable to all monomer systems, we have presented simple kinetic experiments which can be used to infer backbone sequencing of many conjugated monomers, given that one has a suitable method for quantifying monomer conversion.

PTBnDT(C_{12})-*stat*-PTBT synthesised using different catalysts exhibited a variation in optoelectronic and morphological properties, those with a more block-like structure synthesised from Pd(2,4-Me$_2$Ph)$_3$ and Pd:P(*o*-tolyl)$_3$ demonstrate a lower HOMO while maintaining a similar bandgap to the more random polymers synthesised with Pd:XPhos and Pd:P(*o*-OMePh)$_3$ systems. The more block-like systems displayed less aggregation indicated by the absence of secondary oxidation peaks in the CV and large aggregates in the AFM, they demonstrate good miscibility with PC$_{61}$BM leading to domains in the order of 50-100 nm.

PTBnDT(CO$_2$C$_{12}$)-*stat*-PTBT polymers synthesised using different catalytic systems show more reproducible optoelectronic properties, the diester helps to break up the aggregation of the molecule leading to a more consistent morphology between polymers as well as lowering the HOMO and allowing for a greater V$_{oc}$. As with the PTBnDT(C_{12})-*stat*-PTBT the PTBnDT(CO$_2$C$_{12}$)-*stat*-PTBT with a block-like nature demonstrate good BHJ morphology with potentially favourable domain sizes.

3.4: Experimental

3.4.1: Materials

2,6-Dibromo-4,8-didodecylbenzo[1,2-b:4,5-b']dithiophene, didodecyl 2,6-dibromobenzo[1,2-b:4,5-b']dithiophene-4,8-dicarboxylate, 4,7-dibromo-5,6-bis(octyloxy)benzo[c][1,2,5]thiadiazol, 2,5-bis(trimethylstannyl)thiophene and phenyl-C_{61}-butyric acid methyl ester ($PC_{61}BM$) were provided by Merck ltd. Anhydrous chlorobenzene (99.9 %) was purchased from ACROS Organics and used without further purification. Tris(dibenzylideneacetone)dipalladium(0) (Pd_2(dba)$_3$) was purchased from Sigma Aldrich and recrystallised from chloroform to obtain Pd_2(dba)$_3$.$CHCl_3$. Tris(o-tolyl)phosphine (> 97 %), tris(2,4-dimethylphemyl)phosphine (> 97 %), tris(2,4,6-trimethylphenyl)phosphine (> 97 %), tris(2-methoxyphenyl) phosphine (> 97 %), tricyclohexyl phosphine (> 97 %), triphenoxy phosphite (> 95 %) and XPhos (> 97 %) were purchased from Sigma Aldrich and used without further purification. Tetrabutylammonium hexafluorophosphate (99.9 %), silver nitrate, ferrocene (99.9 %), butylated hydroxytoluene and 2-tributylstannyl thiophene were purchased from Sigma-Aldrich and used without further purification.

3.4.2: Methods

NMR. ^{1}H NMR was run on a Bruker Avance 300 MHz spectrometer in deuterated chloroform at 25 °C. High temperature data was obtained using Bruker Avance III 400 MHz spectrometer at 100 °C in 1,1,2,2-tetrachloroethane.

Optoelectronic properties. UV-Vis spectra where obtained using an Agilent Technologies Cary 60 UV-Vis spectrometer. Samples were made up to a concentration of 0.01 mg/ml by serial dilution in chloroform. Cyclic voltammetry was conducted on a CH-Instruments 600 E potentiostat using a 3 mm Pt disc electrode which was polished with 0.05 μm alumina powder, rinsed with milliQ water, acetone and IPA prior to each use. The counter electrode was a platinum wire coil which was annealed in a blue flame prior to use. The reference electrode was Ag/Ag^+, the silver wire was polished and rinsed with milliQ water, IPA and acetone, the wire was then placed into a glass capillary tube fitted with a vycor frit and filled with 0.01 mM $AgNO_3$ solution. The system was calibrated using the ferrocene(Fc)/ferrocenium(Fc^+) redox couple. 0.100 M tetrabutylammonium hexafluorophosphate ($TBAPF_6$) was used as the supporting electrolyte. Analytes were dissolved at a concentration of 2 mg/ml in a solution of 2

mg/ml of TBAPF$_6$ in chlorobenzene, drop cast onto Pt the disk electrode and allowed to dry under ambient conditions.

Gel permeation chromatography. GPC was run on an Agilent PL220 instrument equipped with differential refractive index (DRI) and viscometry (VS) detectors. The system was equipped with 2 x PLgel Olexis columns (300 x 7.5 mm) and a Olexis 10 μm guard column. The mobile phase was 1,2,4-trichlorobenzene (TCB) with 250 ppm BHT (butylated hydroxytoluene) as the stabilising additive. Samples were run at 1 ml/min at 160 °C. The system was calibrated between M_p = 164 and 6,035,000 using 12 polystyrene narrow standards (Agilent EasyVials) to create a third order calibration. Analyte samples were filtered through a stainless steel frit with 10 μm pore size at 140 °C prior injection. Experimental molar mass (M_n, GPC) and dispersity (D) values of synthesized polymers were determined by conventional calibration using Agilent GPC/SEC software.

TGA Measurements. TGA spectra were recorded on a Mettler Toledo TGA/DSC1. Samples were analysed from 25 to 600 °C at a 10 °C min^{-1} heating rate under a nitrogen atmosphere.

AFM measurements. Polymer and Polymer : PC$_{61}$BM films were spin cast at 2000 RPM for 60 seconds from a 10 mg/ml solution of polymer and 1 : 2 polymer : PC$_{61}$BM in chlorobenzene. Films were cast onto ITO coated glass and annealed at 180 ° C for 5 minutes. Atomic Force Microscopy images were obtained using an Asylum Research MFP-3D AFM, using AC 240-TS probes with a spring constant of 0.67 - 3.51 N/m purchased from oxford instruments in intermittent contact (tapping) mode. Images were analysed and processed using the Igor software package.

3.4.3: Experimental procedures

Polycondensation kinetics. To a dry 100 ml, 3-neck- round bottom flask 275.3 mg (0.500 mmol) 4,7-Dibromo-5,6-bis(octyoxy)-benzo-2,1,3-thiadiazole, 342.3 mg (0.500 mmol) 2,6-dibromo-4,8-di(dodecyl)benzo-[1,2-b:4,5-b']dithiophene and 409.8 mg (1.000 mmol) of 2,5-bis(trimethylstannyl)thiophene were added. The central neck was fitted with a condenser, the top of which was sealed with a rubber septum, and the remaining two necks were fitted with rubber septa. The system was evacuated and refilled with nitrogen gas for three cycles. 48.0 mL of dry, degassed chlorobenzene was cannulated into the flask which thereafter was kept under a positive nitrogen pressure.

To a separate glass sinter vial 31.1 mg (0.030 mmol) of tris(dibenzylideneacetone)dipalladium(0)-chloroform adduct and 54.8 mg of P(*o*-tolyl)$_3$ (0.18 mmol) were added. The glass sinter vial was sealed with a rubber septum, evacuated and back filled with nitrogen for three cycles. 3 ml of dry chlorobenzene was added via a degassed syringe.

The main reaction vessel was refluxed to 133 °C. A t = 0 sample (100 μL) was taken before 2 ml of the fully solvated catalyst solution was added via a degassed syringe. Further 100 μL samples were taken at t = 1, 2, 3, 4, 5, 10, 15, 20, 25, 30, 60, 120, 180, 240, 300 and 1440 min, and quenched by bubbling with air. Monomer conversion was followed by ^{1}H NMR in chloroform-D at 25 °C.

The remaining solution was reduced to a minimum volume (2-5 ml) under vacuum and was precipitated into 150 ml of methanol. The precipitate was filtered through a cellulose thimble and purified by Soxhlet extraction with acetone, hexane and chloroform (a chlorobenzene fraction was obtained for more insoluble materials). The chloroform and chlorobenzene fractions were precipitated into 150 ml of methanol and the precipitate was isolated by vacuum filtration. The resulting polymers were dried under vacuum at 40 °C for 24 hours. The ^{1}H NMR spectra of the resulting polymers were obtained at a concentration of 10 mg/ml in 1,1,2,2-tetrachloroethane at 100 °C.

Synthesis of PTBnDT(C$_{12}$)-*stat*-PTBT Polymers. To a dry 100 ml, 2-neck 100 ml round bottom flask 55.1 mg (0.100 mmol) 4,7-Dibromo-5,6-bis(octyoxy)-benzo-2,1,3-thiadiazole, 68.5 mg (0.100 mmol) 2,6-dibromo-4,8-di(dodecyl)benzo-[1,2-b:4,5-b']dithiophene and 77.8 mg (0.190 mmol) of 2,5-bis(trimethylstannyl)thiophene were added. The central neck was fitted with a condenser, the top of which was sealed with a rubber septum and the remaining neck was fitted with rubber septa. The system was evacuated and refilled with nitrogen gas for three cycles. 8.0 mL of dry, degassed chlorobenzene was cannulated into the flask which thereafter was kept under a positive nitrogen pressure.

To a separate glass sinter vial 4.1 mg (0.004 mmol) of tris(dibenzylideneacetone)dipalladium(0)-chloroform adduct and 0.024 mmol of the chosen ligand were added. The glass sinter vial was sealed with a rubber septum, evacuated and back filled with nitrogen for three cycles. 3 ml of dry chlorobenzene was

added via a degassed syringe. 2.0 ml of the premixed catalyst solution was then added to the reaction mixture.

The reaction mixture was refluxed at 133 °C for 24 hours, the resulting polymeric solution was then reduced under vacuum to approximately 2 ml. The polymer was precipitated into 150 ml of methanol and filtered through a cellulose thimble. The polymer was then purified by Soxhelt extraction with acetone, hexanes and chloroform. The chloroform fraction was precipitated into 150 ml of methanol and collected by vacuum filtration. The polymer was dried under vacuum at 40 °C for 24 hours. The polymers were characterised by ^{1}H NMR (Figure 3.36 – Figure 3.39).

P3.1-XPhos (Figure 3.36) δ(ppm) =: 8.54-8.46 (2H, ss) is assigned to the protons on the BnDT unit, 7.68-6.98 (4H, m) is assigned to the protons on the bridging thiophene units, 4.20 (4H, s) is attributed to the α-protons of the alkoxy side chains situated on the BT unit, 3.12 (4H, s) relate to the α-protons of the dodecyl side chains on the BnDT unit, finally, 2.22-0.5 is assigned to the remaining alkyl protons on both the BT and BnDT units.
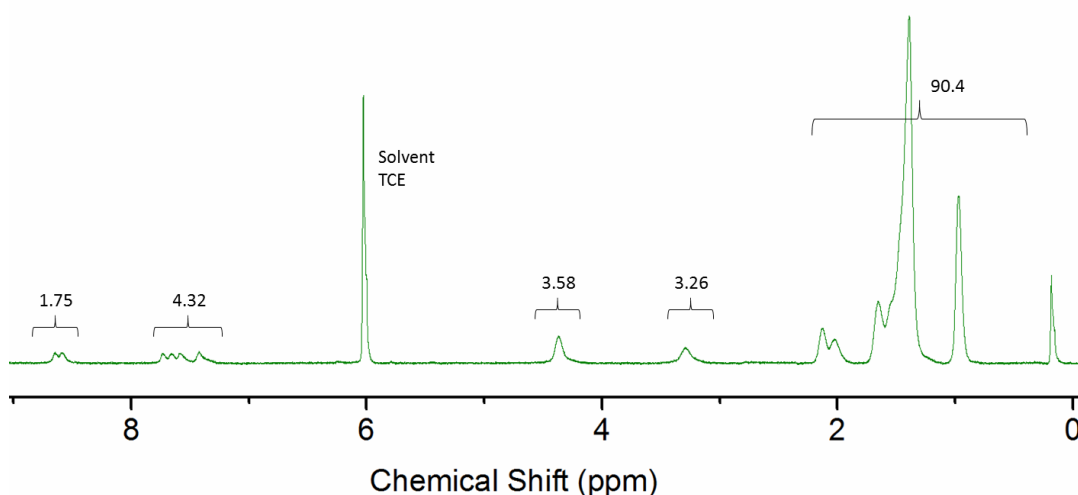
Figure 3.36: ^{1}H NMR of PTBnDT(C$_{12}$)-*stat*-PTBT polymer P3.1-XPhos.

^{1}H NMR of P3.2-DMPP (Figure 3.37) δ(ppm) =: 8.75-8.44 (2H, ss) is assigned to the protons on the BnDT unit, 7.82-7.22 (4H, m) is assigned to the protons on the bridging thiophene units, 4.34 (4H, s) is attributed to the α-protons of the alkoxy side chains situated on the BT unit, 3.25 (4H, s) relate to the α-protons of the dodecyl side chains on the BnDT unit, finally, 2.22-0.5 is assigned to the remaining alkyl protons on both the BT and BnDT units.
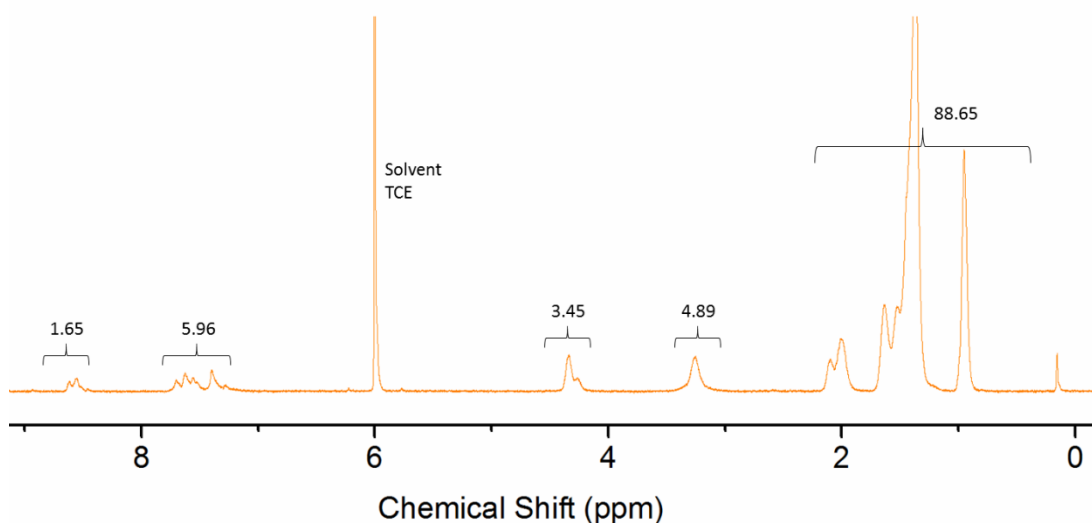
Figure 3.37: ¹H NMR of PTBnDT(C₁₂)-*stat*-PTBT polymer P3.2-DMPP.

¹H NMR of P3.3-oOMeP (Figure 3.38) δ(ppm) =: 8.78-8.38 (2H, ss) is assigned to the protons on the BnDT unit, 7.89-7.15 (4H, m) is assigned to the protons on the bridging thiophene units, 4.35 (4H, s) is attributed to the α-protons of the alkoxy side chains situated on the BT unit, 3.27 (4H, s) relate to the α-protons of the dodecyl side chains on the BnDT unit, finally, 2.22-0.5 is assigned to the remaining alkyl protons on both the BT and BnDT units.
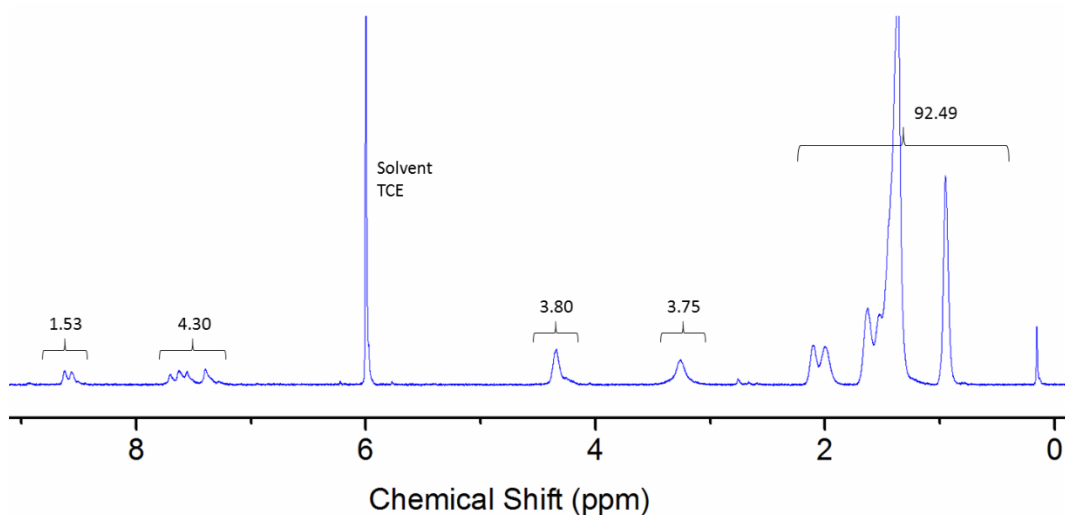
Figure 3.38: ¹H NMR of PTBnDT(C₁₂)-*stat*-PTBT polymer P3.3-oOMeP.

¹H NMR of P3.4-PoTol (Figure 3.39) δ(ppm) =: 8.72-8.43 (2H, ss) is assigned to the protons on the BnDT unit, 7.88-7.10 (4H, m) is assigned to the protons on the bridging thiophene units, 4.34 (4H, s) is attributed to the α-protons of the alkoxy side chains situated on the BT unit, 3.26 (4H, s) relate to the α-protons of the dodecyl side chains on

the BnDT unit, finally, 2.22-0.5 is assigned to the remaining alkyl protons on both the BT and BnDT units.
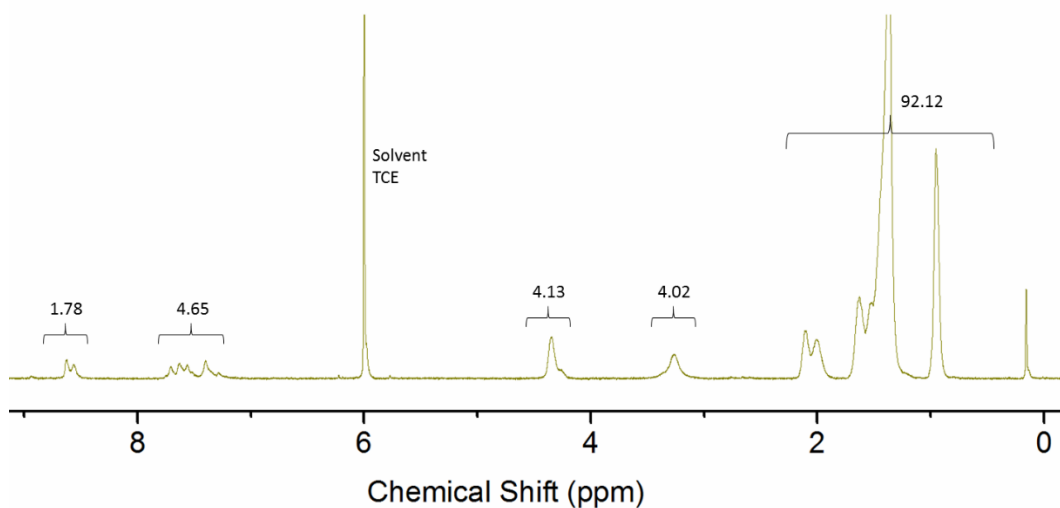
Figure 3.39: ^{1}H NMR of PTBnDT(C$_{12}$)-*stat*-PTBT polymer P3.4-PoTol.

The molecular weight averages of PTBnDT(C$_{12}$)-*stat*-PTBT polymers P3.1-P3.4 were determined by high temperature GPC, the overlaid molecular weight distributions are shown in Figure 3.40 and the averages are summarised in Table 3.2 (Section 3.2.3) along with the T$_D$ as determined by TGA (Figure 3.41).
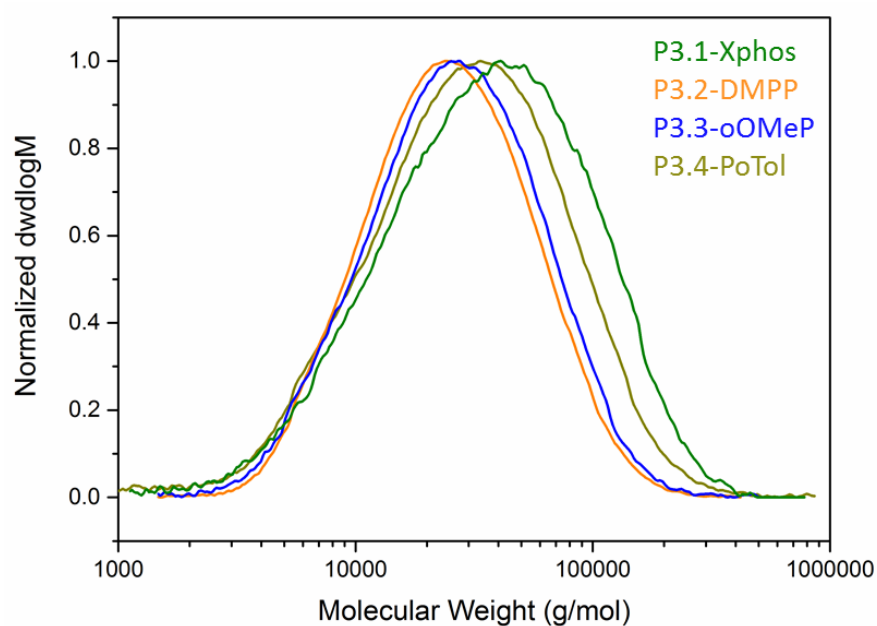
Figure 3.40: Molecular weight distributions (by GPC) of PTBnDT(C$_{12}$)-*stat*-PTBT polymers; P3.1-XPhos, P3.2-DMPP, P3.3-oOMeP and P3.4-PoTol.
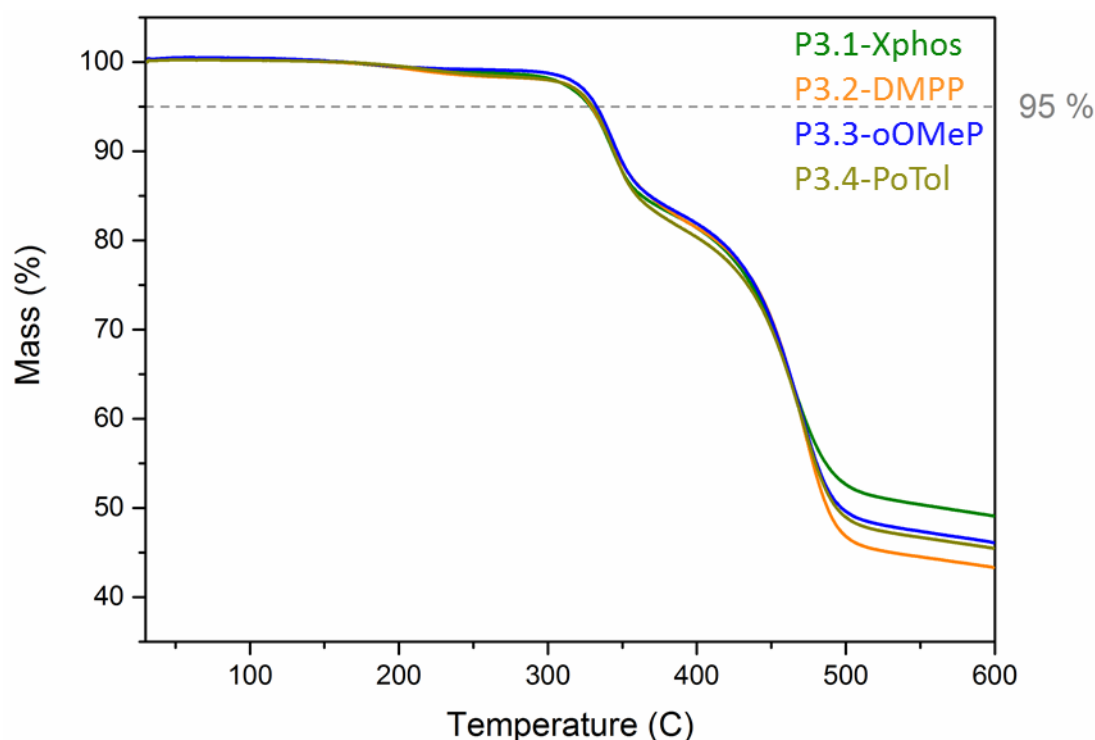
Figure 3.41: TGA traces of PTBnDT(C$_{12}$)-*stat*-PTBT polymers; P3.1-XPhos, P3.2-DMPP, P3.3-oOMeP and P3.4-PoTol..

Synthesis of PTBnDT(CO$_2$C$_{12}$)-*stat*-PTBT Polymers. To a dry 100 ml, 2-neck 100 ml round bottom flask 77.2 mg (0.100 mmol) didodecyl benzo[1,2-b:4,5-b']dithiophene-4,8-dicarboxylate, 68.5 mg (0.100 mmol) 2,6-dibromo-4,8-di(dodecyl)benzo-[1,2-b:4,5-b']dithiophene and 77.8 mg (0.190 mmol) of 2,5-bis(trimethylstannyl)thiophene were added. The rest of the procedure was identical to the synthesis of PTBnDT(C$_{12}$)-*stat*-PTBT polymers reported above. The PTBnDT(CO$_2$C$_{12}$)-*stat*-PTBT polymers P3.5-P3.8 were characterised by ^{1}H NMR (Figures 3.42-3.45).

P3.5-XPhos (Figure 3.42) δ(ppm) =: 8.75-8.32 (2H, ss) is assigned to the protons on the BnDT unit, 8.32-6.59 (4H, m (broad, high signal to noise)) is assigned to the protons on the bridging thiophene units, 4.75 (4H, s) relate to the α-protons of the carboxydodecyl side chains on the BnDT unit, 4.34 (4H, s) is attributed to the α-protons of the alkoxy side chains situated on the BT unit, finally, 2.50-0.5 is assigned to the remaining alkyl protons on both the BT and BnDT units.
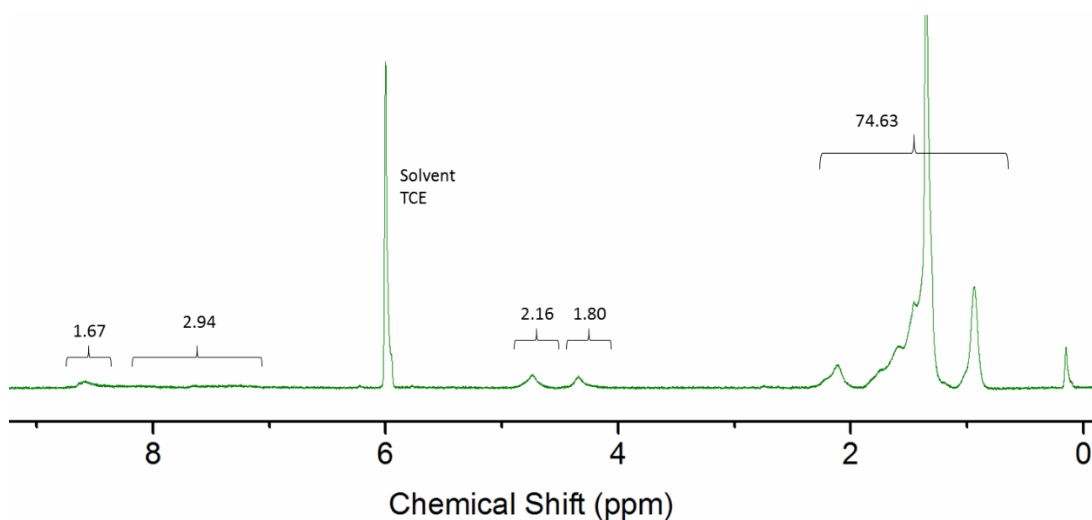
Figure 3.42: ^{1}H NMR of PTBnDT(CO$_2$C$_{12}$)-*stat*-PTBT polymer P3.5-XPhos.

P3.6-DMPP (Figure 3.43) δ(ppm) =: 8.89-8.33 (2H, ss) is assigned to the protons on the BnDT unit, 8.29-6.79 (4H, m (broad, high signal to noise)) is assigned to the protons on the bridging thiophene units, 4.75 (4H, s) relate to the α-protons of the carboxydodecyl side chains on the BnDT unit, 4.36 (4H, s) is attributed to the α-protons of the alkoxy side chains situated on the BT unit, finally, 2.50-0.5 is assigned to the remaining alkyl protons on both the BT and BnDT units.
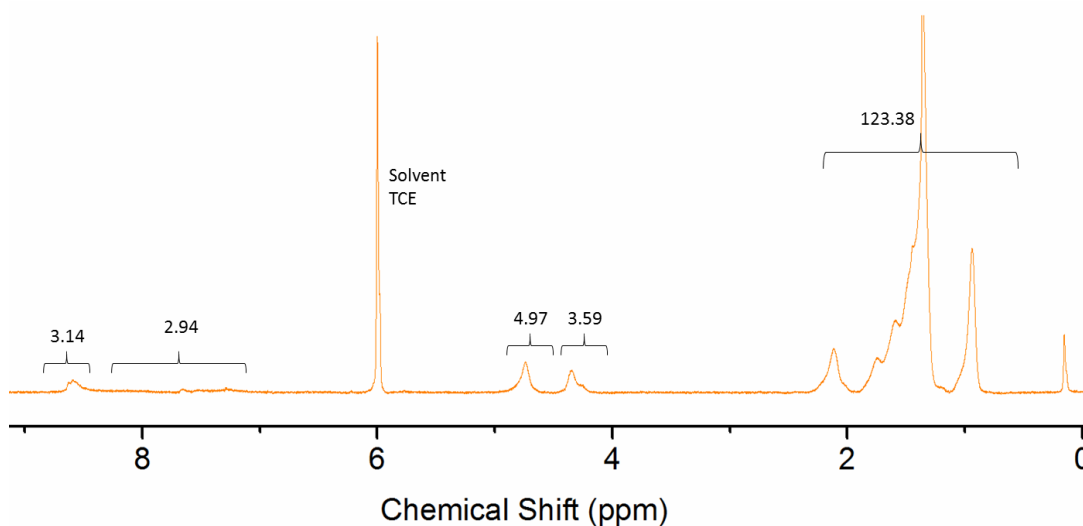
Figure 3.43: ^{1}H NMR of PTBnDT(CO$_2$C$_{12}$)-*stat*-PTBT polymer P3.6-DMPP.

P3.7-oOMeP (Figure 3.44) δ(ppm) =: 8.80-8.34 (2H, ss) is assigned to the protons on the BnDT unit, 8.30-6.79 (4H, m (broad, high signal to noise)) is assigned to the protons on the bridging thiophene units, 4.74 (4H, s) relate to the α-protons of the carboxydodecyl

side chains on the BnDT unit, 4.35 (4H, s) is attributed to the α-protons of the alkoxy side chains situated on the BT unit, finally, 2.50-0.5 is assigned to the remaining alkyl protons on both the BT and BnDT units.
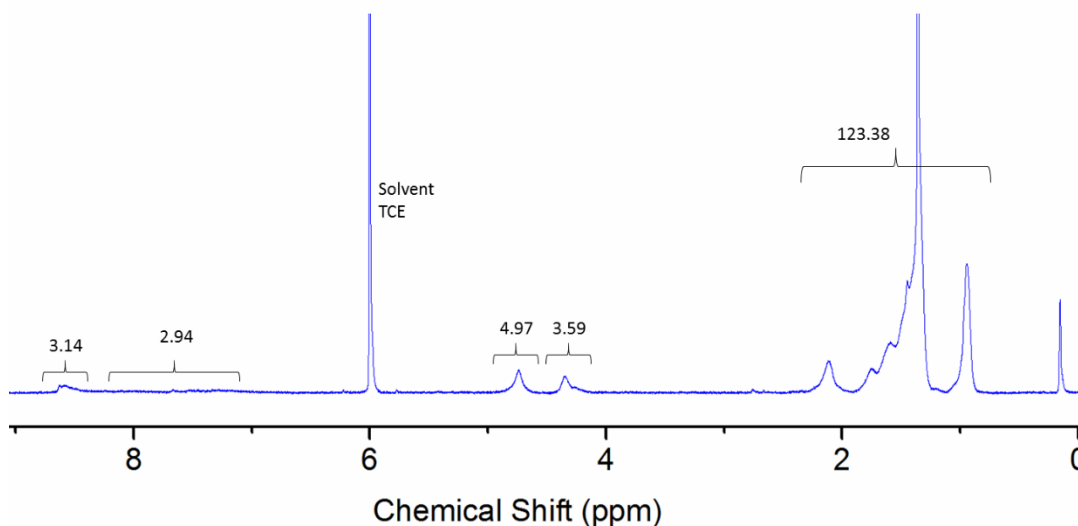
Figure 3.44: ^{1}H NMR of PTBnDT(CO$_2$C$_{12}$)-*stat*-PTBT polymer P3.7-oOMeP.

P3.7-PoTol (Figure 3.44) δ(ppm) =: 8.84-8.27 (2H, ss) is assigned to the protons on the BnDT unit, 8.25-6.94 (4H, m (broad, high signal to noise)) is assigned to the protons on the bridging thiophene units, 4.75 (4H, s) relate to the α-protons of the carboxydodecyl side chains on the BnDT unit, 4.35 (4H, s) is attributed to the α-protons of the alkoxy side chains situated on the BT unit, finally, 2.50-0.5 is assigned to the remaining alkyl protons on both the BT and BnDT units.
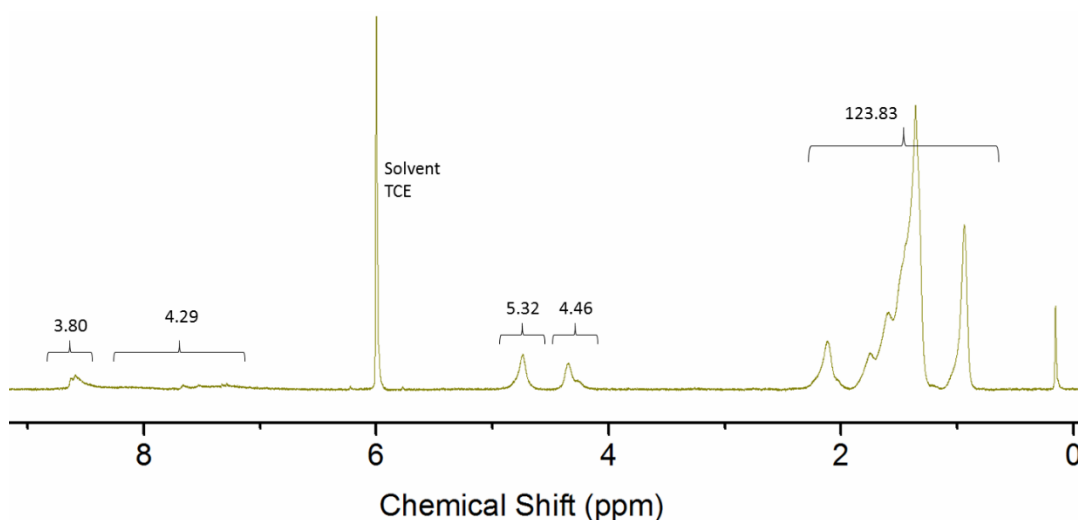
Figure 3.45: ^{1}H NMR of PTBnDT(CO$_2$C$_{12}$)-*stat*-PTBT polymer P3.8-PoTol.

The molecular weight averages of PTBnDT(C_{12})-*stat*-PTBT polymers P3.1-P3.4 were determined by high temperature GPC, the overlaid molecular weight distributions are shown in Figure 3.46 and the averages are summarised in Table 3.4 (Section 3.2.6) along with the T_D as determined by TGA (Figure 3.47).
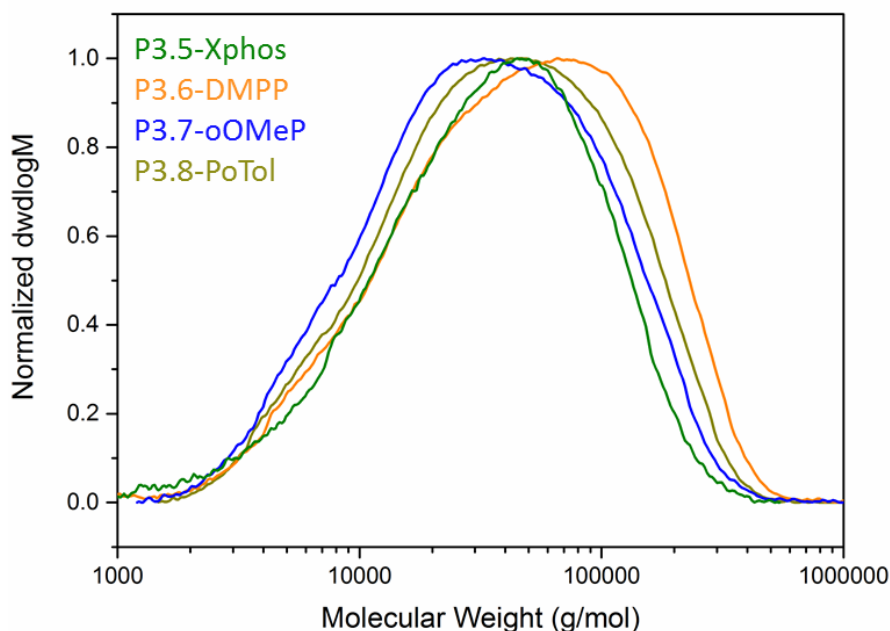
Figure 3.46: Molecular weight distributions (by GPC) of PTBnDT(CO_2C_{12})-*stat*-PTBT polymers; P3.5-XPhos, P3.6-DMPP, P3.7-oOMeP and P3.8-PoTol.
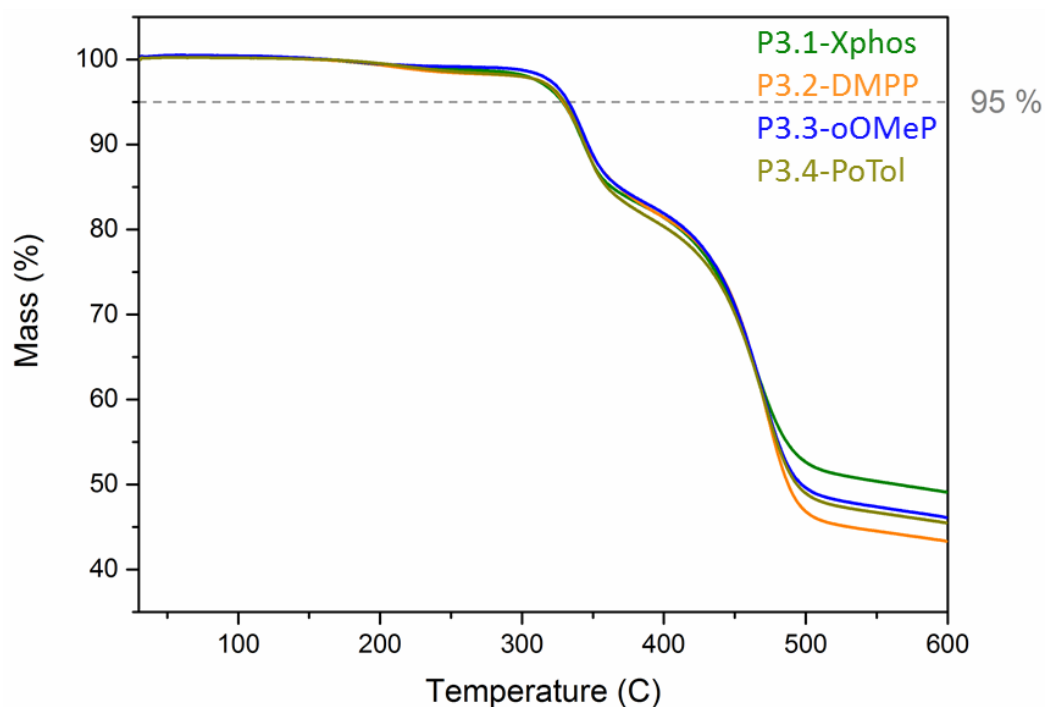
Figure 3.47: TGA plots of PTBnDT(CO_2C_{12})-*stat*-PTBT polymers; P3.5-XPhos, P3.6-DMPP, P3.7-oOMeP and P3.8-PoTol.).

3.5: References

(1)   Cordovilla, C.; Bartolome, C.; Martinez-Ilarduya, J. M.; Espinet, P. *ACS Cat.* **2015**, *5*, 3040.

(2)   Carsten, B.; He, F.; Son, H. J.; Xu, T.; Yu, L. *Chem. Revs.* **2011**, *111*, 1493.

(3)   Espinet, P.; Echavarren, A. M. *Angew. Chem. Inter. Edit.* **2004**, *43*, 4704.

(4)   Bao, Z. N.; Chan, W. K.; Yu, L. P. *J. Am. Chem. Soc.* **1995**, *117*, 12426.

(5)   Farina, V.; Kapadia, S.; Krishnan, B.; Wang, C. J.; Liebeskind, L. S. *J. Org. Chem.* **1994**, *59*, 5905.

(6)   Farina, V.; Krishnan, B. *J. Am. Chem. Soc.* **1991**, *113*, 9585.

(7)   Stille, J. K. *Angew. Chem. Inter. Edit.* **1986**, *25*, 508.

(8)   Wakioka, M.; Kitano, Y.; Ozawa, F. *Macromolecules* **2013**, *46*, 370.

(9)   Gao, J. H.; Wang, W.; Zhang, S. J.; Xiao, S. Q.; Zhan, C.; Yang, M. Y.; Lu, X. H.; You, W. *J. Mater. Chem. A* **2018**, *6*, 179.

(10)   Billingsley, K.; Buchwald, S. L. *J. Am. Chem. Soc.* **2007**, *129*, 3358.

(11)   Niemeyer, Z. L.; Milo, A.; Hickey, D. P.; Sigman, M. S. *Nat. Chem.* **2016**, *8*, 611.

(12)   Darensbourg, D. J.; Andreatta, J. R.; Stranahan, S. M.; Reibenspies, J. H. *Organometallics* **2007**, *26*, 6832.

(13)   Ohtsuka, Y.; Yamamoto, T.; Miyazaki, T.; Yamakawa, T. *Adv. Synth. Catal.* **2018**, *360*, 1007.

(14)   Martin, R.; Buchwald, S. L. *Accounts. Chem. Res.* **2008**, *41*, 1461.

(15)   Junfeng, Y.; Sijia, L.; Jian-Feng, Z.; Jianrong, Z. *Eur. J. Org. Chem.* **2012**, *2012*, 6248.

(16)   Li, W. T.; Yang, L. Q.; Tumbleston, J. R.; Ade, H.; You, W. *Abstr. Pap. Am. Chem, S.* **2014**, *247*.

(17)   Itaru, O.; Masahiko, S.; Hiroki, M.; Tomoyuki, K.; Kazuo, T. *Adv. Mater.* **2012**, *24*, 425.

(18)   Xiao, Z. Y.; Sun, K.; Subbiah, J.; Qin, T. S.; Lu, S. R.; Purushothaman, B.; Jones, D. J.; Holmes, A. B.; Wong, W. W. H. *Polym. Chem.* **2015**, *6*, 2312.

(19)   Leonat, L.; Beatrice Gabriela, S.; Branẑoi, I. V. *Cyclic voltammetry for energy levels estimation of organic materials*, **2013**; 75.

(20)   Bredas, J. L.; Beljonne, D.; Coropceanu, V.; Cornil, J. *Chem. Revs.* **2004**, *104*, 4971.

(21)   Brabec, C. J.; Cravino, A.; Meissner, D.; Sariciftci, N. S.; Fromherz, T.; Rispens, M. T.; Sanchez, L.; Hummelen, J. C. *Adv. Funct. Mater.* **2001**, *11*, 374.

(22)   Sweetnam, S.; Graham, K. R.; Ngongang Ndjawa, G. O.; Heumüller, T.; Bartelt, J. A.; Burke, T. M.; Li, W.; You, W.; Amassian, A.; McGehee, M. D. *J. Am. Chem. Soc.* **2014**, *136*, 14078.

(23)   He, Y.; Li, Y. *Phys. Chem. Chem. Phys.* **2011**, *13*, 1970.

(24)   Hedley, G. J.; Ward, A. J.; Alekseev, A.; Howells, C. T.; Martins, E. R.; Serrano, L. A.; Cooke, G.; Ruseckas, A.; Samuel, I. D. W. *Nat. Comms.* **2013**, *4*, 2867.

(25)   Yang, X. N.; Loos, J.; Veenstra, S. C.; Verhees, W. J. H.; Wienk, M. M.; Kroon, J. M.; Michels, M. A. J.; Janssen, R. A. J. *Nano Letters* **2005**, *5*, 579.

(26)   Shibasaki, K.; Tabata, K.; Yamamoto, Y.; Yasuda, T.; Kijima, M. *Macromolecules* **2014**, *47*, 4987.

(27)   Kohn, P.; Huettner, S.; Huck, W. T. S.; Sommer, J.-U.; Sommer, M. *J. Am. Chem. Soc.* **2012**, *134*, 4790.

(28)   Pirotte, G.; Agarkar, S.; Xu, B.; Maes, W.; Marder, S. R. *J. Mater. Chem. A* **2017**, *5*, 18166.

(29)   Li, L. G.; Niu, W. H.; Zhao, X. L.; Yang, X. N.; Chen, S. W. *Sci. Adv. Mater.* **2015**, *7*, 2021.

(30)   Coropceanu, V.; Cornil, J.; da Silva Filho, D. A.; Olivier, Y.; Silbey, R.; Brédas, J.-L. *Chem. Revs.* **2007**, *107*, 926.

(31)   Menelaou, C.; Tierney, S.; Blouin, N.; Mitchell, W.; Tiwana, P.; McKerracher, I.; Jagadish, C.; Carrasco, M.; Herz, L. M. *J. Phys. Chem. C* **2014**, *118*, 17351.

Chapter 4: Synthesis and Properties of All-Conjugated Block Copolymers
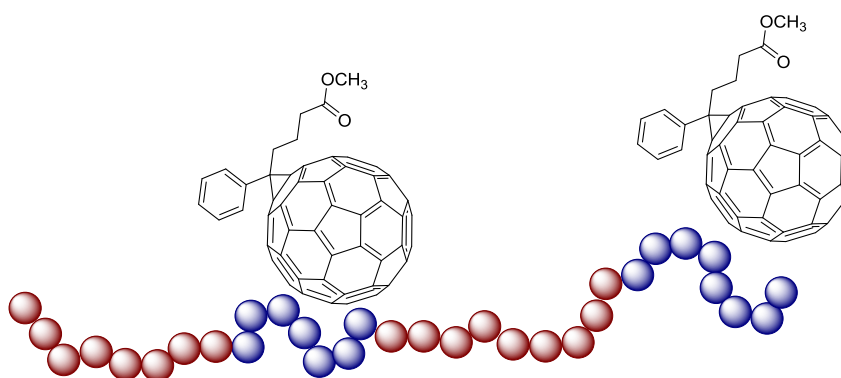
Abstract: Chapters Two and Three have focused on the kinetic studies of the Stille polycondensation and how it can be manipulated to alter the backbone sequence. In Chapter Four the synthesis of all-conjugated block copolymers is investigated. We investigate how well defined all-conjugated block copolymers can self-assemble to help enhance the domain size and morphology of the BHJ in OPV devices. Herein the influence of self-assembly of BnDT blocks can lead to phase separated polymer films the effects on optoelectronic properties and polymer-fullerene blends are investigated.

4.1: Introduction

Conjugated block copolymers are perhaps one of the more neglected areas of research in new materials for photovoltaics, yet in more conventional polymer applications they offer great potential for morphological and microphase separation control.[1,2] Previous investigations of block copolymers for OPVs have often detailed rod-coil type block copolymers; in which an amorphous non-conjugated block would be tethered to a conjugated polymer with the aim of directing self-assembly,[3-5] while others have investigated the coupling of rod-like donor polymers to $PC_{61}BM$ grafted coil polymers (or other polymer acceptors).[6,7] Issues with both types of system arise from lower charge mobility resulting from the presence of non-conjugated "insulating" coil blocks[8] or increased recombination arising from covalently bound donor and acceptor species.[3]

Chapter Four of this thesis focuses on all-conjugated block copolymers. Largely, previous work on rod-rod all-conjugated donor polymers has concentrated on block copolymers incorporating P3HT and its derivatives, with the aim of enhancing BHJ morphology. *rr*-P3HT synthesised by Grignard metathesis polymerisation (GRIM) or a catalytic transfer process has had a variety of polymers grown from it *via* Suzuki-Mayori coupling (Figure 4.1). While these materials have shown desirable microphase separation (P27 - P31), often in the order of 20-40 nm, they are usually ill-defined multi-block/homopolymer mixtures and are unable to achieve competitive PCEs in BHJ-OPV devices.[6,9-11] The microphase separation observed in P27 – P30 arise from the efficient packing and crystalline structure of *rr*-P3HT which phase separates from the fused aromatic blocks. While these polymers may have large band gaps often in the order of 2 eV, and exhibit poor photovoltaic performance they are an important and relatively new milestone in the development of conjugated polymers for organic electronics. These examples demonstrate the possibility of targeting a desired architecture and exploiting this to gain morphological control on the 10 - 30 nm scale which is required for BHJ optimisation.[12,13]

P27
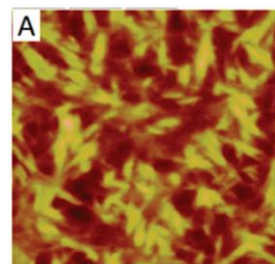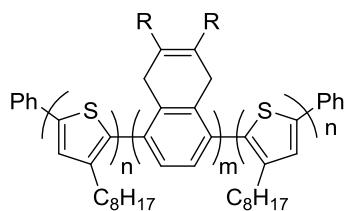
P28
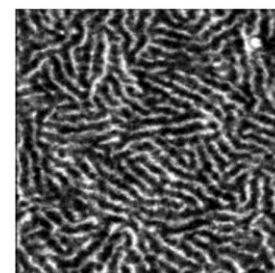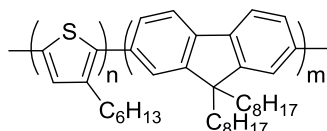
P29
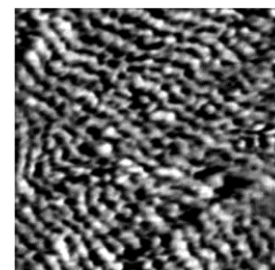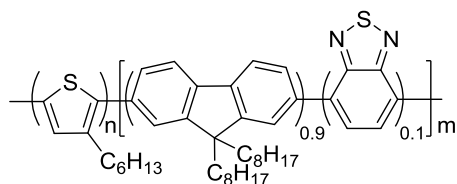
P30
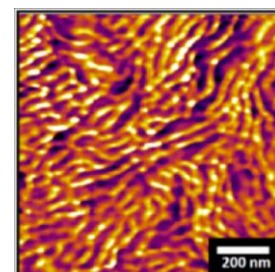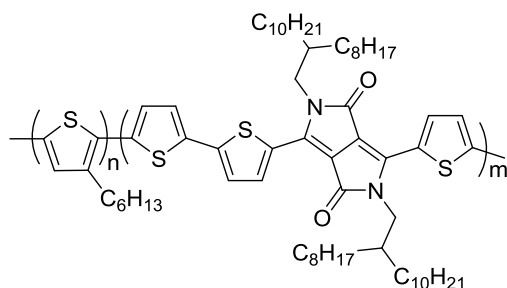
P31
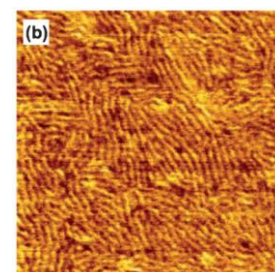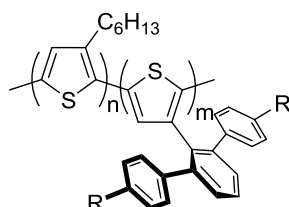
Figure 4.1: P27 – P31; examples of rr-P3HT block copolymers and their microphase separation imaged by AFM.[6,9-11]

Studies into *rr*-P3HT conjugated block copolymers have been popular as *rr*-P3HT exhibits high crystallinity which allows for distinct phase separation when covalently

bound to another species, however, seldom have non-PH3T containing donor-acceptor all conjugated polymers been the subject of detailed investigation in the field of OPVs. One example of such a study by Seferos and co-workers in 2015, P32 (Figure 4.2) was synthesised by the coupling of stannane end functionalised poly-*alt*-(4,8-bis(5-(2-ethylhexyl)thiophen-2-yl)-2-(selenophen-2-yl)benzo[1,2-b:4,5-b']dithiophene) (PBnDT-Th-Se) and bromine terminated poly-*alt*-(1-(6-(4,8-bis(5-(2-ethylhexyl)thiophen-2-yl)benzo[1,2-b:4,5-b']dithiophen-2-yl)thieno[3,4-b]thiophen-2-yl)-3-ethylhexan-1-one) (PBnDT-Th-TT).[14] GPC of the resulting block copolymer showed a large shift in molecular weight although a low molecular weight shoulder was still visible due to inefficient coupling and a challenging purification. Seferos examined a range of Se:TT block ratios, 1:1.59, 1:1.16 and 1:0.85, and found that the 1:1.16 demonstrated the greatest degree of microphase separation (Figure 4.2) and gave a PCE of 5.8 %, which was greater than the equivalent statistical copolymer (PCE = 5.4 %). Interestingly, when the group examined the performance of devices based on a blend of PBnDT-TH-Se and PBnDT-Th-TT they observed an increase in PCE of approximately 1 % for each block ratio for which they offered little explanation. It is possible that the physical blend of the two homopolymers works to enhance charge extraction and limit recombination yielding the higher observed J_{sc}, although little evidence is provided to draw a sound conclusion.

In 2017 Sivula *et al.* investigated the optoelectronic properties of another donor-acceptor block copolymer without the use of *rr*-P3HT.[15] Sivula achieved a better defined block copolymer (Figure 4.2, P33) by removing homopolymer impurities through a lengthy preparative GPC method. P33 exhibited a low band gap of 1.38 eV and demonstrated some ordering in the annealed film (Figure 4.2), however, the polymers performance in a photovoltaic device was not reported.
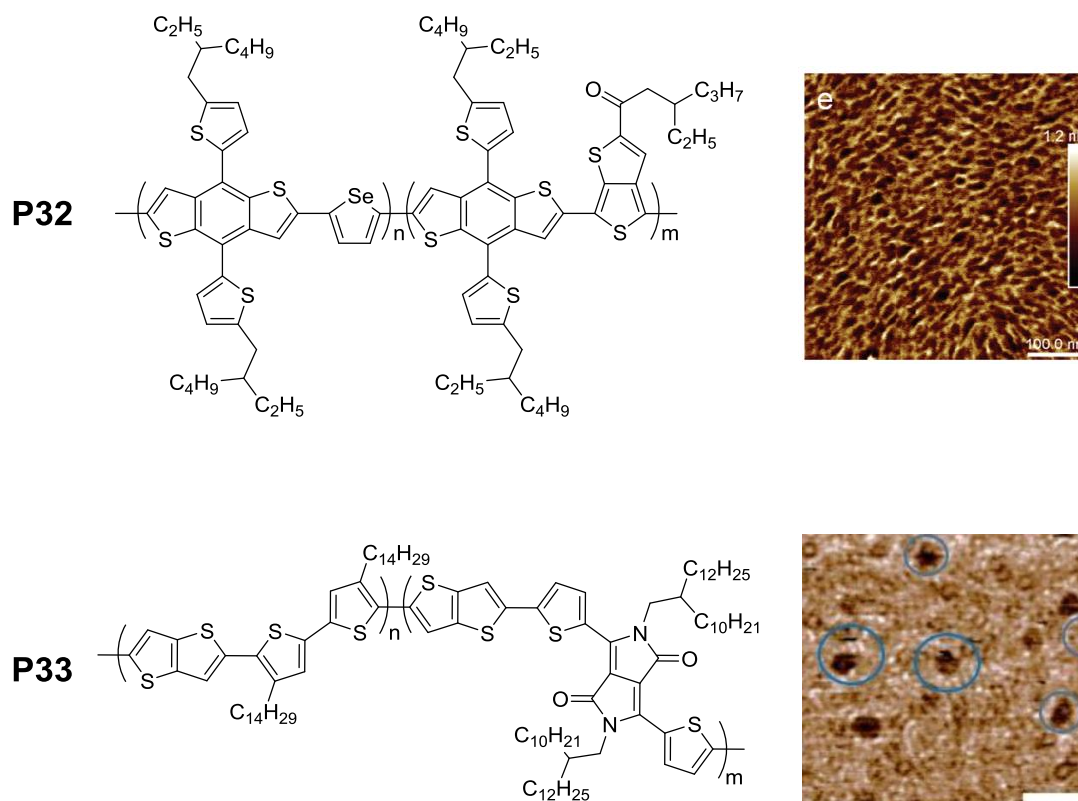
Figure 4.2: Chemical structures and AFM of films of P32 and P33. Scale bar for p33 is 400 nm.[14,15]

Block copolymer investigations have also been extended to the covalent bonding of polymer electron donors and fullerene (or non-fullerene) electron acceptors in an attempt to gain more control over the BHJ, and maximise the PCE of devices. In 2017 Hiorins *et al.* demonstrated that by using PCBM-P3HT block copolymers as a compatibilising agent in a PCBM:P3HT blend that PCE could be enhanced. Addition of just 0.4 weight % of the PCBM-P3HT block copolymer resulted in microphase separation and improved J_{sc} and PCE from 11.04 to 11.70 mA/cm^2 and 3.6 % to 4.2 %, respectively.[16] The increase in J_{sc} validated the theory that the phase separation of block copolymers could be used to improve BHJ morphology and enhance charge transport.

Owing to the naturally occurring block-like structure of the statistical copolymers discussed in Chapter Two and Chapter Three in this chapter the synthesis, characterisation and photovoltaic properties of well-defined block copolymers are reported. A PTBnDT block which exhibits a higher crystallinity, resulting from extensive π-stacking and inter-digitation of side chains, is coupled with a more amorphous and soluble PTBT block with the aim of gaining some morphological control of the morphology of the BHJ.

4.2: Results and Discussion

4.2.1: Synthesis of BnDT(C$_{12}$) Based Block Copolymers

Block copolymers were synthesised by the coupling of bromine end functionalised PTBT and PTBnDT with a 2,5-bis(trimethylstannyl) thiophene as a linker. PTBT and PTBnDT blocks were synthesised to desired molecular weights by utilising the extended Carothers equation,[17]

$$X_n = \frac{1 + r}{1 + r - 2r\rho}$$

where X_n is the degree of polymerisation, r ($r < 1$) is the ratio of difunctional monomers (or homopolymers) and ρ is the conversion of the limiting reagent. Each time, the brominated monomer was used in excess to yield a more stable bromine end functionality as opposed to the less stable trimethylstannyl end group.[18] PTBnDT blocks with both dodecyl and carboxylate-dodecyl side chains were synthesised (Scheme 4.1 and Section 4.2.5, Scheme 4.2 respectively).
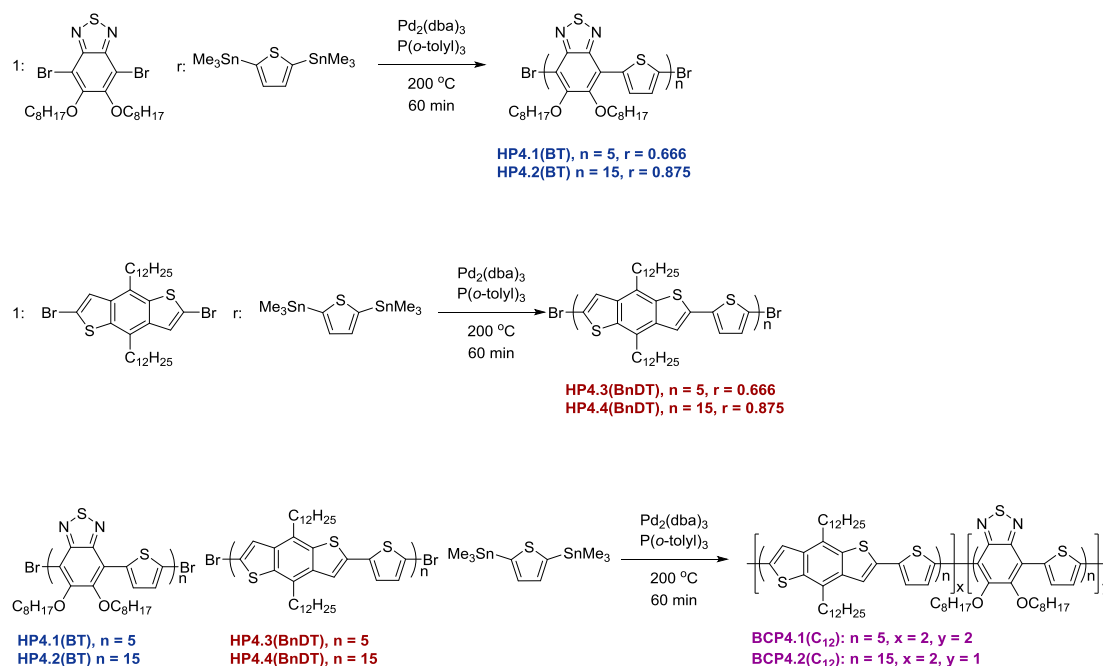
Scheme 4.1: Synthetic scheme for PTBnDT(C$_{12}$) based block copolymers.

Multiblock copolymers incorporating the dodecyl side chains on the BnDT unit were synthesised by coupling PTBT (HP4.1(BT) and (HP4.3(BnDT) to yield BCP4.1(C$_{12}$) (Scheme 4.1). Each homoblock was first purified by Soxhlet extraction and its molecular

weight characterised by high temperature GPC. HP4.1(BT) molecular weight analysis was in good agreement with the theoretical molecular weight, yielding PTBT with an average DP of 6. HP4.3(BnDT) shows a slightly higher molecular weight than predicted, with an average DP of 8. The higher molecular weight is a result of the more rigid rod like structure of HP4.3(BnDT) as the backbone contains a greater number of fused aromatic rings,[19,20] this results in a faster elution time when compared to HP4.1(BT) and the polystyrene standards with which the system is calibrated. Analysis of the polymer resulting from the coupling of HP4.3(BnDT)) and HP4.1(BT) shows the resulting polymer contains BT and BnDT(C_{12}) in a ratio of 36:64 with a molecular weight of 15,200 g/mol. The average polymer chain contains two HP4.1(BT) blocks and two HP4.3(BnDT) blocks (6 + 6 BT units and 8 + 8 BnDT(C_{12}) units, giving the ratio 42:58 and a theoretical M_n of 14,600 g/mol).

4.2.2: Characterisation of BnDT(C_{12}) Based Block Copolymers

Each of the homoblocks demonstrates a symmetrical molecular weight distribution, with relatively low dispersity (Table 4.1 and Figure 4.3). Molecular weight distributions (by high temperature GPC) of the BCP4.1(C_{12}) polymer (Figure 4.3) is monomodal and is devoid of any shoulders, with little overlap with the homopolymer building blocks indicating minimal presence of homoblock impurities. The narrow dispersity of the constituent homoblocks results in a relatively well-defined block copolymer, without the need for a lengthy purification process.

Table 4.1: Molecular weight averages of HP4.1(BT) and HP4.3(BnDT) homo and block copolymers, monomer ratios by side chain α-CH$_2$ ^{1}H NMR analysis.

Polymer	M_n^{Th} (g/mol)	M_n (g/mol)	M_w (g/mol)	Đ	% BT (NMR)	% BnDT (NMR)
HP4.1(BT)	2900	2700	3700	1.40	100	0
HP4.3(BnDT)	3700	4600	6600	1.45	0	100
BCP4.1(C_{12})	14600	15200	32300	2.13	36	64
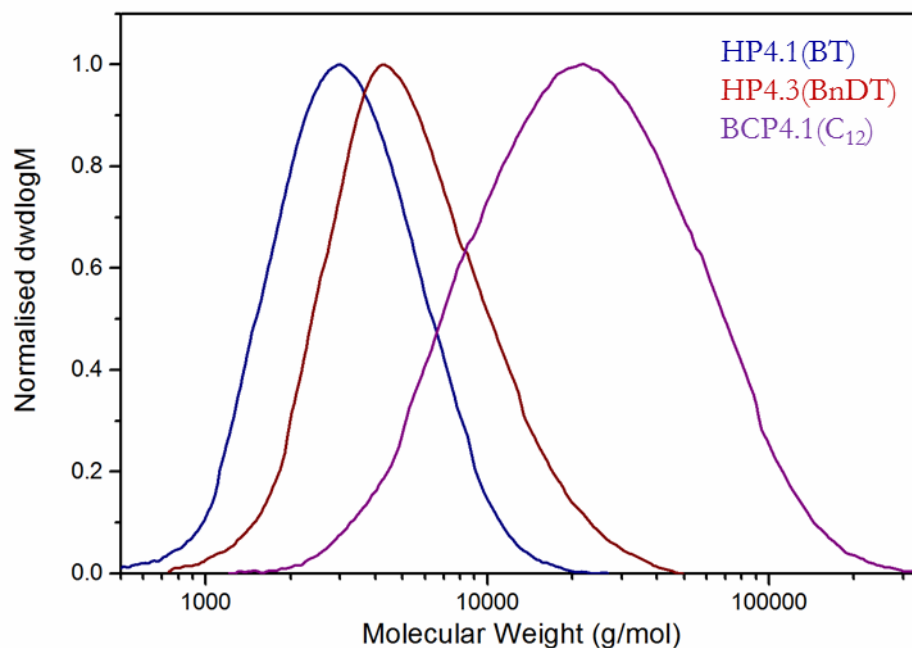
Figure 4.3: GPC molecular weight distributions of HP4.1(BT) (blue), HP4.3(BnDT) (red) and BCP4.1(C$_{12}$) (purple).

Longer chain homoblocks of DP 15 were also targeted to investigate the effect of block length on polymer film and BHJ morphology. HP4.2(BT) and HP4.4(BnDT) (DP 15) where achieved with good accuracy (allowing for the over estimation of rigid rod polymers by PS-standard calibration) with HP4.2(BT) achieving a M_n of 8,400, corresponding to a DP of 17 and HP4.4(BnDT) with an M_n of 9,500 g/mol and a DP of 16. The block copolymer of the two homoblocks (HP4.2(BT) and HP4.4(BnDT) attained a M_n of 28,300 and a BT:BnDT ratio of 35:65 which is indicative of a triblock copolymer containing two HP4.4(BnDT) blocks and one HP4.2(BT); it should be noted; that the ordering of these blocks cannot be discerned.

Table 4.2: Molecular weight averages of HP4.2(BT) and HP4.4(BnDT) homo and block copolymers, monomer ratios by side chain α-CH$_2$ ^{1}H NMR analysis.

Polymer	M_n^{Th} (g/mol)	M_n (g/mol)	M_w (g/mol)	Đ	% BT (NMR)	% BnDT (NMR)
HP4.2(BT)	7200	8400	11900	1.41	100	0
HP4.4(BnDT)	9200	9500	14600	1.53	0	100
BCP4.2(C$_{12}$)	25600	28300	69400	2.45	35	65

Once again, the homoblocks show symmetrical molecular weight distributions with low dispersity considering the synthetic method employed (Table 4.2 and Figure 4.4). The molecular weight distribution of the BCP4.2(C$_{12}$) block copolymer (Figure 4.4) presents

a monomodal distribution devoid of any shoulders indicating efficient block coupling and again, minimal presence of homoblock impurities. The increased dispersity to 2.45 (when compared to the homoblocks (Table 4.2) is indicative that the di-block and tetra-block species are likely to be present.

Absence of the homoblocks in both the BCP4.1(C$_{12}$) and BCP4.2(C$_{12}$) was achievable owing to the lower solubility of higher molecular weight polymers. All homopolymers were isolated in chloroform fractions of the Soxhlet extraction. The higher molecular weight of the BCP4.1(C$_{12}$) and BCP4.2(C$_{12}$) block copolymers (by 3-4 times that of their homoblock constituents) results in lower solubility and consequently the block copolymers were isolated in the chlorobenzene faction of the Soxhlet extraction. As such block copolymers could easily be isolated from their homoblock impurities in contrary to other systems discussed in Section 4.1 of this thesis.[14,15]
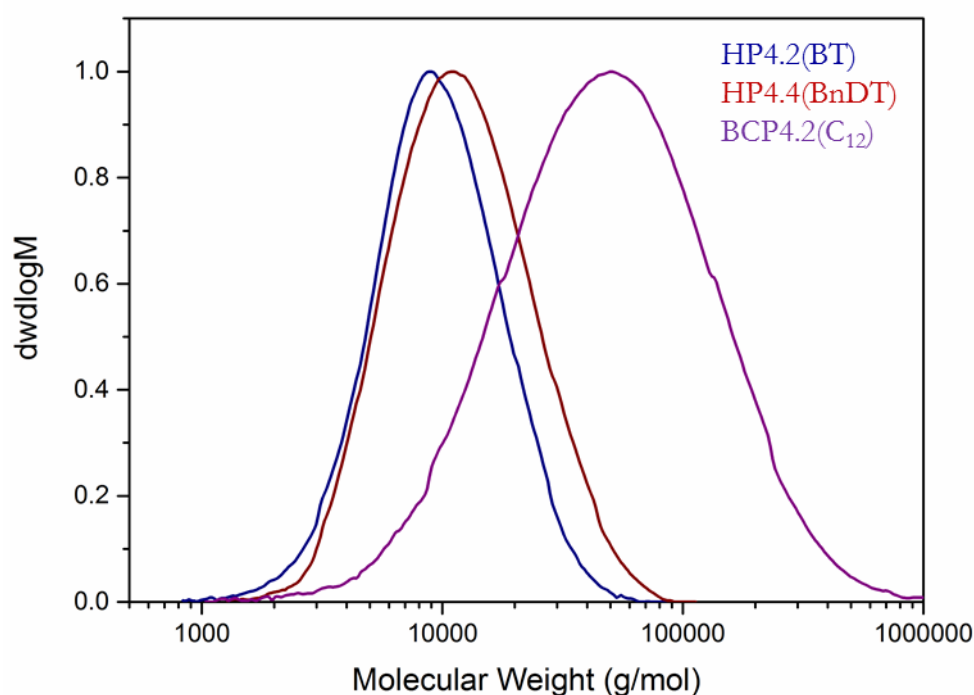
Figure 4.4: GPC traces of HP4.2(BT) DP 17 (blue), HP4.4(BnDT) DP 16 (red) and BCP4.2(C$_{12}$) (purple).

4.2.3: Optoelectronic Properties of BnDT(C$_{12}$) Based Block Copolymers

The optoelectronic properties of the homoblocks HP4.1(BT), HP4.2(BT), HP4.3(BnDT) and HP4.4(BnDT), and block copolymers BCP4.1(C$_{12}$) and BCP4.2(C$_{12}$) were analysed by CV and UV-vis spectroscopy and are summarised in Table 4.3. The HOMO of the polymer was estimated using the onset to the oxidation peak in CV vs. a ferrocene/ferrocinium standard (-4.8 eV),[21,22] the band gap E$_g^{opt}$ was calculated using the

onset to absorption from UV/Vis spectroscopy and finally the LUMO was estimated by addition of the optical band gap E_g^{opt} to the HOMO.

Table 4.3: Optoelectronic properties of homoblocks HP4.1(BT), HP4.2(BT), HP4.3(BnDT) and HP4.4(BnDT), and block copolymers BCP4.1(C_{12}) and BCP4.2(C_{12}).

Polymer	HOMO (eV)	LUMO (eV)	E_g^{opt} (eV)	$\lambda_{max}^{soln.}$ (nm)	λ_{max}^{film} (nm)
HP4.1(BT)	-5.3	-3.6	1.72	541	602
HP4.2(BT)	-5.3	-3.6	1.72	564	657
HP4.3(BnDT)	-5.2	-3.1	2.06	474	499
HP4.4(BnDT)	-5.5	-3.4	2.05	503	510
BCP4.1(C_{12})	-5.5	-3.8	1.77	507	512
BCP4.2(C_{12})	-5.4	-3.6	1.75	512	514

The HP4.1(BT) homoblock shows on distinct peak in the region of 540 nm, which can be assigned to intra-molecular charge transfer (ICT) between the more electron rich thiophene and the electron deficient BT unit.[23,24] The λ_{max} value for HP4.1(BT) shows a significant red shift from solution to film of 61 nm (Figure 4.5). This can be assigned to significant increase in intermolecular interaction in the form of π-stacking due to more efficient packing of smaller molecular species, also evident in the shoulder at $\lambda = 680$ nm. Similarly for HP4.3(BnDT) (Figure 4.5), the emergence of a shoulder and a red shift in the onset to absorption is observed, which is a result of significant π-stacking interactions of the fused aromatic systems. The λ_{max} of PTBnDT(C_{12}) in solution occurs at a shorter wavelength (474 nm) when compared to that of the HP4.1(BT) homopolymer (541 nm), the higher energy ICT state is a result of the absence of an electron deficient accepting species. [25]
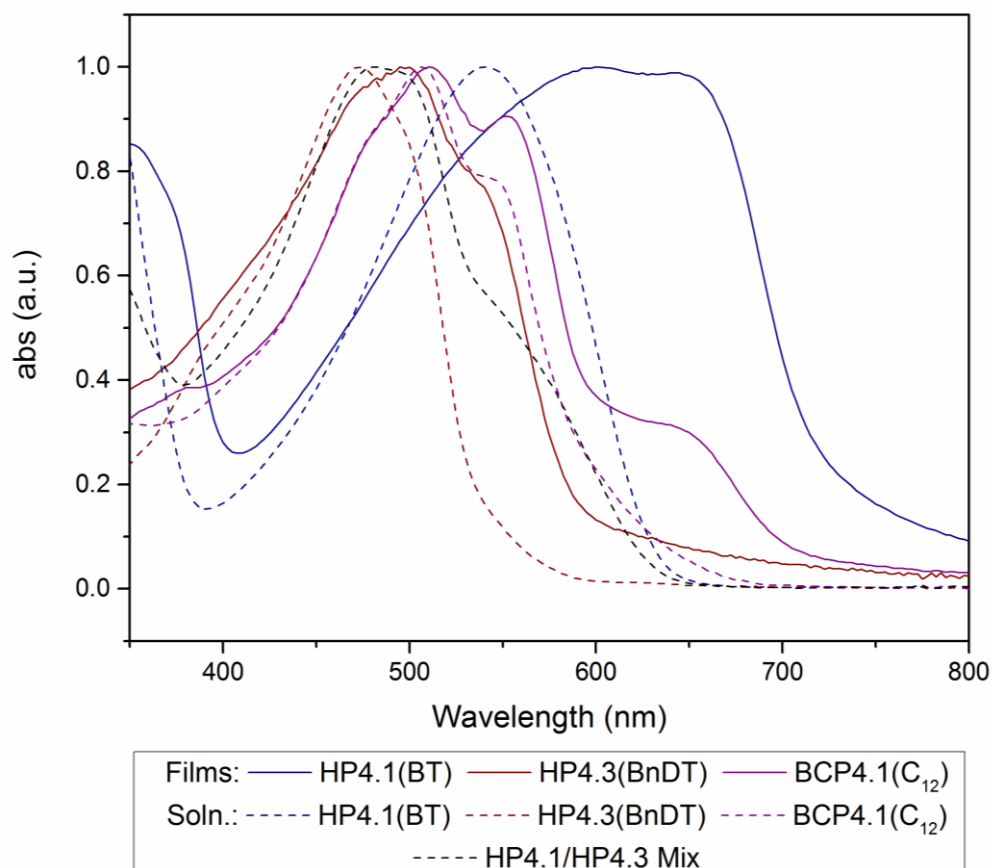
Figure 4.5: Normalised UV-vis spectra of: polymer films (solid lines) HP4.1(BT), HP4.3(BnDT) and BCP4.1(C$_{12}$). UV/vis was also run in dilute chlorobenzene solution (dashed lines). A solution phase mixture of HP4.1(BT and HP4.3(BnDT) was also run for comparison.

The UV-vis spectrum of the thin film of *BCP4.1(C12)* presented in Figure 4.5 shows optical contributions from both the HP4.1(BT) and the HP4.3(BnDT) blocks in an approximately 1:2 ratio, which is in agreement with the BT:BnDT(C$_{12}$) ratio observed by ^{1}H NMR (Table 4.1). The significant red shift of the HP4.1(BT) block occurs in a similar manner to the homopolymer HP4.1(BT) suggesting the blocks optical properties in a thin film are largely independent of one-another even when covalently bound. Unlike in the individual homoblocks a shoulder is observed in the region of 480 nm which can be assigned to π-π* transition between adjacent BT and BnDT(C$_{12}$) regions within the polymer. The emergence of this shoulder suggests a significant amount of ICT despite the relatively low concentration of donor-acceptor interface along the backbone. Interestingly, when comparing the *BCP4.1(C12)* spectrum with a mixture of the homoblocks HP4.1(BT) and HP4.3(BnDT) (Figure 4.5) the block copolymer exhibits a more pronounced shoulder in the region of 560 nm which is indicative of a greater extent of aggregation in solution. Aggregation in solution has been shown to be beneficial (providing that the polymers maintain their solubility) and can lead to more ordered

domains and higher degrees of crystallinity in final films, which can help to enhance J_{sc}.[26] The more discrete peaks observed in the *BCP4.1(C12)* trace in Figure 4.5 are indicative of ICT between the covalently bound acceptor and donor blocks, the homopolymer mix shows a broad featureless peak which might be expected from the mixing of two separate chromophores contributions.
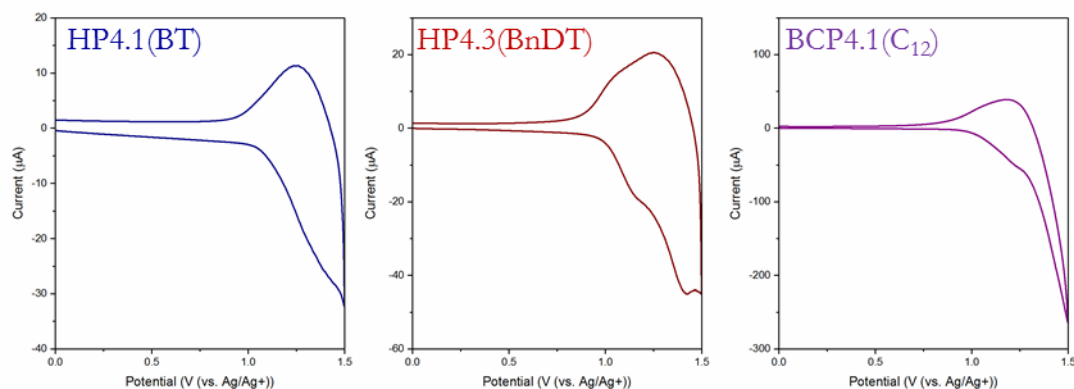
Figure 4.6: Cyclic volatammogram for the oxidation of HP4.1(BT) film (blue trace), HP4.3(BnDT) film (dark red trace) and *multi*-PTBnDT(C$_{12}$)-*b*-PTBT film (purple trace).

The cyclic voltammogram (Figure 4.6) for both the homoblocks shows a quasi-reversible one electron reduction, in the case of the BTBnDT(C$_{12}$)-*short* film a second peak/shoulder can be seen which can be assigned to the difference in oxidation potential of crystalline and amorphous regions of the polymer film.[27] This can also be seen, although to a much lesser extent in the *multi*-PTBnDT(C$_{12}$)-*b*-PTBT film indicating that crystalline properties of the HP4.3(BnDT) block are maintained when coupled to the more amorphous HP4.1(BT) block.
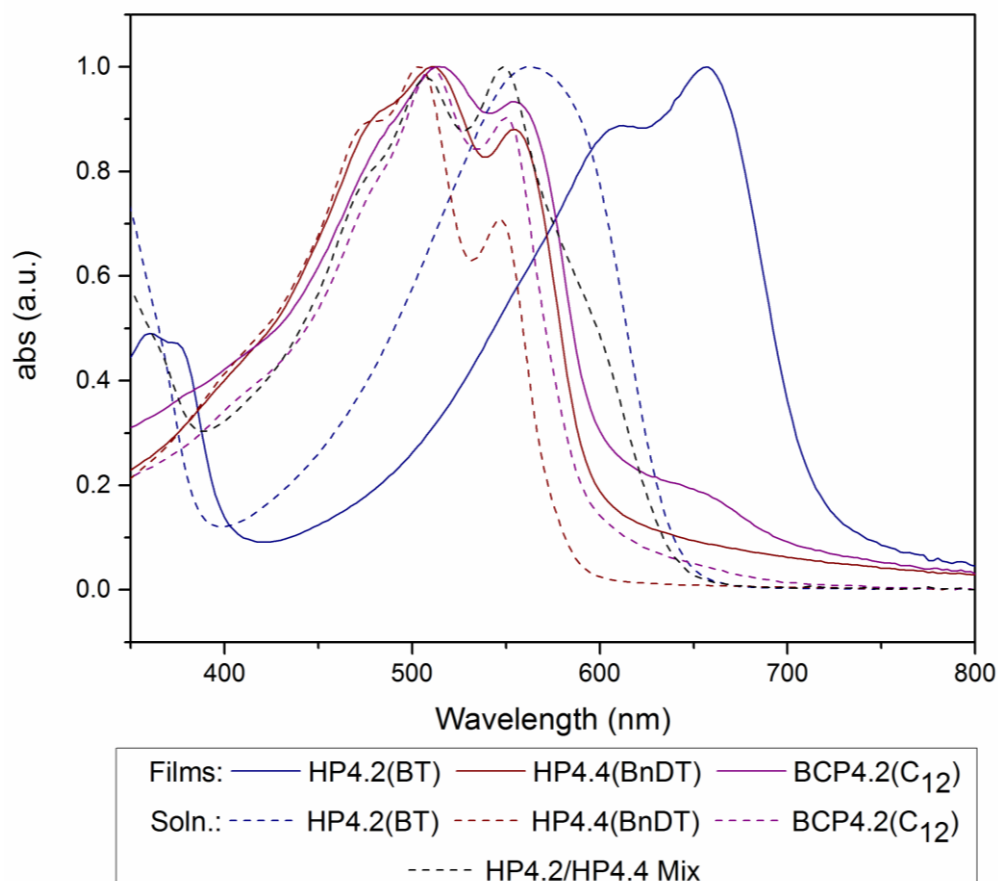
Figure 4.7: Normalised UV-vis spectra of: polymer films (solid lines) HP4.2(BT), HP4.4(BnDT) and BCP4.2(C$_{12}$). UV/vis was also run in dilute chlorobenzene solution (dashed lines). A solution phase mixture of HP4.1(BT and HP4.3(BnDT) was also run for comparison.

The λ_{max} values for the HP4.2(BT) are red shifted when compared to those of HP4.1(BT) (Table 4.3) which is to be expected owing to the greater maximum conjugation length of HP4.2(BT).[28] Similarly to HP4.1(BT), HP4.2(BT) experiences a bathochromic shift between the solution and the film spectra is observed, the shoulder for HP4.2(BT) is more pronounced indicating a greater degree of π-stacking in the solid state for the higher molecular weight homopolymer. Comparing the UV-vis spectra of HP4.3(BnDT) (Figure 4.5) and HP4.4(BnDT) (Figure 4.7) one can draw similar conclusions to the logic employed in the comparison of the PTBT polymers above. A red shift of the higher molecular weight species is observed owing to the longer conjugation length of the species and once again a more pronounced shoulder in the region of 580 nm signals a greater degree of π-stacking and aggregation in both the solution and film. The shoulder at 480 nm for HP4.4(BnDT) is more pronounced than for its lower molecular weight counterpart suggesting that the π-π* transitions have a stronger contribution to the optical properties in the higher molecular weight HP4.4(BnDT) species. Figure 4.7 shows the thin film and solution (dashed line) UV-Vis spectra of BCP4.2(C$_{12}$) and demonstrates that

both of the component blocks (HP4.2(BT) and HP4.4(BnDT)) contribute to the polymers absorption spectra. Surprisingly, the mixture of HP4.2(BT) and HP4.4(BnDT) (Figure 4.7, dashed line) shows a lower onset to absorption than the BCP4.2(C_{12}) (solid line) in solution, this could possibly be due to the disruption of aggregation of BCP4.2(C_{12}) owing to its molecular weight and other di/multiblock impurities. Both the mixture of homopolymers and BCP4.2(C_{12}) block copolymer exhibit π-stacking in the solution phase.
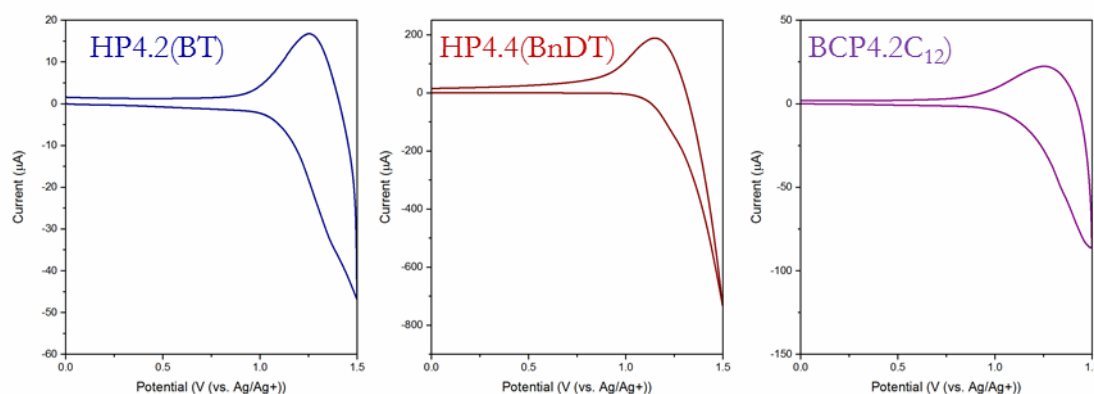
Figure 4.8: Cyclic voltammograms for the oxidation of HP4.2(BT) film (blue trace), HP4.4(BnDT) film (dark red trace) and BCP4.2(C12) film (purple trace).

Figure 4.8 shows the CV for each of the long homopolymers and the resulting triblock copolymer. Each demonstrates a quasi-reversible one electron oxidation. Unlike the HP4.3(BnDT), the HP4.4(BnDT) shows little evidence of a shoulder at lower potential which would be assigned to more crystalline domains. The higher molecular weight HP4.4(BnDT) is less crystalline as disorder and torsional strain along the longer backbone inhibits packing and a slower nucleation rate is expected for higher molecular weight polymers.[29]

4.2.4: Characterisation of BnDT(CO$_2$C$_{12}$) Based Block Copolymers

Similar to the BCP4.1(C_{12}) and BCP4.2(C_{12}) polymers described above, polymers BCP4.3($C_{12}CO_2$) and BCP4.4($C_{12}CO_2$), in which the BnDT unit bears dodecylcarboxylate side chains in the 4- and the 8-positions, were synthesised (Scheme 4.2). The addition of the electron withdrawing esters has been shown to lower the HOMO of the polymer whilst helping to increase the solubility of the rigid aromatic system leading to more easily processable polymers with a higher V_{oc}.[30]

As previously, HP4.5(BnDTCO^2) (DP 5) and HP4.6(BnDTCO$_2$) (DP = 15) were targeted, the resulting homopolymers where then coupled with HP4.1(BT) and

HP4.2(BT) polymers respectively. The molecular weight of the HP4.5(BnDTCO$_2$) and its corresponding block copolymers are presented in Table 4.4 and the molecular weight distribution in Figure 4.9. The targeted molecular weight of 3,700 g/mol was exceeded by 3,000 g/mol, while GPC is expected to overestimate the molecular weight of such rigid polymers this discrepancy is beyond even this overestimation. Due to the higher solubility of the BnDT(CO$_2$C$_{12}$) polymer it is likely that higher molecular weight species were extracted in the chloroform fraction of the Soxhlet extraction (an issue that did not arise with the less soluble BnDT(C$_{12}$) system). This is also verified by the increase in dispersity of the HP4.5(BnDTCO$_2$)polymer when compared with its C$_{12}$ baring counterpart. The average DP of the HP4.5(BnDTCO$_2$)is 9.
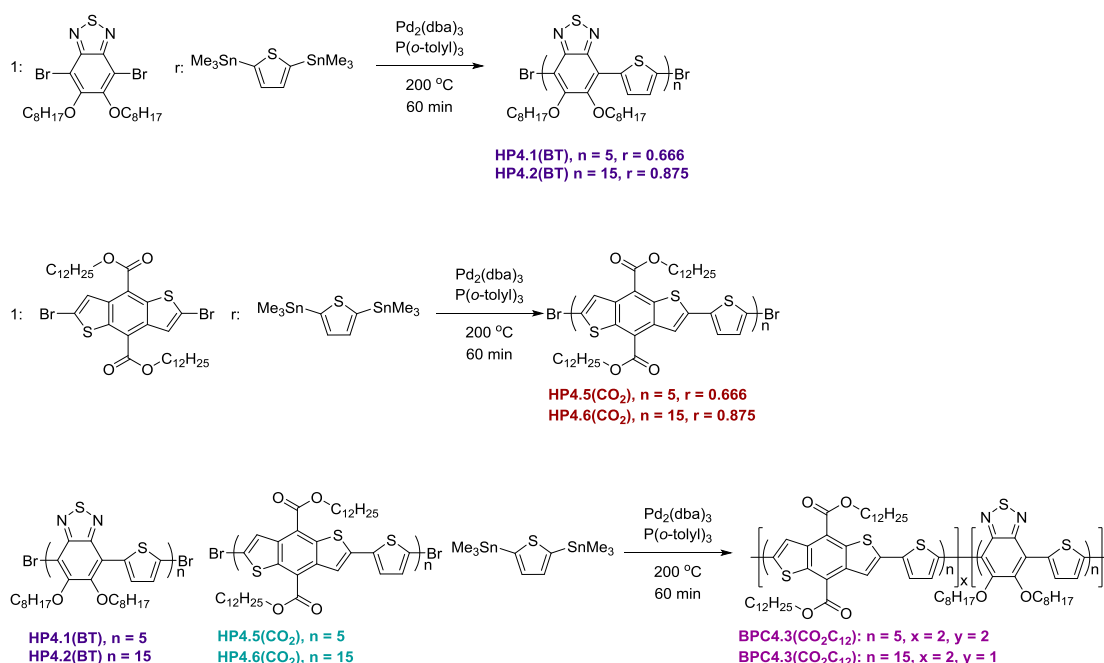
Scheme 4.2: Synthesis of PTBnDT(CO$_2$C$_{12}$) based block copolymers.

Table 4.4: Molecular weight averages of short PTBT and PTBnDT(CO$_2$C$_{12}$) homo and block copolymers, monomer ratios by side chain α-CH$_2$ ^{1}H NMR analysis.

Polymer	M_n^{Th} (g/mol)	M_n (g/mol)	M_w (g/mol)	$Đ$	% BT (NMR)	% BnDT (NMR)
HP4.1(BT)	2900	2700	3700	1.40	100	0
HP4.5(BnDTCO$_2$)	3700	6700	10900	1.62	0	100
BCP4.3(C$_{12}$CO$_2$)	18800	14100	34000	2.41	35	65
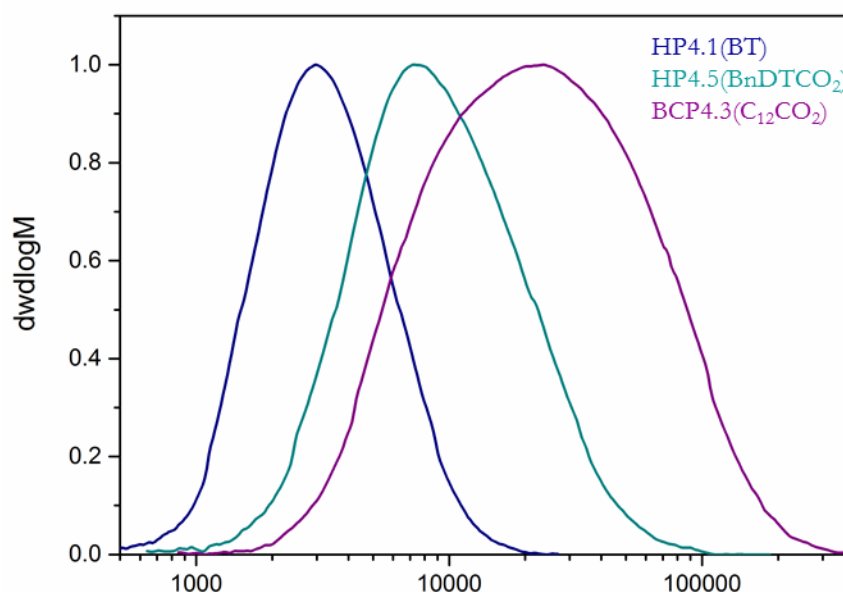
Figure 4.9: GPC traces of HP4.1(BT) DP 6, HP4.5(BnDTCO$_2$) DP 9 and BCP4.3(C$_{12}$CO$_2$).

Coupling of HP4.5(BnDTCO$_2$)with HP4.1(BT) resulted in a shift to higher molecular weight observed by GPC (Figure 4.9, purple trace), yielding a polymer with an M_n of 14,100 g/mol and a BT:BnDT ratio of 35:65. The monomer ratio by ^{1}H NMR suggests that the average composition of the block copolymer should be 2(PTBT)$_6$-2(PTBnDT(CO$_2$C$_{12}$)$_9$, giving a BT:BnDT ratio of 40:60, however, the expected number average molecular weight of this polymer would be 18,800 g/mol which is higher than the experimental value of 14,100 g/mol. On examination of Figure 4.9 it is apparent that there is a large overlap between the block copolymer BCP4.3(CO$_2$C$_{12}$) and polymer HP4.5(BnDTCO$_2$). The higher solubility of the block copolymer instilled by the dodedcylcarboxylate side chains means it, like PTBnDT(CO$_2$C$_{12}$)-*short,* are both extracted in the chloroform fraction of the Soxhlet extraction. This makes separation of the homopolymer from the desired block copolymer challenging.

Synthesis of the HP4.6(BnDTCO$_2$) block (target DP 15) resulted in a polymer with a M_n of 7,500 corresponding to a DP of 11, slightly under that of the target. There is, however, a dispersity of 1.54 and a slight shoulder towards higher molecular weight (Figure 4.10, cyan trace) and the M_w of the homopolymer is close to that of the targeted species (Table 4.5).

Table 4.5: Molecular weight averages of long PTBT and PTBnDT(CO$_2$C$_{12}$) homo and block copolymers, monomer ratios by side chain α-CH$_2$ ^{1}H NMR analysis.

Polymer	M_n^{Th} (g/mol)	M_n (g/mol)	M_w (g/mol)	Đ	% BT NMR	% BnDT NMR
HP4.2(BT)	7200	8400	11900	1.41	100	0
HP4.5(BnDTCO$_2$)	11200	7500	11800	1.58	0	100
BCP4.4(C$_{12}$CO$_2$)	15900	14400	32000	2.23	54	46

Coupling of the HP4.6(BnDTCO$_2$) with HP4.2(BT) results in a copolymer with a M_n of 14,400 g/mol and a BT:BnDT ratio of 54:46 which is indicative of a diblock copolymer P(TBT)$_{17}$-b-P(TBnDT(CO$_2$C$_{12}$))$_{11}$ which has a theoretical M_n of 15,900 and a BT:BnDT ratio of 61:39. The slight excess of BnDT in the experimental values can once again be assigned to the presence of some HP4.6(BnDTCO$_2$) homopolymer impurity (seen in the low molecular weight shoulder of the purple trace in Figure 4.10) resulting from the increased solubility of the block copolymer and difficulty in purification.
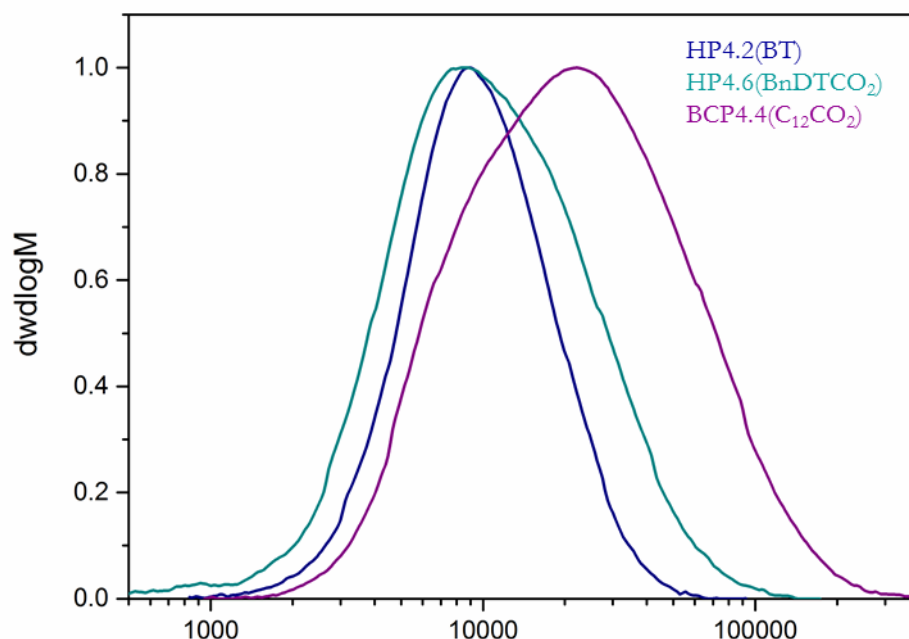
Figure 10: GPC traces of HP4.2(BT) DP 17, HP4.6(BnDTCO$_2$) DP 11 (cyan) and BCP4.3(C$_{12}$CO$_2$).

4.2.5: Optoelectronic Properties of BnDT(CO$_2$C$_{12}$) Based Block Copolymers

The optoelectronic properties of BCP4.3(C$_{12}$CO$_2$) and BCP4.4(C$_{12}$CO$_2$) and their corresponding homoblocks are summarised in Table 4.6. The HP4.5(BnDTCO$_2$) and HP4.6(BnDTCO$_2$) homoblocks possess markedly lower LUMOs and corresponding E$_g$ when compared to their C$_{12}$ equivalents resulting from the presence of the electron withdrawing carboxylate groups.[31] HP4.5(BnDTCO$_2$) exhibits aggregation in solution, indicated by the shoulder in the region of 620 nm in Figure 4.11 (dashed line) as expected. This shoulder, which appears in the presence of significant π-stacking, is more pronounced in the film of HP4.5(BnDTCO$_2$) Similarly, significant π-stacking in the *BCP4.3(C12CO2)*block copolymer is observed (Figure 4.11). The UV-vis spectrum of *BCP4.3(C12CO2)*is dominated by the PTBnDT(CO$_2$C$_{12}$) component, conversely, however, the physical blend of HP4.1(BT) and HP4.5(BnDTCO$_2$) is dominated by the HP4.1(BT) constituent (Figure 4.11). The presence of the HP4.1(BT) chains significantly disrupts the π-stacking of the HP4.5(BnDTCO$_2$) polymer chain resulting in decreased absorption at 630 nm.

Table 4.6: Optoelectronic properties of homoblocks HP4.1(BT), HP4.2(BT), HP4.5(BnDTCO$_2$) and HP4.6(BnDTCO$_2$), and block copolymers **BCP4.3(C$_{12}$CO$_2$)** and **BCP4.4(C$_{12}$CO$_2$)**

Polymer	HOMO (eV)	LUMO (eV)	Eg^{opt} (eV)	λ_{max} (nm) solution	λ_{max} (nm) film
HP4.1(BT)	-5.3	-3.6	1.72	541	602
HP4.2(BT)	-5.3	-3.6	1.72	564	657
HP4.5(BnDTCO$_2$)	-5.5	-3.7	1.84	563	567
HP4.6(BnDTCO$_2$)	-5.5	-3.7	1.84	567	621
BCP4.3(C$_{12}$CO$_2$)	-5.5	-3.7	1.78	576	625
BCP4.4(C$_{12}$CO$_2$)	-5.5	-3.7	1.75	575	625

Each of the polymers in Figure 4.12 exhibits a one electron quasi-reversible oxidation, the slight shoulder in the HP4.5(BnDTCO$_2$) trace is indicative of the presence of crystalline domains as previously discussed.
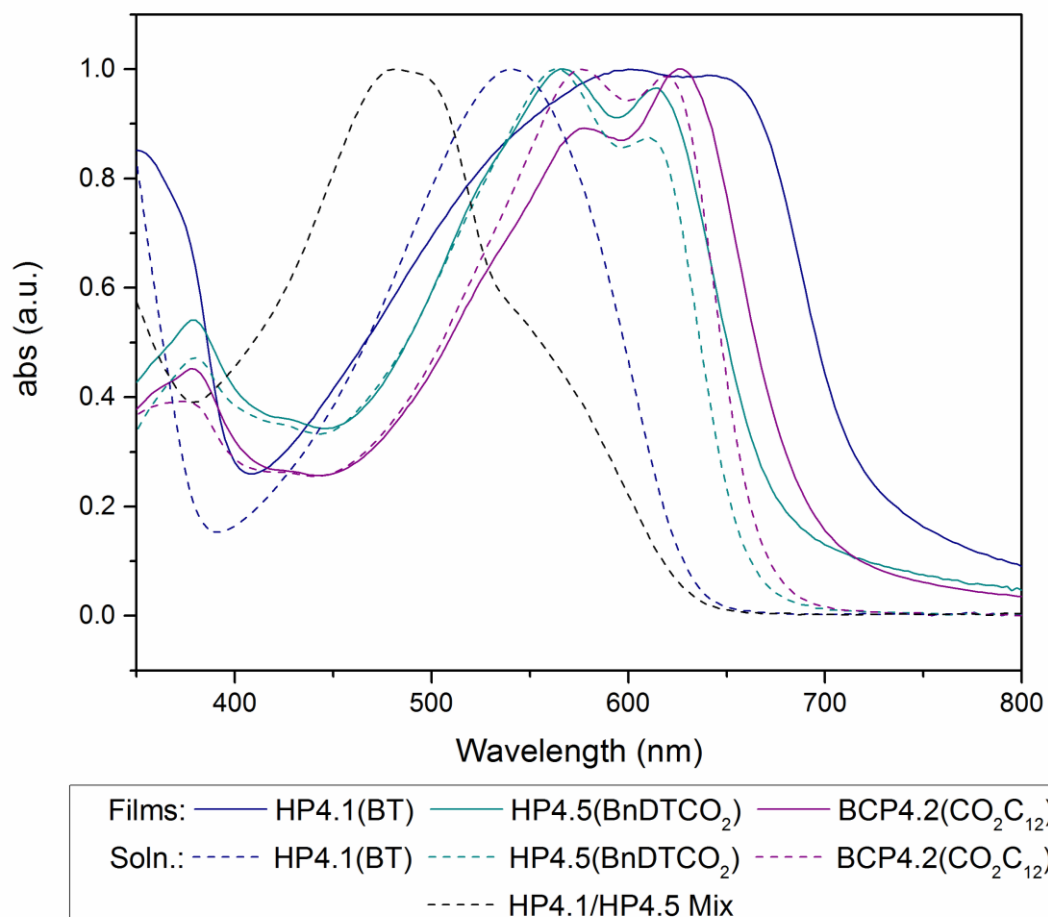
Figure 4.11: Normalised UV-vis spectra of: polymer films (solid lines) HP4.1(BT), HP4.5(BnDTCO$_2$) and BCP4.3(CO$_2$C$_{12}$). UV/vis was also run in dilute chlorobenzene solution (dashed lines). A solution phase mixture of HP4.1(BT and HP4.3(BnDT) was also run for comparison.
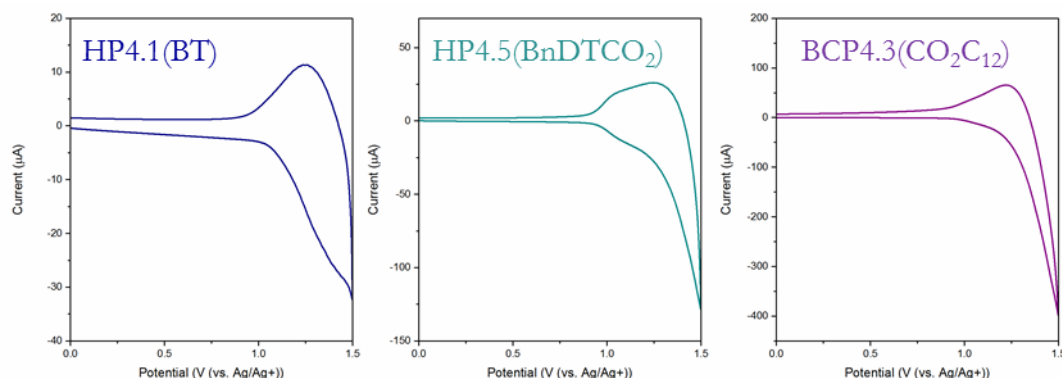
Figure 4.12: Cyclic voltammograms for the oxidation of HP4.1(BT) film, HP4.5(BnDTCO2) film and BCP4.3(CO$_2$C$_{12}$) film.

As expected, the HP4.6(BnDTCO$_2$) polymer exhibits similar behaviour to HP4.5(BnDTCO$_2$) polymer in solution and thin film, a large degree of π-stacking can be inferred from Figure 4.13. Interestingly, the block copolymer BCP4.4(CO$_2$C$_{12}$) (Figure 4.13) shows a lower degree of π-stacking than the constituents from which it is composed. The decrease in π-stacking is also observed in the physical blend of HP4.2(BT) and HP4.6(BnDTCO$_2$) where no aggregation shoulder is observed (Figure 4.13, dashed line), which suggests that the homopolymer impurities are responsible for the disruption of inter-chain interactions. This ability of homoblocks to disrupt one another's ability to π-stack could potentially be used as a handle to influence the morphology of the polymer films and of the BHJ.
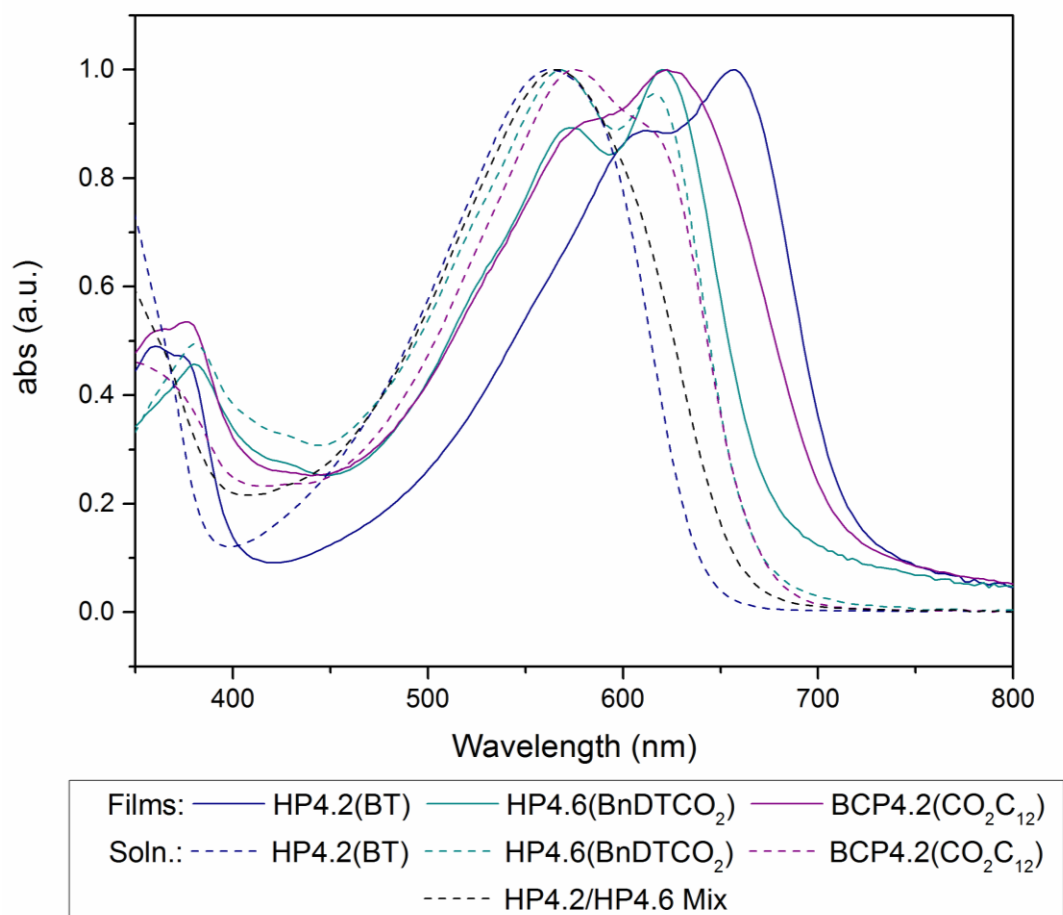
Figure 4.13: Normalised UV-vis spectra of: polymer films (solid lines) HP4.2(BT), HP4.6(BnDTCO₂) and BCP4.4(CO₂C₁₂). UV/vis was also run in dilute chlorobenzene solution (dashed lines). A solution phase mixture of HP4.1(BT and HP4.3(BnDT) was also run for comparison.
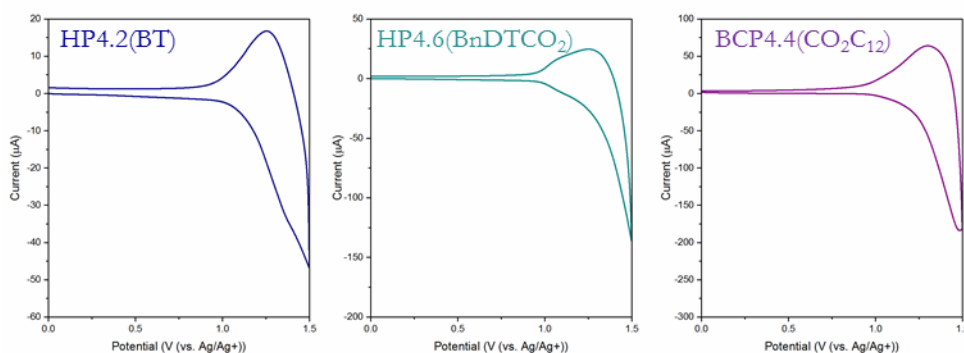
Figure 4.14: Cyclic voltammograms for the oxidation of HP4.2(BT) film, HP4.6(BnDTCO₂) film and BCP4.4(CO₂C₁₂) film.

Analysis of the CV of each of the polymers (Figure 4.14) yields similar results to the previously analysed shorter polymers discussed above, a single one electron quasi-reversible oxidation process and some indication of crystalline domains in the HP4.6(BnDTCO₂) polymer film.

4.2.6: Morphological Studies of Block Copolymers and Their Blends

The morphological properties of the thin films of the homopolymers, block copolymers and respective polymer : $PC_{61}BM$ blends were investigated by AFM in intermittent contact (tapping) mode. Figure 4.15 shows the AFM height and phase images of HP4.1(BT), HP4.3(BnDT) and BCP4.1(C_{12}). The HP4.1(BT) film is very smooth and shows few instances of aggregation whereas the HP4.3(BnDT) shows the formation of high aspect ratio needle like crystals presumably due to the polymer's superior ability to π-stack. The two very different sets of properties of the homopolymers leads to microphase separation of the block copolymer BCP4.1(C_{12}) with domain sizes of approximately 50 nm (Figures 4.15c and 4.15f).

Figure 4.16 shows the same polymers when blended with $PC_{61}BM$ (polymer:$PC_{61}BM$ 1:1.5), the HP4.1(BT) shows a good degree of mixing, creating smooth homogenous films, while the HP4.3(BnDT) shows large scale phase separation with the $PC_{61}BM$ with some domains over 1 μm in size. The BCP4.1(C_{12}):PCBM film demonstrates a smaller feature sizes when compared with that of the HP4.3(BnDT)-$PC_{61}BM$ blend demonstrating that the covalent bonding of the HP4.1(BT) polymer improves the miscibility of the HP4.3(BnDT) polymer with the $PC_{61}BM$.
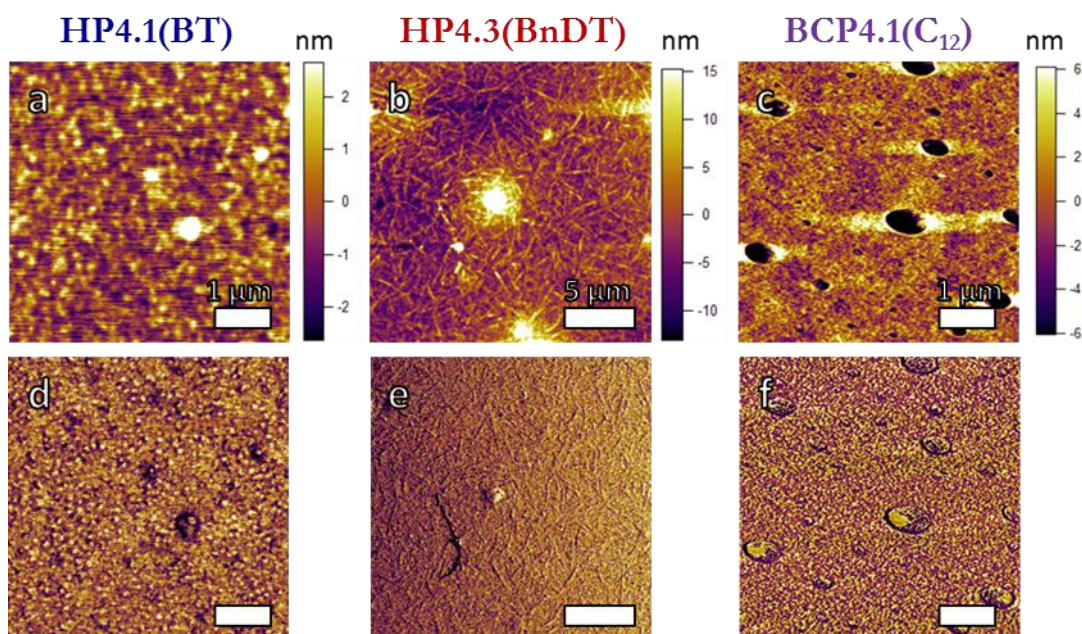
Figure 4.15: a-c; AFM height images, d-f; AFM phase images, a,d; HP4.1(BT), b,e; HP4.3(BnDT), c,d; BCP4.1(C_{12}). Scale bars a,c,d and f are 1μm, scale bars b and e are 5 μm.
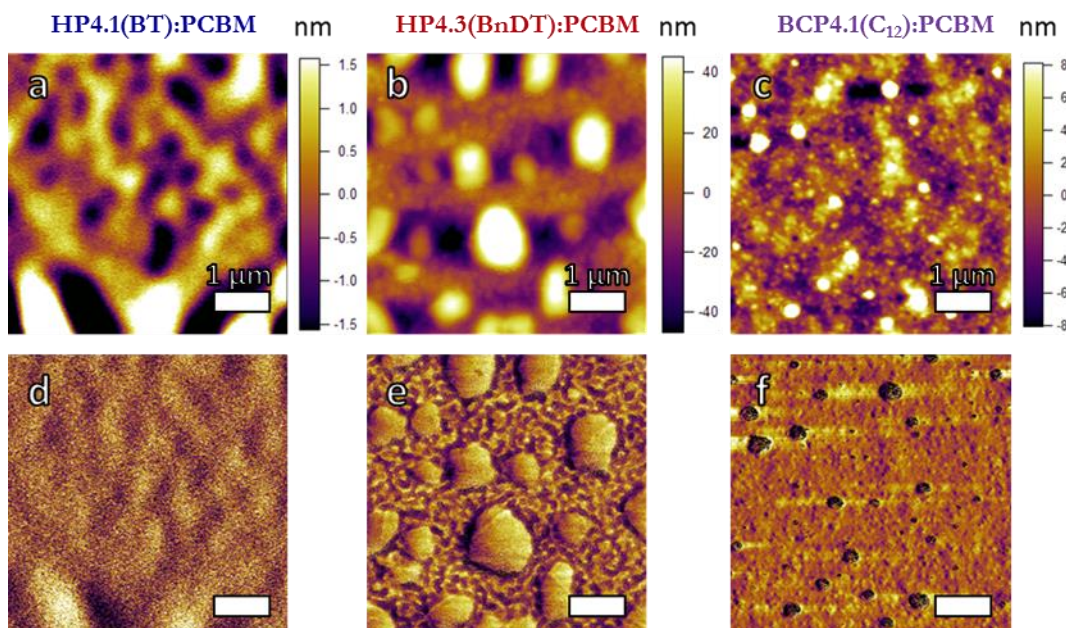
Figure 4.16: a-c; AFM height images, d-f; AFM phase images, a,d; HP4.1(BT):PC$_{61}$BM blend, b,e; HP4.3(BnDT):PC$_{61}$BM blend, c,d; BCP4.1(C$_{12}$):PC$_{61}$BM blend. All scale bars are 1 μm.

AFM height and phase images of the HP4.2(BT), HP4.4(BnDT) and BCP4.2(C$_{12}$) polymers are presented in Figure 4.17. Both the HP4.2(BT) and HP4.4(BnDT) demonstrate smooth homogenous films. HP4.4(BnDT) exhibits no crystal-like structures, in contrast to HP4.3(BnDT) as the larger chains are less likely to form crystalline domains due to disorder along the backbone forcing less efficient molecular packing. The block copolymer BCP4.2(C$_{12}$) produces a smoother film. Unlike the BCP4.1(C$_{12}$), no extended system of interconnecting phases is observed, suggesting that the BCP4.2(C$_{12}$) polymer lacks the ability to phase separate.

The PC$_{61}$BM blends of HP4.2(BT) and HP4.4(BnDT) (Figure 4.18) demonstrate, similarly to their shorter counter parts, a smooth film with a few minor aggregates and large-scale phase separation respectively. The phase separated domain sizes for the BCP4.2(C$_{12}$) blend are much larger (in the order of 5 μm) than the lower molecular weight counterpart (in the order of 1 μm) which is attributed to the reduced solubility and miscibility of the higher molecular weight polymer with PC$_{61}$BM. Examination of the block copolymer-PC$_{61}$BM blend (Figure 4.18c and 4.18f) shows some small interconnecting domains in the order of 100 nm, which are towards the upper limit of domain sizes desired for BHJ-OPV applications.
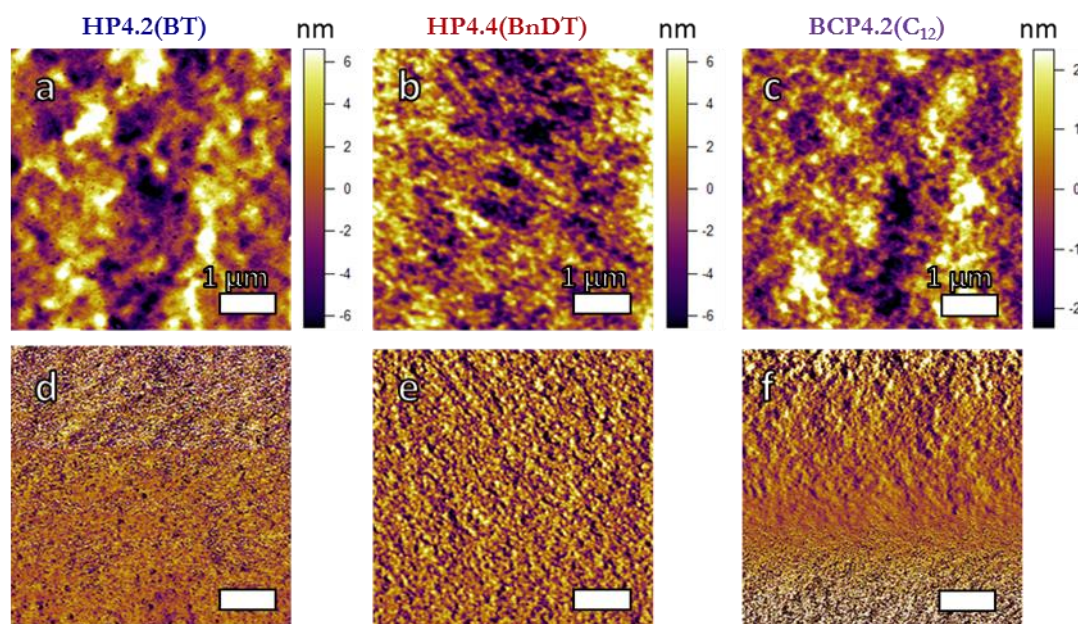
Figure 4.17: a-c; AFM height images, d-f; AFM phase images, a,d; HP4.2(BT), b,e; HP4.4(BnDT), c,d; BCP4.2(C$_{12}$). All scale bars are 1μm.
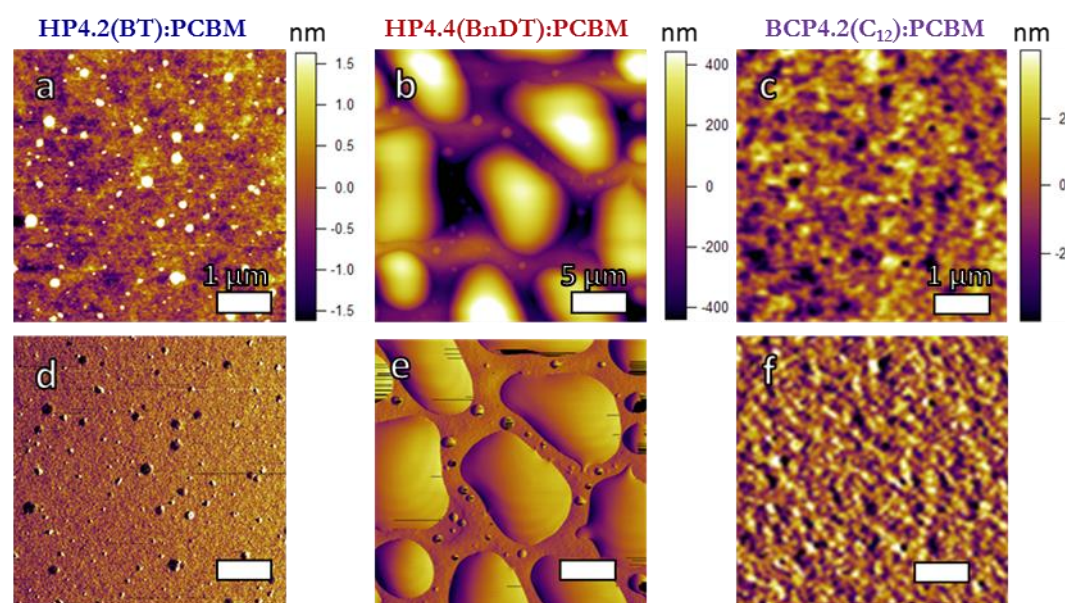
Figure 4.18: a-c; AFM height images, d-f; AFM phase images, a,d; HP4.2(BT):PC$_{61}$BM blend, b,e; HP4.4(BnDT): PC$_{61}$BM blend, c,d; BCP4.2(C$_{12}$): PC$_{61}$BM blend. Scale bars a,c,d and f are 1μm, scale bars b and e are 5 μm.

The height and phase images are of HP4.5(BnDTCO$_2$)and BCP4.3(C$_{12}$CO$_2$) polymer films were also studied (Figure 4.19). The HP4.5(BnDTCO$_2$)film is smooth and shows no evidence of the formation of crystallites unlike its HP4.3(BnDT) counterpart. Despite the difference in homoblock film morphology the block copolymer BCP4.3(CO$_2$C$_{12}$) shows phase separation with interconnecting domains of 50-100 nm in size, similar to the BCP4.1(C$_{12}$) film. The phase separation of block copolymers, containing BnDT(C$_{12}$) or the more soluble BnDT(CO$_2$C$_{12}$), can then be assigned to the differing intermolecular

interactions (π-stacking) of each block with PTBT and has little dependence on the relative solubility of the homoblocks in the casting solvent.

The $PC_{61}BM$ blend of HP4.5($BnDTCO_2$) shown in Figure 4.20 exhibits little evidence of phase separation or formation of large (> 1 μm) domains unlike the HP4.3(BnDT) equivalent which is assigned to its greater solubility and miscibility with $PC_{61}BM$, however, there are some instances of large features/aggregates. The BCP4.3(CO_2C_{12})-$PC_{61}BM$ blend shows a smoother film than its constituent homoblocks and there is some evidence of phase separation on the submicron level.
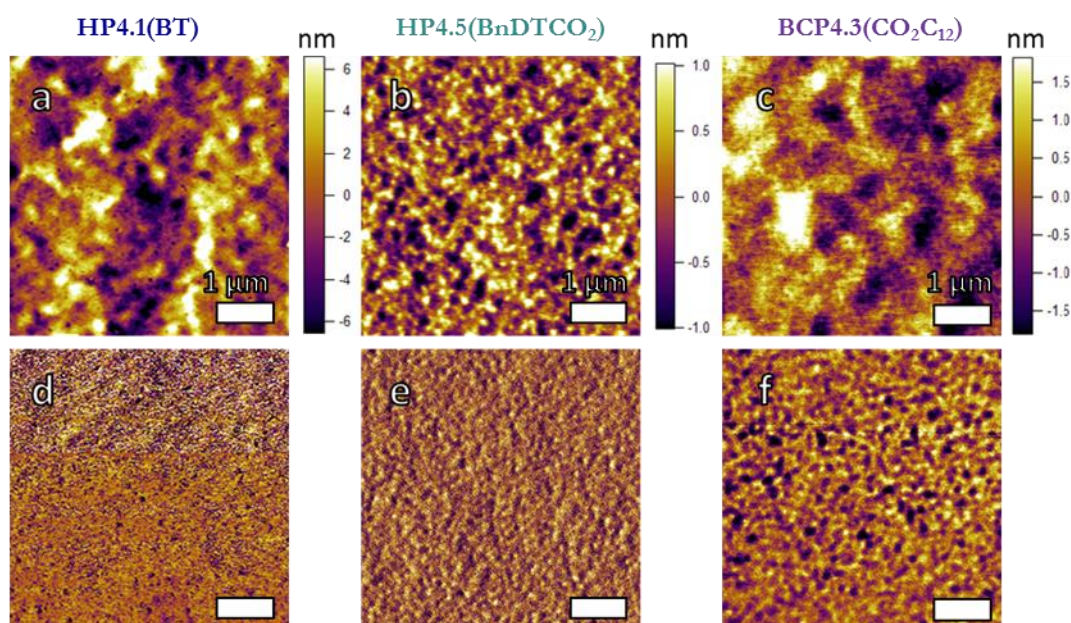
Figure 4.19: a-c; AFM height images, d-f; AFM phase images, a,d; HP4.1(BT), b,e; HP4.5($BnDTCO_2$), c,d; BCP4.3(CO_2C_{12}) All scale bars are 1μm.
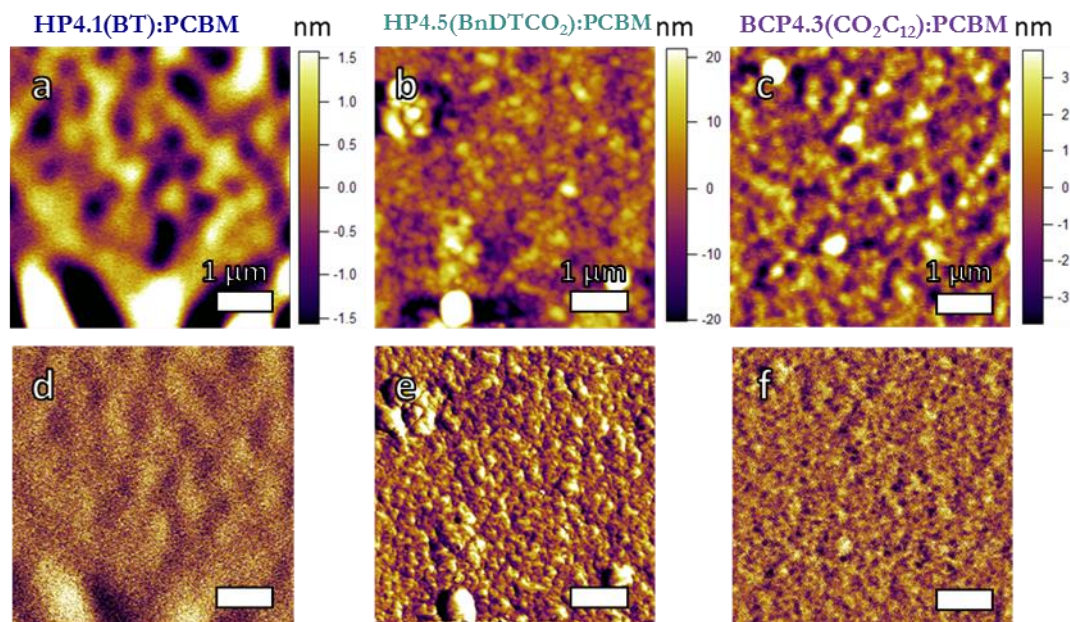
Figure 4.20: a-c; AFM height images, d-f; AFM phase images, a,d; HP4.1(BT):$PC_{61}BM$ blend, b,e; HP4.5(BnDTCO$_2$) blend, c,d; BCP4.3(CO_2C_{12}):$PC_{61}BM$ blend. All scale bars are 1 μm.

The film of the HP4.6(BnDTCO$_2$) polymer shown in Figure 4.21b demonstrates a very similar morphology to the HP4.4(BnDT) film in Figure 4.17b, however, the block copolymer BCP4.4($C_{12}CO_2$) (Figure 4.21c and 4.21f) shows larger phase separated domains, (possibly due to the homopolymer impurities previously discussed) when compared with BCP4.2(C_{12}) (Figure 4.17c and 1.17f). When examining the $PC_{61}BM$ polymer blends of BCP4.4($C_{12}CO_2$) and its constituent blocks it is clear to see that both HP4.2(BT) (Figure 4.22a and 4.22d) and HP4.6(BnDTCO$_2$) (Figure 4.22b and 4.22e) phase separate from the $PC_{61}BM$, small 200 nm spherulites can be seen in the HP4.2(BT) : $PC_{61}BM$ film and in addition, the HP4.6(BnDTCO$_2$) : $PC_{61}BM$ film the shows much more pronounced phase separation with feature sizes of 5-10 μm. Despite the various degrees of phase separation from the $PC_{61}BM$ (of the two homopolymers) the block copolymer BCP4.4($C_{12}CO_2$) shows good mixing with the $PC_{61}BM$ (Figure 4.23c and 4.23f) with smaller domains although some 1 μm aggregates are still present, which are also observed in the polymer film (Figure 4.21c and 4.21f).
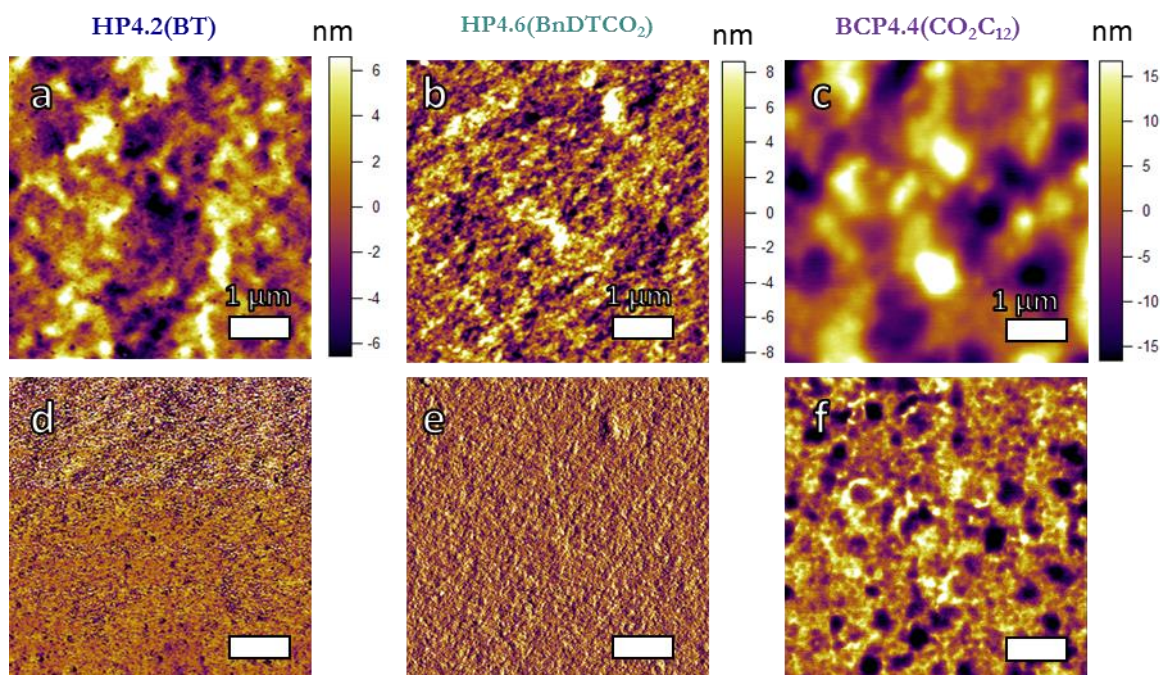
Figure 4.21: a-c; AFM height images, d-f; AFM phase images, a,d; HP4.2(BT), b,e; HP4.6(BnDTCO$_2$), c,d; BCP4.4(C$_{12}$CO$_2$). All scale bars are 1μm.
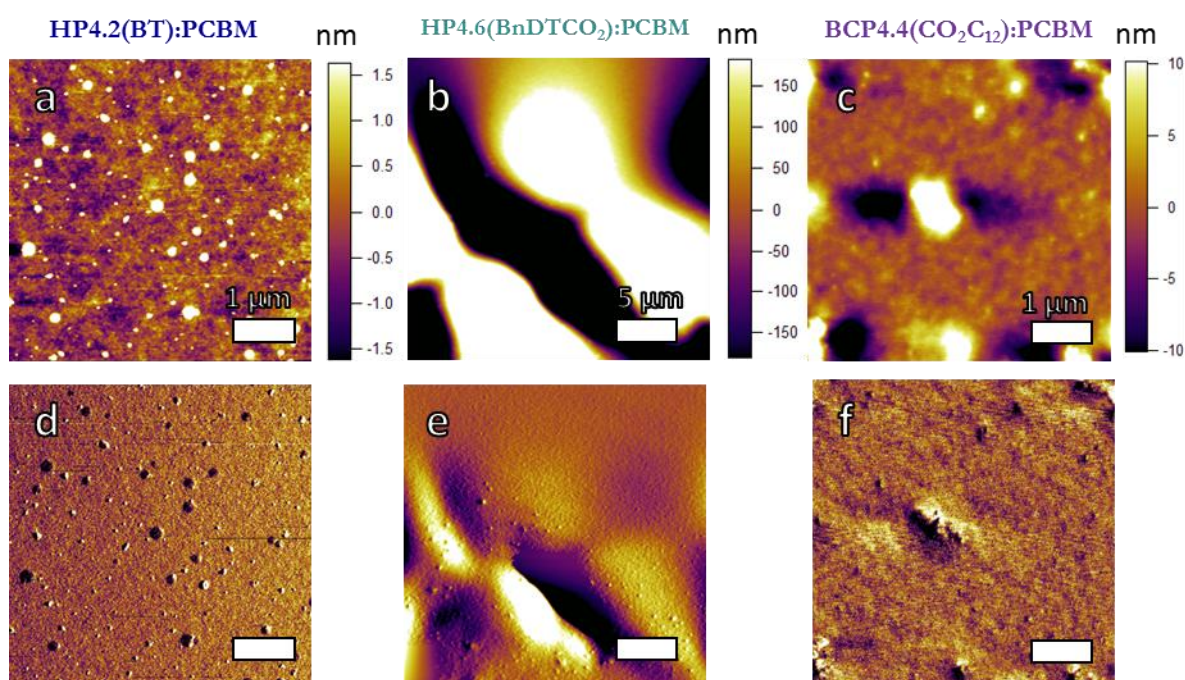
Figure 4.22: a-c; AFM height images, d-f; AFM phase images, a,d; HP4.1(BT):PC$_{61}$BM blend, b,e; HP4.6(BnDTCO$_2$) PC$_{61}$BM blend, c,d; BCP4.4(C$_{12}$CO$_2$):PC$_{61}$BM blend. Scale bars a,c,d and f are 1 μm, scale bars b and e are 5 μm.

The morphology studies of block copolymers comprised of PTBT, PTBnDT(C$_{12}$) and PTBnDT(CO$_2$C$_{12}$) homopolymers of various lengths have demonstrated that one can take advantage of the different properties of the homoblocks and their interactions with the PC$_{61}$BM acceptor to gain some control over the domain size exhibited in the BHJ

polymer-fullerene blend. Both the BCP4.1(C_{12}) and BCP4.3($C_{12}CO_2$) show signs of phase separation in the polymer film although when blended with $PC_{61}BM$ it is difficult to characterise any submicron domains. Both the BCP4.2(C_{12}) and BCP4.4($C_{12}CO_2$) block copolymer films show little evidence of phase separation on the order of < 100 nm which is also reflected in the $PC_{61}BM$ blends. To examine if these morphologies give rise to more favourable devices by increasing charge extraction and minimising recombination, OPV devices were made (described in Section 4.3) the photovoltaic properties of these devices are summarised along with their statistical counter parts in Table 4.7.

4.2.7: Photovoltaic Performance of Block Copolymers

Table 4.7: Summary of photovoltaic properties of devices made using various block copolymers, all values are an average of four devices.

Polymer	HOMO (eV)	E_g (eV)	V_{oc} (V)	J_{sc} (mA/cm^2)	FF	PCE (%)
PTBT-*stat*-PTBnDT(C_{12})	-5.3	1.78	0.72	9.8	64	4.50
BCP4.1(C_{12})	-5.5	1.71	0.78	3.19	36	0.90
BCP4.2(C_{12})	-5.4	1.75	0.59	2.10	29	0.51
PTBT-*stat*-PTBnDT(CO_2C_{12})	-5.4	1.74	0.82	11.1	64	5.84
BCP4.3(CO_2C_{12})	-5.5	1.78	0.82	8.00	52	3.40
BCP4.4(CO_2C_{12})	-5.5	1.75	0.85	7.68	53	3.43

Both of the polymers containing PTBnDT(C_{12}) blocks exhibit poor PCEs (Figure 4.23) when compared with their statistical counterpart owing largely to a low J_{sc} and FF, indicating poor charge generation and transport. The slightly higher J_{sc} and FF for the BCP4.1(C_{12}) device can, perhaps, be attributed to the microphase separation seen in the polymer film. Large aggregates seen in the polymer-$PC_{61}BM$ films of the PTBnDT(C_{12}) based block copolymers may also be the major source of current loss due to poor charge extraction and transport. The considerably lower V_{oc} provided by the BCP4.2(C_{12}) may be a result of the low intensity absorption peak centred at 650 nm (Figure 4.7) and the higher HOMO of the triblock copolymer providing poor charge extraction pathways.
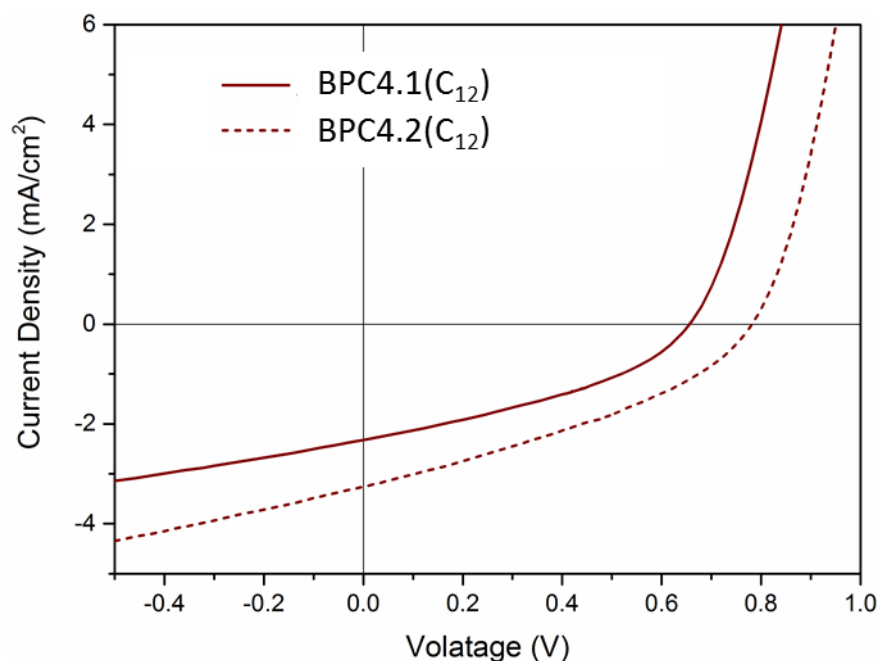
Figure 4.23: Current-Voltage curves for *BCP4.2(C12)* (solid line) and *multi*-PTBnDT(C$_{12}$)-*b*-PTBT (dashed line).

Block copolymers constructed with PTBnDT(CO$_2$C$_{12}$) blocks show a considerably improved performance than those which incorporate PTBnDT(C$_{12}$) blocks although they are still inferior in comparison to the PTBT-*stat*-PTBnDT(CO$_2$C$_{12}$) reference (Figure 4.24). The higher solubility of PTBnDT(CO$_2$C$_{12}$) and its increased miscibility with PC$_{61}$BM lead to more favourable BHJ morphologies with less aggregates. Most noticeably BCP4.3(C$_{12}$CO$_2$) and BCP4.4(C$_{12}$CO$_2$) both provide a high V$_{oc}$ of 0.82 and 0.85 V respectively, despite their HOMOs only being marginally deeper than those of their PTBnDT(C$_{12}$) counterparts. Examination of Figures 4.11c and 4.14c shows that the peak centred at 650 nm has a much higher intensity than those of the PTBnDT(C$_{12}$) based block copolymers (Figure 4.5 and Figure 4.7). The higher efficiency of the PTBnDT(CO$_2$C$_{12}$) block-based devices must also be accredited to the increase in J$_{sc}$ and FF as well as the high V$_{oc}$ values. The similar band gap of the PTBnDT(CO$_2$C$_{12}$) polymers to those of PBnDT(C$_{12}$) polymers as well as their deeper HOMO suggests that increased charge transport and a decrease in recombination is responsible for the increased J$_{sc}$ rather than an increase in exciton formation and charge generation.
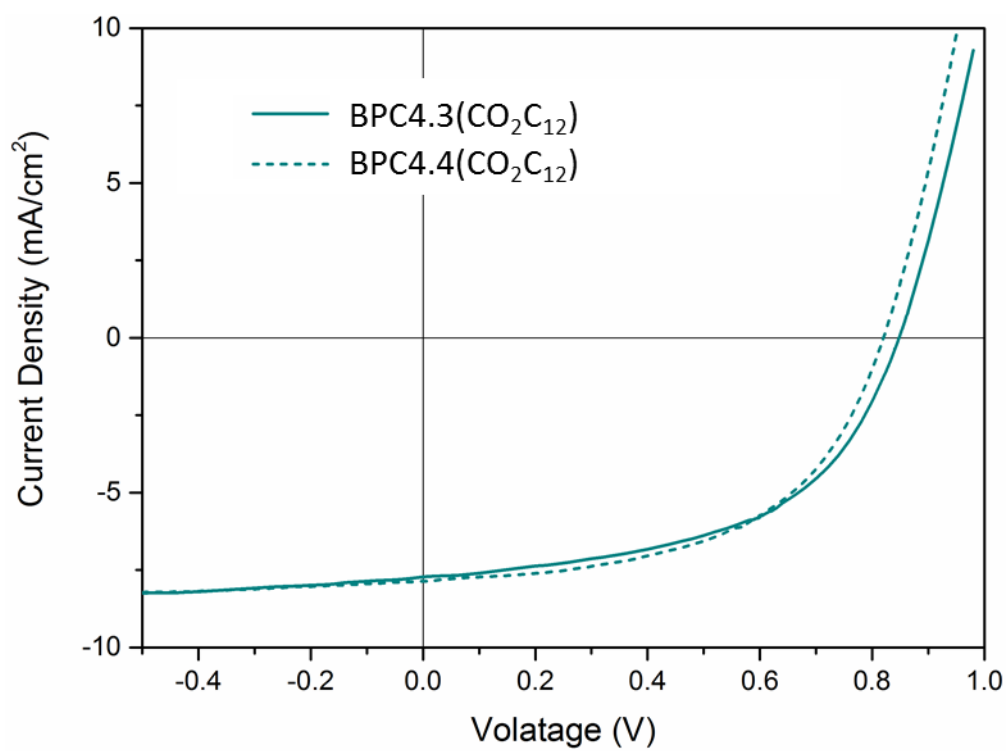
Figure 4.24: Current-Voltage curves BCP4.3(CO$_2$C$_{12}$) (solid line) and BCP4.4(CO$_2$C$_{12}$) (dashed line).

4.3: Conclusions

In this work a variety of block copolymers were synthesised, characterised and tested in OPV devices. The block copolymer films demonstrate a degree of phase separation and suggest a possible means for morphological control. PTBnDT(C_{12}) based block copolymers performed poorly in devices, a result of the insolubility of the PTBnDT(C_{12}) blocks and poor mixing with $PC_{61}BM$. On the other hand, using PTBnDT(CO_2C_{12}) blocks which also demonstrate phase separation in the polymer film but better mixing with $PC_{61}BM$ exhibit much higher PCEs, which, when optimised may compete with those of the statistical counterpart PTBT-*stat*-PTBnDT(CO_2C_{12}). The better definition in backbone structure of the block copolymers may also provide a solution to the issues of batch-to-batch variation which can be experienced when producing statistical copolymers and is disadvantageous from an industrial stand point.

This work has demonstrated that block copolymers may be a viable route to morphological control and efficient devices; further investigation should be carried out on varying block length and sequence, to optimise these systems and attain PCEs which exceed or are comparable to that of the statistical polymercounterparts.

4.4: Experimental

4.4.1: Materials

2,6-dibromo-4,8-didodecylbenzo[1,2-b:4,5-b']dithiophene (BnDT(C_{12})), 4,7-dibromo-5,6-bis(octyloxy)benzo[c][1,2,5]thiadiazol (BT), 4,8-didodecyl-2,6-dibromobenzo[1,2-b:4,5-b']dithiophene-4,8-dicarboxylate (BnDT(CO_2C_{12})), 2,5-bis(trimethylstannyl) thiophene and phenyl-C_{61}-butyric acid methyl ester (PC$_{61}$BM) were provided by Merck ltd. Anhydrous chlorobenzene (99.9 %) was purchased from ACROS Organics and used without further purification. Tris(dibenzylideneacetone)dipalladium(0) (Pd$_2$(dba)$_3$) was purchased from Sigma Aldrich and recrystallised from chloroform to obtain Pd$_2$(dba)$_3$.CHCl$_3$. Tri(*o*-tolyl)phosphine was purchased from Sigma Aldrich and recrystallised from hexane. Tetreabutylammonium hexafluorophosphate (99.9 %), silver nitrate, ferrocene (99.9 %) and butylated hydroxytoluene were purchased from Sigma Aldrich and used without further purification.

4.4.2: Methods

NMR. ^{1}H NMR was run at 398 K in 1,1,2,2-tetrachloroethane-D$_2$ using Bruker Avance III 400 MHz spectrometer.

Optoelectronic properties. UV-Vis spectra were obtained using an Agilent Technologies Cary 60 UV-Vis spectrometer. Samples were prepared to a concentration of 0.01 mg/ml by serial dilution in chlorobenzene. Films were spincast from a 10 mg/ml solution in chlorobenzene onto ITO coated glass (2000 rpm for 60 seconds) and annealed for 5 minutes at 180 °C. Cyclic voltammetry was conducted on a CH-Instruments 600 E potentiostat using a 3 mm glassy carbon disc electrode which was polished with 0.05 μm alumina powder, rinsed sequentially with, acetone, IPA and milliQ water. Prior to use the electrode surface was cleaned by cycling the voltage from + 1.2 to -1.2 V (vs Ag/Ag$^+$) in 0.5 M H$_2$SO$_4$ 20 times at a scan rate of 20 mV/s. The counter electrode was a platinum wire coil which was annealed in a blue flame prior to use. The reference electrode was Ag/Ag$^+$, the silver wire was polished and rinsed sequentially with, acetone, IPA and milliQ water the wire was then placed into a glass capillary tube fitted with a vycor frit and filled with 0.010 mM AgNO$_3$ solution. The system was calibrated using the ferrocene(Fc)/ferrocenium(Fc$^+$) redox couple. 0.100 M tetrabutylammonium hexafluorophosphate (TBAPF$_6$) was used as the supporting electrolyte. Analytes were dissolved at a concentration of 2 mg/ml in a solution of 2 mg/ml of TBAPF$_6$ in

chlorobenzene, drop cast onto the glassy carbon disk electrode and allowed to dry under ambient conditions.

Gel permeation chromatography. GPC was run on an Agilent PL220 instrument equipped with differential refractive index (DRI) and viscometry (VS) detectors. The system was equipped with 2 x PLgel Olexis columns (300 x 7.5 mm) and an Olexis 10 μm guard column. The mobile phase was 1,2,4-trichlorobenzene (TCB) with 250 PPM BHT (butylated hydroxytoluene) as the stabilising additive. Samples were run at 1 ml/min at 160 °C. The system was calibrated between M_p = 164 and 6,035,000 using 12 polystyrene narrow standards (Agilent EasyVials) to create a third order calibration. Analyte samples were filtered through a stainless steel frit with 10 μm pore size at 140 °C prior injection. Experimental molar mass (M_n, GPC) and dispersity (D) values of synthesized polymers were determined by conventional calibration using Agilent GPC/SEC software.

TGA Measurements. TGA spectra were recorded on a Mettler Toledo TGA/DSC1. Samples were analysed from 25 to 600 °C at a 10 °C min^{-1} heating rate under a nitrogen atmosphere.

AFM measurements. Polymer and Polymer:$PC_{61}BM$ films were spin cast at 2000 RPM for 60 seconds from a 10 mg/ml solution of polymer and 1:2 polymer:$PC_{61}BM$ in chlorobenzene. Films were cast onto ITO coated glass and annealed at 180 °C for 5 minutes. Atomic Force Microscopy images were obtained using an Asylum Research MFP-3D AFM, using AC 240-TS probes with a spring constant of 0.67 - 3.51 N/m purchased from oxford instruments in intermittent contact (tapping) mode. Images were analysed and processed using the Igor software package.

Device fabrication. ITO substrates were sonicated in IPA, acetone and deionised water for 5 minutes each and dried with nitrogen. A 10 nm ZnO electron transport layer was doctor bladed onto the ITO surface, the substrate was then annealed at 100 °C for 10 minutes. Polymer : $BC_{61}BM$ blends 1:1.5, 25 mg/ml in 1,2-dichlorobenzene were then doctor-bladed onto the ZnO layer at 80 °C and allowed to dry, after which a 10 nm PEDOT:PSS hole transport layer was doctor bladed on top. Finally, a 100 nm layer of silver was thermally evaporated onto the stack as the back electrode.

4.4.3: Synthesis

Synthesis of poly-5,6-bis(octyloxy)-4-(thiophen-2-yl)benzo[c][1,2,5]thiadiazole (HP4.1(BT) and HP4.2(BT)). To a dry 5 ml microwave vial 275.2 mg (0.500 mmol) of BT, 136.6 mg (0.333 mmol) for DP5 (HP4.1(BT)) or 179.3 mg (0.438 mmol) for DP 15 (HP4.2(BT)) of 2,5-bis(trimethylstannyl)thiophene, 10.4 mg (0.010 mmol) of Pd$_2$(dba)$_3$.CHCl$_3$ and 9.1 mg (0.030 mmol) P(o-tolyl)$_3$ was added. The flask was sealed with an aluminium crimp top on silicon septum before being evacuated and refilled with nitrogen for three cycles finally 2.5 ml of dry chlorobenzene was added. The vial was heated by microwave irradiation to 200 °C for 60 minutes. The polymer was precipitated into 150 ml of methanol and purified by Soxhlet extraction with acetone, hexane and finally chloroform.

Synthesis of poly-4,8-didodecyl-2-(thiophen-2-yl)benzo[1,2-b:4,5-b']dithiophene (HP4.4(BnDT) and HP4.4(BnDT)). To a dry 5 ml microwave vial 342.4 mg (0.500 mmol) of (BnDT(C$_{12}$), 136.6 mg (0.333 mmol) for DP5 (HP4.3(BnDT)) or 179.3 mg (0.438 mmol) for DP 15 (HP4.4(BnDT)) of 2,5-bis(trimethylstannyl)thiophene, 10.4 mg (0.010 mmol) of Pd$_2$(dba)$_3$.CHCl$_3$ and 9.1 mg (0.030 mmol) P(o-tolyl)$_3$ were added. The flask was sealed with an aluminium crimp top and silicon septum before being evacuated and refilled with nitrogen for three cycles, finally 5 ml of dry chlorobenzene was added. The vial was heated *via* microwave irradiation to 200 °C for 60 minutes. The polymer was precipitated into 150 ml of methanol and purified by Soxhlet extraction with acetone then hexane and finally chloroform.

Synthesis of poly-4,8,-didodecyl-2-(thiophen-2-yl)benzo[1,2-b:4,5-b']dithiophene-4,8-dicarboxylate (HP4.5(BnDTCO$_2$) and HP4.6(BnDTCO$_2$)). To a dry 5 ml microwave vial 386.4 mg (0.500 mmol) of (BnDT(CO$_2$C$_{12}$)), 136.6 mg (0.333 mmol) for DP 5 (HP4.5(BnDTCO$_2$) or 179.3 mg (0.438 mmol) for DP 15 HP4.6(BnDTCO$_2$) of 2,5-bis(trimethylstannyl) thiophene, 10.4 mg (0.010 mmol) of Pd$_2$(dba)$_3$.CHCl$_3$ and 9.1 mg (0.030 mmol) P(o-tolyl)$_3$ were added. The flask was sealed with an aluminium crimp top and silicon septum before being evacuated and refilled with nitrogen for three cycles finally 5 ml of dry chlorobenzene was added. The vial was heated *via* microwave irradiation to 200 °C for 60 minutes. The polymer was precipitated into 150 ml of methanol and purified by Soxhlet extraction with acetone then hexane and finally chloroform.

Synthesis of multi-poly-a-4,8-didodecyl-2-(thiophen-2-yl)benzo[1,2-b:4,5-b']dithiophene-block-b-poly-5,6-bis(octyloxy)-4-(thiophen-2-yl)benzo[c][1,2,5]thiadiazole (BCP4.1(C_{12})). To a dry 5 ml microwave vial 69.0 mg (0.015 mmol) of HP4.3(BnDT) (M_n = 4,600 g/mol), 40.5 mg (0.015 mmol) HP4.1(BT) (M_n = 2,700 g/mol), 2.6 mg (0.0025 mmol) of Pd$_2$(dba)$_3$.CHCl$_3$ and 2.3 mg (0.0075 mmol) of P(*o*-tolyl)$_3$ was added. The flask was sealed with an aluminium crimp top on silicon septum before being evacuated and refilled with nitrogen for three cycles finally 5 ml of dry chlorobenzene was added. The vial was heated *via* microwave irradiation to 200 °C for 60 minutes. The polymer was precipitated into 150 ml of methanol and purified by Soxhlet extraction with acetone then hexane and finally chloroform. The purified blockcopolymer was characterised by ^{1}H NMR (Figure 4.25), the peaks at δ = 4.34 and 3.25 ppm are assigned to the α-alkyl protons on the BT and BnDT units respectively, the relative integration of these peaks indicates the ratio of BT:BnDT (35:65) which were used to estimate the average number of blocks per a polymer (2 HP4.1(BT) and 2 HP4.3(BnDT)). The remaining signals δ = 8.65, 7.85-7.00, 2.20-0.50 ppm to the single protons on the BnDT(C$_{12}$) core, protons of the flanking thiophene units and the allylic protons on both the BT and BnDT(C$_{12}$) units respectively.

The ^{1}H NMR of BPC4.1(C$_{12}$) (Figure 4.25) is assigned as follows, δ(ppm)=: 8.63 (2H, s) to the protons on the BnDT unit, 7.59 (4H, s) to the protons on thee thiophene units within the BT homoblock (HP4.1)BT)), 7.38 (4H, s) to the protons on the thiophene in the BnDT homo block (HP4.3(BnDTC$_{12}$)), 4.34 (4H, s) is attributed to the α-protons on the alkoxy side chains situated on the BT units, 3.21 is assigned to the α-protons on the dodecyl side chains on the BnDT units, 2.50-0.50 is assigned to the remaining alkyl protons on both the BT and BnDT side chains.

Figure 4.25: ^{1}H NMR of BCP4.1(C$_{12}$).

Synthesis of ABA-(poly-A-4,8-didodecyl-2-(thiophen-2-yl)benzo[1,2-b:4,5-b']dithiophene-block-b-poly-5,6-bis(octyloxy)-4-(thiophen-2-yl)benzo[c][1,2,5]thiadiazole) (BCP4.2(C12)). To a dry 5 ml microwave vial 114.0 mg (0.012 mmol) of HP4.4(BnDT) (M_n = 9,500 g/mol) , 50.4 mg (0.006 mmol) of HP4.2(BT) (M_n = 8,500 g/mol), 2.6 mg (0.0025 mmol) of Pd$_2$(dba)$_3$.CHCl$_3$ and 2.3 mg (0.0075 mmol) of P(o-tolyl)$_3$ was added. The flask was sealed with an aluminium crimp top on silicon septum before being evacuated and refilled with nitrogen for three cycles finally 5 ml of dry chlorobenzene was added. The vial was heated *via* microwave irradiation to 200 °C for 60 minutes. The polymer was precipitated into 150 ml of methanol and purified by Soxhlet extraction with acetone then hexane and finally chloroform. The purified blockcopolymer was characterised by ^{1}H NMR (Figure 4.26), the peaks at δ = 4.37, and 3.24 ppm are from the α-alkyl protons on the BT and BnDT(C$_{12}$) units respectively, the relative integration of these peaks indicates the ratio of BT:BnDT(C$_{12}$) (31:69) which can be used to estimate the average number of blocker per a polymer (1 HP4.2(BT) and 2 HP4.4(BnDT)). The remaining signals δ = 8.63, 7.85-7.00, 2.20-0.50 ppm to the single protons on the BnDT(C$_{12}$) core, protons of the flanking thiophene units and, the allylic protons on both the BT and BnDT(C$_{12}$) units respectively.

The ^{1}H NMR of BPC4.2(C$_{12}$) (Figure 4.26) is assigned as follows, δ(ppm)=: 8.66 (2H, s) to the protons on the BnDT unit, 7.40 (4H, s) to the protons on the thiophene units within the BT homoblock (HP4.1)BT)), 7.38 (4H, s) to the protons on the thiophene in the BnDT homo block (HP4.3(BnDTC$_{12}$)), 4.38 (4H, s) is attributed to the α-protons on the alkoxy side chains situated on the BT units, 3.26 is assigned to the α-protons on the dodecyl side chains on the BnDT units, 2.50-0.50 is assigned to the remaining alkyl protons on both the BT and BnDT side chains.
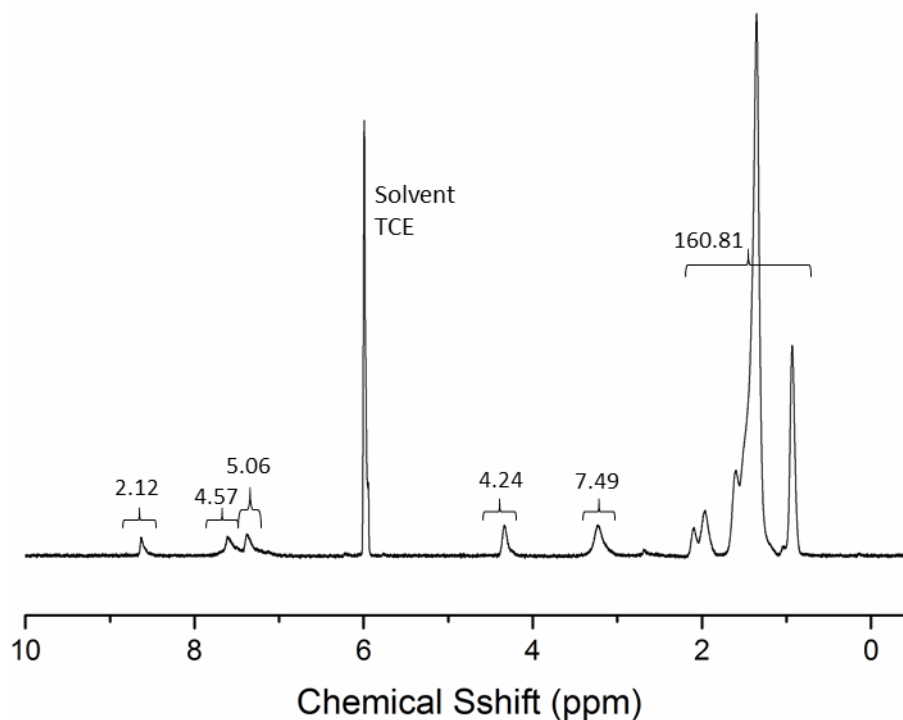

Figure 4.26: BCP4.2(C$_{12}$).

Synthesis of multi-poly-4,8,-didodecyl-2-(thiophen-2-yl)benzo[1,2-b:4,5-b']dithiophene-4,8-dicarboxylate-block-b-poly-5,6-bis(octyloxy)-4-(thiophen-2-yl)benzo[c][1,2,5]thiadiazole (BCP4.3(CO$_2$C$_{12}$).

To a dry 5 ml microwave vial 100.5 mg (0.015 mmol) of HP4.5(BnDTCO$_2$)(M_n = 6,700 g/mol) , 40.5 mg (0.015 mmol) of HP4.1(BT) (M_n = 2,700 g/mol), 2.6 mg (0.0025 mmol) of Pd$_2$(dba)$_3$.CHCl$_3$ and 2.3 mg (0.0075 mmol) of P(o-tolyl)$_3$ was added. The flask was sealed with an aluminium crimp top and silicon septum before being evacuated and refilled with nitrogen for three cycles. Finally, 5 ml of dry chlorobenzene was added. The

vial was heated *via* microwave irradiation to 200 °C for 60 minutes. The polymer was precipitated into 150 ml of methanol and purified by Soxhlet extraction with acetone then hexane and finally chloroform. The purified block copolymer was characterised by ^{1}H NMR (Figure 4.27), the peaks at δ = 4.72 and 4.34 ppm are from the α-alkyl protons on the BnTD(CO_2C_{12}) and BT units respectively, the relative integration of these peaks indicates the ratio of BT:BnDT(CO_2C_{12}) (56 : 44) which were used to estimate the average number of blocks per polymer crimp top on silicon septum before being evacuated and refilled with nitrogen for three (1 HP4.2(BT) and 1 HP4.6(BnDTCO2)). The remaining signals δ = 8.62, 8.40-6.60, 3.90-0.50 ppm to the single protons on the BnDT(CO_2C_{12}) core, protons of the flanking thiophene units and, the allylic protons on both the BT and BnDT(CO_2C_{12}) units respectively.

The ^{1}H NMR of BPC4.3(CO_2C_{12}) (Figure 4.26) is assigned as follows, δ(ppm)=: 8.63 (2H, s) to the protons on the BnDT(CO_2C_{12}) unit, 7.70-7.62 (4H, s) to the protons on the bridging thiophene units, 4.72 is assigned to the α-protons on the dodecyl side chains on the BnDT(CO_2C_{12}) units 4.34 (4H, s) is attributed to the α-protons on the alkoxy side chains situated on the BT units, 2.50-0.50 is assigned to the remaining alkyl protons on both the BT and BnDT side chains.
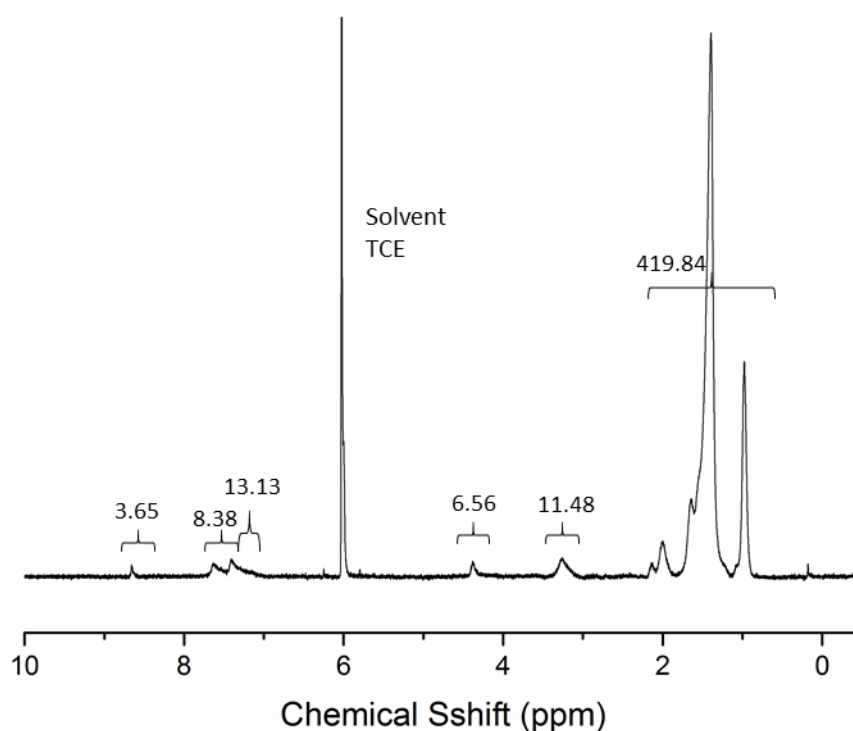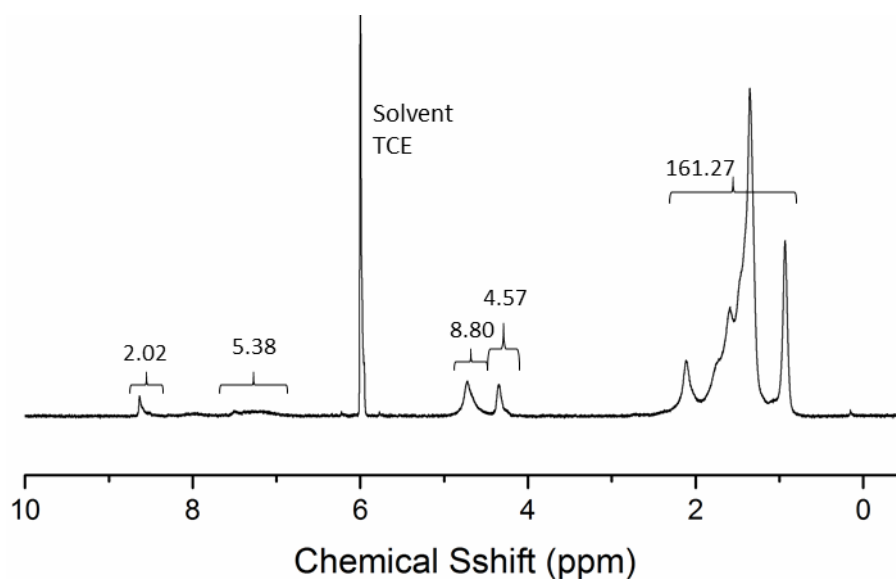

Figure 4.27: (BCP4.3(CO_2C_{12}).

Synthesis of *AB*-poly-4,8,-didodecyl-2-(thiophen-2-yl)benzo[1,2-b:4,5-b']dithiophene-4,8-dicarboxylate-*block-b*-poly-5,6-bis(octyloxy)-4-(thiophen-2-yl)benzo[c][1,2,5]thiadiazole (BCP4.4(CO$_2$C$_{12}$)).

To a dry 5 ml microwave vial 90.0 mg (0.012 mmol) of HP4.6(BnDTCO$_2$) (M_n = 7500 g/mol), 50.4 mg (0.015 mmol) of HP4.2(BT) (M_n = 8400 g/mol), 2.6 mg (0.0025 mmol) of Pd$_2$(dba)$_3$.CHCl$_3$ and 2.3 mg (0.0075 mmol) of P(*o*-tolyl)$_3$ was added. The flask was sealed with an aluminium crimp top on silicon septum before being evacuated and refilled with nitrogen for three cycles finally 5 ml of dry chlorobenzene was added. The vial was heated via microwave irradiation to 200 °C for 60 minutes. The polymer was precipitated into 150 ml of methanol and purified by Soxhlet extraction with acetone then hexane and finally chloroform. The purified blockcopolymer was characterised by ^{1}H NMR (Figure 4.28), the peaks at δ = 4.74 and 4.35 ppm assigned to the α-alkyl protons on the BnTD(CO$_2$C$_{12}$) and BT units respectively, the relative integration of these peaks indicates the ratio of BT:BnDT(CO$_2$C$_{12}$) (33:67) which were used to estimate the average number of blocker per polymer (2 HP4.1(BT) and 2 PTBnDT(CO$_2$C$_{12}$)-*short*). The remaining signals δ =: 8.64, 8.50-6.50, 3.90-0.50 ppm to the single protons on the BnDT(CO$_2$C$_{12}$) core, protons of the flanking thiophene units and, the allylic protons on both the BT and BnDT(CO$_2$C$_{12}$) units respectively.

The ^{1}H NMR of BPC4.3(CO$_2$C$_{12}$) (Figure 4.26) is assigned as follows, δ(ppm)=: 8.70 (2H, s) to the protons on the BnDT(CO$_2$C$_{12}$) unit, 7.64-7.62 (4H, s) to the protons on the bridging thiophene units, 4.75 is assigned to the α-protons on the dodecyl side chains on the BnDT(CO$_2$C$_{12}$) units 4.38 (4H, s) is attributed to the α-protons on the alkoxy side chains situated on the BT units, 2.50-0.50 is assigned to the remaining alkyl protons on both the BT and BnDT side chains.
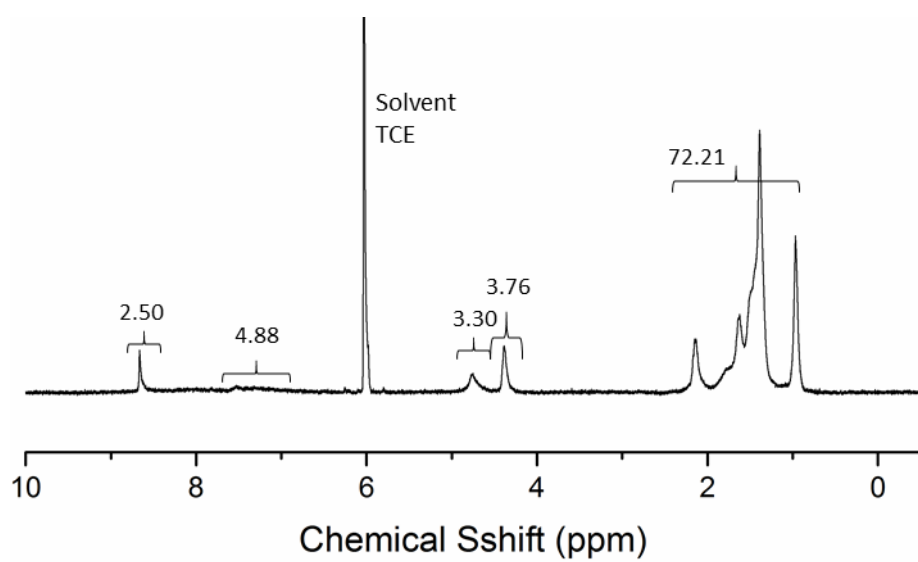
.

Figure 4.28: (BCP4.4(CO$_2$C$_{12}$).

4.5: References

(1)   Hamley, I. W. *The Physics of Block Copolymers*; Oxford University Press, 1998.

(2)   Mitchell, V. D.; Jones, D. J. *Polym. Chem.* **2018**, *9*, 795.

(3)   Mok, J. W.; Lin, Y. H.; Yager, K. G.; Mohite, A. D.; Nie, W. Y.; Darling, S. B.; Lee, Y.; Gomez, E.; Gosztola, D.; Schaller, R. D.; Verduzco, R. *Adv. Funct. Mater.* **2015**, *25*, 5578.

(4)   Liu, C. L.; Lin, C. H.; Kuo, C. C.; Lin, S. T.; Chen, W. C. *Prog. Polym. Sci.* **2011**, *36*, 603.

(5)   Yassar, A.; Miozzo, L.; Gironda, R.; Horowitz, G. *Prog. Polym. Sci.* **2013**, *38*, 791.

(6)   Ku, S.-Y.; Brady, M. A.; Treat, N. D.; Cochran, J. E.; Robb, M. J.; Kramer, E. J.; Chabinyc, M. L.; Hawker, C. J. *J. Am. Chem. Soc.* **2012**, *134*, 16040.

(7)   Heuken, M.; Komber, H.; Erdmann, T.; Senkovskyy, V.; Kiriy, A.; Voit, B. *Macromolecules* **2012**, *45*, 4101.

(8)   Tao, Y. F.; McCulloch, B.; Kim, S.; Segalman, R. A. *Soft Matter* **2009**, *5*, 4219.

(9)   Izuhara, D.; Swager, T. M. *Macromolecules* **2011**, *44*, 2678.

(10)   Verduzco, R.; Botiz, I.; Pickel, D. L.; Kilbey, S. M., II; Hong, K.; Dimasi, E.; Darling, S. B. *Macromolecules* **2011**, *44*, 530.

(11)   Pan, C.; Sugiyasu, K.; Aimi, J.; Sato, A.; Takeuchi, M. *Angew. Chem. Inter. Edit.* **2014**, *53*, 8870.

(12)   Li, L. G.; Niu, W. H.; Zhao, X. L.; Yang, X. N.; Chen, S. W. *Sci. Adv. Mater.* **2015**, *7*, 2021.

(13)   Yang, X. N.; Loos, J.; Veenstra, S. C.; Verhees, W. J. H.; Wienk, M. M.; Kroon, J. M.; Michels, M. A. J.; Janssen, R. A. J. *Nano Letters* **2005**, *5*, 579.

(14)   Gao, D.; Gibson, G. L.; Hollinger, J.; Li, P.; Seferos, D. S. *Polym. Chem.* **2015**, *6*, 3353.

(15)   Gasperini, A.; Johnson, M.; Jeanbourquin, X.; Yao, L.; Rahmanudin, A.; Guijarro, N.; Sivula, K. *Polym. Chem.* **2017**, *8*, 824.

(16)   Raissi, M.; Erothu, H.; Ibarboure, E.; Bejbouji, H.; Cramail, H.; Cloutet, E.; Vignau, L.; Hiorns, R. C. *J. Mater. Chem. A* **2017**, *5*, 7533.

(17)   Odian, G. *Principles of Polymerization*; Wiley, 2004.

(18)   Carsten, B.; He, F.; Son, H. J.; Xu, T.; Yu, L. *Chem. Revs.* **2011**, *111*, 1493.

(19) Skotheim, T. A.; Reynolds, J. *Handbook of Conducting Polymers, 2 Volume Set*; CRC Press, **2007**.

(20) Striegel, A. M., Yau, W. W., Kirkland, J. J. and Bly, D. D. In *Modern Size-Exclusion Liquid Chromatography* **2009**.

(21) Leonat, L.; Beatrice Gabriela, S.; Branzoi, I. V. *Cyclic voltammetry for energy levels estimation of organic materials*, **2013**, *75*.

(22) Gritzner, G.; Kuta, J. *Pure Appl. Chem.* **1984**, *56*, 461.

(23) Bredas, J. L.; Beljonne, D.; Coropceanu, V.; Cornil, J. *Chem. Revs.* **2004**, *104*, 4971.

(24) Lee, W.; Choi, H.; Hwang, S.; Kim, J. Y.; Woo, H. Y. *Chem. Eur. J.* **2012**, *18*, 2551.

(25) Meng, B.; Miao, J. H.; Liu, J.; Wang, L. X. *Macromol. Rapid Comm.* **2018**, *39*.

(26) Kim, N. K.; Jang, S. Y.; Pace, G.; Caironi, M.; Park, W. T.; Khim, D.; Kim, J.; Kim, D. Y.; Noh, Y. Y. *Chem. Mater.* **2015**, *27*, 8345.

(27) Sweetnam, S.; Graham, K. R.; Ngongang Ndjawa, G. O.; Heumüller, T.; Bartelt, J. A.; Burke, T. M.; Li, W.; You, W.; Amassian, A.; McGehee, M. D. *J. Am. Chem. Soc.* **2014**, *136*, 14078.

(28) Meier, H.; Stalmach, U.; Kolshorn, H. *Acta Polymerica* **1997**, *48*, 379.

(29) Yu, L.; Davidson, E.; Sharma, A.; Andersson, M. R.; Segalman, R.; Müller, C. *Chem. Mater.* **2017**, *29*, 5654.

(30) Shibasaki, K.; Tabata, K.; Yamamoto, Y.; Yasuda, T.; Kijima, M. *Macromolecules* **2014**, *47*, 4987.

(31) Guo, Z.; Lee, D. Y.; Liu, Y.; Sun, F. Y.; Sliwinski, A.; Gao, H. F.; Burns, P. C.; Huang, L. B.; Luo, T. F. *Phys. Chem. Chem. Phys.* **2014**, *16*, 7764.

Chapter 5: Conclusions and Outlook

5.1: Conclusions

This thesis started with a seemingly simple question; "why does the statistical polymer PTBnDT(C_{12})-*b*-PTBT out perform its alternating counterpart PTBnDT(C_{12})TBT?". Investigation of the differing structures resulting from these systems led us to develop a means of monitoring monomer conversion and inferring the polymer backbone structure. The hypothesised structure was a gradient or block like copolymer owing to the varying rates of conversion of the BnDT(C_{12}) and BT monomers and the hypothesised chain like growth of the polymer. Further evidence in support of the block-like structure was provided by scanning tunnelling microscopy in collaboration with Dr. Giovanni Costantini and Daniel Warr at the *University of Warwick*. The block like structure of the statistical copolymer resulted in a lower HOMO and better polymer $PC_{61}BM$ miscibility imparting a higher V_{oc} and J_{sc}, respectively, in BHJ-OPV devices. This initial work highlights some key flaws in the Stille polycondensation, with large variety of monomers available for contemporary organic semiconducting polymers one must consider carefully how they interact in a cross coupling, which is seldom well understood in the context of polymerisation.

The differing rates of monomer conversion were hypothesised to be a result of varying stability in the palladium intermediates (L_2Pd^{II}(BnDT)Br and L_2Pd^{II}(BT)Br) in the Stille catalytic cycle as well as BnDT's ability to associate to the catalytic centre perhaps leading to a more chain like growth process. The strongly electron withdrawing BT moiety destabilises the 16 electron palladium centre and the equilibrium for oxidative addition for this monomer lies further to the left than for the more electron donating BnDT species. In Chapter 3 the ability of more electron donating phosphine ligands to stabilise the L_2Pd^{II}(BT)Br) intermediate was investigated. The investigation demonstrated that more electron donating species could favour more rapid conversion of the BT monomer. It was also demonstrated that adding longer side chains to the phenyl groups (P(*o*-OMePh)$_3$ and XPhos) could also inhibit the conversion of BnDT. It was hypothesised that this is due to the disruption of π-stacking interaction between the ligand and monomeric species as well as increased steric demand. This work provided an important demonstration that, when using a statistical polymerisation, careful consideration must be afforded to catalyst choice. While previous work has focused on achieving high molecular weights, this thesis revealed that the catalytic system can largely influence backbone structure and concurrently the photovoltaic performances of the statistical conjugated polymers. In this instance polymers with a more block-like structure (resulting from a greater difference in rate of conversion between BT and BnDT) showed better

miscibility with $PC_{61}BM$ and evidence of microphase separation in the order of 50-100 nm which could be favourable for BHJ-OPV devices.

The favourable properties of the block-like polymers discussed in Chapter 2 and Chapter 3 led to the investigation of better defined block copolymers, where individual blocks were synthesised and characterised before coupling. Block copolymers (baring either C_{12} or CO_2C_{12} side chains on the BnDT donor unit) demonstrated some degree of phase separation in the polymer film and good miscibility with $PC_{61}BM$. This is one of the first reports of well-defined block copolymers without the utilisation of a well understood chain growth mechanism such as GRIM. The BT homo blocks displayed good miscibility with $PC_{61}BM$ while BnDT block showed poor mixing, when coupled the resulting block copolymers where shown, in some instances, to form favourable domain sizes in the polymer:$PC_{61}BM$ BHJ blend. Block copolymers were tested in devices, those containing BnDT(C_{12}) exhibited a poor photovoltaic assigned to their lower solubility resulting in poor devices. BnDT(CO_2C_{12}) containing block copolymers showed promising photovoltaic performance albeit lower than the statistical counterpart. This work has demonstrated that block copolymers may be (after optimisation) a viable way to influence the morphology of the polymer : $PC_{61}BM$ BHJ resulting in a higher device performance although optimisation is needed.

Further to identifying useful block copolymers for morphology control of blends and applications in OPVs this work reinforces the findings and conclusions presented in Chapter 2. This thesis started with a question "Why does the statistical copolymer outperform its alternating counterpart?" Chapter 2 highlighted how the structure of the polymer may be more block or gradient like in leading to improved miscibility with PCBM and some control over BHJ morphology. While one might predict that these donor-block acceptor-block copolymers might have poor optical properties (owing to the low frequency of donor-acceptor coupling along the back bone) we have shown that block copolymers can be used to create devices with acceptable PCEs and impressive V_{oc}'s and thus demonstrating the validity of the findings in Chapter 2.

5.2: Outlook

This work has demonstrated that following the kinetics of the Stille polycondensation can give good insight into the backbone sequence of statistical conjugated polymers, and to the best of our knowledge, is the first report of such work. While this project has mainly focussed on monomers Merck ltd. are working to commercialise, there are many more systems which similar investigations can be applied to. Block-donor-polymers have been shown, in this work, to provide a means for controlling BHJ morphology, however, with an ever growing monomer library and the introduction of non-fullerene acceptors there is extensive for similar work to follow and an ever growing variety of systems.

While block copolymers have been shown to have favourable morphological properties they are much more synthetically demanding. The work in this thesis has perhaps opened the way for more simple synthesis of block like copolymers through careful catalyst choice and perhaps the possibility of altering monomer conversion rates during a reaction by feeding in a variety of ligands.

Finally this work has highlighted some key limitations of the Stille coupling and demonstrated that in the context of polymerisation of conjugated monomers there is still much fundamental work to be done. The efficiency, possibility of homo coupling and core mechanistic understanding are all areas for future work, with *in-situ* ^{31}P NMR potentially being a valuable tool to study what effect the addition of the monomer to the palladium centre has.